



AUTHOR:

TITLE:

YEAR:

OpenAIR citation:

This work was submitted to- and approved by Robert Gordon University in partial fulfilment of the following degree:

OpenAIR takedown statement:

Section 6 of the “Repository policy for OpenAIR @ RGU” (available from <http://www.rgu.ac.uk/staff-and-current-students/library/library-policies/repository-policies>) provides guidance on the criteria under which RGU will consider withdrawing material from OpenAIR. If you believe that this item is subject to any of these criteria, or for any other reason should not be held on OpenAIR, then please contact openair-help@rgu.ac.uk with the details of the item and the nature of your complaint.

This is distributed under a CC _____ license.



Development and Testing of Inorganic
Membranes for Hydrogen Separation and
Purification in a Catalytic Membrane Reactor

By

Abubakar Alkali

A Thesis submitted in partial fulfilment for the degree of

Doctor of Philosophy

School of Engineering

Robert Gordon University

Aberdeen, Scotland United Kingdom

MAY 2016

ABSTRACT

Palladium membranes have been identified as the membranes of choice in hydrogen separation and purification processes due to their infinite selectivity to hydrogen when defect free. Despite their potentials in hydrogen processes, palladium membranes pose challenges in terms of cost and embrittlement which occurs when palladium comes in contact with hydrogen at temperatures below 573 K. The challenges posed by palladium membranes have encouraged research into nonpalladium based membranes such as Silica and Alumina. This thesis investigates hydrogen permeation and separation in palladium membranes and also the use of nonpalladium membranes, Silica and Alumina membranes in hydrogen permeation.

In this study, hydrogen permeation behavior was investigated for 3 types of membranes, Palladium, Silica and Alumina. Thin palladium films were deposited onto a 30 nm porous ceramic alumina support using both conventional and modified electroless plating methods. The hydrogen separation and purification behavior of the membranes were investigated including the effect of annealing at higher temperatures. Gas permeation through Silica and Alumina membranes was investigated for 5 single gases including hydrogen. The Silica and Alumina membranes were fabricated using the dip coating method and their hydrogen permeation behavior of investigated at different coatings.

A thin Palladium (Pd1) membrane with a thickness of 2 μm was prepared over porous ceramic alumina support using the electroless plating method and a maximum hydrogen flux of $80.4 \text{ cm}^3 \text{ cm}^{-2} \text{ min}^{-1}$ was observed at 873 K and 0.4 bar after annealing the membrane. The hydrogen flux increased to $94.5 \text{ cm}^3 \text{ cm}^{-2} \text{ min}^{-1}$ at same temperature and pressure for the Palladium membrane (Pd2) prepared using the modified electroless plating method. The hydrogen flux increased to $98.1 \text{ cm}^3 \text{ cm}^2 \text{ min}^{-1}$ for the palladium/silver (Pd/Ag) membrane prepared using the codeposition electroless plating method and the PdAg membrane avoided the hydrogen embrittlement at low temperature.

Hydrogen purity for the membrane was also investigated for a reformat gas mixture and a maximum hydrogen purity of 99.93% was observed at 873 K and 0.4 bar. The hydrogen purity was observed to increase as a result of the addition

of sulphur which suppresses the inhibition effect of the carbon monoxide in the reformat gas mixture. The presence of CO and CO₂ was observed to lead to an increase of the exponential factor n above 0.5 as a result of the inhibiting effect of these compounds on hydrogen permeation.

The value of the exponential factor n depicting the rate limiting step to hydrogen permeation in the palladium and palladium-alloy membranes was also investigated. Deviations from Sievert's law were observed from the Palladium membranes investigated in this work. In single gas hydrogen permeation investigation for the Pd1 membrane prepared using the conventional electroless plating method, the value of the exponential factor n = 0.5 in accordance with Sievert's law. However, for the mixed gas hydrogen separation investigation n=0.62 at 573 K which decreased to 0.55 when the membrane was annealed at 873 K. For the Pd2 membrane prepared using the modified electroless plating method, n=1 at 573 K but the value decreased to 0.76 for the mixed gas hydrogen separation investigation at same temperature which depicts a deviation from Sievert's law. In all the investigations carried out for the Pd3 palladium alloy membrane prepared using the co-deposition Pd/Ag electroless plating method at same conditions with the Pd1 and Pd2 membranes, n=0.5 in accordance with Sievert's law.

For the Nonpalladium based Silica and ceramic Alumina membranes, investigations were carried out for hydrogen permeation and 5 other single gases; He, CO₂, CH₄, N₂ and Ar. For the Silica membranes, a maximum hydrogen permeance of $3.12 \times 10^{-7} \text{ mol m}^{-2} \text{ s}^{-1} \text{ Pa}^{-1}$ at 573 K and 0.4 bar was observed which increased to $4.05 \times 10^{-7} \text{ mol m}^{-2} \text{ s}^{-1} \text{ Pa}^{-1}$ at 573 K and 0.4 when the membrane was modified with Boehmite sol prior to deposition of the Silica layer. The permeance for hydrogen and the 5 single gases was investigated for the alumina membrane at 5 successive coatings. It was observed that the commercial alumina membrane displayed a maximum hydrogen permeance of $9.72 \times 10^{-7} \text{ mol m}^{-2} \text{ s}^{-1} \text{ Pa}^{-1}$ at 573 K and 0.4 bar which increased to $9.85 \times 10^{-7} \text{ mol m}^{-2} \text{ s}^{-1} \text{ Pa}^{-1}$ at same temperature and pressure when the membrane was modified with Boehmite sol.

DEDICATION

This work is dedicated to the Glory of the Almighty Allah (S.W.T)

ACKNOWLEDGEMENT

My appreciation goes to my wife Zainab and my children Khalifa, Baba, Anisa and Bashir for their invaluable support at all times.

I must extend my deepest appreciation to my mother Hajiya Inno Balarabe Alkali for her motherly support and prayers at all times which gives me lots of strength. It is extremely important that I make special mention of my late father Alkali Balarabe Sokoto in all that I do. Words cannot describe my appreciation to him.

It is imperative that I express my profound appreciation to my supervisor Professor Edward Gobina for his professional support and guidance throughout this work. I am encouraged by Professor Gobina's rare creativity of combining a positive atmosphere with academic work to motivate his students towards success.

I remain grateful to my sponsors, the Petroleum Technology Development Fund (P.T.D.F), a parastatal of the Nigerian government for funding this project and for all their support and encouragement.

My gratitude also goes to my colleagues Mohammed Nasir Kajama, Ngozi Nwogu, Habiba Shehu, Edidiong Okon and Ifeyinwa Orakwe for their useful contributions.

TABLE OF CONTENTS

ABSTRACT	i
DEDICATION	iii
ACKNOWLEDGEMENT	iv
TABLE OF CONTENTS	v
TABLE OF FIGURES	x
LIST OF TABLES	xvii
NOMENCLATURE	xix
ABBREVIATIONS	xx
CONVERSIONS	xxi
CHAPTER 1	2
1.0 Introduction and Motivation	2
1.1 Environmental Pollution	2
1.2 Energy Insecurity	3
1.3 Membrane Technology	3
1.4 Motivation	4
1.5 The Hydrogen Energy System	6
1.5.1 Hydrogen Fuel	7
1.6 Scope of This Work	8
1.7 Membrane Requirement	9
1.8 Publications/Conferences Undertaking In This Work.	10
1.8.1 Journal Publications	10
1.8.2 International Conferences	10
1.9 Thesis Outline	11
1.10 References	13
CHAPTER 2	17
2.0 Literature Review	17
2.1 Hydrogen Production	17
2.2 Inorganic Membranes for Hydrogen Separation & Purification	18
2.3 Membrane Reactors for Hydrogen Production	21
2.4 Gas Transport Mechanisms	25
2.4.1 Viscous Flow	25
2.4.2 Solution Diffusion	26

2.4.3 Knudsen Flow.....	26
2.4.4 Molecular Sieve.....	26
2.5 Gas permeation through porous membranes	27
2.6 Methods for Fabrication of Membrane	29
2.6.1 Electroless Plating (ELP).....	29
2.6.2 Electrodeposition (EDP).....	31
2.6.3 Chemical Vapour Deposition (CVD).....	32
2.6.4 Physical Vapour Deposition (PVD).....	33
2.6.5 Photocatalytic Deposition (PCD)	34
2.7 References	34
CHAPTER 3	38
3.0 Palladium and Palladium - Silver Composite Membranes.	38
3.1. Background.....	38
3.2 Hydrogen Permeation through Palladium Membranes	39
3.3 Materials and Equipments	43
3.3.1 Materials	43
3.3.2 Equipments.....	46
3.3.3 List of Gases.....	49
3.3.4 Chemicals	49
3.4 Experimental Procedure	51
3.4.1 Helium Leak Test.....	53
3.4.2 Support Modification: Sensitization, Activation and Calcination.	54
3.4.3 Deposition of the Palladium Layer.....	57
3.4.4 Modified Electroless Plating Method.....	59
3.4.5 Co-deposition: Electroless Plating of Pd/Ag Composite Membrane	60
3.4.6 Electroless Plating of the Pd/Ag Layer	61
3.4.7 Hydrogen Permeation to Test for Embrittlement	62
3.4.8 Hydrogen Permeation at Higher Temperature	62
3.5 References	63
CHAPTER 4	66
4.0. Silica Membranes for Hydrogen Separation and Purification.	66
4.1. Background.....	66
4.2. The Dip Coating Method.....	67
4.3. Chemical Vapour Deposition (CVD) in Silica Membranes.....	69

4.4. Silica Membranes Vs Palladium Membranes for Hydrogen Separation and Purification	70
4.5 Materials and Equipment	70
4.5.1 Materials	71
4.5.2 Equipments	72
4.5.3 Gases	72
4.5.4 Alumina Support Tubes	73
4.6 Experimental Procedure.....	73
4.6.1 Conventional Method for Preparation of Silica Membranes.....	73
4.6.2 Modified Method for Preparation of Silica Membranes	74
4.6.3 Gas Permeation Test Plant.....	75
4.7 References.....	76
CHAPTER 5.....	78
5.0. Alumina Membranes for Hydrogen Separation and Purification	78
5.1. Background	78
5.2 Methodology	79
5.3 Experimental Procedure.....	80
5.4 Determination of Boehmite Layer Thickness.....	81
5.5 References.....	81
CHAPTER 6.....	83
6.0. Results and Discussion	83
6.1: Palladium Membrane Prepared Using Conventional Electroless Plating Method (Pd1)	84
6.1.1 Helium Leak Test After Palladium Layer Deposition.....	85
6.1.2 Permeation Test for Pure N ₂ Gas Through Pd1 Membrane.....	86
6.1.3 Single Gas Permeation Test for Pd1 Membrane.	89
6.1.4 Effect of Annealing on Hydrogen Permeation Through Pd1 Membrane	91
6.1.5 Mixed Gas Transport Tests for Pd1 Membrane.....	93
6.1.6 Hydrogen Transport, Rate Limiting Step and n-value in Pd1 Membrane.....	98
6.1.7 Hydrogen Embrittlement.....	100
6.1.8 Observations for Pd1 Membrane	101
6.2 Palladium Membrane Produced Using the Modified Electroless Plating Method (Pd2)	102

6.2.1: He & N ₂ Permeation Through Pd2 membrane.....	103
6.2.2 Single Gas Hydrogen Permeation Through Pd2 Membrane.....	105
6.2.3 Effect of Annealing on Hydrogen Permeation Through Pd2 Membrane	108
6.2.4 Mixed Gas Separation and Hydrogen Purity for Pd2 Membrane.....	109
6.2.5 Hydrogen Purity for Pd2 Membrane	112
6.2.6 Observations for Pd2 membrane	113
6.3 Results for Pd/Ag Composite Membrane.....	114
6.3.1 Helium & N ₂ Leak Test	115
6.3.2 Single Gas Permeation Test for Pd3 Membrane at Low Temperature	116
6.3.3 Effect of Annealing Pd3 Membrane on Hydrogen Permeation....	119
6.3.4 Gas Separation and Hydrogen Purity.....	120
6.3.5 Summary of observations for Pd3 membrane.....	125
6.4 Silica Membranes SL1 & SL2	126
6.4.1 Single Gas Permeation Test for SL1 Membrane after first dip...126	
6.4.2 Gas Permeation Through SL1 Membrane after second dip	138
6.4.3 Modification of the Alumina support with Boehmite sol for silica deposition.....	148
6.4.4 Single Gas Permeation Tests for the SL2 membrane after first dip	149
6.4.5 Single Gas Permeation Tests for the Modified Silica Membrane after Second Dip.....	158
6.4.6 Gas Permeance against Kinetic Diameter	168
6.4.7 Gas Permeance against Molecular Weight	168
6.4.8 Observations for SL1 and SL2 membranes	169
6.5 Ceramic Alumina Membranes	170
6.5.1 Single Gas Permeation Test for the Commercial Ceramic Alumina Support AM0	170
6.5.2. Gas Permeance against Kinetic Diameter for the AM0 Membrane	177
6.5.3 Gas Permeation Tests for the Modified Alumina Membrane AM1	178
6.5.4 Gas permeance and Selectivity after Second Dip for the AM1 Membrane	183
6.5.5 Gas Permeance and Selectivity after Third Dip	187
6.5.6 Gas permeance after fourth Dip	191
6.5.7 Hydrogen Permeance after fifth Dip	193

6.5.8 Observations for the AM0 and AM1 Membranes.....	194
6.5.9 References	195
CHAPTER 7	200
7.0 Conclusions and Recommendations for Future Work.....	200
7.1 Validation of Results	200
7.2 Conclusions.....	201
7.2 Recommendations for Future Work	204
Appendices.....	206
Appendix A: GC Method for Gas Analysis.....	207
Appendix B: Typical GC Chromatogram Result for Single Gas Hydrogen Permeation Test.....	210
Appendix C: Typical GC Chromatogram Result for Mixed Gas Hydrogen Permeation Test.....	212
Appendix D: Membrane Characterization: SEM and EDXA for Pd1 Membrane	214
Appendix E: Calculation of Hydrogen Flux	218
Appendix F: Sample Calculation of Gas Permeance and Selectivity	220
Appendix G: Calculation of Thickness for Silica Membrane.....	222
Appendix H: Membrane Characterisation for Ceramic Alumina Membrane...	226
Appendix I: Calculation of Thickness for Modified Ceramic Alumina Membrane AM1	229

TABLE OF FIGURES

Figure 2.1. Classification of Membrane Reactors Based on Permselectivity	22
Figure 2.2: Membrane reactors based on catalytic activity	24
Figure 2.3: Gas Transport Mechanism in Inorganic Membranes: a) Surface Diffusion (b) Viscous Flow (c) Solution - Diffusion (d) Molecular Sieve (e) Knudsen Diffusion	25
Figure 2.4: A Schematic of the Electroless Plating Process	Error!
Bookmark not defined.	
Figure 2.5: A Schematic Diagram of the Vacuum Electrodeposition Process	32
Figure 2.6: A Schematic of Forced Flow Chemical Vapour Deposition	33
Figure 2.7: A Schematic of Magnetic Sputtering Method	34
Figure 3.1: A Schematic of hydrogen permeation across a palladium membrane.....	40
Figure 3.2: A Diagram showing the effect of driving force on gas permeation across the membrane	42
Figure 3.3: Pictures of alumina support (A) Big membrane (B) Small membrane.....	44
Figure 3.4: Pictures showing the determination of diameter of alumina support using vernier caliper (A) Outer diameter (B) Inner diameter....	45
Figure 3.5: Design specification of the custom tubes for electroless plating method	46
Figure 3.6: A Picture of the gas chromatograph for gas analysis used in this work	51
Figure 3.7: Concept schematic of a gas permeation test plant.....	52
Figure 3.8: Picture of ceramic alumina support in the oven for drying ...	53
Figure 3.9: A Picture of membrane in the furnace for calcination	54
Figure 3.10: A Picture of the sensitization and activation solutions with distilled water during support modification before electroless plating	55

Figure 3.11: A Picture of water jacket and plating solution during electroless plating	58
Figure 3.12: A Picture of the gas permeation test plant in the CPIMT laboratory	58
Figure 3.13: A Picture of the set up for surface modification with Boehmite before plating	60
Figure 4.1: A Picture of the dip coating set up for the preparation of composite silica membranes	68
Figure 4.2: A Picture of Silica membrane dried at room temperature using the WEIR 413D motor power rotatory drier	74
Figure 5.1: A Picture of the dip coating set up for the modification of ceramic alumina support with Boehmite	80
Figure 6.1: Helium permeance against inlet pressure for the tubular alumina support	83
Figure 6.2: A Picture of tubular ceramic alumina support (A) Before and (B) after sensitization and activation showing clear color change	84
Figure 6.3: A Picture of the palladium membrane Pd1 prepared using conventional electroless plating	85
Figure 6.4: Helium permeance against inlet pressure for the palladium membrane Pd1	86
Figure 6.5: Nitrogen flux against feed pressure for the Pd1 membrane .	87
Figure 6.6: H ₂ /N ₂ selectivity against feed pressure for the Pd1 membrane	87
Figure 6.7: Hydrogen flux against square root of partial pressure difference for the Pd1 membrane	89
Figure 6.8: Arrhenius Vant-Hoff plot for single hydrogen permeation through Pd1 membrane	90
Figure 6.9: Hydrogen flux against square root of partial pressure difference after annealing the Pd1 membrane	92
Figure 6.10: Hydrogen flux against partial pressure difference for hydrogen separation from gas mixture through Pd1 membrane	93

Figure 6.11: CO and CO ₂ flux in the permeate stream against feed pressure before annealing the Pd1 membrane.....	94
Figure 6.12: Hydrogen flux against partial pressure difference for hydrogen separation from gas mixture after annealing Pd1 membrane..	94
Figure 6.13: Flux of CO and CO ₂ in the permeate stream against feed pressure after annealing the Pd1 membrane	96
Figure 6.14: A Picture of the peeled Pd1 membrane after hydrogen embrittlement	101
Figure 6.15: A Picture of the Pd2 membrane prepared using modified electroless plating method.....	103
Figure 6.16: Helium flux against inlet pressure for the Pd2 membrane	104
Figure 6.17: N ₂ flux against feed pressure for the Pd2 membrane	104
Figure 6.18: Hydrogen flux against partial pressure difference for the Pd2 membrane.....	105
Figure 6.19: H ₂ /N ₂ selectivity against feed pressure for the Pd2 membrane	106
Figure 6.20: Hydrogen flux against partial pressure difference for the annealed Pd2 membrane	108
Figure 6.21: Hydrogen flux agaist partial pressure difference for hydrogen separation from gas mixture for the Pd2 membrane	110
Figure 6.22: Hydrogen flux against partial pressure difference for hydrogen separation from gas mixture after annealing the Pd2 membrane	110
Figure 6.23: A Picture of the Pd3 membrane prepared using codeposition electroless plating method.....	114
Figure 6.24: Helium permeation against inlet pressure for the Pd3 membrane.....	115
Figure 6.25: N ₂ flux against feed pressure for the Pd3 membrane	115
Figure 6.26: Hydrogen flux agaist partial pressure difference for the Pd3 membrane at low temperature to test for embrittlement	116
Figure 6.27: H ₂ /N ₂ selectivity against feed pressure for the Pd3 membrane	117

Figure 6.28: Hydrogen flux against partial pressure difference for the Pd3 membrane at high temperature	118
Figure 6.29: Hydrogen flux against partial pressure difference after annealing the Pd3 membrane	119
Figure 6.30: Hydrogen flux against partial pressure difference for mixed gas separation for the Pd3 membrane.....	120
Figure 6.31: Hydrogen flux against partial pressure difference for hydrogen separation from gas mixture after annealing the Pd3 membrane	121
Figure 6.32: Hydrogen permeation against inverse square root of temperature for the SL1 membrane after first dip	127
Figure 6.33: Helium permeance against inverse square root of temperature for the SL1 membrane.....	130
Figure 6.34: Nitrogen permeance against inverse square root of temperature for the SL1 membrane after first dip	131
Figure 6.35: H ₂ /N ₂ selectivity against inlet pressure after first dip for the SL1 membrane	132
Figure 6.36: CO ₂ permeance against inverse square root of temperature for the SL1 membrane after first dip	133
Figure 6.37: H ₂ /CO ₂ selectivity against inlet pressure for the SL1 membrane after first dip	134
Figure 6.38: CH ₄ permeance against inverse square root of temperature for the SL1 membrane after first dip	135
Figure 6.39: H ₂ /CH ₄ selectivity for the SL1 membrane after first dip	136
Figure 6.40: Ar permeance against the inverse square root of temperature for the SL1 membrane after first dip	137
Figure 6.41: H ₂ /Ar selectivity for the SL1 membrane after first dip	137
Figure 6.42: H ₂ permeance against inverse square root of temperature for the SL1 membrane after second dip	138
Figure 6.43: (a) He permeance and (b) CO ₂ permeance against inverse square root of temperature for the SL1 membrane after the second dip	140

Figure 6.44: (a) CH ₄ and (b) N ₂ permeance against inverse square root of temperature for the SL1 membrane after the second dip	142
Figure 6.45: Ar permeance against square root of temperature for the SL1 membrane after the second dip	143
Figure 6.46: Hydrogen permeance against inverse square root of temperature for the SL2 membrane after first dip	148
Figure 6.47: Helium permeance against inverse square root of temperature for the SL2 membrane after first dip	150
Figure 6.48: H ₂ /He selectivity for the SL2 membrane after first dip	150
Figure 6.49: CO ₂ permeance against inverse square root of temperature for the SL2 membrane after first dip	151
Figure 6.50: H ₂ /CO ₂ selectivity for the SL2 membrane after first dip ...	152
Figure 6.51: CH ₄ permeance against inverse square root of temperature for the SL2 membrane after first dip	152
Figure 6.52: H ₂ /CH ₄ selectivity at different temperature for the SL2 membrane after the first dip	153
Figure 6.53: N ₂ permeance against inverse square root of temperature for the SL2 membrane after the first dip	154
Figure 6.54: H ₂ /N ₂ selectivity at different temperature for the SL2 membrane after first dip	155
Figure 6.55: Ar permeance against the inverse square root of temperature for the SL2 membrane after first dip	156
Figure 6.56: H ₂ /Ar selectivity at different temperature for the SL2 membrane after first dip	156
Figure 6.57: Hydrogen permeance against inverse square root of temperature for the SL2 membrane after second dip	157
Figure 6.58: Helium permeance against the inverse square root of temperature for the SL2 membrane after second dip	158
Figure 6.59: H ₂ /He selectivity at different temperatures for the SL2 membrane after second dip	158
Figure 6.60: CO ₂ permeance against inverse square root of temperature for the SL2 membrane after second dip	159

Figure 6.61: H ₂ /CO ₂ selectivity at different temperature for the SL2 membrane after second dip	160
Figure 6.62: CH ₄ permeance against inverse square root of temperature for the SL2 membrane after second dip.....	161
Figure 6.63: H ₂ /CH ₄ selectivity at different temperature for the SL2 membrane after second dip	162
Figure 6.64: N ₂ permeance against inverse square root of temperature for the SL2 membrane after second dip	162
Figure 6.65: H ₂ /N ₂ selectivity for the SL2 membrane after second dip..	163
Figure 6.66: Ar permeance against the inverse square root of temperature for the SL2 membrane after second dip.....	164
Figure 6.67: H ₂ /Ar selectivity at different temperature for the SL2 membrane after second dip	165
Figure 6.68: Hydrogen permeance against feed pressure for the ceramic alumina support AM0	168
Figure 6.69: Gas permeance against temperature at 0.05 bar for the Alumina support AM0.....	170
Figure 6.70: H ₂ /N ₂ selectivity against feed pressure for the alumina support AM0	171
Figure 6.71: gas permeance against kinetic diameter at 573 K and 0.05 bar for the alumina support AM0	174
Figure 6.72: Hydrogen permeance against feed pressure for the modified AM1 membrane after first dip	175
Figure 6.73: Gas permeance against temperature at 0.05 bar for the AM1 membrane after first dip	177
Figure 6.74: H ₂ /N ₂ selectivity against feed pressure for the AM1 membrane	177
Figure 6.75: Hydrogen permeance against feed pressure for the alumina membrane AM1 after second dip	181
Figure 6.76: Gas permeance against temperature at 0.05 bar for the AM1 membrane after the second dip.....	181

Figure 6.77: Hydrogen permeance against feed pressure for the AM1 membrane after third dip	185
Figure 6.78: Gas permeance against temperature at 0.05 bar for the AM1 membrane after third dip	185
Figure 6.79: H ₂ and CO ₂ permeance against feed pressure for the AM1 membrane after fourth dip	189
Figure 6.80: Hydrogen permeance against feed pressure for the AM1 membrane after fifth dip	190

LIST OF TABLES

Table 3.1: Specification for small and big membranes used in this work	43
Table 3.2: Composition of sensitization and activation solutions	55
Table 3.3: Composition of the plating solution	57
Table 3.4: Composition of the Boehmite solution for modification of the Alumina support.....	60
Table 3.5: Pd/Ag Plating bath composition.....	61
Table 6.1: Average H ₂ purity in the dry gas reformat before and after annealing the Pd1 membrane	98
Table 6.2: Flux of CO in the permeate stream for mixed gas separation before and after annealing Pd2 membrane	109
Table 6.3: Average hydrogen purity in the dry gas reformat before and after annealing Pd2 membrane	112
Table 6.4: Flux of CO in the permeate stream before and after annealing Pd3 membrane	122
Table 6.5: Average hydrogen purity in the dry gas reformat for Pd3 membrane	122
Table 6.6: Comparison of activation energy for composite membranes	123
Table 6.7: Technical targets for hydrogen separation using membranes (U.S DOE)	124
Table 6.8: Ideal selectivity for hydrogen in relation to He, CO ₂ , CH ₄ , N ₂ and Ar for the SL1 membrane after first dip.....	129
Table 6.9: H ₂ /He selectivity at different temperature and pressure for the SL1 membrane after second dip	144
Table 6.10: H ₂ /CH ₄ selectivity at different temperature and pressure for the SL1 membrane after second dip	144
Table 6.11: H ₂ /CO ₂ selectivity at different temperature and pressure for the SL1 membrane after second dip	145

Table 6.12: H ₂ /N ₂ selectivity at different temperature and pressure after second dip.....	145
Table 6.13: H ₂ /Ar selectivity at different temperature and pressure for the SL1 membrane after second dip.....	146
Table 6.14: Comparison of hydrogen permeance SL1 and SL2 at 573 K and 0.04 bar after the first and second dips.....	165
Table 6.15: H ₂ /N ₂ and H ₂ /He selectivity for the Alumina support AM0 .	172
Table 6.16: H ₂ /CO ₂ and H ₂ /CH ₄ selectivity for the Alumina support AM0	173
Table 6.17: H ₂ /Ar selectivity for the Alumina support AM0.....	173
Table 6.18: H ₂ /N ₂ and H ₂ /He selectivity for the AM1 membrane after first dip	179
Table 6.19: H ₂ /CO ₂ and H ₂ /CH ₄ selectivity for the Alumina membrane AM1 after first dip	179
Table 6.20: H ₂ /Ar selectivity for the Alumina membrane AM1 after first dip	180
Table 6.21: H ₂ /He selectivity for the Alumina membrane AM1 after second dip	183
Table 6.22: H ₂ /CO ₂ and H ₂ /CH ₄ selectivity for the Alumina membrane AM1 after second dip	183
Table 6.23: H ₂ /Ar selectivity for the Alumina membrane AM1 after second dip	184
Table 6.24: H ₂ /N ₂ and H ₂ /CO ₂ selectivity for the alumina membrane AM1 after third dip	186
Table 6.25: H ₂ /CO ₂ and H ₂ /CH ₄ selectivity for the Alumina membrane AM1 after third dip	187
Table 6.26: H ₂ /Ar selectivity for the Alumina membrane AM1 after third dip	187
Table 6.27: H ₂ /CO ₂ selectivity for the Alumina membrane AM1 after fourth dip	189

NOMENCLATURE

A	Membrane Area	m^2
C	Molar Concentration	mol/ml
C _{permeate}	Concentration of permeate	(mol/m ²)
D	Diffusion Coefficient	(m ² /s)
E _a	Activation Energy	(kJ/mol)
ΔH	Heat of reaction	(K.cal/mol)
I.D	Internal Diameter	(mm)
J	Gas Permeance	(mol m ⁻² s ⁻¹ Pa ⁻¹)
J _{kn}	Knudsen diffusion	
J _v	Viscous flow	
K _o	Knudsen Coefficient	(mol.m/m ² .s.Pa)
L	Thickness	μm
M	Molecular Weight	
O.D	Outer Diameter	(mm)
P	Partial Pressure	(bar)
Q ₀	Pre-exponential factor	(mol.m./m ² .s,Pa)
R	Gas constant	(8.314)
T	Temperature	(K)
V	Volume	(ml.cm ³)
r	Pore radius	(nm)

V	Volume	(ml.cm ³)
V ₀	Viscous flow coefficient	(Kg/m.s)

Special Symbols

$\alpha_{A/B}$	Selectivity of specie A respective B
λ	Mean free path
τ	Turtuosity
ε	Porosity
π	Pi

ABBREVIATIONS

Ag	Silver
CH ₄	Methane
CO	Carbon Monoxide
CO ₂	Carbon Dioxide
C ₃ H ₈	Propane
CUSO ₄	Copper Sulphate
CVD	Chemical Vapor Deposition
DOE	Department of Energy
EDXA	Energy Dispersive X-Ray Analysis
ELP	Electroless Plating
Fe	Iron
H ₂	Hydrogen

CHAPTER 1

CHAPTER 1

1.0 Introduction and Motivation

The current high energy demand and challenges caused by rapid depletion of fossil fuels have motivated research into alternative and renewable sources of energy such as hydrogen. Currently, the major sources of energy are the fossil fuels including crude oil, coal and natural gas [1]. However, these fossil fuels are environmentally unfriendly because they cause pollution and are also exhaustible. The use of fossil fuels as the major source of energy has led to 2 critical challenges facing the global energy system: environmental pollution and energy insecurity [2].

1.1 Environmental Pollution

Presently, fossil fuels contribute about 86% of the world's energy supply and 90% of greenhouse emissions. They have been identified as the major sources of environmental pollution through anthropogenic emission of carbon dioxide which is the major source of global warming and climate change. There is now global focus on climate change and after several attempts at international climate change conferences, nations are yet to agree terms with a commitment on emission targets for each country based on their individual contributions to carbon emission [3]. There is currently a strict global emission regime aimed at cutting down carbon emission based on the Kyoto protocol [3].

The Kyoto protocol is an international agreement on climate change set by the United Nations Organization (UNO) which was adopted in Kyoto, Japan in December 1997 and has been referred to as one of the most contentious policy issues on environmental protection [3]. The protocol sets target on reducing the global greenhouse gas (GHG) emissions [4]. The implementation of the global emission targets is now one of the most critical issues in international political arena as countries and continents try to cut the best deal.

1.2 Energy Insecurity

Oil and gas resources are depleting rapidly and are envisaged to run out in a few decades which mean the world is faced with a scary but realistic future without oil [5]. A world without oil and gas will create an energy vacuum if other energy sources are not economically available before oil runs out.

Already some wells are drying out in Saudi Arabia, the country with the largest oil reserves and even where new oil wells are discovered, it is becoming increasingly difficult to hit oil because oil production is getting economically unviable [6]. Oil companies are finding it increasingly difficult to achieve economies of scale thereby leading to downsizing and mergers and in some cases, outright closures. Oil is said to deplete finally in 30-40 years from now and this calls for renewed commitment to identifying alternative and renewable sources of energy including hydrogen [6].

The challenges associated with oil are more compounded with fluctuating oil prices which always cast a shadow of uncertainty over the global economy thereby limiting free trade amongst nations. Oil is also said to be the major cause of the current global armed conflicts, insurgencies and mistrust amongst nations [7]. The focus now is on energy sources that are environmentally friendly and inexhaustible so as to combat climate change and ensure energy security.

1.3 Membrane Technology

Membrane separation is one of the enabling technologies in hydrogen production. Among the various membranes, Palladium membranes have received an ever – increasing attention in the separation of hydrogen mainly due to their ability to exclusively separate hydrogen from other gases and as a result of its high mobility in palladium lattice' and application over a wide range of temperatures [8].

Palladium membranes are the preferred choice in hydrogen separation and purification due to their infinite selectivity to hydrogen when defect free [9].

Challenges in Palladium membranes for hydrogen processes have encouraged research into other alternatives to palladium membranes such as silica and alumina for hydrogen separation and purification [10]. The adoption of hydrogen as the global energy carrier is faced with challenges including hydrogen storage, scaling up to full commercial levels and the need for public awareness and sensitization about the hydrogen energy system.

The use of inorganic membranes for hydrogen processes is also facing challenges such as cost, how to achieve uniform densification, examination and treatment of defects during the deposition of the metallic layer and poisoning by impurities such as carbonaceous compounds which impeded hydrogen permeation [11]. Electroless plating method for deposition of palladium layer over porous supports also has several challenges such as the threat of impurities during surface modification for Al₂O₃ supports, the long duration which makes it prone to errors and contamination. The need arises to fabricate thin defect free composite palladium membranes with high hydrogen flux and selectivity for hydrogen separation and purification especially for use in fuel cell processes and petroleum refining applications [12]. All these challenges to the hydrogen energy system have made it imperative that sustained research is encouraged in palladium and other inorganic membranes for hydrogen production, separation and purification.

1.4 Motivation

The demand for ultra-pure hydrogen is rising particularly as a result of recent developments in polymer electrolyte membrane fuel cells (PEMFC) [13]. PEMFC's are environmentally and economically viable due to their higher power density, low operating temperatures, cleaner exhausts and compactness compared to the conventional gas turbines and internal combustion engines. Hydrogen is also an important industrial feedstock for the production of fuels and several chemicals. The hydrogen energy system therefore holds a lot of potentials in the current global efforts to ensure energy security and combat global warming due to the use of fossil fuels [5].

Thin defect free palladium membranes are required not only to produce high purity hydrogen but also to meet the practical requirements of mechanical and chemical stability for hydrogen separation and purification at elevated temperatures [8]. The challenge arises on how to prepare thin defect free palladium membranes with enhanced hydrogen permeance and permselectivity. This is because these membranes are often prone to develop pin holes and defects which compromise hydrogen purity [9].

Palladium membranes pose several challenges such high cost and susceptibility to poisoning in the presence of hydrocarbons and sulfur. Palladium membrane also suffer from embrittlement in the presence of hydrogen at temperature below 573 K which causes cracks and breaks in the active palladium layer thus resulting in loss of purity [13]. Further research is pertinent on how hydrogen embrittlement can be suppressed and simultaneously enhance hydrogen permeance and selectivity.

Hydrogen permeation through palladium membranes is normally governed by Sievert's law where the exponential factor $n=0.5$ [14]. The rate limiting step in this case is diffusion of atomic hydrogen through the bulk metal. If the value of n changes from 0.5, then the rate limiting step is no longer bulk diffusion and the deviation from sievert's law could be due to several factors including temperature, pressure, grain size and contaminants such as C, CO, CO₂, CH₄ which reduces the surface reaction rate [15] . There is paucity of knowledge on these factors and more work is required especially on the effect of contaminants and grain size on hydrogen permeation through palladium membranes.

As a result of some of the advantages associated with palladium membranes, research into nonpalladium membranes such as silica for hydrogen processes is highly desirable. Silica membranes overcome some of the disadvantages of palladium membranes as they are more stable at high temperature, robust and also less expensive which provides options for commercialization [10]. Silica membranes have the advantage of operating at higher temperatures and harsher conditions compared to palladium [10]. Also, silica membranes are tolerant of sulfur impurities and this is critical because most reactant streams in hydrogen processes contain sulfur including natural gas-derived streams [10].

The preparation of Silica membranes with good hydrogen permeance and selectivity is one of the options being proposed to compliment the use of palladium membranes for hydrogen separation and purification. It is pertinent to promote research into silica membranes especially in the use of graded intermediate layers such as AlOOH to create more stable γ -alumina layers in case of alumina supports [10]. It is also imperative that investigations into hydrogen permeation and transport properties of silica membranes at elevated temperature are encouraged so as to provide a better understanding of the gas transport mechanisms involved. Research into alumina membranes is also highly encouraged as a result of the need for understanding of hydrogen permeation behavior and selectivity through alumina membranes.

1.5 The Hydrogen Energy System

The hydrogen energy system is also known as the hydrogen economy and it seeks to promote and sustain the importance of hydrogen as a source of energy [16]. The concept of hydrogen economy is often explained in two parts: On one hand it covers the production of hydrogen and its use in chemical and petrochemical industries, in mineral oil processing and in the upgrading of coal. On the other hand, the hydrogen economy envisages the use of hydrogen as the main energy carrier in a global energy system (17) Hydrogen fuel has been identified as the most ideal energy carrier to replace fossil fuels and avoid an impending energy vacuum when oil and gas resources finally deplete [18].

Hydrogen can form the foundation of a sustainable modern energy system and its most significant effect on civilization will be in transportation. It is projected that in the next 5-10 years, hydrogen would be the fuel for cars, buses, trains and aircrafts. Already there are hydrogen powered cars and buses on the road in several countries (17).

Moreover, within the next 5-10 years, there will be a surge of industries for hydrogen production, storage, transportation and utilisation. It is also envisaged that in the next 10 years, many gasoline stations will be converted to hydrogen [18]. High purity hydrogen is relevant as an energy carrier especially with the

recent development of hydrogen fuel cell vehicles (HFCV) which are planned for full commercialization in 2015.

1.5.1 Hydrogen Fuel

Hydrogen is the most abundant element on the planet. It is a light, odourless, colourless and tasteless gas and found in the air at about 100 ppm (0.01%). It is also called the 'clean fuel' due to the fact that only water is produced during its combustion. Hydrogen is an energy carrier mainly due to its reaction with oxygen to produce energy and water.

The energy from hydrogen is based on equation 1 as follows [2]:



The energy yield of hydrogen is 2.75 times greater than the yield of hydrocarbons and when used in fuel cell vehicles, hydrogen emits only water vapour while fossil emits the environmental pollutant CO₂. Apart from its use in fuel cells, hydrogen is also used in petroleum refining, production of ammonia (49%), hydrotreating and hydrocracking during petroleum refining (37%), methanol production (8%) and other miscellaneous uses (6%) [2].

Hydrogen is considered as one of the most efficient fuels because the combustion of 1kg of hydrogen can lead to the release of up to 120 MJ/kg including about 20 MJ/kg in the residual water vapour. In contrast, the equivalent of energy from oil and gas would require 2.5 – 2.75 kg of fuel [2]. This shows that hydrogen has about 150% efficiency factor over oil and natural gas in terms of heat of combustion. Despite its high heat of combustion, hydrogen has a very low volumetric energy density. For example, methane is 8 times heavier than hydrogen gas which puts hydrogen at a disadvantage when in mixture with gases [19]. This makes separation and purification of hydrogen from gas mixtures more critical to the development of a hydrogen economy. The use of separation

membranes will enable the optimum recovery of pure hydrogen from mixed gas streams.

1.6 Scope of This Work

The major aspect of this work involves substantial experimental work on the preparation of composite inorganic membranes namely, palladium, palladium-silver, silica and alumina membranes. Electroless plating method was used to deposit thin metallic palladium layers over porous alumina supports while the dip coating/sol gel method was used to prepare composite silica membranes over porous alumina supports and also to deposit γ -alumina layers over porous α -alumina support.

The aim of the project is to prepare composite membranes with high hydrogen flux and selectivity for high purity hydrogen from mixed gas streams. The future scaling up of the process is also taking into consideration in selecting the appropriate material for membrane fabrication in terms of cost, commercialization and stability in harsh operating conditions [10].

Based on the above aim of the project, its key objectives are as follows:

1. To prepare thin defect free composite palladium membranes with enhanced hydrogen flux and selectivity with a view to achieving high hydrogen purity for fuel cells and related applications.
2. To investigate the method of electroless plating with a view to optimizing the method to reduce the processing time involved and also the threat of impurities while maintaining membrane quality with high hydrogen flux and selectivity.
3. To investigate the effect of any possible defects, pinholes, contaminants, grain size, temperature or pressure on the rate limiting step and the pressure exponential n on hydrogen permeation properties in palladium and palladium-silver membranes.
4. To investigate hydrogen permeation through silica and alumina membranes with a view to understanding their suitability in hydrogen processes.

5. To identify the effect of introducing an intermediate γ -alumina layer on the porous α -alumina support prior to deposition of the silica layer for hydrogen permeation and selectivity.
6. To investigate the hydrogen permeation behavior of an unmodified commercial alumina membrane and compare same with that of another alumina membrane modified with a AlOOH sol. The significance of modifying the membrane is to deposit the more stable γ -alumina layer for enhanced hydrogen permeation.
7. To investigate the gas transport mechanism in both the commercial and modified alumina membranes for a better understanding of hydrogen permeation behavior through alumina support/membranes.

1.7 Membrane Requirement

The United States Department of Energy (DOE) has established 4 important characteristics for membranes in hydrogen separation. These are as follows [20]:

- 1- An operating temperature of 250 – 500⁰ C
- 2- A flux of 150 cm³ cm⁻² min⁻¹
- 3- A cost of \$1000 per m⁻²
- 4- A durability of 5 years

Porous silica and alumina ceramic membranes are recognised for their chemical stability in harsh operating conditions. These porous membranes usually exhibit high hydrogen permeability and low selectivity. However, Palladium membranes provide excellent hydrogen selectivity but they present high cost, are thermally and chemically unstable and suffer from embrittlement when in contact with hydrogen at low temperatures [20]. The strong interaction with hydrogen at low temperatures results in the cracking and peeling off of the active palladium layer.

In particular, the high cost and limited availability of palladium has encouraged research into alternative membrane materials such as silica and alumina to serve as options to palladium [20]. However, the cost implications can be ameliorated by combining thin palladium films with alumina and/or by employing less

expensive techniques for fabrication of the Pd film [8]. In terms of the techniques for fabrication of Pd films, a thickness of 50 μm can be achieved by cold rolling, less than 1 μm by electroless plating and about 1 μm by chemical vapour deposition [20].

1.8 Publications/Conferences Undertaking In This Work.

1.8.1 Journal Publications

1. Alkali, A. & Gobina, E. (2014). Hydrogen permeation behavior and annealing in Pd & Pd/Ag membranes at high temperature. International Journal of Advanced Research in Engineering and Technology (IJARET), 5(5), 205-212.
2. Alkali, A. & Gobina, E. (2014). Gas separation properties of a Hydrogen Permeable Macroporous Ceramic membrane at high temperature. International Journal of Advanced Research in Engineering and Technology (IJARET), 5(5), 40-50.

Paper in Preparation:

1. Alkali, A. & Gobina, E. Electroless plating of palladium and palladium alloy membranes for hydrogen separation and purification: A review.

1.8.2 International Conferences

Oral Presentation:

1. Alkali, A. & Gobina, E. (2014). Hydrogen permeation behavior and n-value in composite palladium membranes. American Society of Mechanical Engineers (ASME) 12th Fuel Cell Engineering and Technology Conference in Boston, Massachusetts U.S.A. 30th June – 2nd July 2014.
2. Alkali, A. & Gobina, E. (2014). Hydrogen permeation behavior in Palladium and Palladium alloy composite membranes. Materials challenges in Alternative & Renewable Energy (MCARE) conference held in Tampa, Florida U.S.A. 17th – 20th Feb. 2014.

3. Alkali, A. & Gobina, E. (2014). Hydrogen separation & Purification using composite Inorganic membranes. Fuel Cell Seminar & Exposition held in Mohegan Sun, Connecticut, U.S.A. 3rd – 5th November 2012.
4. Alkali, A. & Gobina, E. (2014). An investigation into the hydrogen separation, purification and transport behaviour of a ceramic alumina membrane and its comparison with a gamma alumina membrane modified with AlOOH sol. European Fuel Cell Conference held in Rome, Italy. 11th – 13th December, 2013.

Poster Presentation:

1. Alkali, A. & Gobina, E. (2011). Hydrogen separation & Purification Using Composite Inorganic Membranes. International Hydrogen Research Showcase. University of Birmingham, 13th – 15th April 2011.
2. Alkali, A. & Gobina, E. (2011). Hydrogen preparation in palladium and palladium alloy membranes at high temperature. International Conference on Inorganic Membranes. University of Twente, Enschede, Netherlands. 9th – 13th July 2012

Field Trip:

December 2014: Attended a field trip at the University of Birmingham Centre for Hydrogen and Fuel Cell Research (School of Chemical Engineering) under Professor Robert Steinberger-Wilkens. I was also at the University's school of Metallurgy and Materials working on Membrane Separation.

1.9 Thesis Outline

This thesis is structured into 7 chapters. A summary of the contents of each chapter is as follows:

Chapter 1. This chapter presents a concise introduction to the research including the motivation for the research. The scope, aims and objectives of the research

are also presented. The relevance of the hydrogen energy system and membrane technology to the global search for a sustainable energy system is also discussed. The membrane requirement is also presented including hydrogen transport through inorganic membranes.

Chapter 2: This chapter presents a review of relevant literature for inorganic membranes for hydrogen separation & purification including the different gas transport mechanisms. The different methods of preparation of composite palladium membranes including electroless plating are also presented.

Chapter 3: This chapter concentrates on palladium membranes and it presents the experimental methodology for palladium and palladium-silver membranes including the electroless plating method and materials used in preparation of the composite palladium membranes over porous alumina support. Three composite palladium membranes were prepared and tested namely Pd1 (which is a Pd membrane prepared using the conventional electroless plating), Pd2 (a Pd membrane prepared using the modified electroless method) and Pd3 (which is a Pd/Ag membrane also prepared using the conventional electroless plating method).

Chapter 4: This chapter concentrates on silica membranes and it presents a background of the current work done in silica membranes for hydrogen processes. It also presents the methodology for the dip coating used in the fabrication of silica membranes for gas permeation tests. Two composite membranes SL1 and SL2 were prepared using the dip coating method and the results of their hydrogen permeance and selectivity investigated at different coatings for single hydrogen streams.

Chapter 5: This chapter concentrates on alumina membranes and also presents an analysis of current work for these membranes in hydrogen processes. The dip coating methodology used in modifying the ceramic alumina membranes for hydrogen processes is also presented. Two membranes AM1 and AM2 were prepared and investigated for hydrogen permeance and selectivity and also the permeance of 5 other single gases at high temperature. AM1 is a commercial α -alumina membrane without any modification while AM2 is a γ -alumina

membrane prepared using the dip coating method by modification of the support with AlOOH sol. Both membranes were investigated for hydrogen permeation and selectivity at five different coatings.

Chapter 6: This chapter presents the results and discussions for the palladium and nonpalladium membranes. The palladium membranes are the Pd1, Pd2 and the Pd3 (palladium-alloy, Pd/Ag) membrane while the nonpalladium membranes are silica (SL1 and SL2 membranes) and ceramic alumina (AM1 and AM2 membranes).

Chapter 7. This chapter presents the conclusions and recommendations that were drawn from the investigations carried out on all the membranes prepared in this work. Options for future work are also presented.

Appendices: Some print outs of experimental results from the Gas Chromatograph analytical equipment and SEM and EDXA are presented. The method for calculation of hydrogen flux, gas permeance and selectivity and determination of membrane thickness are also presented.

1.10 References

1. Dincer, I. & Zamfirescu, Z. (2014). Fossil fuels and Alternatives. *Advanced Power Generation Systems*. 3: 95 – 141.
2. Balat, M. (2008). Potential importance of hydrogen as a future solution to environmental and transportation problems. *International journal of hydrogen energy*. 33: 4013-4029.
3. Feroz, E. H., Raab, R.L., Ulleberg, G, T. & Alsharif, K. (2009). Global warming and environmental production efficiency ranking of the Kyoto protocol nations. *Journal of environmental management*, 90: 1178-1183.
4. Nabuurs, G.J., Dolman, A.J., Verkaik, Kuikman, P.J., Van Diepen, C.A., Whitmore, A.P., Daamen, W.P., Oenema, O & Kabat, P. (2000). Article 3.3 and 3.4 of the Kyoto Protocol: Consequences for industrialised countries' commitment, the monitoring needs and possible side effects. *Environmental Science & Policy*, 3 (2-3): 123-134

5. Dunn, S. (2002). Hydrogen futures: toward a sustainable energy system. *International journal of hydrogen energy*, 27: 235-264.
6. Bockris, O'M, J. & Veziroglu, N.T. (2007). Estimates of the price of hydrogen as a medium for wind and solar sources. *International journal of hydrogen energy*, 32: 1605-1610
7. Colgan, D.J. (2014). Oil, Domestic politics and international conflicts. *Energy research & social science*, 1: 198-205.
8. Yun, S. & Oyama, T.S. (2011). Correlations in palladium membranes for hydrogen separation: A review. *Journal of membrane science*, 375 (1-2): 28-45.
9. Morreale, B. D., Ciocco, V. M., Enick, R. M., Morsi, B. I., Howard, B. H., Cugini, V. A. & Rothenberger, S. K. (2003). The permeability of hydrogen in bulk palladium at elevated temperatures and pressures. *Journal of Membrane Science*, 212 (2003) 87-97.
10. Khatib, J. S. & Oyama, S. T. (2013) Silica membranes for hydrogen separation prepared by chemical vapour deposition (CVD). *Separation and Purification Technology*, 111: 20 – 42.
11. Ahmad, L. A. & Mustafa, N. N. N. (2006). Sol – gel synthesised of nanocomposite palladium – alumina ceramic membrane for H₂ permeability: Preparation and characterization. *International journal of hydrogen energy*, 32: 2010-2021
12. Schlesinger, M. & Paunovic, M. (2010). *Modern electroless plating*. Chapter 18, Wiley & sons, Inc. 447-458.
13. Hatlevik, O., Gade, K.S., Keeling, K.M., Thoen, M.P., Davidson, A.P. & Way, J.D. (2010). Palladium and palladium alloy membranes for hydrogen separation and production: History, fabrication strategies, and current performance. *Separation and Purification Technology*, 73: 59-64.
14. Guazzone, F., Engwall, E. E. & Ma, H, Y. (2006). Effects of surface activity, defects and mass transfer on hydrogen permeance and *n*-value in composite palladium-porous stainless steel membranes. *Catalysis Today*, 118: 24-31.
15. Hengyong. L.H. & Li, W. (2008). Study of *n* value and α/β palladium hydride phase transition within the ultra thin palladium composite membrane. *Journal of membrane science*, 324: 44-49.

16. Muradov, N.Z. & Veziroglu, N.T. (2008). 'Green' Path from fossil – based to hydrogen economy: An overview of carbon neutral technologies. *International journal of hydrogen energy*, 33 (23): 6804-6839.
17. Fischer, M., Kreysa, G. & Sandstede, G. (1987). The hydrogen economy: a challenge for chemical engineering. *International journal of hydrogen energy*, 12: 39-46.
18. Nowotny, J., Sorrell, C.C., Sheppard, L.R. & Bak, T. (2005). Solar hydrogen: Environmentally safe fuel for the future. *International Journal of hydrogen energy*, 30: 521-544.
19. Levin, B.L. & Chahine, R. (2009). Challenges for renewable hydrogen production from biomass. *International journal of hydrogen energy*, 3: 1-8.
20. Santucci, A., Enea, T.S. & Basile, A. (2013). Alternatives to palladium in membranes for hydrogen separation: nickel, niobium and vanadium alloys, ceramic supports for metal alloys and porous glass membranes. Woodhead publishing company, chapter 4.

CHAPTER 2

CHAPTER 2

2.0 Literature Review

2.1 Hydrogen Production

Hydrogen can be produced in several ways such as through electrolysis of water, steam methane reforming, gasification of coal and partial oxidation of natural gas [1]. The raw gas contains a number of gaseous impurities which must be removed to make the hydrogen in its pure form. The methods for hydrogen separation are: pressure swing adsorption (PSA), cryogenic distillation, solvent adsorption and membrane separation. Membrane separation has been identified as one of the most promising technology due to a number of attributes such as its low cost, low energy consumption and simple equipment [1].

Steam reforming of methane is the most widely used method for hydrogen production. However, despite its significance in hydrogen production processes, the steam methane reforming poses several challenges prominent amongst which is the restriction caused by the thermodynamic equilibrium [2]. Steam reforming also produces carbon dioxide which is an environmental pollutant. The steam methane reforming process is performed in fixed bed reactors. Due to the endothermic reaction high temperatures ($>800^{\circ}\text{C}$) are required which results in enormous drastic operating conditions [2]. Membrane reactors provide promising options in overcoming these challenges including high temperature and high pressure.

Membrane reactors could perform both the reaction and the separation process simultaneously (Process intensification) and can also shift the thermodynamic equilibrium in the water – gas shift reaction to convert carbon monoxide to hydrogen [3].

High temperatures are required for the endothermic reaction as shown in equations 2 and 3 [3]:



The water-gas shift reaction involves the exothermic reaction of carbon monoxide with steam [3]:



The selective removal of hydrogen from the reaction stream using membranes will result in a shift of the thermodynamic equilibrium to the products side. This shift will lead to high feed conversion and high purity hydrogen recovery at low temperatures [4]. Metals of groups 8-10 of the periodic table are normally used as catalysts in steam methane reforming [2].

2.2 Inorganic Membranes for Hydrogen Separation & Purification

Membranes are physical barriers that allow a selective transport of mass specie and are selected depending on the application [3]. Membranes are classified as either organic, inorganic or hybrids of organic/inorganic. Inorganic membranes can further be classified into metallic and ceramic membranes. The metallic membranes are usually in the dense phase while the ceramics can be either porous or nonporous. The organic membranes can be further classified as either polymeric or biological [4]. A membrane has the unique ability to selectively allow a component to pass through it while rejecting other components.

They serve as filters to separate one gas from the feed mixture in form of permeate; the rejected components are passed as retentate [5]. In selecting a membrane, there is the need to consider some key factors such as the membrane permeability, selectivity, durability, mechanical integrity, resistance to poisoning etc.

These factors must be balanced with the cost implications for optimum value and efficiency of the membrane [1]. Membranes could be used either as self –

supporting OR as composites (supported). As self supporting, the membranes exist in stand – alone form as tubes or films without any substrate to give added mechanical and thermal strength to the metal layer [1].

The major requirement with the unsupported membranes is that they should be thick enough so that they can have the necessary thermal and mechanical strength to withstand harsh conditions e.g. high temperature incorporation of seals. However, this thickness makes them expensive and also, they yield low hydrogen flux since flux is inversely proportional to thickness [1]. As a result of the challenges posed by the self supporting membranes in form of thin films such as their inability to withstand high temperature, much attention is now directed in the use of composite membranes in which a thin layer is deposited on a porous support e.g. a thin Palladium film deposited on α – Al_2O_3 support. The support provides the necessary mechanical and thermal strength for the membrane to withstand harsh conditions while the thin film enhances the flux [1].

The supports can be either ceramic, glass, stainless steel and other porous materials and can enable the preparation of highly effective ultra thin Pd and Pd-alloy membranes with significant thermal stability and mechanical strength [1]. Ceramic supports such as alumina are widely used due to their stability, resistance to corrosion and ability to withstand high temperatures [1]. The stainless steel supports also present a good choice because they have a similar thermal expansion coefficient to Palladium films compared to glass supports that are prone to cracks [6]. Unsupported thick membranes cause several challenges including low permeance, low chemical stability and high cost. However, supported/composite type membranes of thin films on a porous support yield high hydrogen flux and excellent separation properties because the flux depends on the thickness and the membrane materials [1].

According to the International Union of Pure and Applied Chemistry (IUPAC), porous membranes can be classified based on their pore sizes as follows [7]:

- Macroporous >50 nm,
- Mesoporous 2 nm < pore size < 50 nm
- Microporous < 2 nm

Despite their potentials to make a significant impact in addressing the current energy crisis, inorganic membranes have certain challenges that need to be addressed for effective gas separation and purification. Some of these challenges are as follows [4]:

- Thickness: A membrane should be thin for effective target separation.
- High Surface activity.
- Defect – free surface for deposition.
- Stability and strength to sustain harsh operating conditions.

The most important properties that make a membrane effective in separation and purification processes are permeability and selectivity [3]. Permeability is defined as 'the flux of mass through a membrane per unit of area and time at a given gradient and is a product of diffusivity and solubility [1]. Diffusivity and solubility allow the permeate to pass through the membrane and hydrogen has an extremely high diffusivity in palladium which gives it a very high selectivity [1]. Permeance is the total flux in terms of the membrane's ability to drive the gas through it and it describes the relationship between permeability and thickness of the membrane denoted in molar units as ($\text{mol m}^{-2} \text{s}^{-1} \text{Pa}^{-1}$) [4]. Higher flux denotes that a smaller membrane area is required and therefore, a lower cost of the process.

In palladium membranes, pinholes and cracks could develop in the film from preparation stages and membrane exposure to unfavourable conditions and these defects can result in the membrane having a finite selectivity [1]. A high selectivity denotes a high hydrogen throughput at ultra pure levels and

translates to lower cost of the process since low pressure ratio i.e. the driving force, is required for the separation [3].

2.3 Membrane Reactors for Hydrogen Production

A membrane reactor is a multifunctional device which provides process intensification in reactions by combining a separation process with a chemical reaction in one unit [8]. As a result of this process intensification capability of these reactors, they have been widely applied for a range of chemical reactions such as dehydrogenation reactions (equilibrium limited), selective oxidations and in reaction coupling processes to produce thermodynamically beneficent products [8]. The use of membrane reactors for hydrogenation and dehydrogenation reactions essentially involves a catalyst and a membrane with the former providing conversion and the latter controlling transfer to and from the catalyst [8].

In membrane reactors based on supported palladium membranes, the membrane can be used as a permselective material for separation and also as a base-component catalyst for dehydrogenation reaction. However in such cases, the reaction would be very slow due to the small surface area and the membrane doesn't act as the primary catalyst [8]. A classification of membrane reactors based on permselectivity is shown in figure 2.1. Two main challenges are encountered in the direct dehydrogenation of alkanes to alkenes by fluid catalytic cracking or as by-product in pyrolysis/cracking furnaces.

These challenges are [9]:

1. The endothermic nature of the direct dehydrogenation reaction as shown in equation 4.



$$\Delta H^0_{733 \text{ K}} = 130 \text{ kJ/mol}$$

2. Slow activity of the commercial catalysts leading to coke formation. Platinum Alumina ($\text{Pt}/\text{Al}_2\text{O}_3$) and chromia/alumina ($\text{Cr}_2\text{O}_3/\text{Al}_2\text{O}_3$) are the types of catalysts used in the direct dehydrogenation.

The above problems have made it necessary to consider the catalytic membrane reactor concept in the dehydrogenation of alkanes to alkenes which is now a more widely used concept compared to direct dehydrogenation [8]. The process intensification resulting from the ability of the membrane reactor to combine separation and reaction provides advantages such as an energy efficiency and an increase in conversion at a lower temperature [10].

In the catalytic dehydrogenation of n-butane in a membrane reactor at high temp, E. Gobina and R. Hughes [10] prepared a composite Pd/Ag alloy membrane for the catalytic dehydrogenation of n-butane in a membrane reactor. In Gobina's work, increases in the n-butane conversion up to 6 fold above the equilibrium value were achieved at 397°C using oxygen as the sweep gas [10].

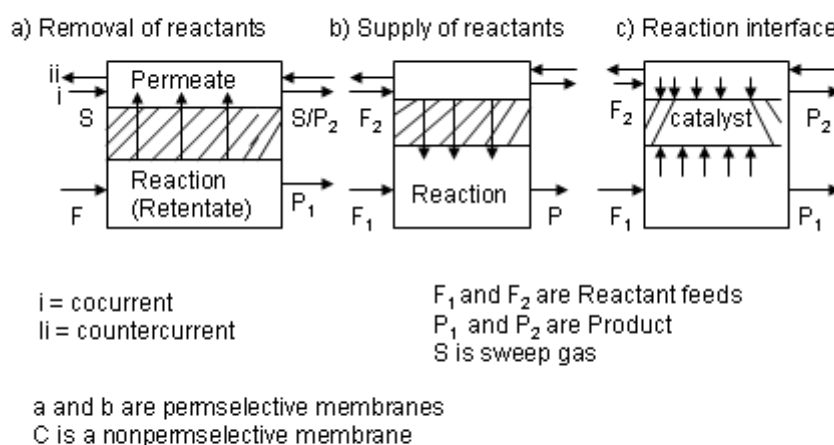


Figure 2. 1. Classification of Membrane Reactors Based on Permselectivity

There are 3 possibilities that are involved in membrane reactor processes as shown in figure 2.1. These are follows [8]:

1. Selective removal of one of the products from the reaction zone (Extractor): This is also referred to as 'cheating the equilibrium and applies to equilibrium limited reaction where the reactant conversion increased beyond the equilibrium value.

The process involves removing the product as it is being formed to improve conversion and is the most widely used concept in membrane reactors.

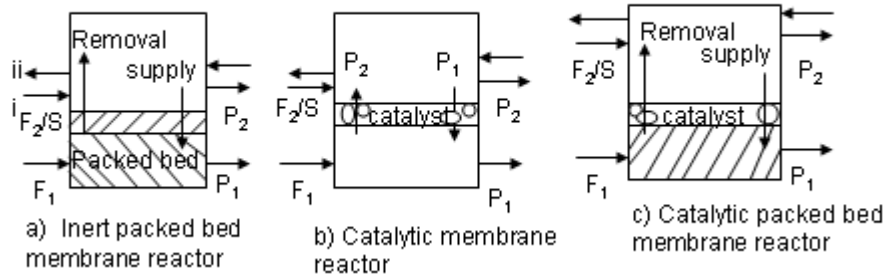
2. Supply of reactants to the reaction zone (Distributor) via a membrane so as to establish a concentration profile along the reactor.

3. The establishment of a well defined reaction interface between 2 reactant streams.

In catalytic membrane reactors, palladium membranes can be used in catalytic membrane reactors for 2 reasons as shown in figure 2.2 [8]. These are as follows:

- 1) In a dehydrogenation reaction using a packed bed catalyst by removal of the hydrogen as a product in equilibrium limited reaction: In this case, the establishment of the chemical equilibrium is restricted but reactant conversion is enhanced with the removal of the produced hydrogen. Membrane has no primary catalytic function.

- 2) In a hydrogenation reaction by supplying hydrogen to the reaction: In this case where the membrane has a primary catalytic function, diluted hydrogen can be used to perform the hydrogenation reaction or hydrogen can be passed through the membrane to support the hydrogenation reaction.



i = cocurrent
 ii = countercurrent

F_1 and F_2 are Reactant feeds
 P_1 and P_2 are Product
 S is sweep gas

a and b are permselective membranes
 C is a nonpermselective membrane

Figure 2.2: Membrane reactors based on catalytic activity

The use of a sweep gas is highly recommended in order to balance the reaction and permeation rates and also enhance the driving force for optimum results [11].

2.4 Gas Transport Mechanisms

There are 5 molecular transport mechanisms through membranes as follows: viscous flow, solution diffusion, Knudsen flow, molecular sieving and surface diffusion. These are shown in figure 2.3:

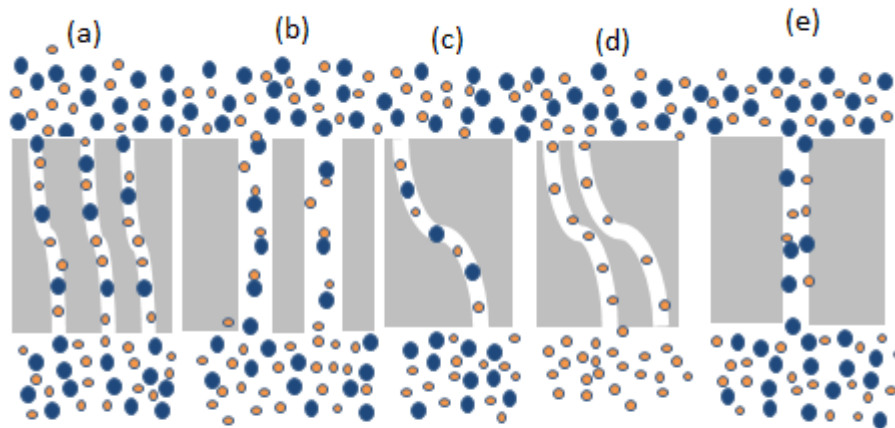


Figure 2.3: Gas Transport Mechanism in Inorganic Membranes: a) Surface Diffusion (b) Viscous Flow (c) Solution - Diffusion (d) Molecular Sieve (e) Knudsen Diffusion

2.4.1 Viscous Flow

This mechanism is also known as poiseuille flow regime and it is usually dominant in macro porous membranes with large pore sizes over 50 μm . Due to the much larger pore diameter than the mean free path, the flow properties are dominated by collisions between the molecules [3].

2.4.2 Solution Diffusion

The solution diffusion model is based on the 3 key steps namely: sorption, diffusion and desorption of the gas through the membrane. The 3 steps explain the relationship of the membrane and the gas from the membrane surface to the permeation of the membrane as a result of an applied pressure gradient and the desorption of the gas at the low pressure side [3].

2.4.3 Knudsen Flow

In Knudsen flow the molecules will collide more with the pore walls than with other molecules. This flow regime applies to separation based on differences in molecular weight and it occurs when the distance between molecular collisions (the mean free path) is larger than the pore diameter [3]. Under circumstances of very low pressures and small pore sizes, the molecules will bounce from wall to wall as against colliding with one another. The concentration gradient is the driving force in this transport regime [3]. The pore diameter is larger than the mean free path in viscous flow while the reverse is the case in Knudsen [1].

2.4.4 Molecular Sieve

Molecular sieve involves very small pores where the sieves allow molecules of same or smaller sizes to the sieve diameter to pass through while molecules that are bigger than the sieve diameter are unable to pass through [12]. In ultramicropore applications, the pore sizes are usually similar to the molecular sieves such that the molecules come into contact with the potential field of the pore walls.

2.5 Gas permeation through porous membranes

In gas transport through membranes, there are 2 important processes namely sorption and diffusion. Sorption describes the interaction between the gas molecules and the surface of the membrane while diffusion describes the rate of gas mobility through the membrane. Sorption can occur physically or chemically depending on the driving force [13]. Chemisorption usually occurs in palladium membranes with strong interaction between the gas molecules and the membrane surface while physisorption occurs in porous ceramic and silica membranes during weak interaction of the gas molecules with the membrane surface. Silica membranes exhibit molecular sieving or activated diffusion transport mechanism. The permeation behavior of a gas through a membrane is usually presented as permeance or permeability [14].

To obtain the permeability of the membrane, the unit thickness of the membrane is used to normalize the permeance [213]. Permeance in $\text{mol m}^{-2} \text{s}^{-1} \text{Pa}^{-1}$ is defined as the quantity of gas crossing a unit area in unit time or flux per unit pressure difference between the high pressure and the low pressure sides of the membrane [13] [14] as shown in equation 5.

$$J = \left(\frac{Q/22.4}{A \times P} \right) \text{ (mol/m}^2\text{/s/Pa)} \dots \text{Eq. 5}$$

Where J is gas permeance, Q is permeate flow rate, A is membrane area for permeation and P is the pressure difference across the membrane

Selectivity denotes the relationship between gas permeance and the permeance of another gas [14]. If J_{H_2} is the permeance of hydrogen and J_{N_2} is the permeance of nitrogen through the alumina membrane, then the ideal selectivity of hydrogen relative to nitrogen can be represented as follows [14]:

$$\alpha_{H_2/N_2} = \frac{J_{H_2}}{J_{N_2}} \dots \text{Eq. 6}$$

Where J_{H_2} is the permeance of hydrogen and J_{N_2} is the permeance of nitrogen

Gas separation can occur in porous membranes when the mean free path is larger than the pore size of the membrane. This results in the gas molecules colliding more frequently with the pore wall. In this case, the Knudsen diffusion is the governing transport mechanism. In Knudsen diffusion, hydrogen shows an inverse square root dependence on both the temperature and molecular weight [13]. In porous media, gas phase flow is dependant on the ratio of number of molecule-molecule collisions to that of molecule-wall collisions [15]. The Knudsen number describes the applicable gas flow and is represented by the equation:

$$K_n = \frac{\lambda}{d_p} \dots\dots\dots \text{Eq. 7}$$

Where λ = Mean free path, d_p = Pore diameter

The properties of gas-phase flow through porous media depend on the molecular of collision during gas permeation. The mean free path λ is the distance travelled by a gas molecule during molecular collisions and is given by [15]:

$$\lambda = \frac{\kappa T}{\sqrt{2P\pi}d^2} \dots\dots\dots \text{Eq. 8}$$

Where T is the temperature, P is the pressure, d is the pore diameter

Viscous flow occurs when collisions between molecules is dominant as against collision between the molecules with the pore walls.

$$J_v = \frac{\epsilon r^2 P}{8\pi\eta RT} \frac{d_p}{d_x} \dots\dots\dots \text{Eq. 9}$$

Knudsen diffusion occurs when the mean free path is larger than the pore size in which case the Knudsen number $K_n \gg 1$ [15].

In Knudsen diffusion, light molecules pass through the membrane pores faster than heavy molecules under same concentration gradient. Impliedly, the Knudsen diffusion is dependent on the square root of the molecular weight of the diffusing gases.

The Knudsen diffusion J_{kn} is given as [15]:

$$J_{kn} = \frac{\varepsilon 8r}{3\tau\sqrt{2\pi RTM}} \frac{dP}{dx} \dots\dots\dots \text{Eq. 10}$$

Where ε is the porosity, τ is the tortuosity, r is the mean pore radius, R is gas constant, T is the temperature and M is molecular weight.

While viscous flow predominates when $K_n \ll 1$. When $K_n=1$ the mean free path and the pore size are similar, the flow mechanism is governed by a combination of viscous and Knudsen gas flow mechanisms and $J_{tot} = J_v + J_{kn}$.

The combined effect of viscous and Knudsen transport mechanisms govern the flow regime when the mean free path is comparable to the pore diameter. The total flux through the porous layers is represented by the equation [15]:

$$J_T = J_v + J_{kn} = \frac{\varepsilon}{\tau x} \left(\frac{r^2 P \Delta P}{8\eta RT} + \frac{8r \Delta P}{3\sqrt{2\pi RTM}} \right) \dots\dots\dots \text{Eq. 11}$$

Where J_v and J_{kn} denote the contributions of viscous and Knudsen transport respectively.

2.6 Methods for Fabrication of Membrane

There are several methods for preparation of composite inorganic membranes for hydrogen processes. Some of these methods are as follows:

2.6.1 Electroless Plating (ELP)

The Electroless plating method for the deposition of dense films over porous substrates has assumed increasing importance and wider applications in the fabrication of composite Pd and palladium alloy membranes for hydrogen production, separation and purification. It involves plating metallic films on a

substrate by reducing metal complex ions in solution using a reducing agent without applying an external electric source [16]. A schematic of the electroless plating process is shown in figure 2.4. Some of the several advantages the electroless plating method enjoys over other methods include its uniformity and easiness of coating over any surface of any shape, no energy supplies required, low cost, simple equipment and it also avoids accumulation of the deposits around the substrate edges to ensure in uniformity of coating [16]. However, it also has its drawbacks such as the time consuming procedure as a result of the several treatment steps involved [1]. The mechanism of electroless plating for the fabrication of palladium-based composite membranes has been well investigated and the experience is that the method has a near perfect throwing power due to its applicability in both conducting and nonconducting surfaces and is applicable as long as the plating solution has access to the substrate surface [16]. In the preparation of composite membranes using the electroless plating method, a porous support such as stainless steel, Vycor glass and ceramic alumina is required onto which a dense metallic film is deposited [16].

Steel is more commonly used in the process industry. One of the reason being that it has more toughness compared to ceramics. However, ceramics also enjoy some advantages such as better and less challenging management of cracks and pin holes. Surface defects and pin holes are more easily repaired for ceramics than for steel. Prior to the deposition of the metal on the support, the sensitization and activation steps are carried out on the porous substrate so as to create catalytic sites on the non-metallic surfaces and to also stimulate the adsorption of the metal ions, enhance strong adhesion of the Pd nuclei on the substrate and eliminate the induction period of the metal to ensure better uniformity of coating and improved membrane quality.

In the case of palladium deposition, it can coexist with Tin during the sensitization step and this could affect the activity of Palladium towards hydrazine reducer thus slowing the rate of reaction and leading to a decrease in the deposition rate of the Pd metal [17]. On the upside, it creates catalytic sites and also reduces the time it takes for the commencement of the deposition of palladium seeds onto the porous support which is also known as the induction

period. The pre-treatment steps to deposit Pd nuclei onto the substrate also reduce the induction period and improve the plating efficiency [18]

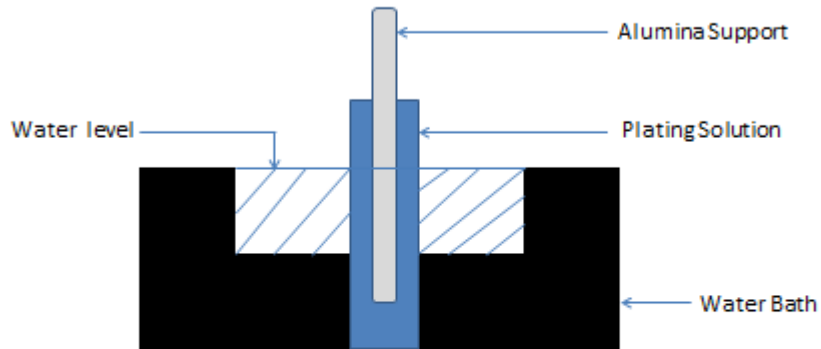


Fig. 2.4: A Schematic of Electroless Plating Set Up

2.6.2 Electrodeposition (EDP)

The Electrodeposition technique unlike the ELP, uses external electric power as shown in figure 2.5. In this method, metal ions found at the anode are moved towards the cathode in an electric field. Electrons are accepted by the ions and deposited as metal atoms on the cathode [19]. The electrodeposition bath is equipped with a vacuum system, a temperature controller and a power supply. It has a platinum mesh as the anode and a sample holder as the cathode electrode. Positive metallic ions formed at the anode are moved towards a cathodic membrane substrate using an applied electric field and are deposited on the cathode as atoms [20].

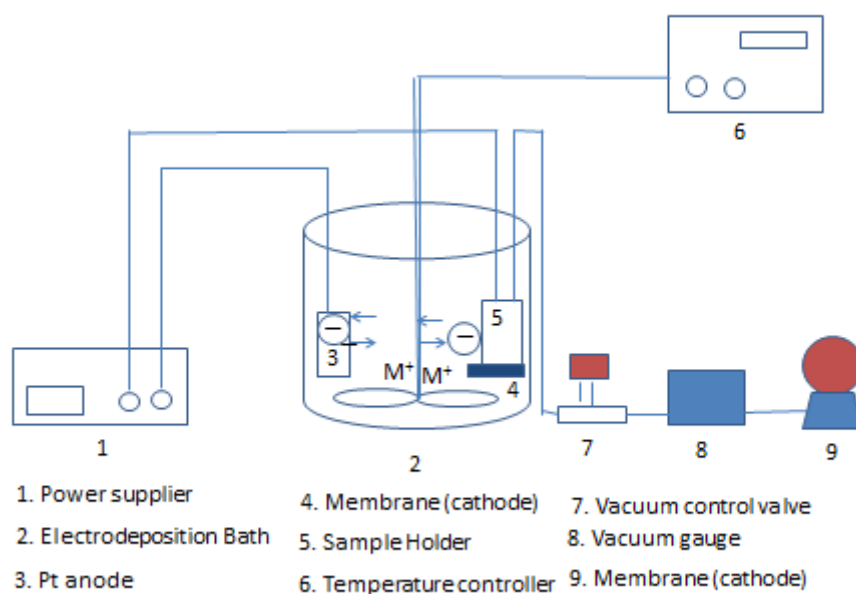


Figure 2.5: A Schematic Diagram of the Vacuum Electrodeposition Process

2.6.3 Chemical Vapour Deposition (CVD)

The CVD method is used to deposit thin films on a support through the thermal deposition of a volatile precursor on the surface of the substrate as shown in figure 2.6. The method can be used to obtain the desired thickness of the membrane; however, volatile palladium precursors and high purity constituents are required [21]. The CVD technique can be used to obtain very thin palladium or palladium alloy films. For example, Naotsugu itoh and co workers [21] used the forced flow chemical vapour deposition (CVD) technique to prepare a palladium membrane with a thickness of 4 μm given a hydrogen flux of 0.1 – 0.2 mol/m²/s and selectivity exceeding 5000 (H₂/N₂) at 300⁰ C [21].

The technique has its drawbacks some of which are that it is prone to contamination by the residual carbon. In a forced flow CVD, the vapour of volatile palladium precursor such as Palladium diacetate, (CH₃COO)₂ Pd, enters through a porous support and decomposes on the surface [21].

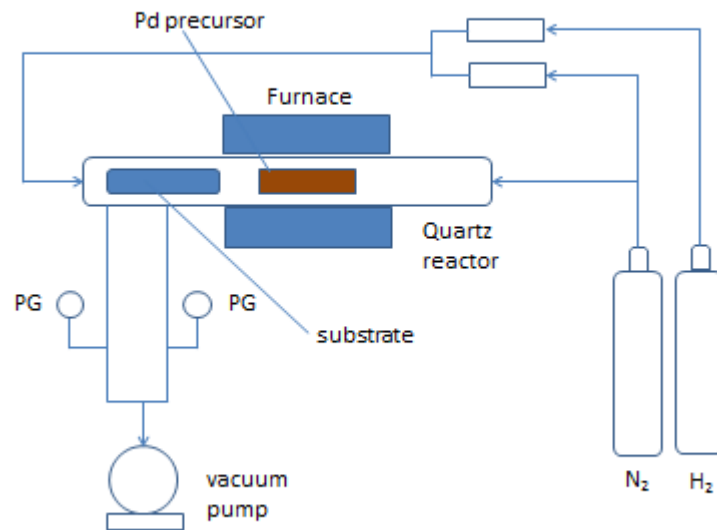


Figure 2.6: A Schematic of Forced Flow Chemical Vapour Deposition

2.6.4 Physical Vapour Deposition (PVD)

In the PVD method for fabrication of thin palladium membranes, high – energy sources such as a beam of electrons or ions are used to transfer materials at atomic level through bombardment of a palladium precursor. This technique involves coating through vaporization as in CVD but the major difference between the two is that the PVD does not involve chemical deposition at the surface [1]. In magnetron sputtering, the collisions of the Argon ions excited by the plasma leads to the atomisation of the precursor which is then deposited on the surface of the substrate [1]. The technique has its challenges such as being expensive in terms of equipment because there is a very high power density required for the evaporation of the solid precursor [1].

2.6.5 Photocatalytic Deposition (PCD)

The photocatalytic deposition method involves the use of a photocatalyst under UV irradiation to fabricate palladium and palladium -alloy membrane. A Schematic of the magnetron sputtering process is shown in figure 2.7.

In this method, metallic palladium or palladium-alloy ions are reduced when TiO_2 absorbs UV irradiation and the reduced metals are then deposited on the TiO_2 surface to form a layer [22].

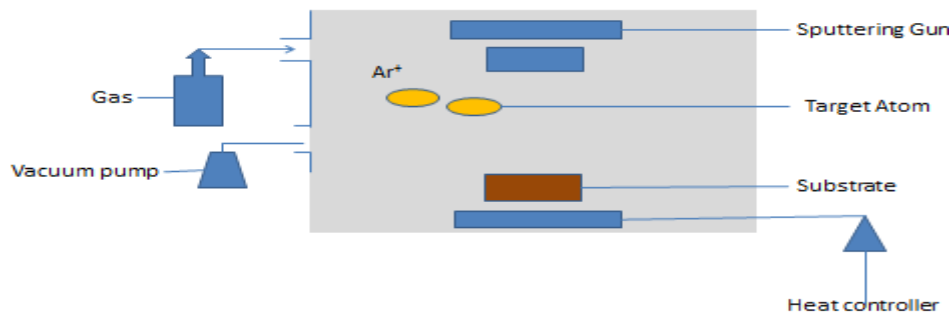


Figure 2.7: A Schematic of Magnetic Sputtering Method

2.7 References

1. Yun, S. & Oyama, T.S. (2011). Correlations in palladium membranes for hydrogen separation: A review. *Journal of membrane science*, 375 (1-2): 28-45.
2. Amin, N,A,S. & Yaw, T.C. (2009). Thermodynamic equilibrium analysis of combined carbon dioxide reforming with partial oxidation of methane to syngas. *International journal of hydrogen energy*, Volume 32, 12: 1789-1798.
3. Lu, G. Q., Diniz da Costa, J.C., Duke, M., Giessler, S., Socolow, R., Williams, R.H. & Kreutz, T. (2007). Inorganic membranes for hydrogen production and purification: A critical review and perspective. *Journal of colloid and interface science*, 314: 589-603.

4. Zhang, L., Park, I., Shqau, K., Winston, H. & Verweij, H. (2009). Supported Inorganic Membranes: Promises and Challenges. *Journal of minerals, metals and materials society*, 61 (4): 61-71.
5. Scholes, A. C., Kentish, E.S. & Stevens, W.G. (2008). Carbon Dioxide separation through polymeric membrane systems for flu gas applications. *Recent patents on chemical engineering*. 1: 52-66.
6. Cheng, Y. S., Pena, M.A., Fierro, J.L., Hui, D.C.W. & Yeung, K.L. (2002). Performance of alumina, zeolite, palladium, Pd-Ag alloy membranes for hydrogen separation from town gas mixture. *Journal of membrane science*, 204: 329-340.
7. Ahmad, L. A. & Mustafa, N. N. N. (2006). Sol – gel synthesised of nanocomposite palladium – alumina ceramic membrane for H₂ permeability: Preparation and characterization. *International journal of hydrogen energy*, 32: 2010-2021.
8. Dittmeyer, R., Hollein, V. & Daub, Kristian. (2001). Membrane reactors for hydrogenation and dehydrogenation processes based on supported palladium. *Journal of molecular catalysis*. 173: 135-184.
9. Weyten, H., Luyten, J., Keizer, K., Willems, L. & Leysen, R. (2000). Membrane performance for dehydrogenation reactions in a catalytic membrane reactor. *Catalysis today* 56: 3-11.
10. Gobina, E. & Hughes, R. (1996). Reaction assisted hydrogen transport during catalytic dehydrogenation in a membrane reactor. *Applied catalysis*. 137 (1): 119-127.
11. Hughes, R. (2001). Composite palladium membranes for catalytic membrane reactors. *Journal of membrane technology*. 2001 (131). 9-13.
12. Suda, H. & Haraya, K. (1997). Gas permeation through micropores of carbon molecular sieve membranes derived from Kapton polyimide. *Journal of physical chemistry*, 101: 3988-3994.
13. Lee, D. & Oyama, S.T. (2002). Gas permeation characteristics of a hydrogen selective supported silica membrane. *Journal of Membrane Science*. 210: 291-306.
14. Li, X. & Liang, B. (2012). Permeance of pure vapors in porous γ -Al₂O₃/ α -Al₂O₃ ceramic membrane, *Journal of the Taiwan Institute of Chemical Engineering*, (43): 339-346.

15. Yuliya, W., Mudimu, A-O., Braun, G. & Brunner, G. (2010). Gas transport through ceramic membranes under super-critical conditions. *Desalination*. 250: 1056-1059.
16. Schlesinger, M. & Paunovic, M. (2010). *Modern electroless plating*. Chapter 18, Wiley & sons, Inc. 447-458.
17. Li, A., Xiong, G., Gu, J. & Zheng, L. (1996). Preparation of Pd/ceramic composite membrane 1. Improvement of the conventional preparation technique. *Journal of membrane science* 110: 257-260.
18. Yeung, K.L., Christianiansen, S. & Varma, A. (1999). Palladium composite membranes by electroless plating technique: Relationship between plating kinetics, film microstructure and membrane performance. *Journal of membrane science*. 159: 107-122.
19. Nam, S-E., Lee, S-K. & Lee, K-H. (1998). Preparation of a palladium alloy composite membrane supported in a porous stainless steel by vacuum electrodeposition. *Journal of membrane science*, 153: 163-173.
20. Ngamlerdkopin, K. & Tantavichet, N. (2014). Electrodeposition of nickel – copper alloys to use as a cathode for hydrogen evolution in an alkaline media. *International journal of hydrogen energy*, 39, 16:8194-8203.
21. Itoh, N., Akiha, T. & Sato, T. (2005). Preparation of thin palladium composite membrane tube by a CVD technique and its hydrogen permselectivity. *Catalysis Today*, 104: 231-237.
22. Li, X., Liu, T.M., Fan, Y.Q. & Xu, N.P. (2008). Preparation of composite palladium-silver alloy membranes by photocatalytic deposition. *Thin Solid films* 516: 7282-7285.

CHAPTER 3

CHAPTER 3

3.0 Palladium and Palladium - Silver Composite Membranes.

3.1. Background

Metals in group 10 and some metallic elements in groups 3-5 can dissolve hydrogen; however only palladium has the unique ability to transport hydrogen through the metal as a result of the higher solubility of hydrogen in the bulk over several temperature ranges [1] [2]. Palladium membranes have received an ever – increasing attention in the separation of hydrogen mainly due to their ability to exclusively separate hydrogen from other gases [3]. Despite its significance in hydrogen separation and purification, pure palladium membranes suffer from hydrogen embrittlement when in contact with hydrogen below 300^o C and 2 MPa. The embrittlement causes cracking, blistering and reduced ductility in the metallic layer [1]. The cost challenge posed by palladium is balanced by the fact that 80% of the cost of the membranes are in the support costs.

Poisoning is a major constraint encountered in palladium membranes due to the susceptibility of palladium to surface deactivation resulting in α and β phases which promote recrystallization and leads to bulk defects commonly referred to as embrittlement [1]. In both fcc and bcc phases, palladium face – centred – cubic (fcc) lattice are retained but the crystal unit cell lattice parameter increases for pure palladium in the α phase from 0.3890 nm to 0.3895 nm and for the β occurs during exposure to hydrocarbons or sulphur [1]. The hydrogen embrittlement is caused by the formation of palladium hydride (PdH_x) which could lead to pinholes that eventually results in the failure of the membrane [3]. The mechanism associated with the embrittlement involves the transformation from α to β – phases when there is hydrogen diffusion through the membranes at temperatures below 300^oC and pressures below 2 MPa [4]. The physical dimension of the unit cells in the crystal lattice for the β phase is larger than that of α - phase by about 3% which causes strains in the metal. This strain caused by the growth of the beta phases results in the embrittlement of the material [1].

In order to relieve the problems of hydrogen embrittlement and poisoning and improve hydrogen permeability, palladium is usually alloyed with metals such as

Ag, Cu, Ni, Y, Pt and Au [1]. Alloying palladium with these metals drastically reduces the critical temperature for the transformation from α to β phases [1]. In alloying, the elements of group 11 are used: Ag, Cu, Au. The main advantage of alloying is to avoid the hydrogen embrittlement which leads to peeling off of the active palladium layer and renders the membrane inactive. The embrittlement occurs when palladium comes in contact with palladium at temperatures below 300⁰ C. The alloying also enhanced hydrogen permeation and increases the resistance of the membrane to the effect of H₂S [1].

In terms of material cost, Pd/Ag alloy membranes are less expensive while Au is more expensive compared to the others. Pure palladium for hydrogen permeation and separation is hampered by high solubility of hydrogen below 300⁰ C which leads to the formation of a separate Pd-hydride phase which distorts the lattice to cause embrittlement. At temperatures below 300⁰ C when hydrogen comes in contact with Pd, the B – phase in the lattice grows by about 3% larger than the A-phase which cause strains in the metal leading to embrittlement. Alloying lowers the critical temperature[1] [2] . Moreover, the alloys are resistant to sulphur poisoning and the alloying reduces the difference in size of the lattice between α and β phases to cushion the strain during the absorption – desorption of hydrogen [1] [2]. Several experimental studies show higher hydrogen permeance for palladium alloy membranes compared to pure palladium membranes [2] [3].

3.2 Hydrogen Permeation through Palladium Membranes

Hydrogen permeation through palladium membranes can be described by the equation [5].

$$J = \frac{Q}{L} (P^{n_{high}} - P^{n_{low}}) \dots \dots \dots \text{Eq. 12}$$

Where J is Gas flux, Q is Permeability constant, n is pressure exponent, P^{n_{high}} is hydrogen partial pressure in the feed side, P^{n_{low}} is hydrogen partial pressure in the permeate side and L is palladium membrane thickness.

The permeation is defined by the solution diffusion transport model based on external mass transfer, surface adsorption and desorption, transition to and from the bulk palladium and diffusion within the palladium [6] and can be represented in figure 3.1.

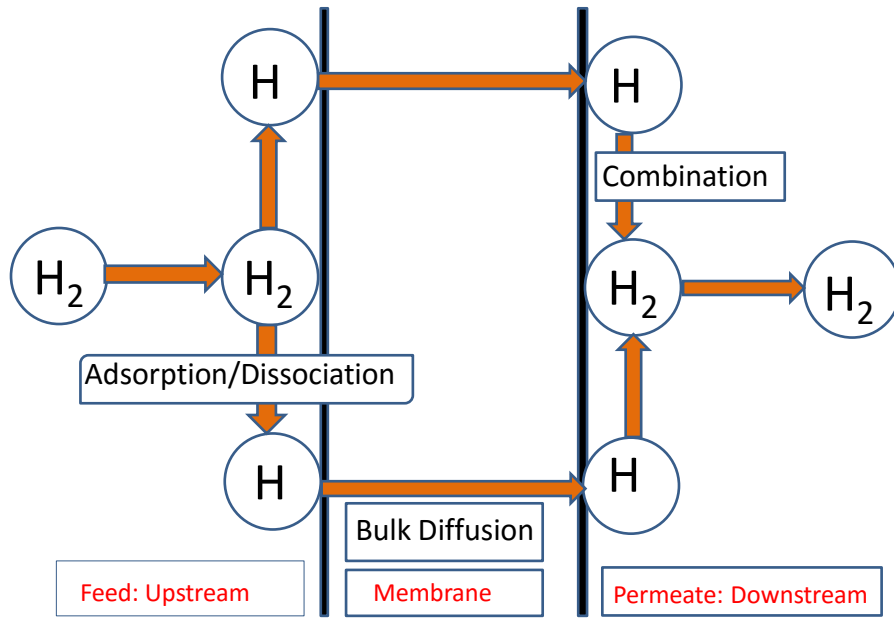


Figure 3.1: A Schematic of hydrogen permeation across a palladium membrane

The series of steps in figure 3.1 are explained as follows [7]:

1. External mass transfer where the hydrogen molecules undergo internal diffusion from the bulk of the gas phase onto the membrane surface on the high pressure side.
2. The hydrogen molecules are dissociated into atoms through a reversible dissociative adsorption also on the high pressure side.
3. The hydrogen atoms are dissolved into the bulk palladium layer through a reversible dissolution process.
4. The hydrogen atoms undergo diffusion into the bulk metallic layer.

5. The hydrogen atoms undergo reversible movement from the bulk metallic layer to the membrane surface.
6. The hydrogen molecules undergo reversible recombination desorption at the low pressure side.
7. External mass transfer of hydrogen molecules on the membrane surface at the low pressure side.

The value of the pressure exponential n in equation 2 indicates the rate limiting step for hydrogen permeation through the membrane [7]. If bulk diffusion of atomic hydrogen is the rate limiting step, $n=0.5$. If the surface processes i.e. either hydrogen dissociative adsorption on the high pressure feed side or the atomic hydrogen recombination and desorption at the low pressure permeate side controls hydrogen permeation, then $n=1$. However, when both surface processes and bulk diffusion control hydrogen permeation through the membrane, then n will vary between 0.5 and 1 [8].

Normally the H_2 flux through palladium membranes is expected to follow Sievert's law which states that hydrogen permeation through the membrane is directly proportional to the square root of the partial pressure difference in the feed and permeate sides [9]. In respect of Sievert's driving force, the value of pressure exponent $n=0.5$. The activation energy is expressed according to the Arrhenius Vant-Hoff equation which describes the effect of temperature in hydrogen permeation across palladium membranes as shown in equation 13 [10]:

$$J = A_0 \exp \left(-\frac{E_a}{RT} \right) \dots\dots\dots \text{Eq. 13}$$

Where A_0 is the pre-exponential factor, E_a is the activation energy, R is the gas constant and T is the temperature.

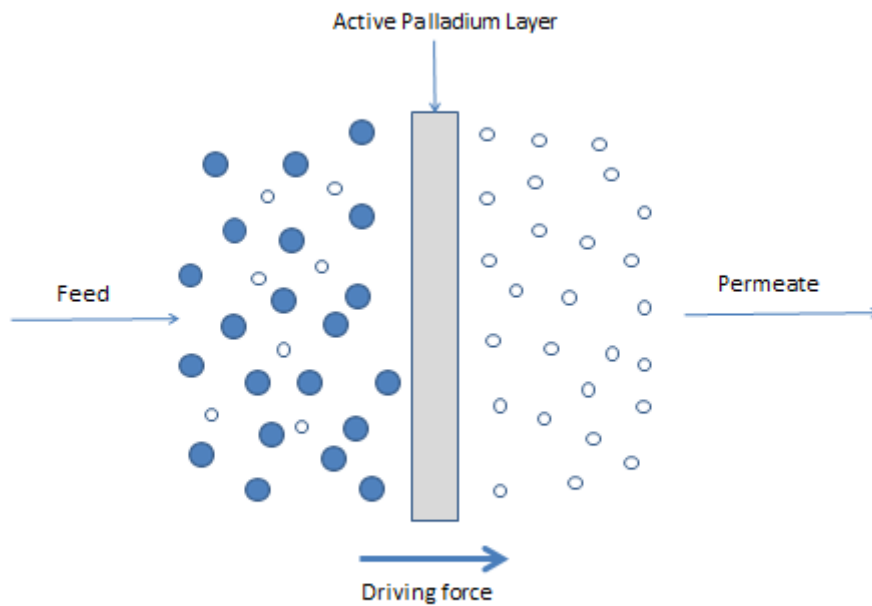


Figure 3.2: A Diagram showing the effect of driving force on gas permeation across the membrane

Based on Sievert's law, the most important driving force for the transport of hydrogen in palladium membranes is the pressure difference across the membrane. Figure 3.2 shows an illustration of the effect of the driving force on gas permeation through the composite membrane. Gas molecules attempting to permeate through the membrane are faced with resistance by the composite membrane. However, the driving force lowers the membrane resistance to permeation thus allowing some molecules pass through while others are rejected. The remaining molecules are referred to as retentate while the molecules that pass through by the action of the driving force are referred to as the permeate.

3.3 Materials and Equipments

This section presents the methodology used in this work for the fabrication of the membranes. The materials, equipments, gases and chemicals used are also explained in this section.

3.3.1 Materials

The starting support used in this work is ceramic alumina obtained from CTI SA (Ceramiques Techniques & Industrielles SA, France). There are 2 types of this support in the C.P.I.M.T laboratory at the Robert Gordon University Aberdeen, the big and small membranes with specifications shown in Table 3.1 below.

Table 3.1: Specification for small and big membranes used in this work

Specifications	Big Size Membrane	Small Size Membrane
I.D (mm)	20.07	7.34
O.D(mm)	26	10
Effective Length (m)	0.32	0.34
Average Pore size	6000 nm	30 nm

In preparing the composite palladium membrane, i.e. deposition of the palladium layer over the porous alumina support, only the small support was used because of the cost implications of the material. Obviously if the big size is to be used, it will demand more palladium for the coating which is a bit expensive. During the cause of this study, a 5g bottle of the palladium precursor PdCl_2 sold for about £250 (Two hundred and fifty British pounds). A picture of the Alumina membrane support is shown in Figure 3.3 (A) Big support (B) Small support while figure 3 (A) and (B) show the determination of the O.D and I.D of the alumina support using vernier caliper.

There are several membrane supports which would have been used for this study such as glass and stainless steel but Alumina was chosen for the study due to

the advantages it enjoys over other types of support such as its ability to withstand high temperature and resistance to corrosion [1].

Table 3.1 shows the outer and inner diameter specifications of both the big and small membranes while figure 3.4 shows the method for determination of O.D and I.D of the tubular support using vernier caliper. For the silica membranes, the same type of support was used to deposit successive silica layers over the porous support. However, for the silica membranes, only the big support was used because the silica precursor i.e. silicone elastomer was not expensive as was the case for palladium membranes.



(A)



(B)

Figure 3.3: Pictures of alumina support (A) Big membrane (B) Small membrane

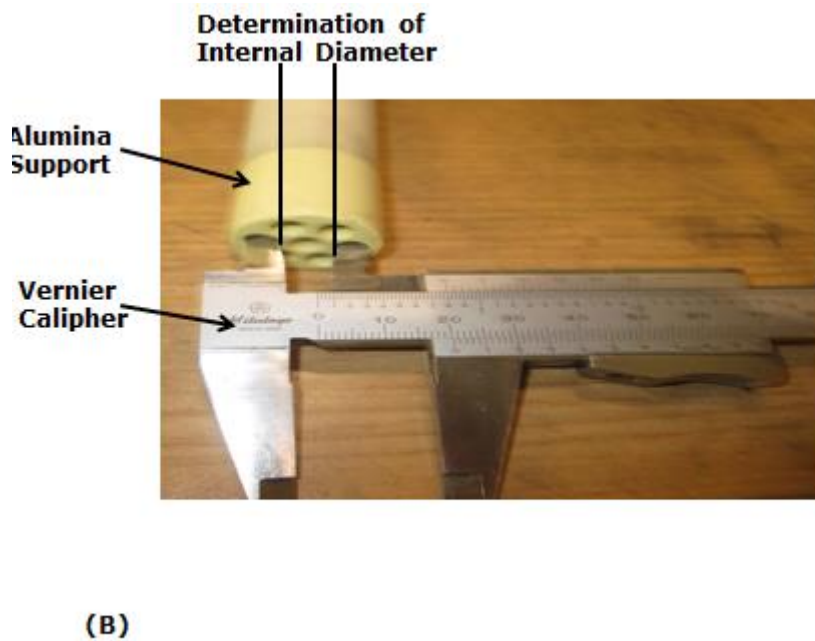
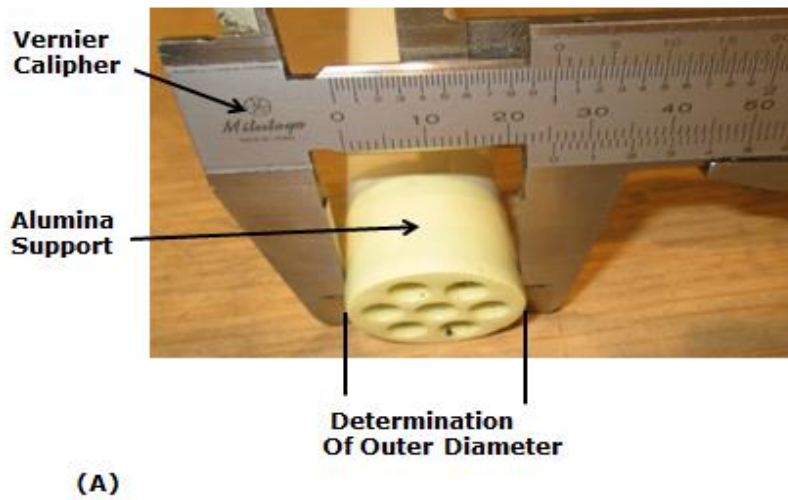


Figure 3.4: Pictures showing the determination of diameter of alumina support using Vernier caliper (A) Outer diameter (B) Inner diameter

Diameter is the length of a straight line through the centre of a circle. Inner diameter is the length of a straight line inside of a tube. For outside coating, inner diameter is not used in determining the gas permeance and flux.

3.3.2 Equipments

1. Custom test tubes 350 ml: These test tubes were ordered purposely for this investigation and used in both the support modification (sensitization & activation) and the plating process proper. Prior to the plating process there were only the 1000 ml and 500 ml tubes available in the laboratory but these larger tubes will need a large quantity of the palladium precursor i.e. PdCl_2 which is expensive. To ameliorate this problem, this researcher (Abubakar Alkali) designed the smaller new custom built 350 mL cylinders which were supplied by Vitrum engineers Aberdeen. A design of the specification for the custom tubes drawn up by the researcher with the assistance of vitrum prior to producing the tubes is shown in Figure 3.5.

Glass cylinder - simplified drawing

For aqueous solutions, polymeric solutions and suspensions

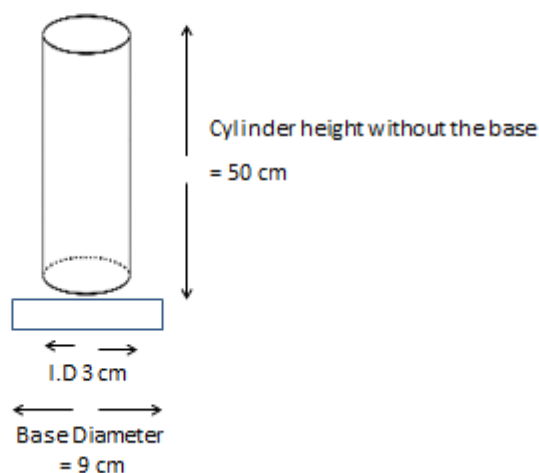


Figure 3.5: Design specification of the custom tubes for electroless plating method

This idea has helped greatly in reducing the cost associated with this project by reducing the quantity of palladium by about 50%. Also the new 340 mL glass

cylinders fit very well for the size of the porous alumina support (small size) which has an O.D of 10.7 mm and 34 cm long.

2. Vernier Caliper: This was used to determine the Internal and Outer Diameter of the membrane as shown in Figure 3.4.

3. Beakers: Both 200, 500 and 100 ml beakers were used in preparation of solution prior to transferring same into the test tube for sensitization, activation and plating.

4. Water Jacket: The water Jacket is a big container with an electricity supplier ON/OFF control switch into which clean tap water was poured to the neck level and heated to a particular temperature. The test tube containing the plating solution is placed into this jacket and the temperature of the plating solution controlled to the desired plating temperature.

5. Furnace (Carbolite): 5 – 1050⁰ C, type RWF 11/23: This equipment was used to calcine the support at higher temperature.

6. Oven (Carbolite): This equipment was used to dry the support when a few hours drying is required.

7. Magnetic stirrer: This equipment was inserted into test tube during each sensitization, activation and plating procedure and placed onto the electric stirrer to ensure proper mix of the plating solution for uniform modification of the support and even coating of the palladium layer over the porous support.

8. Fume Cupboard: As these experiments involved using chemicals some of which are toxic, it is necessary to use the fume cupboard in preparation of solutions for health and safety purposes. The plating solution contains NH₄OH solution which has a very distressing and foul smell. To avoid the spread of this smell, the preparation of the plating solution was conducted in the fume cupboard. The fume cupboard also housed the retentate tube during gas permeation test and serves as the medium through which the gas in the retentate is guided away from the laboratory and escapes outside into the atmosphere.

9. Drier (Carbolite) 1 – 300⁰ C, PF120(201): This equipment was used to dry the membrane after the sensitization and activation step and also after the metallic layer deposition.

10. Graphite seals: These were used to seal the support from any contact with the solution to avoid internal deposition. This is necessary since all the plating was done using the outer deposition technique.

11. Magnetic stirrer FB15045 (Fisher Scientific): After preparing each solution, the test tube containing the solution is placed on the stirrer so as to ensure the components are properly diluted and well mixed. This is necessary to achieve an evenly coated palladium layer.

12. Thermometer Exia11CT4 (Digitron): For temperature measurements for the plating bath and the plating solution. The equipment was also used to measure the temperature of the reactor during high temperature permeation and membrane annealing.

13. Mass flow meter (Agilent Technologies ADM1000): This equipment was used as part of the gas permeation set up to measure gas flow.

14. Pressure Gauge

15. Weighing balance

16. Heating Tape

17. Swagelok Fittings

18. Thermocouple

19. Power regulator (Barnstead Electro Thermal).

3.3.3 List of Gases

Both single and mixed gases used in this study were of certified grade and supplied by BOC Industrial gases UK. The cylinders have specifications: Some of the gases used are extremely dangerous and flammable hence adequate care was taken during gas permeation experiments based on health and safety standards.

The gases used are as follows:

1. Hydrogen: (high purity 99.995%, P=175 bar): This gas was used in single gas permeation tests. It was used also during reduction of palladium membrane to activate the palladium layer prior to gas permeation test.
2. Helium: (Purity 99.99%, P=230 bar) This gas was used as a carrier gas to calibrate the GC, perform Helium leak tests.
3. Argon: (Purity 99.995%, P=230) This is another inert gas like Helium and used as a carrier gas to calibrate the GC.
4. Nitrogen: (Purity 99.99%, P=230 bar): This gas was used in single gas permeation tests.
5. Gas Mixture: A hydrogen mixture with the composition. ($H_2 = 50\%$, $CO=28\%$, $CO_2=10\%$, $CH_4 = 8\%$, $N_2=4\%$) was used in all the hydrogen separation experiments.

3.3.4 Chemicals

All the chemicals used in this study are of laboratory analytical grade and supplied by Sigma Aldrich or Fischer Scientific. The chemicals were used in preparing the plating bath for electroless plating deposition and also surface modification of the membrane in the 2 step sensitization and activation.

The chemicals used are as follows:

1. Stannous Chloride: SnCl_2 (99%) CAS No. CAS 7772-99-8: This chemical was used in preparing the solution for support modification i.e sensitization step prior to depositing the metallic layer.
2. Hydrochloric Acid HCl (0.1 M) CAS No. 7647-01-0. This chemical was used in preparing the solution for activation and sensitization. It was also used in preparing the plating bath.
3. Ammonia hydroxide NH_4OH : This chemical was used to prepare the plating bath solution for deposition of the palladium layer.
4. Palladium Chloride PdCl_2 (99.9%): CAS 7647-10-1: This chemical was used as the palladium precursor in the plating bath solution for deposition of the palladium layer.
5. Hydrazine hydrate (35%) N_2H_4 : CAS No. 10217-52-4: This chemical was used in preparing the plating bath solution for deposition of the palladium layer.
6. EDTA (99.9+%): CAS No. 6381-92-6. This chemical was used as stabilizing agent in the plating bath solution for deposition of the palladium layer.
7. $\text{Pd}(\text{NH}_3) \text{NO}_2$: This chemical was used to prepare the activation solution for modification of the support.
8. Distilled water: Distilled water was obtained from the Pharmacy and life sciences department in RGU and used in preparing the sensitization and activation solutions for modification of the support.
9. Silver Nitrate AgNO_3 : This chemical was used in preparing the plating bath solution for codeposition of the Pd/Ag layer.

3.4 Experimental Procedure

Figure 3.6 shows a picture of the Gas Chromatograph equipment used in this work for analysis of permeate composition during gas separation experiments.



Figure 3.6: A Picture of the gas chromatograph for gas analysis used in this work

The permeation tests were carried out in a stainless steel shell and tube membrane reactor module. Graphite O-rings were fitted tightly at both ends of the membrane reactor module to prevent gas leakages. Gas flow rates were measured using a digital flow meter and the separation data collected online using a Varian HP 3800 Gas Chromatograph interfaced to a PC and equipped with a T.C.D and F.I.D detectors in series. Inlet and exit pressures were controlled using back-pressure regulators.

The temperature and pressure were monitored using thermocouples and pressure gauges as shown in figure 3.5. Membrane characterization was carried out using a scanning electron microscopy (SEM) and energy dispersive x-ray

analysis (EDXA) to identify both the morphological features and elemental composition. The key components of the gas permeation test are shown in Figure 3.7. Initially, the composite palladium membrane is inserted into the membrane reactor and the seals at both ends placed tightly to prevent leaks. The reactor bolts and nuts were also fitted appropriately to stop gas leaks. Possible gas leaks through the membrane reactor were investigated using soapy water which shows bubbles if there are any gas leakages.

The gas permeation is essentially a cross flow from the feed through the membrane to the permeate while the rejected gas flows out through the retentate. Gases from the cylinder are fed into the reactor through the feed controlled by a pressure regulator.

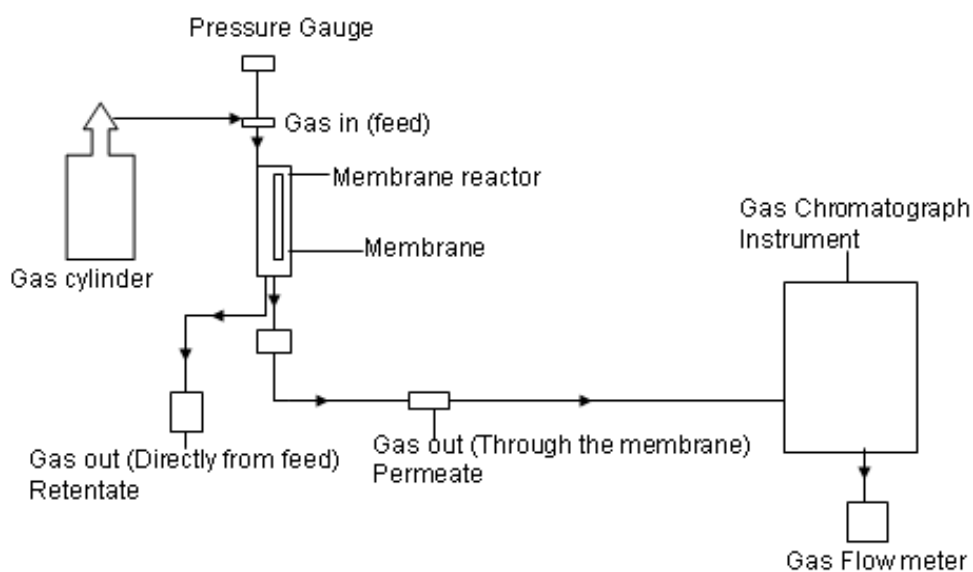


Figure 3.7: Concept schematic of a gas permeation test plant

The permeate is analysed through the Gas Chromatograph (GC Varian model 3800) which provides the composition of the permeate in terms of the gases present, their concentration (Peak area counts) and purity levels.

The flow meter is placed after the GC to enable the measurement of the permeate flow rate. The flow meter gives the composition from which the separate flow rates of the individual gases can be determined. From this process, it can be established that one gas permeates faster than the other and the purity levels, permeability and selectivity of the membrane can also be determined.

3.4.1 Helium Leak Test

Prior to the deposition of the palladium film, it is necessary to determine the suitability of the support for deposition by drying it free from any damp or moisture and also carrying out a Helium leak test. A 30 nm alumina support with specification (I.D. 7.34 mm, O.D. 10 mm, effective length = 34 m) was used for the He leak test. The support was dried in an oven at 65⁰ C as shown in figure 3.7 for 2 hours after which a helium leak test was carried out.



Figure 3.8: Picture of ceramic alumina support in the oven for drying

3.4.2 Support Modification: Sensitization, Activation and Calcination.

Prior to the plating of the palladium layer through the electroless plating method, there is the need to seed the support with Pd nuclei. This involves a two step process of sensitization and activation to create catalytic sites on the non-metallic surfaces. This is a standard practice in electroless plating of palladium over porous supports [11]. The sensitization and activation processes stimulate the adsorption of the metal ions, enhance strong adhesion of the Pd nuclei on the substrate and eliminate induction period of the metal to ensure better uniformity of coating and improved membrane quality [12].

In order to prepare the support for a more uniform deposition, it was calcined at 1100 K for 10 hours at a rate of 2⁰ C per minute after which it was stored overnight at room temperature. A picture of the support in the furnace during calcination is shown in figure 3.9.

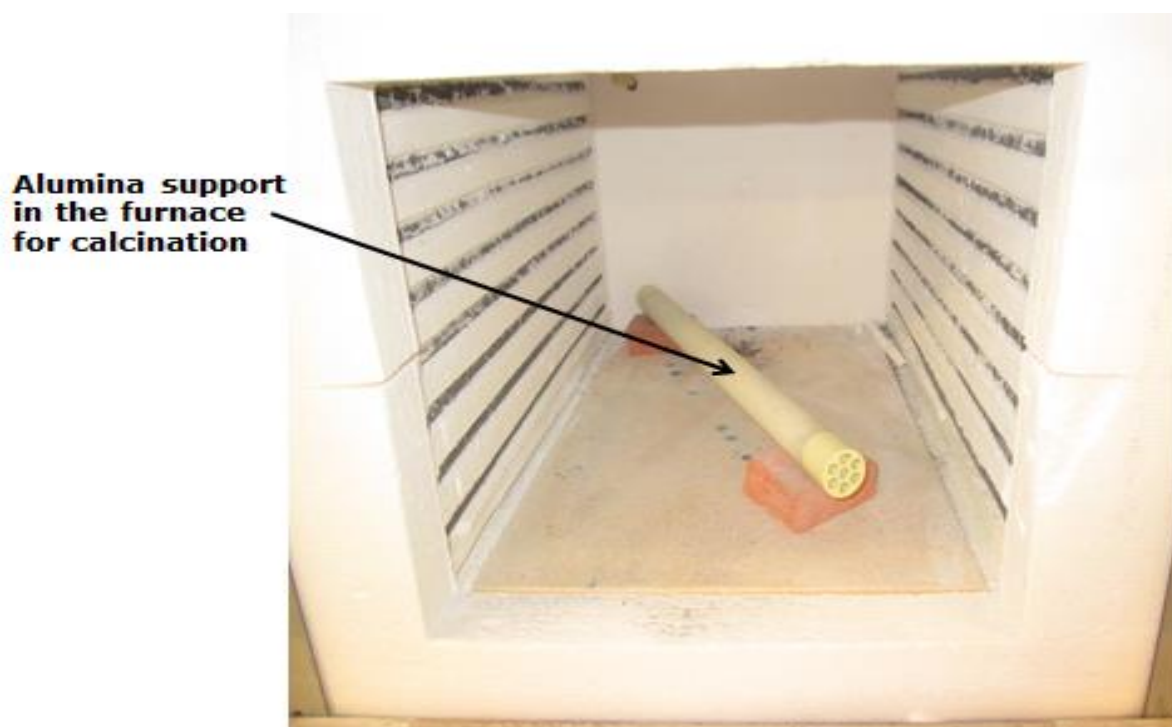


Figure 3.9: A Picture of membrane in the furnace for calcination

The sensitization and activation procedure was carried out using a 0.005 M Sn (11) and a 0.005 M Pd (11) solution respectively. The composition of the sensitization and activation solutions is shown in Table 3.2.

Table 3.2: Composition of sensitization and activation solutions

(Sensitization solution):	SnCl ₂ = 0.36 g Distilled water = 320 mL 0.1 M Hcl = 10 mL
(Activation solution):	Pd (NH ₃) ₄ (NO ₃) ₂ = 1.0 mL Distilled water = 320 mL 0.1M Hcl = 10 mL

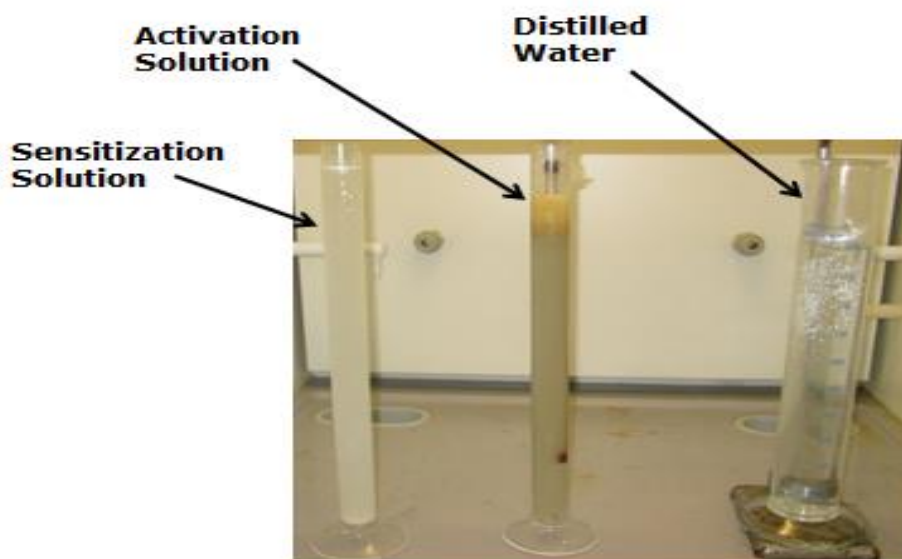


Figure 3.10: A Picture of the sensitization and activation solutions with distilled water during support modification before electroless plating

A picture of the sensitization and activation solutions including distilled water is shown in figure 3.10. After the membrane was allowed to cool down to room temperature, both ends of the support were sealed to ensure that only the outer section of the support comes in contact with the solution. This is necessary since it is the outer section of the support that will be plated. Both the sensitization and activation processes were carried out simultaneously such that both solutions were placed in the fume cupboard.

Another glass cylinder containing distilled water was also placed in the fume cupboard to rinse the support after each step. The support was dipped into the sensitization solution for 5 minutes and rinsed with distilled water; it was then dipped into the activation solution for another 5 minutes and rinsed in distilled water. This procedure was repeated 10 times in order to obtain a uniformly seeded support. After each dipping, the support was rinsed for 10 seconds in distilled water and immersed immediately back into the solution. The 10 seconds time in-between each dip for 10 dips gives a total time of 1 minute 40 seconds.

Practically, the time in-between dippings during the modification will be more than 10 seconds because there is always a time lag of a few seconds before the support is dipped back into the solution or while trying to place the support upright vertical position in the glass cylinder. The total time spent on the 2 step sensitization and activation process is calculated as follows:

Sensitization step = 5 (minutes) × 10 (dips) = 50 minutes

Activation step = 5 (minutes) × 10 (dips) = 50 minutes

Rinsing with distilled water = 90 seconds × 2 = 3 minutes

Total: 1 hour 43 minutes

The actual time spent on the sensitization and activation could be between 2 – 2 ½ hours. This long time duration makes the process prone to errors and contamination. During the sensitization procedure, the support was dipped into the solution and held in an upright vertical position to avoid tilting which could affect the uniformity of coating.

3.4.3 Deposition of the Palladium Layer

After the 2 step sensitization and activation, the support is now ready for deposition of the palladium layer. A picture of the electroless plating set up is shown in figure 3.11. The composition of the electroless plating bath is presented in Table 3.3. A Hydrazine based bath was used to deposit the Pd layer onto the activated support. The support was again sealed at both ends with a plastic protector to prevent internal deposition. The plating solution was stabilised with Na₂EDTA and heated in a water bath. Initially the water bath was prepared and the glass tube containing the plating solution placed into the water bath. The plating solution was heated to a temperature of 60⁰ C.

The temperature of the plating solution was monitored using a thermometer and maintained at 60⁰ C. The activated support was then immersed into the plating solution at a constant plating time of 30 minutes. The plating solution was prepared and placed into the water jacket without the hydrazine reducer. However, the 1M N₂H₄ reducer was added just before the support was inserted into the plating solution. The point at which the hydrazine reducer was added signals the commencement of the electroless plating process and the plating time starts at that point.

Table 3.3: Composition of the plating solution

PdCl ₂	2.2 g
NH ₄ OH	220 mL
EDTA	25 g
1M N ₂ H ₄	10 mL

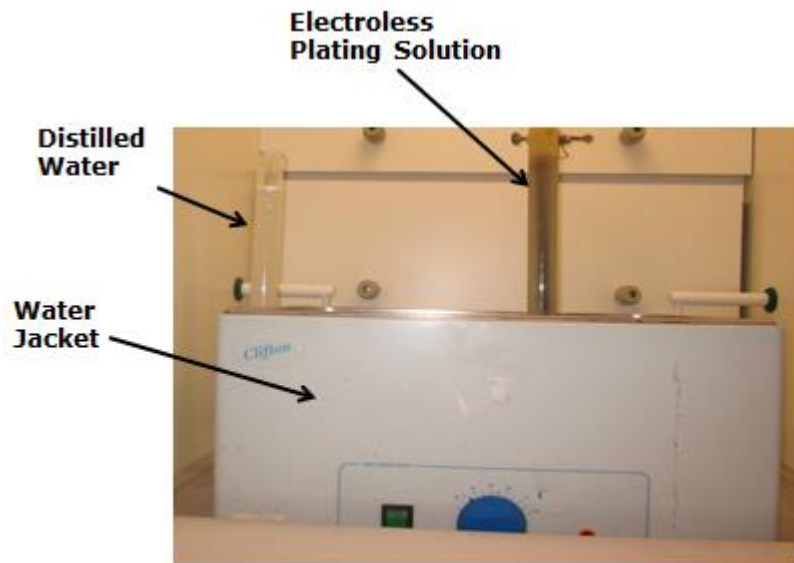


Figure 3.11: A Picture of water jacket and plating solution during electroless plating

The permeation tests were carried out using the permeation test plant in the CPIMT laboratory shown in Figure 3.12.

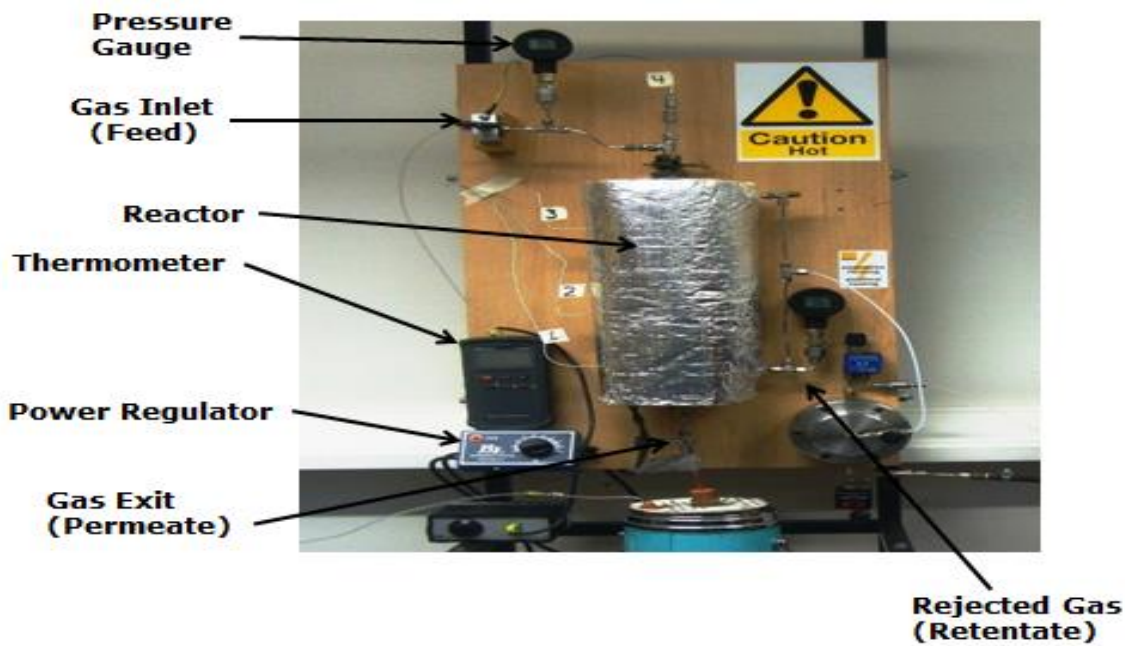


Figure 3.12: A Picture of the gas permeation test plant in the CPIMT laboratory

The feed gas was fed through the gas inlet section of the reactor to enable the contact of the gas with the active membrane layer for permeation and separation purposes. The surface area is determined based on the inner and outer diameter specification and the effective length

3.4.4 Modified Electroless Plating Method

A 30 nm pore alumina support was calcined based on the same calcinations cycle as in membrane Pd1. The calcined support was dried overnight at room temperature after which the support was modified with AlO (OH) sol by dipping into the AlO (OH) sol for 30 minutes. The composition of the Al (OH) sol is shown in Table 3.4 while figure 3.13 shows a picture of the dipping set up. Prior to dipping, both ends of the calcined support were sealed to ensure that there is no deposition on the inner surface of the support. The significance of the modification with AlO (OH) sol is to ensure a smooth and uniform surface which would enhance uniform of coating of the Pd layer during the electroless plating.

The conventional method of modifying the support through a 2 step sensitization and activation is now reduced to a 1 step activation method. In electroless plating, catalytic sites containing palladium nuclei need to be created on the porous support prior to plating.

**10.7 mm O.D Alumina support
during modification with
Boehmite Sol**

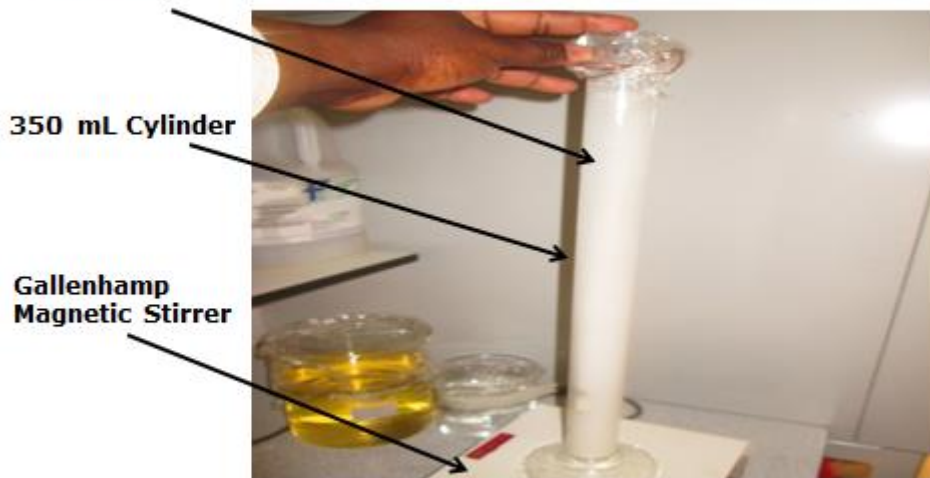


Figure 3.13: A Picture of the set up for surface modification with Boehmite before plating

Table 3.4: Composition of the Boehmite solution for modification of the Alumina support

Boehmite powder	15.5 g
Distilled water	320 mL

The activation procedure was carried out for 5 minutes after which it was rinsed in distilled water. The procedure was repeated 10 times to obtain a uniformly seeded support. After each dipping, the support was rinsed with distilled water. After the modification, the support was dried overnight at room temperature.

3.4.5 Co-deposition: Electroless Plating of Pd/Ag Composite Membrane

The same procedure was used as that for preparing Pd1 membrane in section 3.2.4 except that in this case a different plating bath composition was used containing both palladium and silver precursors.

A 30 nm alumina support with specification (I.D 7.34 mm, O.D. 10.7 mm, and effective length 34 cm) was used. The same calcinations procedure was used as that for the Pd1 and Pd2 membranes. In this case, the 2 step sensitization and activation procedure for conventional electroless plating was carried out on the porous support based on the same procedure and composition of the sensitization and activation solutions as described in section 3.2.3.

3.4.6 Electroless Plating of the Pd/Ag Layer

The composition of the Pd/Ag electroless plating bath is shown in Table 3.5 and kept at 77%/23%. As can be observed, the solution contains both the palladium and silver precursors for codeposition of the Pd/Ag layer. Another method is to prepare 2 different solutions containing the palladium and silver precursors separately in which case the plating would be carried out separately which will result in 2 separate layers of palladium and silver. However, in this study, one plating solution containing both precursors was prepared which resulted in a single Pd/Ag layer. and the composition of the plating solution was kept at 77%/23%.

Another advantage of using a single plating bath for both Pd and Ag precursors is that a uniform composition of both Pd and Ag will be achieved since the same plating time is applied. Both the temperature and plating time were maintained as was used during the preparation of Pd1 membrane i.e. 60⁰ C and 30 minutes. Plating commences after addition of the hydrazine reducer.

Table 3.5: Pd/Ag Plating bath composition

PdCl ₂	2.1 g
AgNO ₃	0.7 g
NaEDTA	31 g
NH ₄ OH	200 mL
1M N ₂ H ₄	10 mL

3.4.7 Hydrogen Permeation to Test for Embrittlement

Prior to the permeation test, the membrane was annealed in flowing hydrogen at 450⁰ C for 2 hours to enhance alloy formation and activate the metallic Pd layer. During the permeation test on membrane Pd1 in section 3.3.1, hydrogen flux was measured through the membrane at 150⁰ C which caused the membrane to peel off and embrittle. This made the membrane inactive for hydrogen permeation. Therefore, the permeation test for the Pd/Ag membrane (Pd3) was measured at 100, 150 and 200⁰ C which are all below the critical temperature of 298⁰ C below which palladium membrane will embrittle. Hydrogen must not come into contact with palladium below 298⁰ C in order to avoid embrittlement. The aim of the test is to investigate hydrogen embrittlement which occurs when hydrogen comes into contact with palladium below 298⁰ C which results in cracks of the active palladium layer.

3.4.8 Hydrogen Permeation at Higher Temperature

After testing the Pd3 membrane at low temperatures, the hydrogen permeation behaviour of the membrane was also investigated at 723, 673 and 623K to ascertain the level of enhancement of hydrogen permeation. This will provide a basis for comparing the hydrogen permeation behaviour of the Pd/Ag membrane (Pd3) with that of the Pd1 and Pd2 membranes. The membrane was annealed in hydrogen at 873K, 773K and 673K for 10 hours to investigate the effect of annealing temperature on hydrogen permeation. The same procedure used in annealing of Pd1 and Pd2 membranes was also used to anneal Pd3 membrane.

The presence of contaminants such as CO and CO₂ is also another problem which retards hydrogen separation from the gas mixture containing these compounds. Another objective of this test is to investigate the response of the PdAg membrane to the inhibiting effect of CO and CO₂ on hydrogen permeation.

The same hydrogen mixture with same composition for Pd1 and Pd2 membranes was used to investigate the gas separation properties of the Pd/Ag membrane Pd3.

3.5 References

1. Yun, S. & Oyama, T.S. (2011). Correlations in palladium membranes for hydrogen separation: A review. *Journal of membrane science*, 375 (1-2): 28-45.
2. Ahmad, A.L. & Mustafa, N.N.N. (2007). Sol-gel synthesised nanocomposite palladium-alumina ceramic membrane for hydrogen permeability: Preparation and characterisation. *International journal of hydrogen energy*, 32: 2010-2021.
3. Nam, S-E., Lee, S-K. & Lee, K-H. (1998). Preparation of a palladium alloy composite membrane supported in a porous stainless steel by vacuum electrodeposition. *Journal of membrane science*, 153: 163-173.
4. Hatlevik, O., Gade, K.S., Keeling, K.M., Thoen, M.P., Davidson, A.P. & Way, J.D. (2010). Palladium and palladium alloy membranes for hydrogen separation and production: History, fabrication strategies, and current performance. *Separation and Purification Technology*, 73: 59-64.
5. Itoh, N., Akiha, T. & Sato, T. (2005). Preparation of thin palladium composite membrane tube by a CVD technique and its hydrogen permselectivity. *Catalysis Today*, 104: 231-237.
6. Ward, L.T. & Dao, T. (1999). Model of hydrogen permeation behaviour in palladium membranes. *Journal of membrane science*. 153: 211-231.
7. Hengyong. L.H. & Li, W. (2008). Study of n value and α/β palladium hydride phase transition within the ultra thin palladium composite membrane. *Journal of membrane science*, 324: 44-49.
8. Chee, C. & Gobina, E. (2010). Ultra-thin palladium technologies enable future commercial deployment of PEM fuel cell systems. *Membrane technology*, Vol. 2010, Issue 3, 6-13.
9. Cheng, Y. S., Pena, M.A., Fierro, J.L., Hui, D.C.W. & Yeung, K.L. (2002). Performance of alumina, zeolite, palladium, Pd-Ag alloy membranes for hydrogen separation from town gas mixture. *Journal of membrane science*, 204: 329-340.
10. Guazzone, F., Engwall, E. E. & Ma, H, Y. (2006). Effects of surface activity, defects and mass transfer on hydrogen permeance and n -value in composite palladium-porous stainless steel membranes. *Catalysis Today*, 118: 24-31.

11. Gabito, J. & Tsouris, C. (2008). Hydrogen transport in composite inorganic membranes. *Journal of membrane science* 312: 132-142.
12. McLeod, L. S., Degertekin, F.L. & fedorov, A.G. (2009). Determination of the rate limiting mechanism for permeation of hydrogen through microfabricated palladium-silver alloy membranes. *Journal of membrane science*. 341: 225-232.

CHAPTER 4

CHAPTER 4

4.0. Silica Membranes for Hydrogen Separation and Purification.

4.1. Background

Silica membranes have long been identified as among the most important membranes in hydrogen processes and are of unique interest as a result of the relevance of hydrogen in fuel cell and other applications [1]. The 2 dominant membranes for hydrogen processes are palladium membranes and silica membranes. Silica membranes display high permeability and selectivity for hydrogen although are not permeable to hydrogen like palladium membranes. Moreover, silica membranes enjoy very distinct advantages over palladium membranes in hydrogen separation because silica membranes don't suffer from hydrogen embrittlement and material poisoning like palladium membranes. Composite silica membranes for hydrogen separation are usually prepared through dip coating method or chemical vapour deposition through which silica layers are deposited on porous supports such as alumina or Vycor glass (CVD) [1]. The high cost of palladium is balanced by the fact that 80% of the cost of the composite palladium membrane is in the support (ceramic alumina, steel or vycor glass).

Silica membranes present high selectivity and stability under harsh operating conditions. Selectivity is achieved on the alter of permeance, hence it is necessary to achieve a balance between both for optimum membrane performance [2]. Very high hydrogen permeance have been reported for silica membranes over a wide range of temperatures with H₂/N₂ selectivity of up to 3000 [2]. For a silica membrane with high hydrogen permeance and selectivity, a thin defect-free layer is deposited over a porous support. However, to further reduce the gas permeation resistance of the membrane for optimum hydrogen throughput, an intermediate layer is usually deposited between the active and the support layers.

The intermediate layer serves as a protection for the active layer against the formation of defects and pinholes [3]. Silica membranes prepared on modified

porous supports have shown high selectivity for hydrogen over Nitrogen. Gu and Oyama [3] prepared a silica membrane by depositing the silica layer on an intermediate multilayer alumina substrate. They reported high permeance of $5.0 \times 10^{-7} \text{ mol m}^{-2} \text{ s}^{-1} \text{ pa}^{-1}$ and good selectivity for hydrogen over Nitrogen over 1500 at 873 K [3]. The Gu and Oyama group in a separate investigation also carried out CVD of tetraethyl orthosilicate on alumina membranes and reported a thin silica membrane with high hydrogen permeance and selectivity of up to $5.0 \times 10^{-7} \text{ mol m}^{-2} \text{ s}^{-1} \text{ Pa}^{-1}$ and 1,500 respectively [3]. Silica membranes have also shown promising results in membrane reactors for hydrogen production using catalysts and yields above equilibrium have been obtained [3].

4.2. The Dip Coating Method

The dip coating method was invented by Jenaer Glaswrk Schott & Gen. in 1939 for depositing silica films over porous supports [4]. Dip coating is widely used in preparation of thin defect free silica membranes. The process involves depositing a wet silica layer over porous support through coating of the dry porous support surface with a particle dispersed sol. The coating procedure is usually repeated several times in order to suppress pinholes or defects.

26 mm O.D Alumina support during deposition of silica layer

1 L Cylinder containing Silica solution

Magnetic Stirrer FB15045

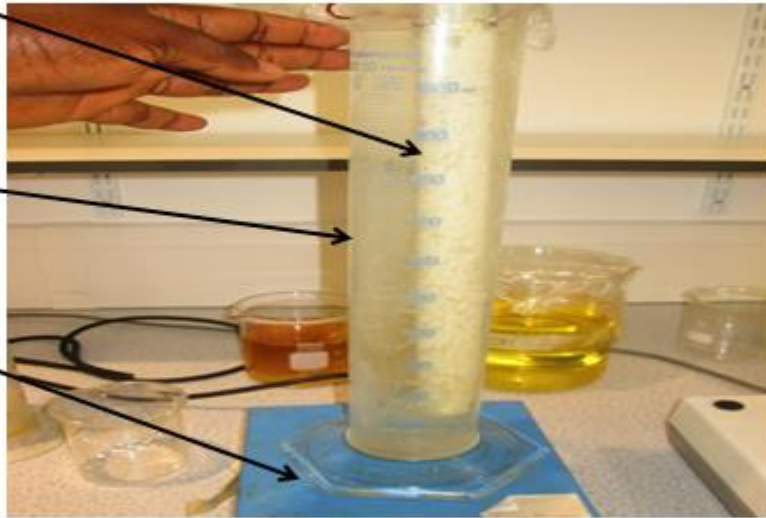


Figure 4.1: A Picture of the dip coating set up for the preparation of composite silica membranes

A picture of the dip coating process for preparation of silica membranes is shown in figure 4.1.

The dip coating procedure involves 3 fundamental steps [1]:

- (1) Dipping the support into the solution.
- (2) Withdrawing the support from the solution.
- (3) Drying the support.

In the dipping step, the layer is deposited over the surface of the porous support by capillary force which drives the solvent suction into the pores of the membrane. During the withdrawal step, the drag force could form an adhering particle layer as a result of the tangential flow of suspension against the support [5]. This tangential flow will either sweep away weakly adsorbed particles and/or drive particles into vacant holes. In both cases, the tangential flow could suppress the possibility of pin holes during dip coating [5].

Several authors have reported high H₂ permeance for silica membranes prepared using the dip coating method. Alfaro. S. et al [5] synthesized silica membrane on porous ceramic alumina support using the dip coating method and reported a hydrogen permeance in the range of $5 \text{ to } 9 \times 10^{-7} \text{ mol m}^{-2} \text{ s}^{-1} \text{ Pa}^{-1}$ and was able to separate hydrogen from a binary H₂/CH₄ gas mixture [6]. Gu & Oyama [3] also used the sequential dip coating method to deposit silica layers over porous alumina support. However, in this case, an intermediate multilayer γ -alumina substrate was deposited over the porous support prior to the deposition of the silica layers. The intermediate layer enhanced the membrane performance with hydrogen permeance of up to $5 \times 10^{-7} \text{ mol m}^{-2} \text{ s}^{-1} \text{ Pa}^{-1}$ and H₂/CO, H₂/CH₄ selectivities of over 1500 [3]. Yoshino. Y. et al [7] also used the dip coating method to deposit a silica layer over an intermediate alumina layer and reported a highly selective membrane to hydrogen with permeance values ranging from 5×10^{-8} to $5 \times 10^{-6} \text{ mol m}^{-2} \text{ s}^{-1} \text{ Pa}^{-1}$ and H₂/N₂ selectivity in the range of 30 – 300.

4.3. Chemical Vapour Deposition (CVD) in Silica Membranes

Silica membranes prepared with CVD have shown enhanced stability and integrity. Unlike the dip coating/sol gel method, the CVD doesn't need repeated coatings. The CVD process involves a system to deliver both reactive and carrier gases such as hydrogen or argon and reactive compounds such as metal halides. These gases flow through the substrate in a reaction chamber where the deposition of the film takes place [1]. The mechanism of the CVD method involves both gas phase and surface reaction. There are several ways through which film is deposited over the porous support in CVD these include thermal decomposition, oxidation and hydrolysis [8].

The reactions can start in the vapor phase leading to film decomposition. Also decomposition can occur through the reaction between the substrate surface and one of the gases in the vapor phase. Several authors have reported hydrogen permeation results for silica membranes prepared through the CVD method [8]. Lee et al [8] prepared a composite silica membrane by depositing a thin silica layer through the CVD of tetraethylorthosilicate (TEOS) over porous alumina support using the CVD method and reported a hydrogen permeance in the order

$10^{-7} \text{ mol m}^{-2} \text{ s}^{-1} \text{ Pa}^{-1}$ at 873 K [8]. Kim S-S et al [9] also used the CVD method to thermally decompose tetraethoxysilane at 600 – 650^o C on α -alumina tube of 110-180 nm pore size and γ -alumina coated membrane of 6-8 nm pore size.

4.4. Silica Membranes Vs Palladium Membranes for Hydrogen Separation and Purification

Silica membranes can withstand higher temperatures than palladium membranes and because several hydrogen production reactions are endothermic and require high temperatures, this is a distinct advantage that silica membranes have over palladium membranes [1]. Palladium membranes also decline in hydrocarbon environments while silica membranes do not suffer from some of these disadvantages associated with palladium because they can withstand much higher temperatures and are less expensive [1]. Currently, most of the research on silica membranes is focused on improving the hydrogen permeation properties of silica membranes by modifying the CVD method to control the pore sizes and film thickness [1]. Silica membranes have high hydrothermal stability which contributes to their application in adsorption processes. Membrane materials are hydrophilic in nature. They contain hydroxyl groups which enable strong H-bonding with water which could lead to rapid filling of the pores which inhibits application of membrane separation in moist gas mixtures. This phenomenon also limits the separation properties of the membranes.

4.5 Materials and Equipment

This section presents the methodology used to prepare the silica membranes over porous ceramic alumina support. Two types of silica membranes were prepared: the one without support modification, and the other where the support was modified with Boehmite sol prior to depositing the silica layer. Membrane characterization was carried out using SEM and EDXA.

A porous alumina support of average pore size 6000 nm (O.D = 26 mm and I.D = 20.07 mm and 6000 nm pore size) was used to prepare composite silica membrane. Both single and multi layer deposition was carried out on the porous

alumina support. The preparation of the membranes was carried out in two parts. In part 1, the composite silica membrane was prepared without any modification of the alumina support while in part 2, the alumina support was modified with Boehmite sol prior to deposition of the silica layer. The investigations were carried out for two separate silica coatings. The modification of the support involves deposition of an intermediate layer of Boehmite sol prior to deposition of the silica layer. The unmodified support was calcined at 873 K at 2° C/min to ensure a smooth surface for deposition of the silica layer. The same calcination cycle was used for the modified support.

For the modified support, two sequential dippings were carried out to investigate the effect of film thickness on hydrogen permeance and membrane selectivity. Film thickness was determined using the weight gain method. The objective is to investigate the effect of support modification with AlO(OH) on the quality of the silica layer coating and by implication the hydrogen permeation behavior of the silica membrane and also that of the other gases. The significance of modifying the support was to provide a uniform and defect free surface for deposition.

This will ensure a more uniform coating of the silica layer and enhance hydrogen permeation through the membrane.

4.5.1 Materials

1. Silicone elastomer SYLGARD 184: This chemical was supplied by Farnell and used as the silica precursor.
2. Aluminium monohydrate AlO (OH): (Boehmite Powder). Supplied by Alcan Chemical Europe and used in modification of the support.
3. 2-methyl butane (Isopentane): This chemical was supplied by Fischer Scientific and used as the solvent to prepare the silica gel.
4. SYLGARD Curing agent: This chemical was supplied by Farnell and used for
5. Acetone: This chemical was supplied by Fischer scientific and used in washing up and preparation.
6. Distilled water: Distilled water was obtained from the pharmacy and life sciences department RGU and used in washing up.

4.5.2 Equipments

The equipments used for both the preparation of silica and AlOOH modified silica membranes are as follows:

1. Test tube 1000 ml
2. Beaker
3. Magnetic stirrer
4. Furnace
5. Fume cupboard
6. Stirrer
7. Graphite seals
8. Plastic seals
9. Drier
10. Gas Flow meter
11. Gas Chromatograph (Varian 3800)

4.5.3 Gases

1. Hydrogen: (Purity 99.995%, P=175 bar): This gas was supplied by BOC gases and used in single gas permeation tests and also during reduction of palladium membrane to activate the palladium layer prior to gas permeation test.
2. Helium: (Purity 99.99%, P=230 bar): This gas was supplied by BOC gases and used as a carrier gas to calibrate the GC, perform helium leak test and in single gas permeation experiments.
3. Argon: (Purity 99.995%, P=230 bar): This is another inert gas like Helium supplied by BOC gases and used as a carrier gas to calibrate the GC, perform helium leak test and in single gas permeation experiments.
4. Nitrogen: (Purity 99.99%, P=230 bar): This gas was supplied by BOC gases and used in single gas permeation tests.
5. Methane: (Purity 99.99%, P=230 bar) This gas was used in single gas permeation test.
6. Carbon Dioxide: (Purity 99.995%, P=50 bar). This gas was used in single gas permeation tests.
7. Gas Mixture: A hydrogen mixture with the composition. ($H_2 = 50\%$, $CO = 28\%$, $CO_2 = 10\%$, $CH_4 = 8\%$, $N_2 = 4\%$).

4.5.4 Alumina Support Tubes

The porous alumina support tubes were supplied by CTI (Ceramiques Techniques Industrielles SA) France with 6000 nm average pore size, I.D = 20.07 mm, O.D = 26 mm and effective length = 0.32 m

4.6 Experimental Procedure

4.6.1 Conventional Method for Preparation of Silica Membranes

To prepare the silica solution, 100 ml of silicone elastomer was weighed into a test tube and diluted with 900 ml 2-methyl butane (isopentane). 9 ml of curing agent were added into the solution. The solution was prepared under continuous stirring for 3 hours to obtain a properly diluted silicone elastomer solution. Silicone elastomer was used due to its advantage of improved adhesion resistance and tensile strength. Prior to deposition of the silica layer, the 6000 nm alumina support was first dried at 65⁰ C for 2 hours after which it was stored overnight at room temperature. The dried support was dipped into the silica solution for 30 minutes.

However, adequate care was taken such that the entire permeable surface area of the support was in contact with the solution. Also, the support was placed central and vertical to avoid tilting sideways which could lead to uneven coating. After the dipping procedure, the support was withdrawn and dried using the WEIR 413D motor powered rotatory drier as shown in Figure 4.2 for 3 hours after which the membrane was stored overnight at room temperature. The dried composite membrane was calcined at 873 K for 10 hours at a rate of 2⁰ C per minute to ensure better adhesion of the silica layer to the support. After the calcination, the membrane was weighed and then inserted into the membrane reactor. The graphite seals were securely tightened to avoid leaks. Gas permeation tests were carried out over the temperature range 298 K – 573 K at a transmembrane pressure difference of 0.05 to 0.4 bar.

The gas flow from the feed (inlet) was controlled through pressure gauges and the permeate and retentate outlets were measured using digital flow meters. In

the CPIMT laboratory at the Robert Gordon University, there are 2 types of mass flow meter: one measures high flow rates in L/min while the other measures low flow rates typically below 1000 mL/min. A uniformly coated silica membrane with a smooth surface was obtained. This membrane was dried in an oven at 65⁰ C for 2 hours prior to permeation tests.

**Motor powered
WEIR 413
electric drier**



**Ceramic Alumina Support
During drying process**

Figure 4.2: A Picture of Silica membrane dried at room temperature using the WEIR 413D motor power rotatory drier.

4.6.2 Modified Method for Preparation of Silica Membranes

In preparing the silica membrane modified with Boehmite sol, 46.1 g of Boehmite powder was diluted in 900 mL of distilled water in a 1000 mL test tube and the resulting solution stirred continuously for 3 hours. Boehmite sol can provide very good intermediate layers for α -Alumina supports including enabling better adhesion of the active layer of the substrate, better control of the coating, ensuring a uniformly seeded layer and reducing the defects of the membrane support.

The same procedure as in section 4.6.1 was used to dry the support after which it was dipped into the Boehmite solution under continuous stirring for 1 hour. In determining the thickness of the membrane, the weight gain method was also used here. However, the thickness for the modified method will be higher than that of the conventional method as a result of the introduction of the intermediate Boehmite layer. The support was dried using the WEIR 413D rotatory drier for 3 hours and stored overnight at room temperature after which the deposition of the silica layer was carried out using the same procedure as in section 4.6.1.

4.6.3 Gas Permeation Test Plant

Gas permeation tests were carried out in a permeation test set up consisting of a tube and shell membrane reactor and a gas flow system comprising of three connected parts: the feed, permeate and retentate. The other parts of the experimental set up consist of the mass flow meter which monitors the gas flow rate. It is pertinent to highlight that the same gas permeation set up used for palladium membranes in chapter 3 section 3.4 was also used for silica membranes.

4.7 Reference

1. Khatib, S.J. & Oyama, S.T. (2013). Silica membranes for hydrogen separation prepared by chemical vapour deposition (CVD). *Separation & purification technology*, 111, 25:20-42.
2. Lee, D. & Oyama, S.T. (2002). Gas permeation characteristics of a hydrogen selective supported silica membrane. *Journal of Membrane Science*. 210: 291-306.
3. Gu, Y. & Oyama, S.T. (2007). Ultrathin, hydrogen-selective silica membranes deposited on alumina-graded structures prepared from size-controlled boehmite sols. *Journal of Membrane science*, 306:216-227.
4. Brinker, C.J. & Hurd, A.J. (1991). Fundamentals of sol-gel dip-coating. *Thin solid films*, 201, 1:97-108.
5. Zhu, J., Fan, Y. & Xu, N. (2010). Modified dip-coating method for preparation of pinhole free ceramic membranes, 367, 1-2:14-20.
6. Alfari, S., Valenzuela, M.A. & Bosch, P. (2008). Hydrogen separation using silica membranes. *International conference on materials science*, Bucharest, Romania.
7. Yoshino, Y., Suzuki, T., Nair, B.N., Taguchi, H. & Itoh, N. (2005). Development of tubular substrates, silica based membranes and membrane module for hydrogen separation at high temperature. *Journal of membrane science*, 267, 1-2:8-17.
8. Lee, D., Zhang, L., Oyama, S.T., Niu, S. & Saraf, R.F. (2004). Synthesis, characterization and gas permeation properties of a hydrogen permeable silica membrane supported on porous alumina. *Journal of membrane science*, 231, 1-2: 117-126.
9. Kim, S-S. & Sea, B-K. (2001). Gas permeation characteristics of silica alumina composite membranes prepared by chemical vapor deposition. *Korean journal of chemical engineering*, 18, 3:322-329.

CHAPTER 5

CHAPTER 5.

5.0. Alumina Membranes for Hydrogen Separation and Purification

5.1. Background

Porous ceramic alumina membranes with different pore sizes can be considered for several gas separation applications including hydrogen by reducing the pore sizes or by improving specific surface properties [1]. Interest is growing in porous ceramic alumina membranes for hydrogen processes due to their ability to withstand harsh operating conditions, thermal and mechanical stability as well as their resistance to corrosion.

The hydrogen permeation and transport behavior in porous alumina membranes has been reported by several authors [2] [3]. Li et al [2] investigated the permeance of hydrogen across porous alumina ceramic membrane which was graded with a top γ - Al_2O_3 layer with a pore diameter 4 nm using the sol-gel technique [2]. In their work, H_2 permeation tests were conducted at temperature from 25°C to 500°C and the group reported a drastic decrease in H_2 permeance with increasing temperature from 25°C to 250°C but for temperatures from 350°C to 500°C , the hydrogen permeance was more stable. The H_2/N_2 selectivity reported by the group was between 2.9 – 3.4 which was lower than the theoretical Knudsen value of 3.74. The lower selectivity value below the theoretical Knudsen value indicates that there was a contribution of viscous flow [2]. Y.S Cheng et al [3] also investigated the hydrogen permeance of a mesoporous commercial alumina membrane with a nominal pore size of 5 nm. Although a hydrogen permeance of over $700\text{ cm}^2\text{ cm}^{-3}\text{ min}^{-1}\text{ bar}^{-1}$ was achieved, the alumina membrane could not separate hydrogen from town gas mixture. For H_2/He selectivity, a separation factor of 1.5 was achieved which was above the theoretical Knudsen value of 1.41 [3].

One of the ways of enhancing hydrogen permeation in alumina membranes is through surface modification with $\text{AlO}(\text{OH})$ Boehmite sol. This modification converts the topmost α - alumina layer to the more stable γ - alumina layer [3]. In this research, we investigated the hydrogen permeance and selectivity of a

commercial alumina support and the effect of temperature and pressure on gas permeance through the membrane. The hydrogen permeation behavior and selectivity of the modified γ -alumina membrane was also investigated to investigate the effect of the modification on hydrogen permeation.

5.2 Methodology

The ceramic alumina support is a macroporous membrane supplied by CTI (Ceramiques Techniques Industrielles SA) France of 6000 nm average pore size, I.D = 20.07 mm, O.D = 26 mm and effective length = 0.32 m. A second alumina support with same specifications was graded with AlOOH sol using the sequential dip - coating method. Both tubes were dried in an oven at 65^o C for 2 hours to remove any water vapor. In the dip coating method for preparation of γ -alumina membrane, the Boehmite sol was prepared into which the support was immersed for 30 minutes under continuous stirring. To prepare the Boehmite sol, 46.1 g of the AlOOH powder was weighed and diluted in 1000 mL of distilled water under constant stirring.

A fresh Boehmite sol was used for each dipping in order to obtain a uniformly coated membrane. Prior to dipping, both ends of the support were sealed with plastic seals to avoid inner deposition. Five sequential dippings were conducted and after each dipping, the modified support was dried using the WEIR 413D rotatory for 4 hours after which it was again dried using the oven for 10 hours at 65^o C. The support was then calcined at 873 K for 24 hours and a permeation test for six single gases carried out. These gases include: H₂, He, CH₄, CO₂, N₂ and Ar. The commercial alumina membrane was named AM0 while the modified alumina membrane was named AM1. The experimental set up for gas permeation consists of a shell and tube membrane reactor module, a gas flow system comprising of three sections; the feed delivery, the membrane system and the measurement system.

Gas permeation tests were conducted for both the modified and unmodified membranes at temperatures ranging from 298K – 573K. Membrane characterization was conducted using Scanning Electron Microscopy (SEM) and

the elemental composition of the membrane was analyzed using Energy Dispersive X-ray Analysis (EDXA).

5.3 Experimental Procedure

The investigation on commercial alumina support was carried out in two parts. In the first part, a fresh unmodified commercial alumina membrane (AM0) was investigated for hydrogen permeance and selectivity and also the permeation of single gases (He, N₂, CH₄, CO₂ and Ar). In the second part, a separate alumina support with the same specifications as the one used in the first part was modified with the AlO (OH) sol using the dip coating method (AM1) in order to plug any defects or pinholes and ensure a uniform surface for gas permeation. A picture of the dip coating method is shown in figure 5.1

The significance of modification of the support with AlOOH sol is to enhance the hydrogen permeation behavior of the membrane and also that of the 5 other single gases. The permeation behavior of the unmodified membrane was then compared with that of the modified membrane to ascertain the effect of the support modification in enhancing hydrogen permeation and membrane selectivity

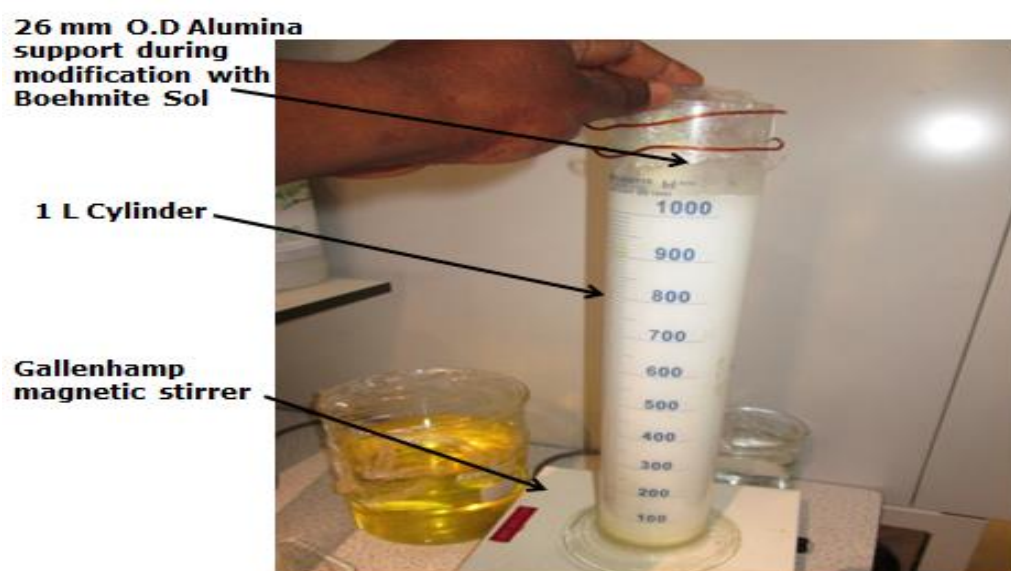


Figure 5.1: A Picture of the dip coating set up for the modification of ceramic alumina support with Boehmite.

5.4 Determination of Boehmite Layer Thickness

After each dipping, the weight of the modified membrane AM2 was measured using the weight gain technique in order to calculate of the thickness of the γ -alumina layer. The amount of AlO (OH) deposited was recorded after each dipping. The amount of deposited AlO (OH) W was measured by subtracting the weight of the alumina support before dipping from the weight after dipping. The calculation of the membrane thickness after each coating is presented in Appendix G. It is necessary to mention that the thickness was not factored into the calculation for gas permeance. Unit thickness is used to standardize permeance measurements to enable calculation of the permeability. Nonetheless, layer thickness affects gas permeation across the membrane and the higher the thickness the higher the membrane resistance to gas permeation.

5.5 References

1. Lee, H-J., Yamuchi, H., Suda, H. & Huraya, K. (2006) Influence of adsorption on the gas permeation performance in the mesoporous alumina ceramic membrane. *Separation and Purification Technology*, (49): 49-55.
2. Li, X. & Liang, B. (2012). Permeance of pure vapors in porous γ -Al₂O₃/ α -Al₂O₃ ceramic membrane, *Journal of the Taiwan Institute of Chemical Engineering*, (43): 339-346.
3. Cheng, Y. S., Pena, M.A., Fierro, J.L., Hui, D.C.W. & Yeung, K.L. (2002). Performance of alumina, zeolite, palladium, Pd-Ag alloy membranes for hydrogen separation from towngas mixture. *Journal of membrane science*, 204: 329-340.

CHAPTER 6

CHAPTER 6

6.0. Results and Discussion

This chapter presents the results and discussions for both palladium and non-palladium-based membranes prepared and investigated in this work. Prior to the electroless deposition of the palladium film, it is necessary to determine the suitability of the support for deposition by drying it free from any damp or moisture and also carrying out a Helium leak test. A 30 nm commercial alumina support with specification (I.D. 7.34 mm, O.D. 10 mm, effective length = 34 m) was dried in the oven at 65⁰ C for 2 hours after which a helium leak test was carried out.

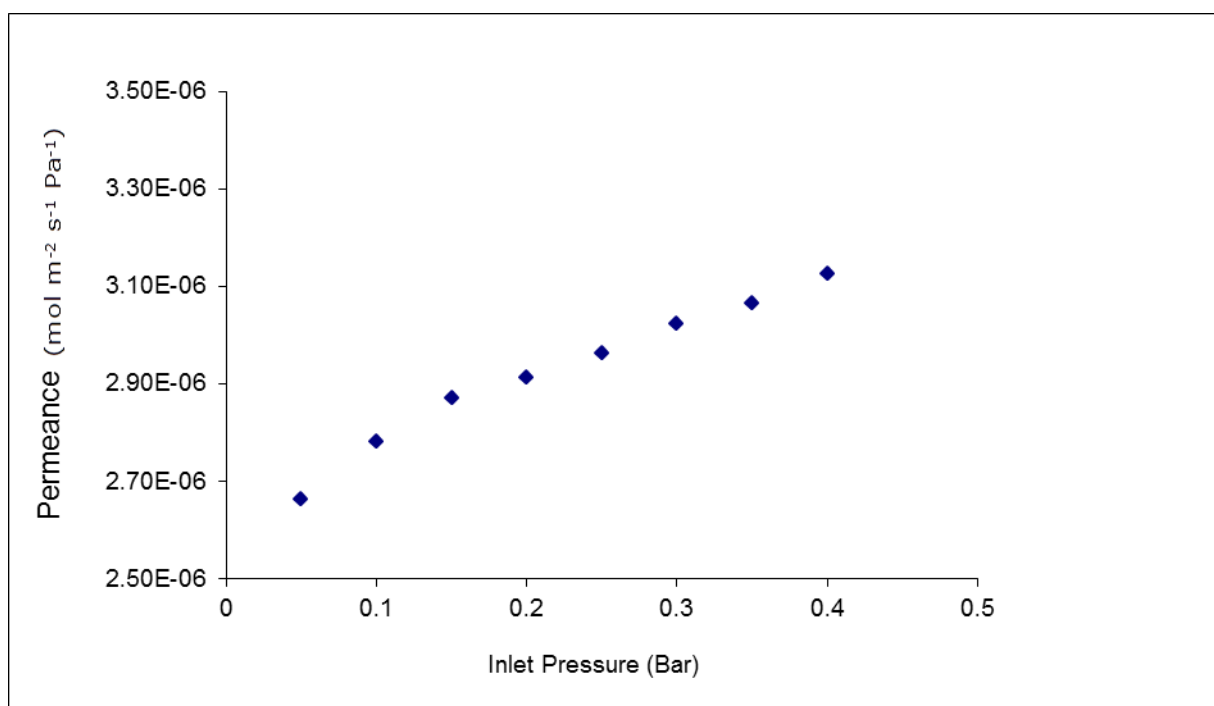


Figure 6.1: Helium permeance against inlet pressure for the tubular alumina support.

Results of the He leak test shown in figure 6.1 show a maximum Helium permeance of $3.13 \times 10^{-6} \text{ mol m}^{-2} \text{ s}^{-1} \text{ Pa}^{-1}$ at room temperature. Since the support is porous, then helium will permeate through it.

The significance of this test is to compare the He permeance before and after deposition of the Pd layer so as to ascertain the quality of the deposited Pd layer. After the deposition of the Pd layer, the permeation of He should be resisted by the Pd membrane because for a dense Pd membrane without defects or any pinholes, only hydrogen should permeate through it.

6.1: Palladium Membrane Prepared Using Conventional Electroless Plating Method (Pd1)

After the sensitization and activation step, it was observed that the support changed colour from white to dark brown due to the deposition of the palladium seeds as a result of nucleation and growth during the activation step. After the sensitization and activation process was completed, the support was dried for 24 hours at room temperature prior to electroless plating for coating Pd layer on the support. It can be observed from figure 6.2 that there was a clear colour change of the support from white (A), (before the sensitization and activation) to brown (B), (after sensitization and activation). A uniformly coated membrane palladium membrane named Pd1 with a smooth surface and of thickness 2 μm was achieved as shown in figure 6.3.



(A)



(B)

Figure 6.2: A Picture of tubular ceramic alumina support (A) Before and (B) after sensitization and activation showing clear color change.

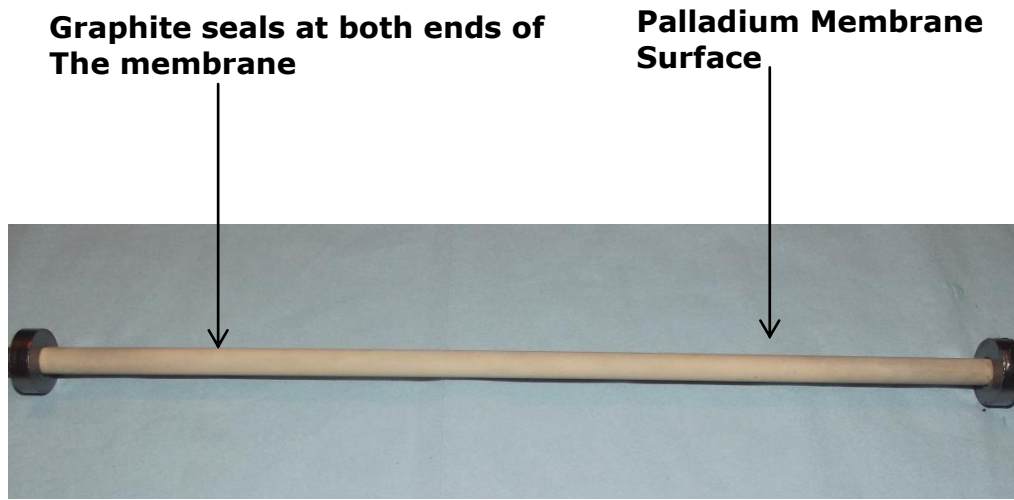


Figure 6.3: A Picture of the palladium membrane Pd1 prepared using conventional electroless plating

6.1.1 Helium Leak Test After Palladium Layer Deposition

A He leak test was carried out after the fabrication of the Pd membrane and the results shown in Figure 6.4. Helium was used to check for any defects or leaks because helium should not permeate a dense palladium membrane. Hence if it is detected in the permeate stream, then it means either the membrane is porous or there is a leak in the seals.

The maximum He permeance after deposition of the Pd layer was $9.67 \times 10^{-8} \text{ mol m}^{-2} \text{ s}^{-1} \text{ Pa}^{-1}$. The maximum He permeance after deposition was lower than the $3.13 \times 10^{-6} \text{ mol m}^{-2} \text{ s}^{-1} \text{ Pa}^{-1}$ which was the maximum permeance for the fresh unmodified alumina support before deposition of the Pd layer. The lower He permeance for the composite Pd membrane indicates that the deposition of the metallic Pd layer was successful. Albeit for a defect free and dense Pd membrane, only H_2 should permeate through when it is dense.

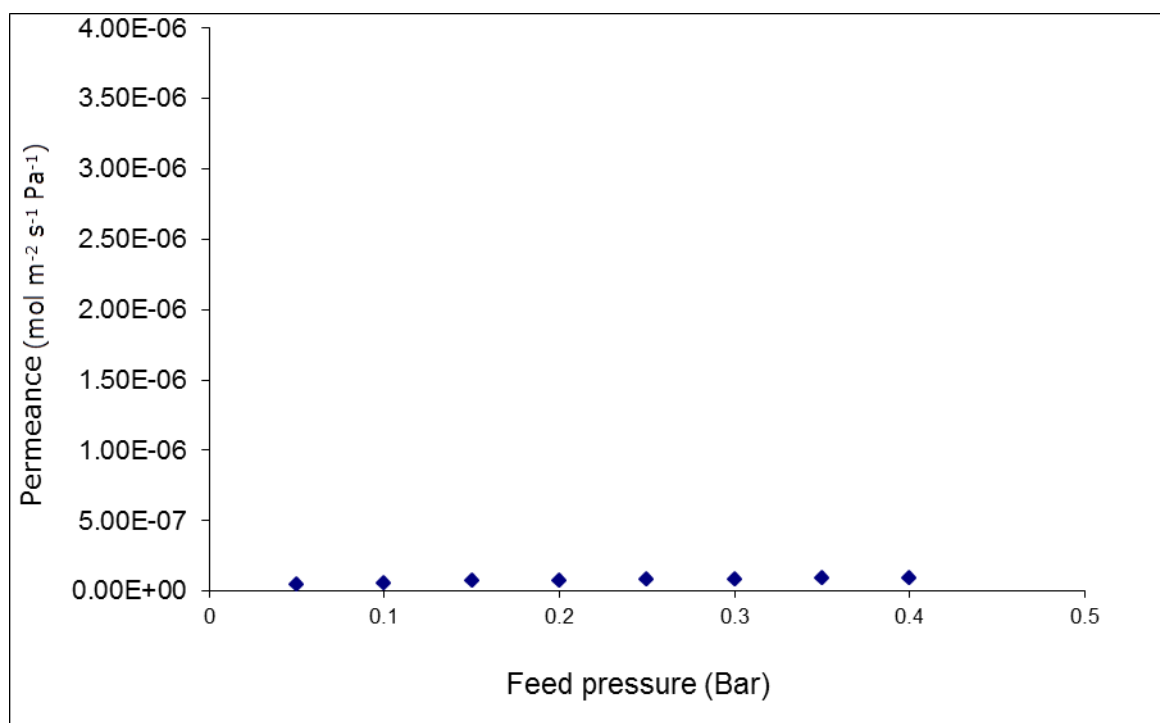


Figure 6.4: Helium permeance against inlet pressure for the palladium membrane Pd1

6.1.2 Permeation Test for Pure N₂ Gas Through Pd1 Membrane

The uniformity of coating and smoothness of the metallic surface is an important criterion in determining the quality and H₂ permeation performance of the palladium membrane [1]. To further investigate the smoothness of the coated active palladium layer, the permeation of Nitrogen through the membrane was investigated at different temperatures and transmembrane pressure difference. The investigation was carried out at a temperature between 623K to 723 K and transmembrane pressure difference 0.05 – 0.4 bar. Figure 6.5 shows the nitrogen flux at feed pressures from 0.05 bar to 0.40 bar.

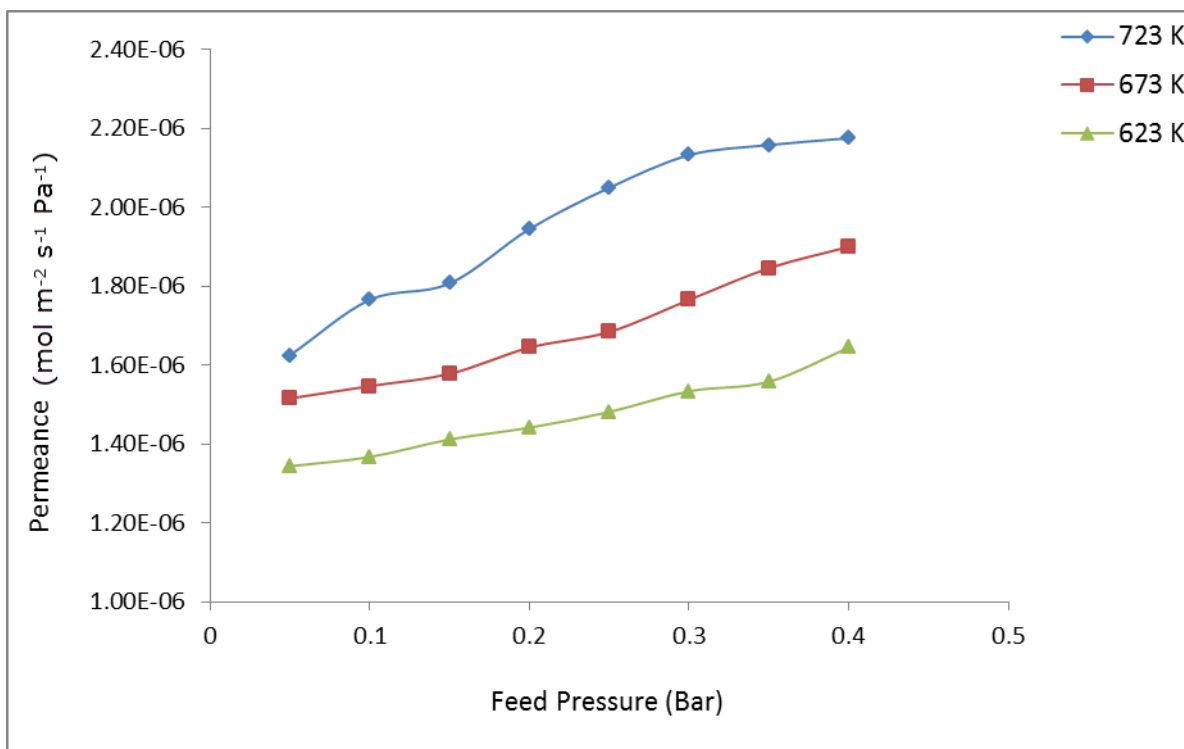


Figure 6.5: Nitrogen Permeance against feed pressure for the Pd1 membrane

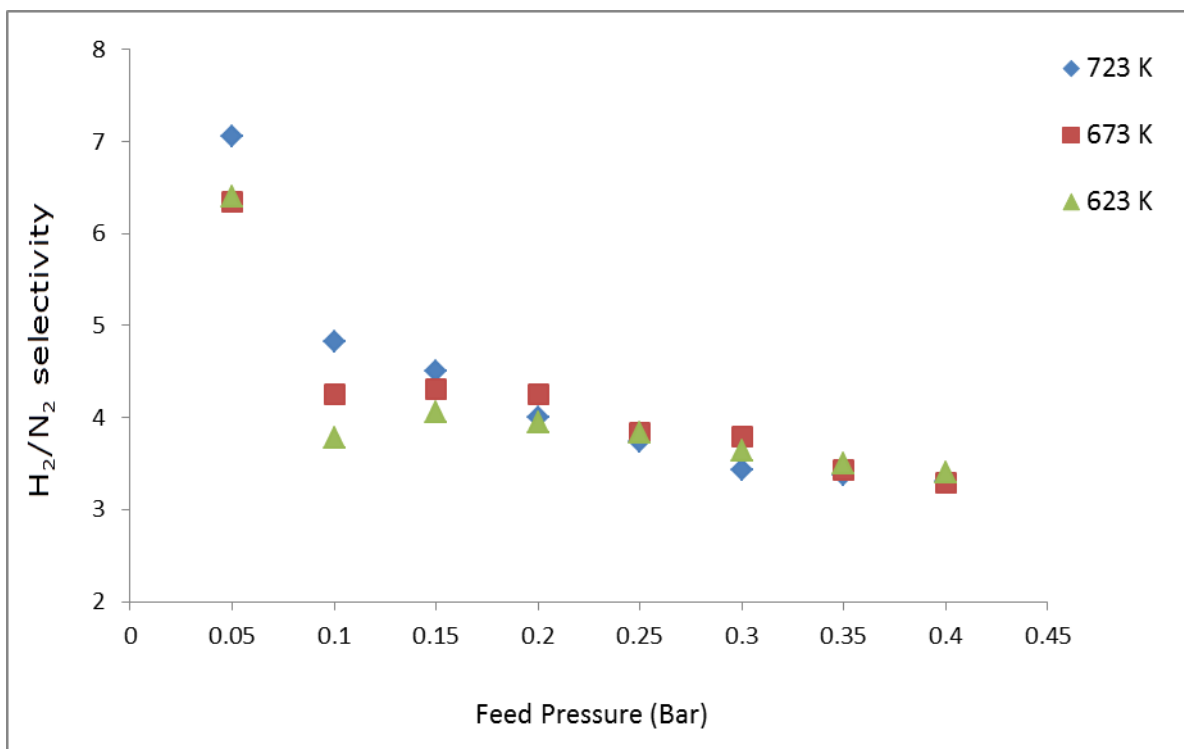


Figure 6.6: H_2/N_2 selectivity against feed pressure for the Pd1 membrane

Figures 6.4 and 6.5 show that both helium and nitrogen permeated through the membrane although both gases displayed low permeance. The maximum permeance for helium was $1.29 \times 10^{-7} \text{ mol m}^{-2} \text{ s}^{-1} \text{ Pa}^{-1}$ at 723 K while the highest flux for nitrogen was $1.9 \text{ cm}^3 \text{ cm}^{-2} \text{ min}^{-1}$ at same temperature and pressure. The highest H_2/N_2 selectivity observed is 24.12 at 673 K and 0.4 bar which is higher than the theoretical H_2/N_2 Knudsen selectivity (3.74). In Figure 6.6 it can be observed that the H_2/N_2 selectivity increased with increasing temperature and pressure as the gases are forced through the membrane pores. In practice, the N_2 molecules must have permeated through the pores because the membrane is porous.

Another factor that could affect the membrane's hydrogen permeation performance is contamination from Tin impurities which occur during the sensitization step during the support modification prior to deposition of the Pd layer. From the EDXA elemental composition in figure D2 (Appendix D) it can be observed that there are Tin impurities which constitutes 3.54 wt% in the membrane. These impurities contaminate the active layer and block sites for hydrogen permeation which retards hydrogen permeation through the membrane [2]. To avoid leakages during the permeation test, the graphite seals were tightly fitted and soap bubbles applied to check for leaks in the membrane tubes. The total time spent on the 2 step sensitization and activation (support modification) process before deposition of the active palladium layer is calculated as follows:

Sensitization step= 5 (minutes) \times 10 (dips) = 50 minutes

Activation step = 5 (minutes) \times 10 (dips) = 50 minutes

Rinsing with distilled water = 90 seconds \times 2 = 3 minutes

Total: 1 hour 43 minutes

This long time duration during sensitization and activation makes the electroless plating process prone to errors and contamination.

6.1.3 Single Gas Permeation Test for Pd1 Membrane.

After the preparation of the composite palladium membrane named Pd1, single and mixed hydrogen permeation tests were conducted to investigate the hydrogen permeation and separation behavior of the membrane. The inlet pressure (feed) was adjusted with a pressure gauge. Prior to the permeation test, the membrane was reduced in flowing hydrogen at 350⁰ C for 10 minutes to activate the palladium layer. The permeation tests for hydrogen were carried out above the critical temperature of 300⁰ C to avoid hydrogen embrittlement.

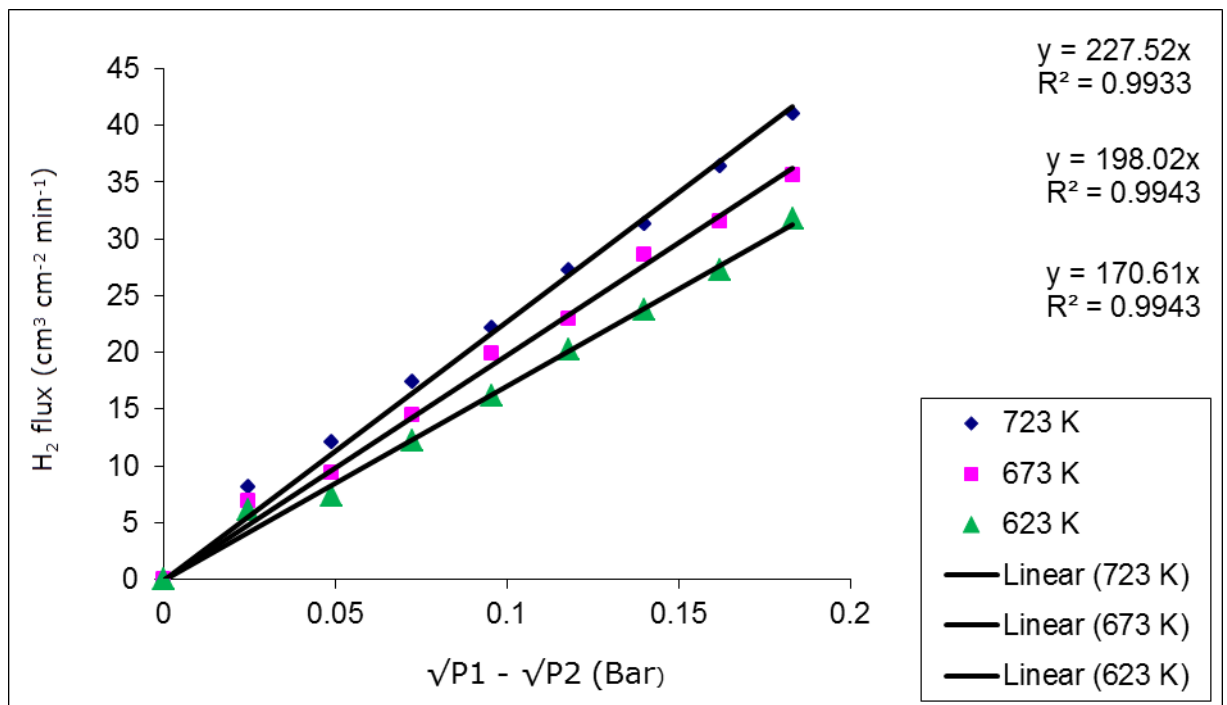


Figure 6.7: Hydrogen flux against square root of partial pressure difference for the Pd1 membrane

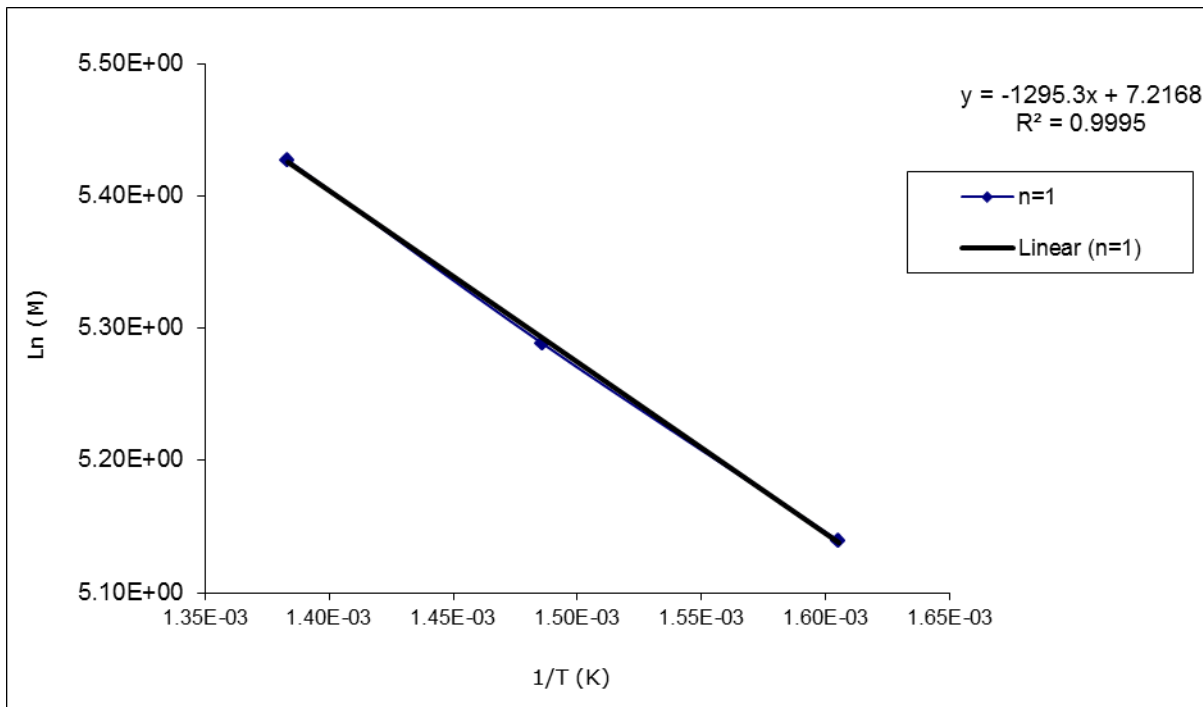


Figure 6.8: Arrhenius Vant-Hoff plot for single hydrogen permeation through Pd1 membrane

Figure 6.7 shows that hydrogen flux is directly proportional to the square root of the partial pressure difference between the high pressure (feed) and low pressure (permeate). This is in accordance with Sievert's law thus the value of the pressure exponential $n = 0.5$ which indicates that the rate limiting step in hydrogen permeation is bulk diffusion [2]. However, n values of 0.5 are usually valid for thick films (>0.5), although several authors have reported n values of 0.5 for thin films (<0.5) [3] [4] [5]. It can also be observed that Hydrogen flux increased with increasing temperature and transmembrane pressure difference. The maximum hydrogen flux observed was $41.0 \text{ cm}^3 \text{ cm}^{-2} \text{ min}^{-1}$ at 723 K and 0.4 bar.

From Figure 6.8, it can be observed that the temperature dependence on hydrogen permeation follows the Arrhenius-vant Hoff behavior with a correlation coefficient of 0.9989. The activation energy was calculated from the slope as 10.77 kJ/mol which represents the effect of temperature on hydrogen permeation through the membrane. Our observed value is in agreement with values reported in literature by several authors [6], [7] [8].

It can also be observed from figure 6.8 that the temperature dependency on Hydrogen permeation between 723 and 673 K was less significant compared to 623 and 673 K. This indicates that at lower temperature, the effect decreased but the hydrogen flux increases. In other words, the hydrogen flux at feed pressure of 0.3 bar increased at 23.8, 28.6 and 31.3 $\text{cm}^3 \text{cm}^{-2} \text{min}^{-1}$ for 623, 673 and 723 K respectively. However the difference in flux between 673 and 623 K was 4.8 $\text{cm}^3 \text{cm}^{-2} \text{min}^{-1}$ which decreased to 2.7 $\text{cm}^3 \text{cm}^{-2} \text{min}^{-1}$ differential H_2 flux between 673 and 723 K. This indicates that the temperature effect was becoming less significant.

6.1.4 Effect of Annealing on Hydrogen Permeation Through Pd1 Membrane

After the permeation test for the Pd1 membrane, it is necessary to investigate how best H_2 permeation through the membrane can be enhanced/maximised. The Pd1 membrane displayed a maximum hydrogen flux of 41.0 $\text{cm}^3 \text{cm}^{-2} \text{min}^{-1}$ at 723 K and 0.4 bar. One way of enhancing hydrogen permeation is to anneal the membrane in hydrogen at high temperature. Annealing is a form of heat treatment and it results in structural transformation for surface morphology, grain size, pore size, removal of water vapour and surface contaminants to enhance Hydrogen permeation [9].

The membrane was annealed at 673, 773 and 873 K for 10 hours in hydrogen and the temperature allowed to cool down to 623 K at which the hydrogen permeation was investigated at each temperature. In other words, the hydrogen permeation was measured at 623 K for each of the annealing temperatures i.e. 673, 773 and 873 K. Annealing temperature can have a significant effect on the morphology and surface properties of palladium membranes which in turn could facilitate hydrogen permeation [10]

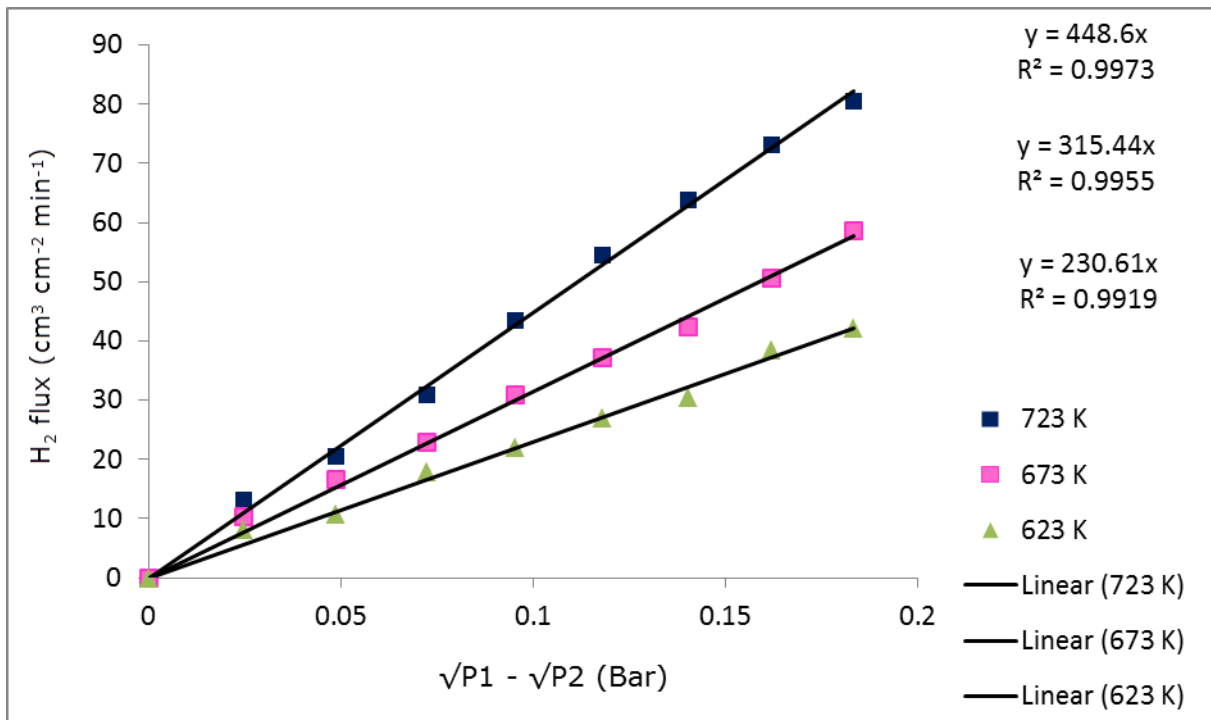


Figure 6.9: Hydrogen flux against square root of partial pressure difference after annealing the Pd1 membrane

As shown in Figure 6.9, results for the annealed Pd1 membrane indicate $n = 0.5$ which implies that hydrogen permeation through the membrane follows Sievert's law as was the case in Figure 6.7 before annealing the membrane. The annealing has no effect on the n value and rate limiting step to hydrogen permeation through the membrane. Hydrogen permeation increases with temperature giving an activation energy of 24.84 kJ/mol which is comparable to values obtained in literature [9] [10]. A maximum Hydrogen flux of 80.4 cm⁻³ cm⁻² min⁻¹ after annealing the membrane at 873 K was observed which is about two-fold higher than that of the Pd1 membrane prior to the annealing. This indicates that annealing the membrane at high temperature increased the hydrogen flux by about two- fold for the Pd1 membrane. The increase in Hydrogen flux for the annealed membranes is attributed to the removal of surface contaminants and also the formation of hydride phases [11].

6.1.5 Mixed Gas Transport Tests for Pd1 Membrane

The performance of the Pd1 membrane was also investigated for hydrogen separation from a dry reformat gas mixture with the composition ($H_2= 50\%$, $CO=28\%$, $CO_2=10\%$, $CH_4= 8\%$, $N_2=4\%$) at 623, 673 and 723 K for a transmembrane pressure difference of 0.05 to 0.4 bar. The significance of this test is to investigate the performance of the membrane in hydrogen separation from the gas mixture. The composition of the permeate stream was analyzed using an online gas chromatograph.

The procedure adopted is to connect the permeate directly to the Gas chromatograph and measure the amount of each gas based on its % composition as displayed on the Gas Chromatograph. From the total gas flow rate measured from the mass flow meter and the percentage composition of hydrogen, it is possible to calculate the flow rate of hydrogen. For example, if the total gas flow rate at the permeate side is 4.22 L/min and hydrogen is 99% from the GC analyser, then the flow rate of hydrogen is given as $4.22 \text{ L/min} \times 99\% = 4.1778 \text{ L/min}$.

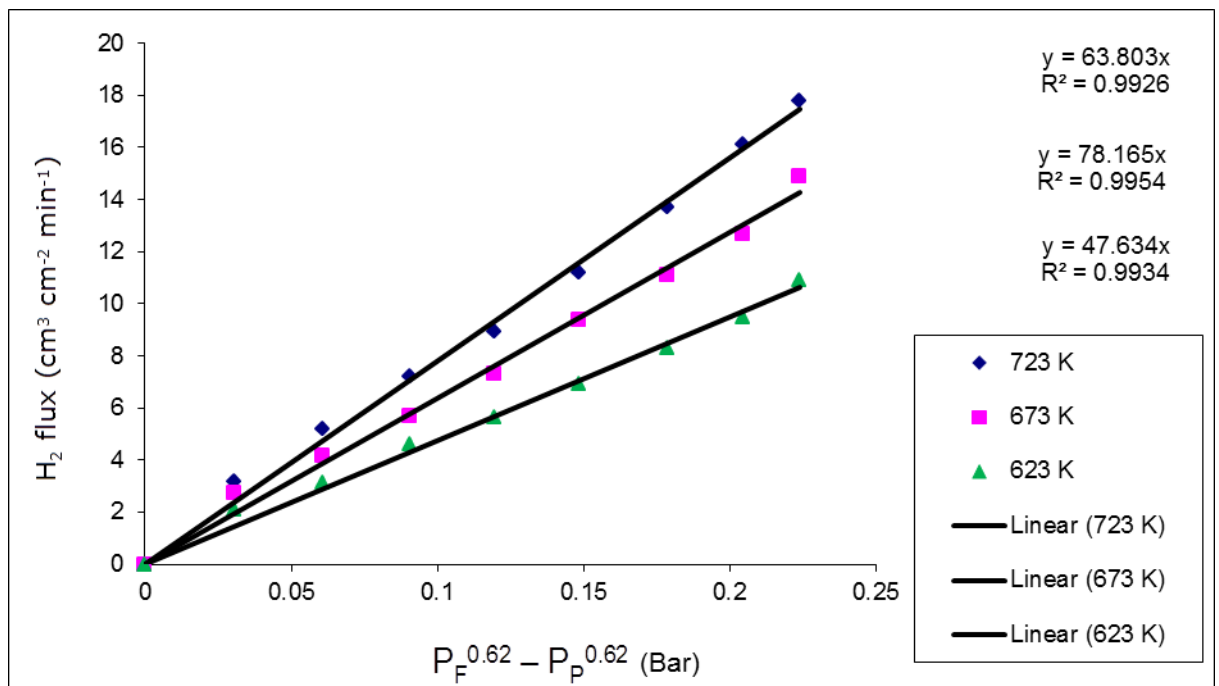


Figure 6.10: Hydrogen flux against partial pressure difference for hydrogen separation from gas mixture through Pd1 membrane.

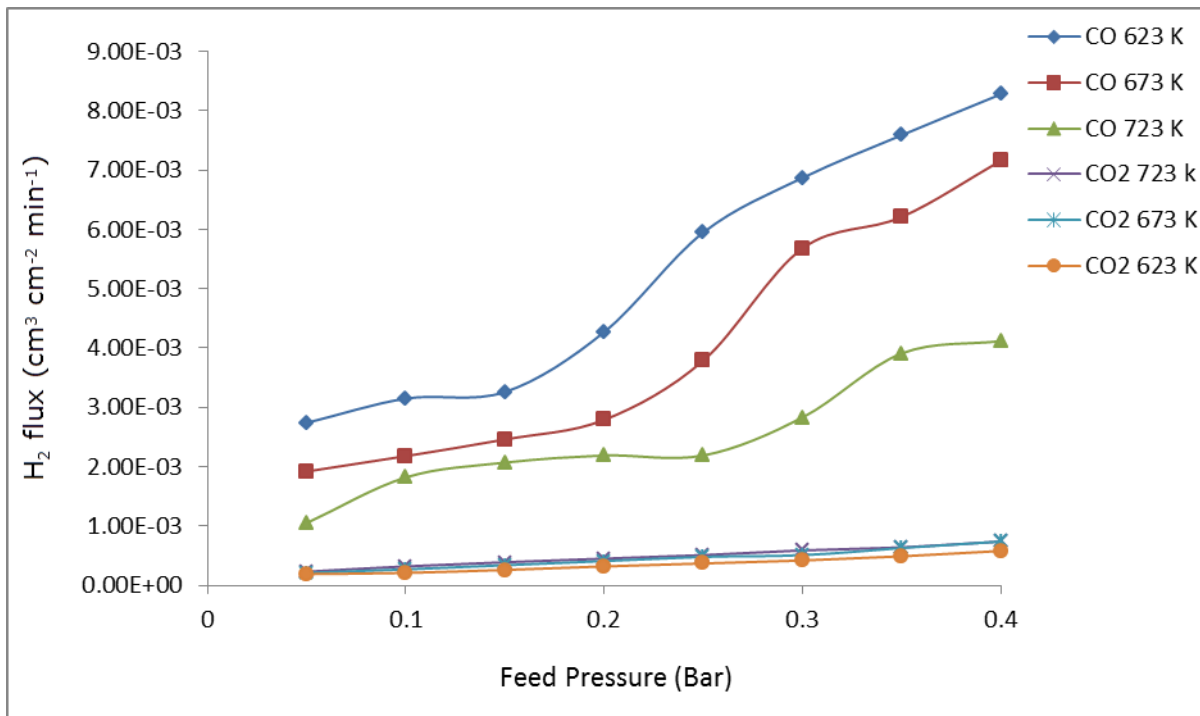


Figure 6.11: CO and CO₂ flux in the permeate stream against feed pressure before annealing the Pd1 membrane

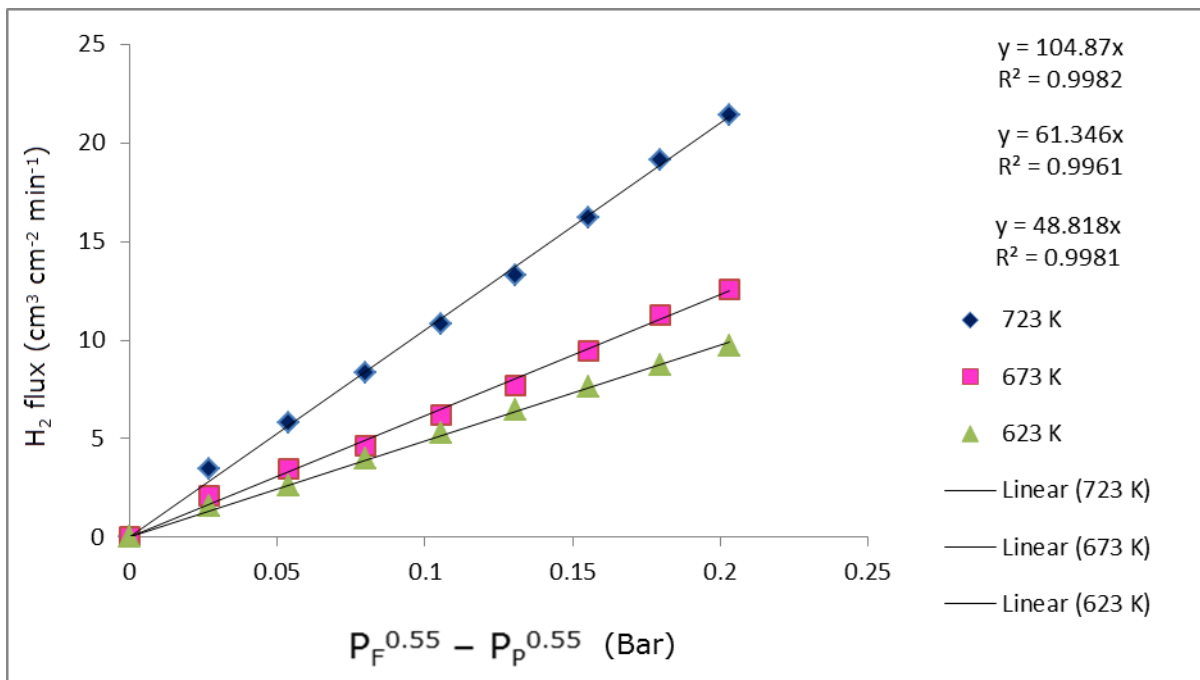


Figure 6.12: Hydrogen flux against partial pressure difference for hydrogen separation from gas mixture after annealing Pd1 membrane

From figure 6.10, it can be observed that the n value increased to 0.62 for the mixed gas separation which indicates a deviation from Sievert's law. The n value decreased to 0.55 when the membrane was annealed at higher temperature as shown in Figure 6.12. The value of the pressure exponential n before and after annealing the membrane indicates that hydrogen permeation through the membrane is determined by both surface processes and bulk diffusion. The temperature dependence on hydrogen permeation before annealing gave activation energy of 11.57 kJ/mol which is higher than the values for single gas permeation before annealing the Pd1 membrane at 10.77 kJ/mol and lower after annealing at 24.84 kJ/mol. The activation energy increased to 28.30 KJ/mol for the gas mixture hydrogen separation when the membrane was annealed at high temperature. In this case, higher temperature annealing led to an increase in the activation energy.

It can also be observed that there was a significant decrease in hydrogen flux compared to the results for single gas permeation. The H_2 flux is more stable with temperature and the maximum H_2 flux observed for Pd1 hydrogen single gas permeation is $41.0 \text{ cm}^3 \text{ cm}^{-2} \text{ min}^{-1}$ at 723 K at a transmembrane pressure difference of 0.4 bar. For the mixed gas separation, the maximum H_2 flux observed was $17.8 \text{ cm}^3 \text{ cm}^{-2} \text{ min}^{-1}$ also at 723 K at a transmembrane pressure difference of 0.05 bar to 0.4 bar. This represents a decrease of more than 2 fold for the mixed gas separation.

The Pd1 membrane should normally display high H_2 flux unless there are impediments such as pin holes, defects or carbonaceous elements/compounds such as CO and CO_2 . From figure 6.11, it can be observed that there is the presence of impurities CO and CO_2 in the permeate stream which suggests that both gases permeated through the membrane. Both gases are part of the composition of the mixed gas stream. Expectedly for a palladium membrane, the membrane should have permeated only hydrogen but this was not the case. The lower H_2 flux in the gas mixture can be attributed to the presence of carbon monoxide in the gas mixture which interacts with the membrane surface to impede hydrogen permeation [2].

This trend has also been observed by several authors [2] [12] [13]. CO inhibits hydrogen permeation through palladium membranes by blocking the sites for hydrogen adsorption and dissociation and decreasing the surface reaction rate. The amount of carbon monoxide is also increased by the presence of carbon dioxide in the mixture through the reaction of carbon dioxide with hydrogen to produce water and carbon monoxide. Invariably this increases the amount of carbon monoxide and by implication, the inhibition to hydrogen permeation [3].

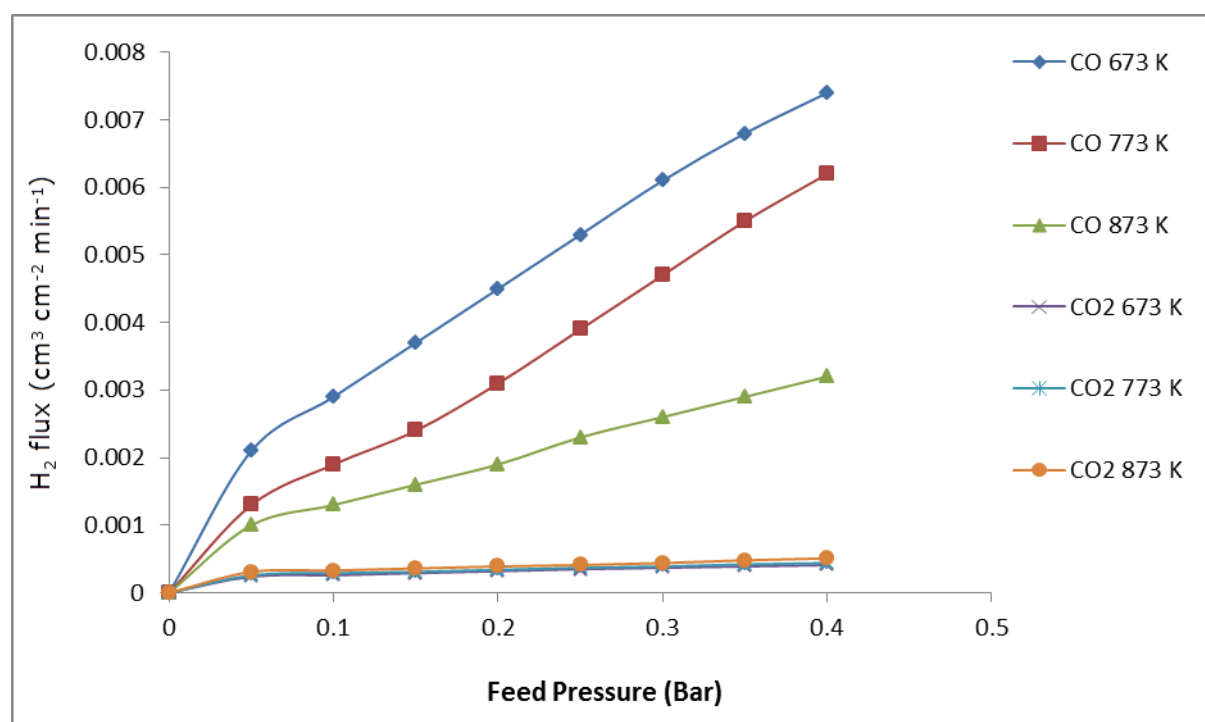


Figure 6.13: Flux of CO and CO₂ in the permeate stream against feed pressure after annealing the Pd1 membrane

Figures 6.11 and 6.13 show the flux of CO and CO₂ in the permeate stream against the feed gas pressure before and after annealing in hydrogen respectively. The CO concentration decreased after annealing which explains why the hydrogen flux increased after annealing the membrane. Annealing at high temperature ensured that there was an enhanced permeation for hydrogen as less CO was able to permeate through the membrane. Decrease in the CO

concentration implies that the surface reaction rate is faster compared to what it was before annealing the membrane.

It can be observed that the maximum flux for CO was $8.28 \times 10^{-3} \text{ cm}^3 \text{ cm}^{-2} \text{ min}^{-1}$ at 723 K and 0.4 bar before annealing which decreased to $7.40 \times 10^{-3} \text{ cm}^3 \text{ cm}^{-2} \text{ min}^{-1}$ at the same temperature and pressure after annealing. Although CO₂ reacts with hydrogen on the palladium surface to produce water and CO, both CO and CO₂ and hydrocarbons cause reduction to hydrogen permeation in palladium and palladium alloy membranes.

However, this reduction is dependant on the operating temperature as reported by several authors such as K. Hou and R. Hughes [14] who investigated the effect of impurities on hydrogen permeation and reported that CO has a significant adverse inhibiting effect on hydrogen permeation through the Pd/Ag membrane at temperatures less than 623 K [14].

In this work, the findings are different from Hou and Hughes' conclusion because the inhibiting effect of CO and CO₂ on hydrogen permeation was observed at temperatures at and above 623 K (i.e 623 – 723 K). Moreover, these findings are for a pure palladium membrane while Hou and Hughes investigated a Pd/Ag membrane. In another investigation, Amano et al [15] reported a significant hindrance to hydrogen permeation through the palladium membrane with addition of CO and CO₂ at temperature below 523 K and 473 K. This corroborates the findings in this project although the temperatures investigated here are higher compared to Amano's. Hara et al [16] also observed significant adverse CO inhibiting effect on hydrogen permeation through palladium membranes at temperatures below 553. K. Amandusson et al [17] also reported the CO effect to be more pronounced at lower temperatures due to the formation of thicker CO layers at lower temperatures.

It can be concluded based on these findings that the inhibition effect of CO and CO₂ on hydrogen permeation through palladium membranes is temperature dependent. Less CO inhibiting effect to hydrogen permeation through palladium membranes is observed at high temperatures compared to lower temperature.

The average Hydrogen purity (%) before and after annealing is shown in Table 6.1.

Table 6.1: Average H₂ purity in the dry gas reformat before and after annealing the Pd1 membrane

Before annealing	
Temperature (K)	H ₂ Purity (%)
723	94.12
673	91.56
623	89.74
After annealing	
873	96.87
773	94.61
673	93.58

From Table 6.1, it can be observed that hydrogen purity increased with temperature and the maximum recovery for pure hydrogen achieved through the membrane is 96.87 % after annealing at 873 K. The hydrogen purity expected under normal conditions for a dense palladium membrane is at least 99.99%. The slightly lower hydrogen purity was mainly due to the impurity gas i.e. CO which inhibits hydrogen permeation across the membrane.

6.1.6 Hydrogen Transport, Rate Limiting Step and n-value in Pd1 Membrane.

Any deviations from Sievert's law can be caused by many factors including defects in the metallic layer, high pressures of hydrogen, temperature, contaminants/carbonaceous compounds and grain boundaries [3]. In Figure 6.7, it can be observed that there is a linear fit with R² values of 0.9933, 0.9943 and 0.9943 for 723, 673 and 623 K respectively. The average correlation coefficient is 0.995. Our observed value for n is 0.5 which indicates that hydrogen permeation through the palladium membrane Pd1 obeys Sievert's law and bulk diffusion controls hydrogen permeation. The thickness of the Pd layer for Pd1

membrane is about 2 μm and our observed n value at temperatures above 723 K is in agreement with those reported in literature and consistent with the values for thin palladium films ($\leq 5 \mu\text{m}$) [18] [19].

For thick membranes n values greater than 0.5 can be attributed to defects and pinholes which is governed by Knudsen or viscous flow transport mechanisms [3] [20]. The n value is reported to decrease with temperature due to the surface reaction rate as the temperature increased [3]. However, higher pressures have been reported to lead to increase in the n value especially in cases of defects where hydrogen permeation is through defects in the thin films [3]. The maximum H_2/N_2 selectivity of the membrane is 7.01 which is above the theoretical Knudsen selectivity of 3.73. A metallic Pd layer with defects /pinholes is likely to deviate from Sievert's law because hydrogen permeation will be other than through the bulk metal.

The observed value of the pressure exponential n is also 0.5 as was observed before the annealing. Although the membrane was annealed at 873, 773 and 673 K, the permeation test was conducted at 623 K and an increase in the hydrogen flux was observed for the annealed membrane. Temperature increase has been reported to affect the n value due to several reasons including the removal of contaminants, reduction in the reaction rate etc [3]. For a palladium membrane with defects, hydrogen permeation occurs via a mixed Knudsen/viscous flow. The hydrogen flux through defects can be expressed by the sum of a term proportional to the pressure difference (Knudsen flow) and a term proportional to the square root of the partial pressure (viscous flow). Hence for a palladium membrane with leaks and defects, the pressure exponent n will be higher than 0.5. A thickness of 1 μm has been reported to be the critical level where the hydrogen desorption reaction (where $n=1$) as part of the surface processes, is the rate limiting step. Deviations from Sievert's law were reported for thickness $< 1 \mu\text{m}$ thickness and also for low temperatures [3].

It can be observed from Figure 6.10 that the value of n has increased to 0.62 which is a deviation from Sievert's law. In this work, the increase in the n value after the test with hydrogen mixture is attributable to the effect of carbonaceous contaminants in the mixture. The contaminants in the mixture i.e CO , CO_2 , CH_4

all have a suppressing effect on hydrogen permeation by competing with hydrogen for sites on the palladium surface. In this regard, the adsorption of the impurities decreases the rate of hydrogen absorption/desorption reactions. When the inhibiting effect of the contaminants to hydrogen permeation is severe, the n value moves to unity or very close to it and the surface processes will control hydrogen permeation. However, in our observed value of $n = 0.62$, the inhibiting effect is not severe hence the value is closer to Sievert's driving force than it is to unity.

As reported by F. Guazzone et al [3], high pressure of hydrogen could cause deviation of Sievert's law in membrane with thickness $>1 \mu\text{m}$. In fact this group of workers concluded that 1.1-2 bara for $>1 \mu\text{m}$ palladium membrane thickness will certainly lead to deviation from Sievert's law. However, in our experiment, the pressure range used is 0.05 – 0.4 bar which is less than the range stated by Guazzone and his group [3]. For high operating pressures, deviations from Sievert's should be expected and n values of 0.5-1 in which case a combination of bulk diffusion and surface processes will control hydrogen permeation through the membrane.

6.1.7 Hydrogen Embrittlement

Hydrogen embrittlement is one of the challenges posed by palladium membranes in hydrogen separation and purification which occurs as a result of $\alpha - \beta$ transition below the critical temperature of 293°C and pressure (2 MPa) which is accompanied by a lattice expansion of 3.4% [21]. This expansion results in an internal stress which leads to defects and peeling of the palladium layer. The Pd1 membrane was used to investigate hydrogen embrittlement in palladium membranes. Since permeation tests using this membrane for both single and mixed gas have been carried out, then we can afford to use the membrane to investigate hydrogen embrittlement. To investigate this phenomenon, hydrogen permeation tests were conducted on the Pd1 membrane at 150°C and transmembrane pressure difference of 0.5 - 0.4 bar. During the permeation test an abnormal smell and noise were observed coming out of the membrane

reactor. At this point, the gas supply was switched off and the reactor removed from its position and the membrane retrieved.

It was discovered that the Pd layer had cracked and peeled off from the substrate as shown in Figure 6.14 which implies that H₂ embrittlement has occurred thus rendering the membrane inactive.

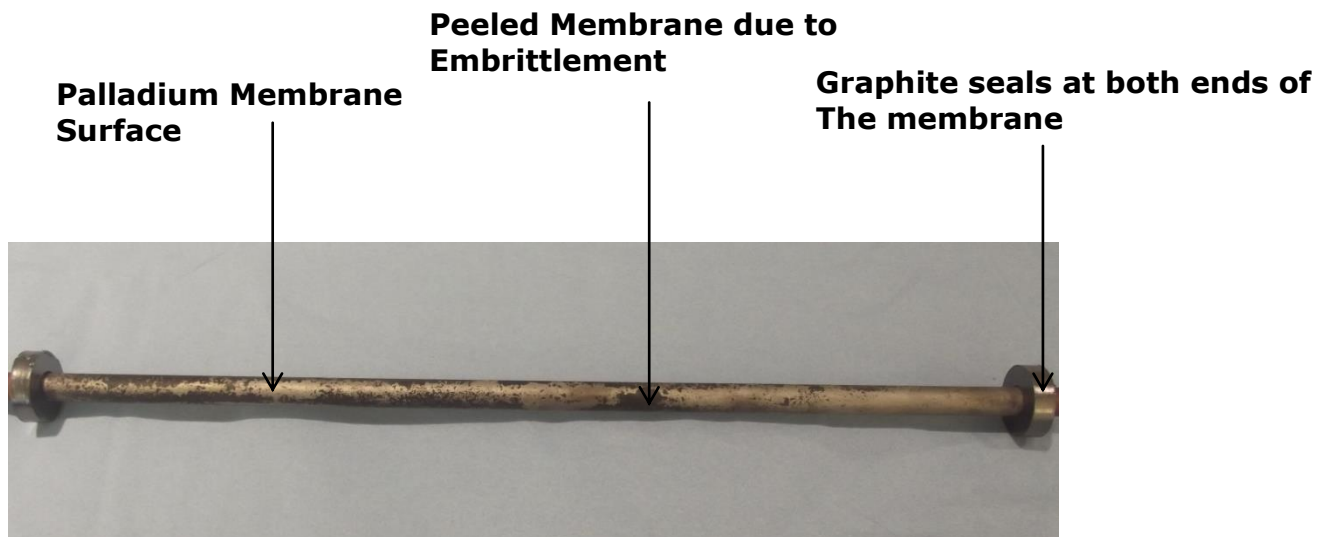


Figure 6.14: A Picture of the peeled Pd1 membrane after hydrogen embrittlement

6.1.8 Observations for Pd1 Membrane

From the investigations carried out on membrane Pd1, the following inference can be drawn:

1. A maximum hydrogen flux of $80.4 \text{ cm}^3 \text{ cm}^{-2} \text{ min}^{-1}$ was observed after annealing the membrane in hydrogen at 873 K. However, the membrane is porous because He and N₂ permeated through the it.
2. The highest percentage hydrogen purity achieved is 96.87 % after annealing the membrane at 873 K.
3. The membrane suffered from hydrogen embrittlement when hydrogen (referred to as 'cold hydrogen') was permeated through the membrane at 150⁰ C.
4. The preparation of the membrane using the electroless plating method took a long time to accomplish. The 2-step sensitization and activation took about 1

hour 45 minutes. It is apparent that the 2 step sensitization and activation process is cumbersome and prone to impurities/errors.

6.2 Palladium Membrane Produced Using the Modified Electroless Plating Method (Pd2)

From the observations for Pd1 membrane, it is necessary to prepare another membrane such that the permeation and purity of hydrogen could be enhanced. The new approach should avoid the threat of impurities from Tin during the sensitization step so as to enhance hydrogen purity and also address the long period it takes in the membrane preparation. The long period for sensitization and activation makes the electroless plating method not only cumbersome but also prone and susceptible to errors and contamination. It is in this regard that a new method was developed which skipped the sensitization step during support modification prior to electroless plating so as to achieve 3 key objectives:

1. Avoid Sn(11) Tin impurities
2. Reduce the overall time duration of the electroless plating process.
3. Prepare a Pd membrane of better quality with better adhesion of the Palladium film on the substrate for enhanced hydrogen permeation.

Although the sensitization step was skipped in the new method, the activation step was conducted for nucleation and growth of the Pd ions prior to the deposition. Also, the alumina support was modified with Boehmite sol using the dip coating technique prior to the activation method to avoid defects on the ceramic support and ensure a smoother surface for uniform coating of the palladium layer.

A uniformly seeded support was obtained from this procedure although the membrane produced is a bit darker compared to the one obtained for the modified support as shown in figure 6.15. For the deposition of the Pd film onto the modified porous support, the same procedure was used as that for the conventional method. A constant plating time of 30 minutes was maintained. A

uniformly seeded palladium membrane named Pd2 of thickness 2 μm was obtained as shown in figure 6.15.

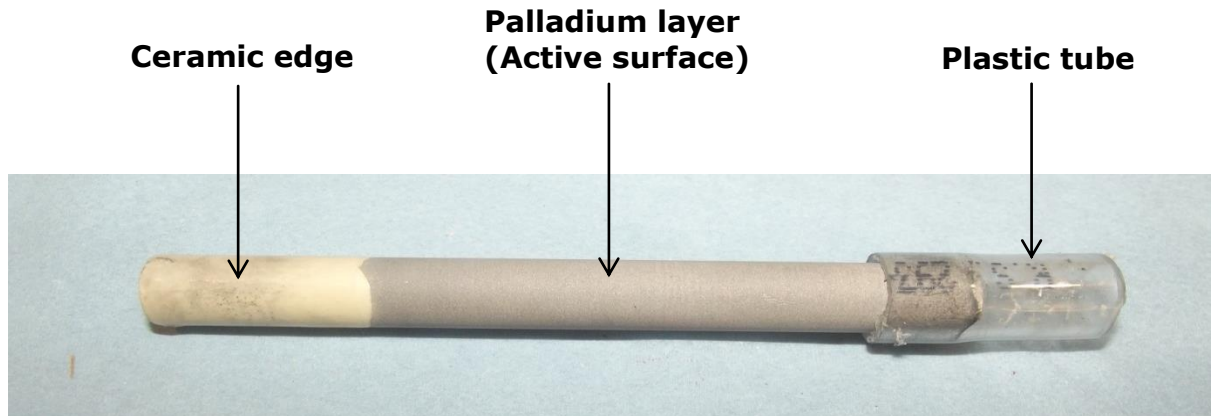


Figure 6.15: A Picture of the Pd2 membrane prepared using modified electroless plating method

6.2.1: He & N₂ Permeation Through Pd2 membrane

A leak test was carried out on the Pd2 membrane as was the case for the Pd1 membrane in order to ascertain whether the membrane is dense or porous. It can be observed from figure 6.16 that Helium permeated through the membrane with a maximum permeance of $9.11 \times 10^{-8} \text{ mol m}^{-2} \text{ s}^{-1} \text{ Pa}^{-1}$. This indicates that the membrane is porous since He was able to permeate through it. However, the He flux observed is lower than that of the Pd1 membrane prepared using conventional electroless plating method. This indicates a more smooth finish and more uniformly coated membrane compared to the Pd1 membrane. The Pd2 membrane was also investigated for Nitrogen permeation and the results in figure 6.17 show that the maximum flux observed is $1.37 \text{ cm}^{-3} \text{ cm}^{-2} \text{ min}^{-1}$ which is lower than that of the Pd1 membrane. The fact that the observed He permeance and N₂ flux for the Pd2 membrane are lower than those of the Pd1 membrane is an indication that the Pd2 membrane has a smoother finish and is more uniformly coated compared to the Pd1 membrane.

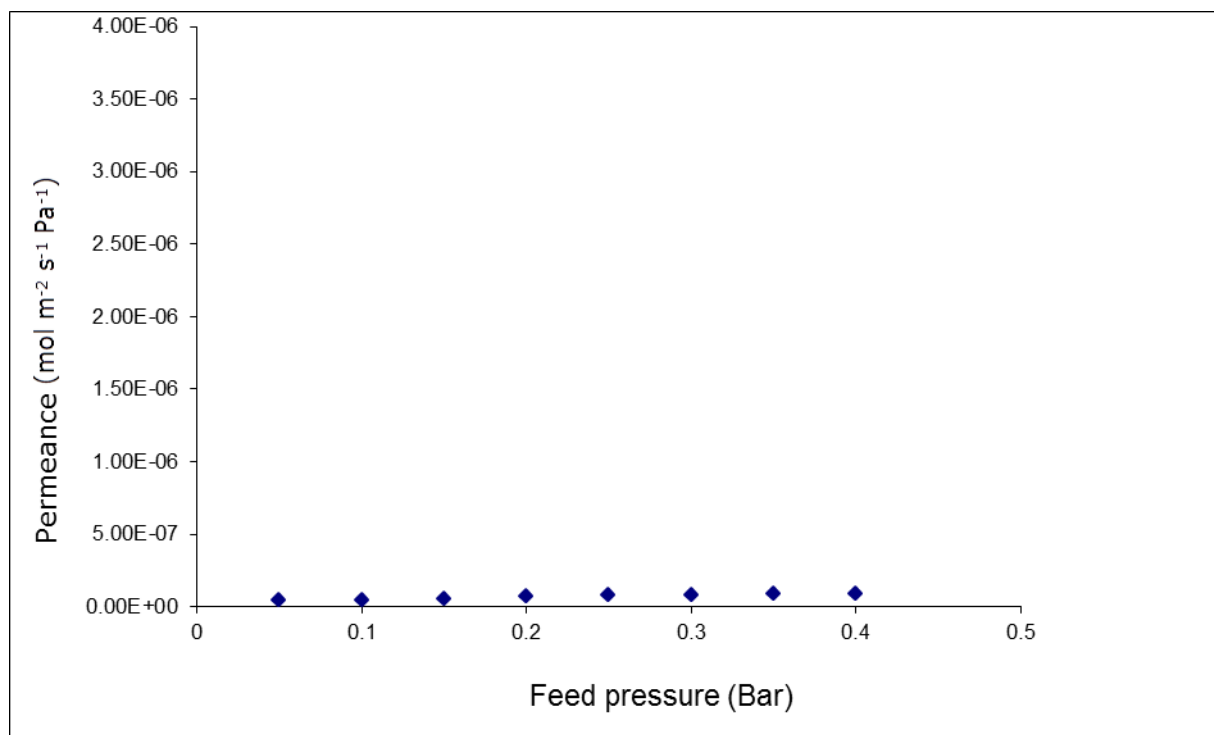


Figure 6.16: Helium flux against inlet pressure for the Pd2 membrane

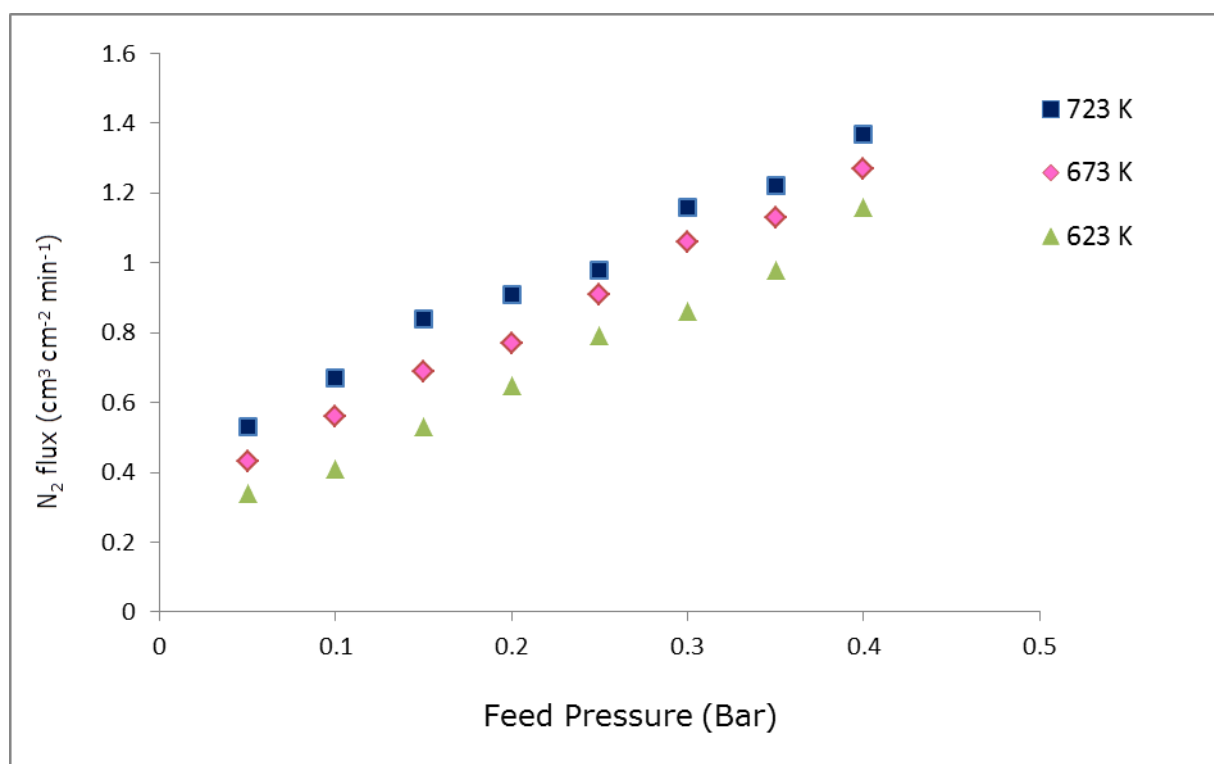


Figure 6.17: N₂ flux against feed pressure for the Pd2 membrane

6.2.2 Single Gas Hydrogen Permeation Through Pd2 Membrane

Single and mixed gas permeation tests were conducted for the Pd2 membrane. Prior to the test, the membrane was reduced in flowing hydrogen at 350⁰ C for 10 minutes to activate the palladium layer just as was done for the Pd1 membrane. Figure 6.18 shows the Hydrogen flux as a function of the partial pressure difference on the feed and permeate sides at 723, 673 and 623 K. It can be observed that there is a deviation from Sievert's law with the value of the pressure exponential $n=1$. At unity, the rate limiting step for hydrogen permeation through the membrane are the surface processes involving hydrogen dissociative adsorption on the palladium layer and/or atomic hydrogen recombination and desorption at the permeate side. The n value at unity indicates a fast rate of hydrogen permeation through the membrane normally associated with thin palladium membranes (<5 μm).

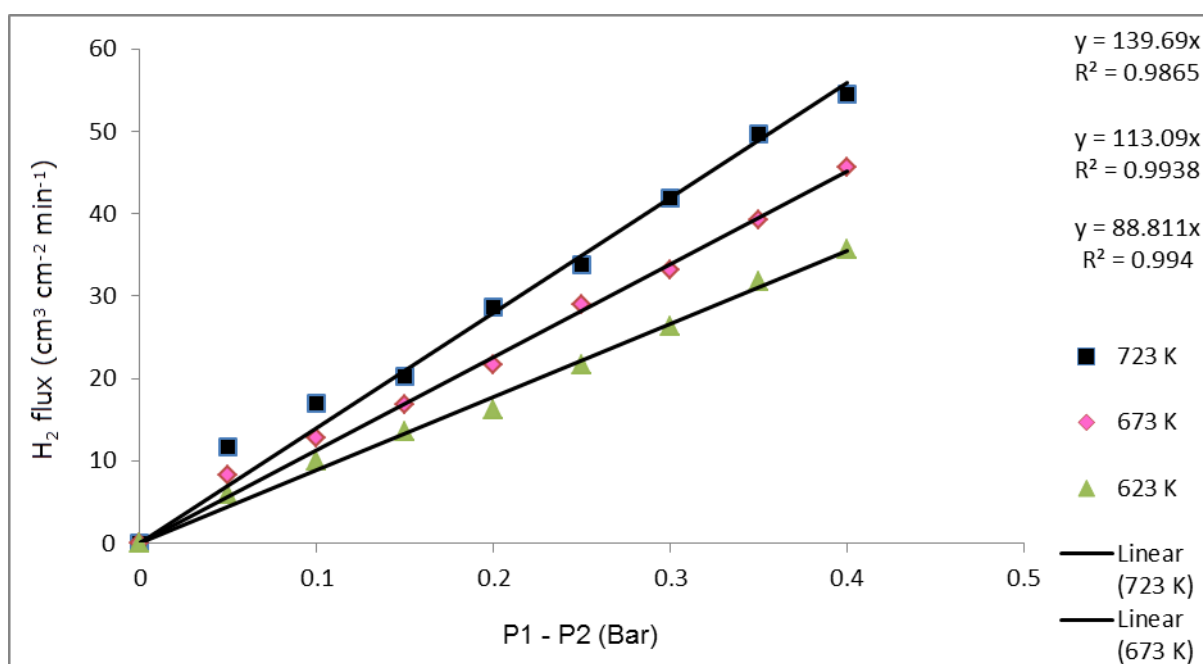


Figure 6.18: Hydrogen flux against partial pressure difference for the Pd2 membrane

The n=1 is for the Pd2 membrane prepared using the modified electroless plating method in which an intermediate Boehmite layer was used which means the hydrogen permeation was controlled by surface processes including hydrogen dissociative adsorption on the palladium surface and/or atomic hydrogen recombination and desorption.

The hydrogen permeation increased with temperature and pressure giving an activation energy of 16.96 kJ/mol. A maximum Hydrogen flux of $54.5 \text{ cm}^3 \text{ cm}^{-2} \text{ min}^{-1}$ was observed at 723 K and a transmembrane pressure differential of 0.4 bar. This indicates an increase of $13.5 \text{ cm}^3 \text{ cm}^{-2} \text{ min}^{-1}$ in hydrogen flux for the Pd2 membrane compared to the Pd1 membrane. Therefore, the new method of skipping the sensitization step has led to the fabrication of a Pd membrane that enhanced hydrogen permeation.

It can be inferred from the Pd1 membrane prepared using the conventional method that there was the hindrance to hydrogen permeation was more pronounced compare to the Pd2 membrane prepared without the sensitization step. It can also be observed from figure 6.19 that the maximum H_2/N_2 selectivity is 40.74 which is higher than that for the Pd1 membrane i.e. 7.05 and is an indication of a more uniform coating and better adhesion of the metallic film to the substrate. The maximum H_2/N_2 selectivity of the Pd2 membrane is higher than the theoretical H_2/N_2 selectivity of 1.41.

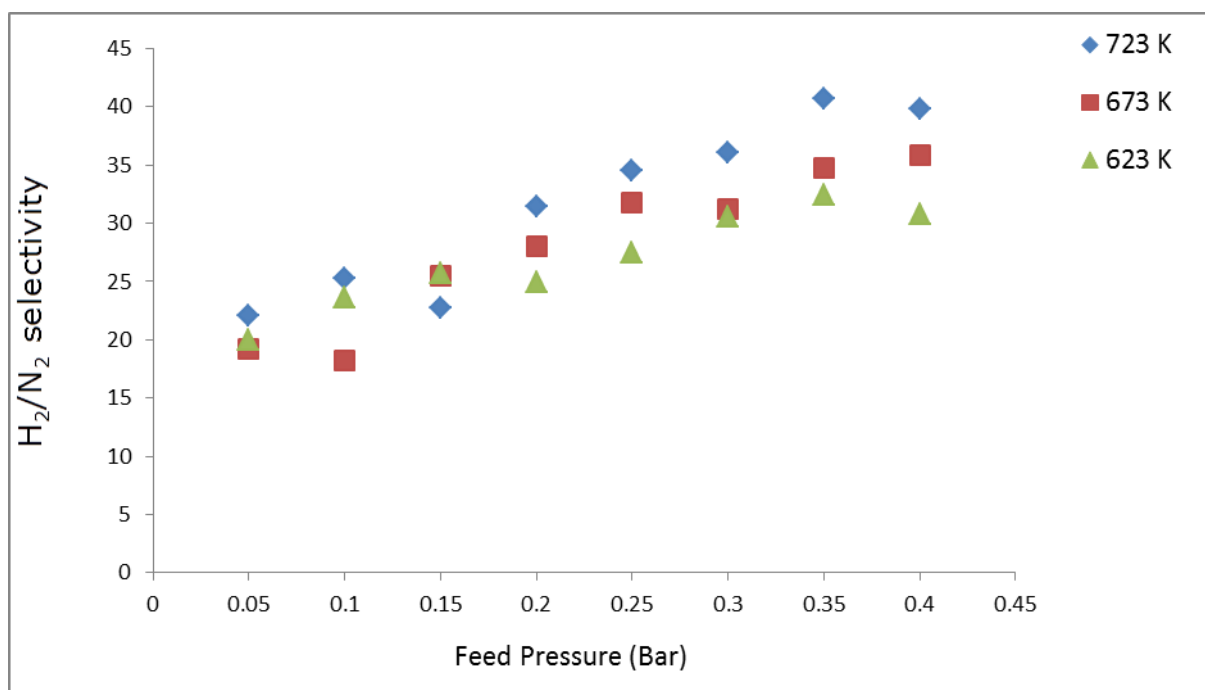


Figure 6.19: H₂/N₂ selectivity against feed pressure for the Pd₂ membrane.

The hindrance to hydrogen permeation from the Pd₂ membrane is from the Tin impurities and also poor adhesion of the Pd layer to the porous substrate. The enhanced H₂ flux for the Pd₂ membrane suggests that despite skipping the sensitization step, catalytic sites were created through the activation process. The creation of these catalytic sites was made possible by the modification of the porous alumina substrate with AlOOH sol which was chemisorbed on the alumina substrate [22]. The time duration for the electroless plating was reduced by 50 minutes which in effect reduced the cumbersome nature of the electroless plating process.

The time used for the modified electroless plating time is as follows:

Activation step = 5 (minutes) × 10 (dips) = 50 minutes

Rinsing with distilled water = 90 seconds × 2 = 3 minutes

Total: 53 minutes

The increased hydrogen flux is an indication that the adhesion of the palladium layer on the porous support has been enhanced and a more uniformly coated membrane was achieved.

6.2.3 Effect of Annealing on Hydrogen Permeation Through Pd2 Membrane

The effect of annealing on hydrogen permeation for the Pd2 composite membrane was also investigated at 873, 773 and 673 K using the same procedure as that for membrane Pd1 and the results shown in Figure 6.18. The temperature dependence on hydrogen permeation gave an activation energy of 9.22 kJ/mol which is lower than the activation energy for hydrogen permeation prior to annealing the Pd2 membrane.

It can also be observed that there is a deviation from Sieverts driving force just as was the case for the membrane before annealing. The pressure exponential n was unity just as was the case before annealing. The fact that the value of the pressure exponential n remains the same after annealing the Pd2 membrane indicates that annealing the membrane at high temperature has no significant effect on the rate limiting step in hydrogen permeation although annealing the membrane at higher temperature enhanced hydrogen permeation performance of the membrane.

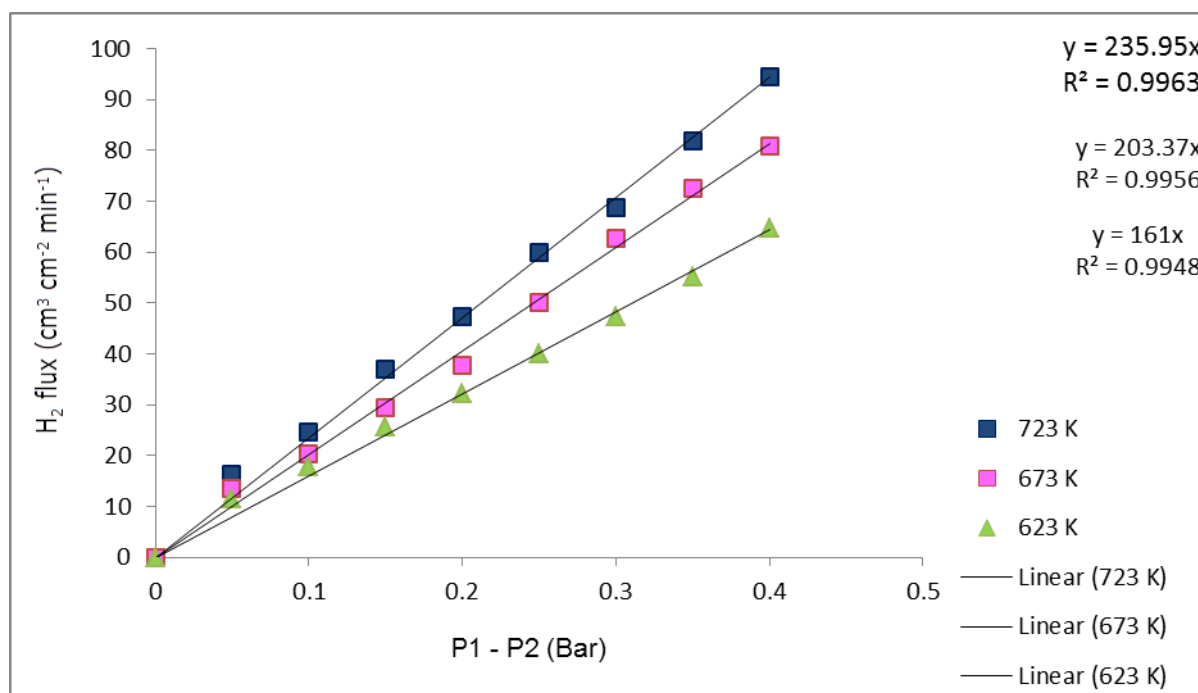


Figure 6.20: Hydrogen flux against partial pressure difference for the annealed Pd2 membrane

It can be observed in Figure 6.20 that the Pd2 membrane displayed hydrogen flux of $94.5 \text{ cm}^3 \text{ cm}^{-2} \text{ min}^{-1}$ at 723 K and transmembrane pressure difference of 0.4 bar which is higher than that of the annealed Pd1 membrane prepared using the conventional method. The temperature dependence on hydrogen permeation also gave activation energy of 14.37 kJmol^{-1} which is consistent with values reported in literature [2] [23]. There is an observed trend in the activation energy in the different investigations for Pd1 and Pd2 membranes. For hydrogen single gas permeation for Pd1, the activation energy was 10.77 kJ/mol which was higher than when the membrane was annealed at 873, 773 and 673 K (8.50 kJ/mol). The same trend was also observed for Pd2 membrane which gave an activation energy of 16.96 kJ/mol for hydrogen single gas permeation but this value decreased to 14.37 kJ/mol when the membrane was annealed.

Also in the Pd2 investigations for gas mix, the activation energy was 11.57 kJmol^{-1} but when the membrane was annealed at 873, 773 and 673 K, the activation energy increased to 28.30 kJ/mol .

6.2.4 Mixed Gas Separation and Hydrogen Purity for Pd2 Membrane

Mixed gas permeation tests were also conducted for the Pd2 membrane for the gas mixture with the composition $\text{H}_2 = 50 \%$, $\text{CO} = 28\%$, $\text{CO}_2 = 10\%$, $\text{N}_2 = 4\%$, $\text{CH}_4 = 8\%$. The procedure for the Pd1 membrane for this investigation was also used for the Pd2 membrane. The Pd2 membrane separated hydrogen from the gas mixture and also enhanced the hydrogen permeation compared to the Pd1 membrane. The flux of CO in the Pd2 permeate stream determined from the GC separation results is shown in Table 6.2.

Table 6.2: Flux of CO in the permeate stream for mixed gas separation before and after annealing Pd2 membrane

	Before annealing	After annealing
	$(\text{cm}^3 \text{ cm}^{-2} \text{ min}^{-1})$	$(\text{cm}^3 \text{ cm}^{-2} \text{ min}^{-1})$

Feed Pressure (Bar)	723 K	673 K	623 K	873 K	773 K	673 K
0.05	5.36E-04	1.06E-03	1.48E-03	4.51E-04	6.43E-04	1.07E-03
0.10	8.12E-03	1.21E-03	1.76E-03	6.10E-04	1.11E-03	1.58E-03
0.15	1.35E-03	1.56E-03	2.07E-03	6.32E-04	1.47E-03	1.73E-03
0.20	2.09E-03	1.96E-03	3.08E-03	1.16E-03	1.72E-03	1.89E-03
0.25	2.27E-03	2.55E-03	3.37E-03	1.56E-03	2.19E-03	2.47E-03
0.30	2.72E-03	3.05E-03	3.90E-03	2.21E-03	2.53E-03	2.63E-03
0.35	3.09E-03	3.57E-03	4.48E-03	2.63E-03	2.62E-03	2.98E-03
0.40	3.21E-03	4.13E-03	5.16E-03	3.09E-03	2.93E-03	3.22E-03

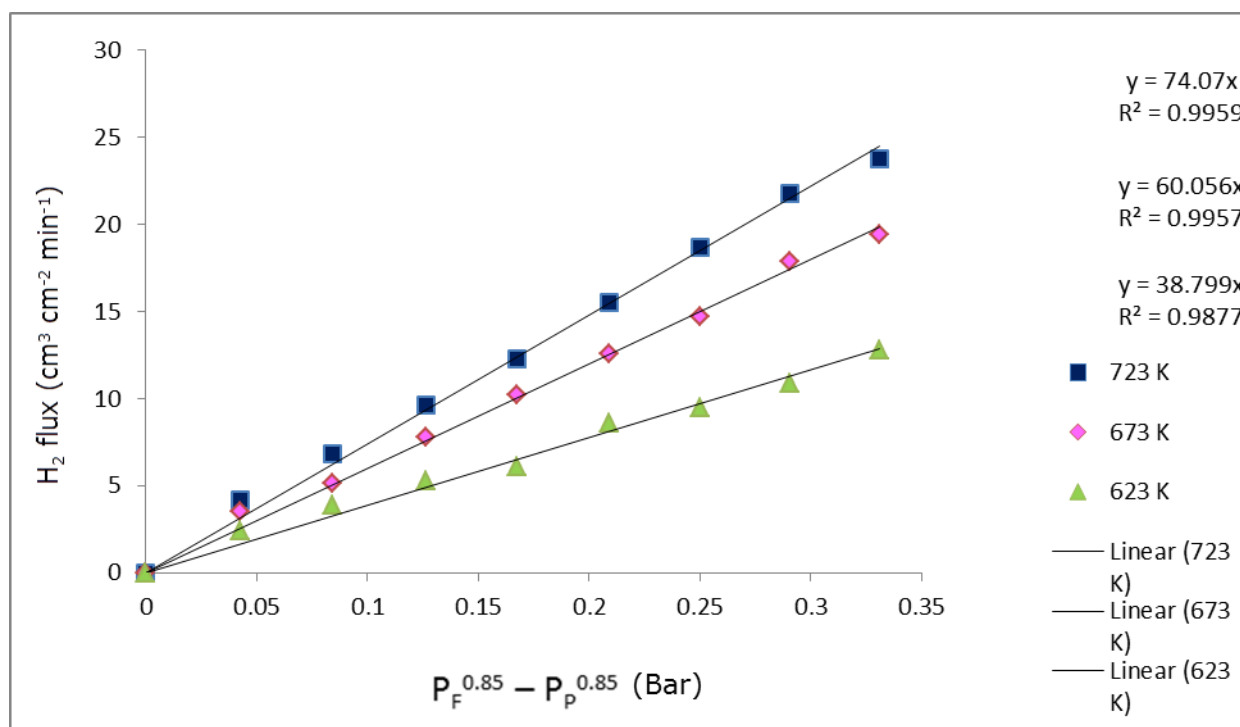


Figure 6.21: Hydrogen flux against partial pressure difference for hydrogen separation from gas mixture for the Pd2 membrane.

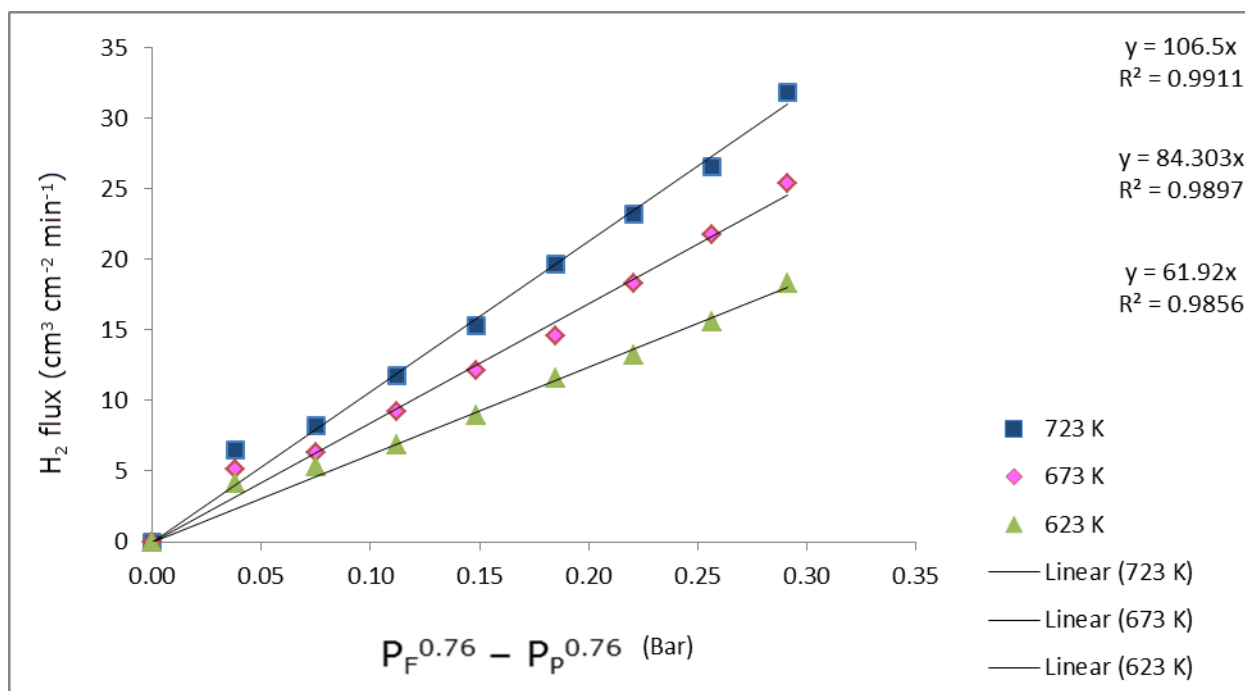
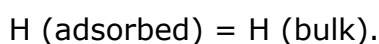


Figure 6.22: Hydrogen flux against partial pressure difference for hydrogen separation from gas mixture after annealing the Pd2 membrane

It can be observed from Figure 6.21 that the maximum H₂ flux is 23.8 cm³ cm⁻² min⁻¹ at 723 K which is higher than the H₂ flux (17.8 cm³ cm⁻² min⁻¹) for the Pd1 membrane prepared using the conventional electroless plating method. However, there was a deviation from Sievert's law both before and after annealing the membrane. The value of the pressure exponent n is equal to 0.85 which reduced to 0.76 after annealing the membrane at high temperature as shown in figure 6.22. This implies that both the surface process and bulk diffusion are responsible for hydrogen permeation through the membrane. The value for the pressure exponential n for the mixed gas separation investigation for Pd2 membrane is unity compared to that of Pd1 membrane which indicates that hydrogen permeation through the Pd2 membrane is faster than through the Pd1 membrane. This is despite the fact that both membranes have comparably same thickness.

The surface processes in hydrogen permeation through composite palladium membranes involve 2 steps [24]:



In the first case, the dissociative adsorption of H_2 molecules which impedes the surface reaction and the preceding transition of atomic hydrogen from surface to the bulk metallic layer. However, both or either of the 2 steps could control hydrogen permeation depending on the rate. If the rate of H_2 dissociative adsorption dominates the surface resistance, then the surface rate will depend on molecular H_2 movement rate at the surface. On the other hand, if the H_2 adsorption rate through the bulk is faster, then the surface resistance will depend on H_2 concentration in the bulk metal.

For mixed gas separation, the Pd2 membrane displayed a better hydrogen separation performance and higher purity compared to the Pd1 membrane.

The higher hydrogen flux for the Pd2 membrane suggests that the Pd2 membrane was more uniformly coated and denser compared to the Pd1 membrane. The concentration of CO in the permeate stream decrease with temperature but increases with pressure as shown in Table 6.2.

This implies that increasing the temperature led to decrease in the CO effect and enhanced hydrogen permeation. As hydrogen and CO compete for available sites for permeation on the membrane surface, temperature increase supports hydrogen permeation hence less of the impurity CO permeates. The same observation was made for the Pd1 membrane although the CO flux is higher for the Pd1 membrane compared to the Pd2 membrane.

It can be observed that hydrogen flux is increasing with temperature as shown in figure 6.22, H_2 flux 723 K > 673 K > 623 K hence hydrogen is winning the competition with CO for available sites for permeation on the membrane surface. Since hydrogen is displacing CO, it shows that the inhibiting effect of CO is reduced by the temperature increase. This is significant because for hydrogen production from Syngas which is mainly CO and H_2 , there is the need to avoid the inhibiting effect of CO on the palladium surface. In this work, it is shown that increasing the temperature will reduce the CO inhibiting effect.

6.2.5 Hydrogen Purity for Pd2 Membrane

Table 6.3: Average hydrogen purity in the dry gas reformat before and after annealing Pd2 membrane

Before annealing	
Temperature (K)	H ₂ Purity (%)
723	96.63
673	93.89
623	92.47
After annealing	
873	96.95
773	95.14
673	94.82

It can be observed from Table 6.3 that higher hydrogen purity was achieved for the Pd2 membrane prepared using the modified electroless plating method. The maximum hydrogen purity observed for the Pd2 membrane was 96.95% after annealing at 873 K.

6.2.6 Observations for Pd2 membrane

From the investigation for Pd2 membrane prepared using the modified electroless plating method, the following observations were made:

1. A maximum hydrogen flux of $94.5 \text{ cm}^3 \text{ cm}^2 \text{ min}^{-1}$ was observed after annealing the membrane at 873 K which is higher than that observed for the Pd1 membrane prepared using the conventional electroless plating.
2. The increased hydrogen purity for the Pd2 membrane is due to less contamination owing to the skipping of the sensitization step. Annealing the membrane also increased the purity of hydrogen because higher temperature promotes hydrogen permeation while impeding the permeation of contaminant CO which retards the permeation of hydrogen through the membrane.
3. The purity of hydrogen increased to 96.95% for the modified electroless plating method after annealing the membrane at 873 K.
4. A deviation from Sievert's law was observed with the value of the pressure exponential n at unity which implies that surface processes control hydrogen

permeation. This was attributed to the adverse effects of CO impurity on hydrogen permeation.

6.3 Results for Pd/Ag Composite Membrane

As shown in figure 6.23, the Pd/Ag membrane produced on ceramic alumina support using the codeposition electroless plating has a shiny surface and smoother compared to Pd1 and Pd2 membranes produced using the conventional and modified electroless plating methods respectively. The Pd3 membrane was tested for both hydrogen single gas permeation and mixed gas separation. The significance of the tests is to investigate hydrogen embrittlement, effect of annealing, hydrogen purity and rate limiting steps to hydrogen permeation through the membrane.

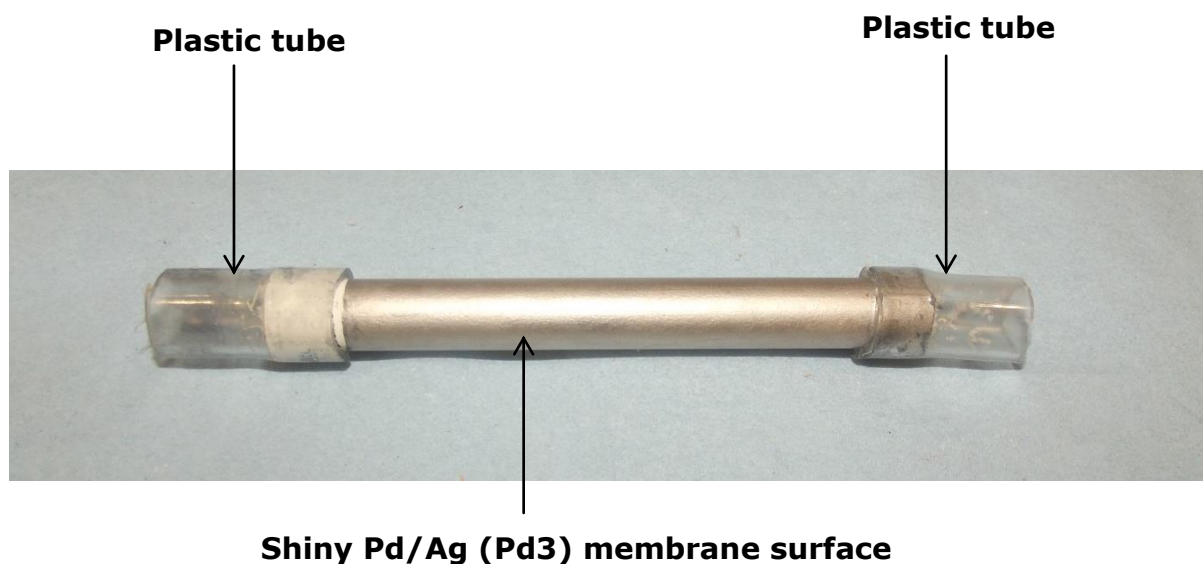


Figure 6.23: A Picture of the Pd3 membrane prepared using codeposition electroless plating method

6.3.1 Helium & N₂ Leak Test

It is necessary to ascertain whether the membrane was dense or porous just as was done for Pd1 and Pd2 membranes. It is for this reason that a Helium permeation test was also carried out for the Pd3 membrane and the membrane was found to be permeable to both He and N₂. The highest He permeance observed was $1.28 \times 10^{-7} \text{ mol m}^{-2} \text{ s}^{-1} \text{ Pa}^{-1}$ as shown in Figure 6.24 and a maximum N₂ permeance of $1.37 \text{ cm}^3 \text{ cm}^{-2} \text{ min}^{-1}$ which indicates that the membrane is porous. This shows that the He permeance is higher than for both Pd1 and Pd2 membranes while the N₂ flux was lower than for both Pd1 and Pd2 Membranes.

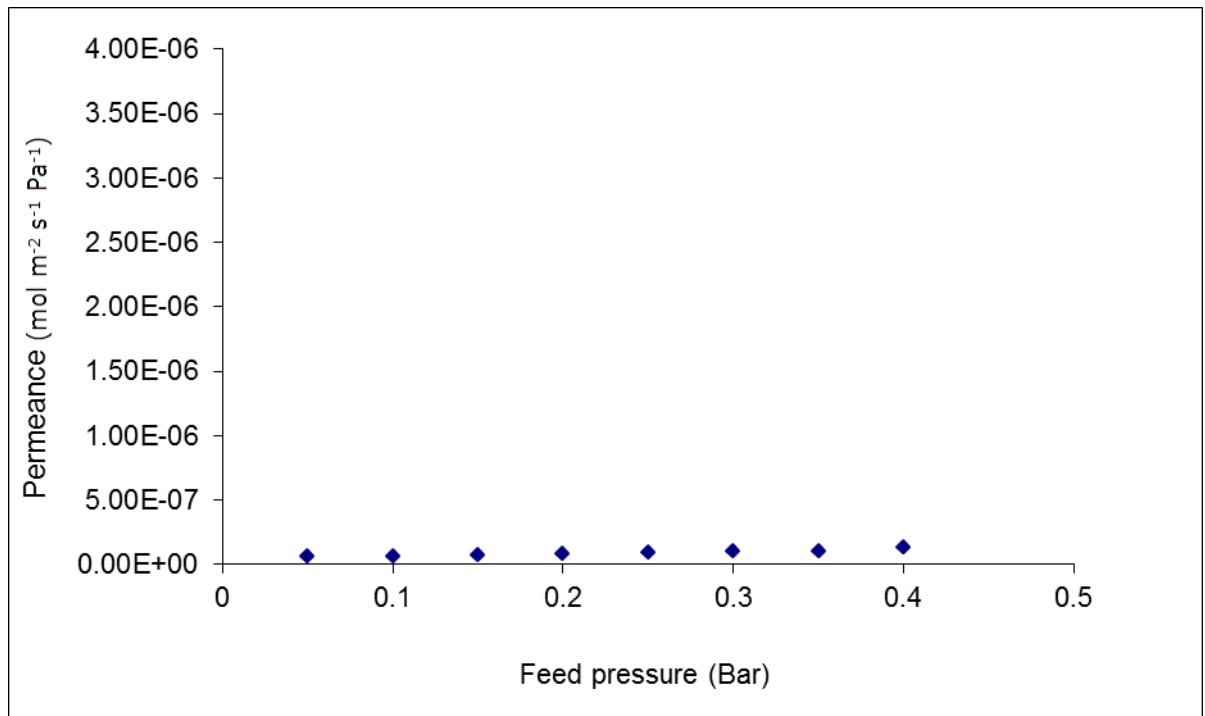


Figure 6.24: Helium permeation against inlet pressure for the Pd3 membrane

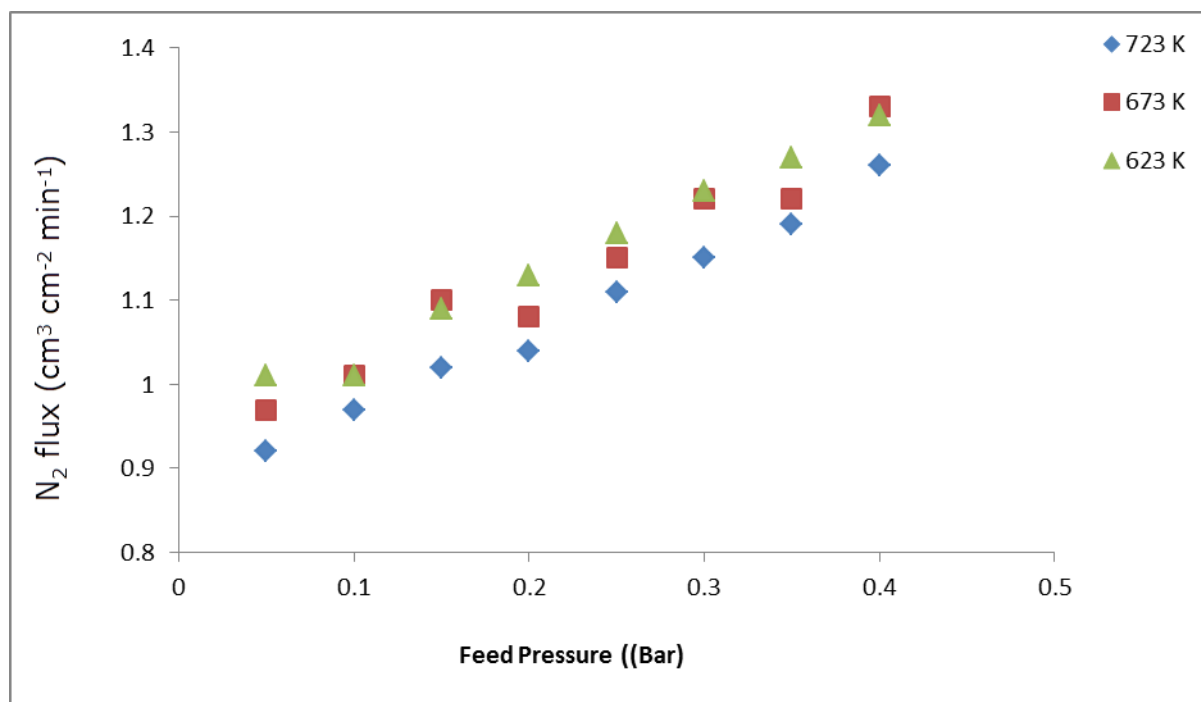


Figure 6.25: N₂ flux against feed pressure for the Pd3 membrane

6.3.2 Single Gas Permeation Test for Pd3 Membrane at Low Temperature

Prior to the permeation tests, the membrane was reduced in flowing hydrogen at 350^o C for 10 minutes to activate the palladium layer. It can be observed from Figure 6.26 that the highest hydrogen flux was 21.8 cm³ cm⁻² min⁻¹ at 473 K at 4734 K and 0.4 bar giving a pressure exponential n value of 0.5 and activation energy of 20.30 kJ/mol. A plot of hydrogen flux against the difference in the square root of the high and low pressure sides gave a linear relationship in conformity with Sievert's law with a pressure exponent n value of 0.5. The rate limiting step is bulk diffusion as was also observed for the Pd1 membrane.

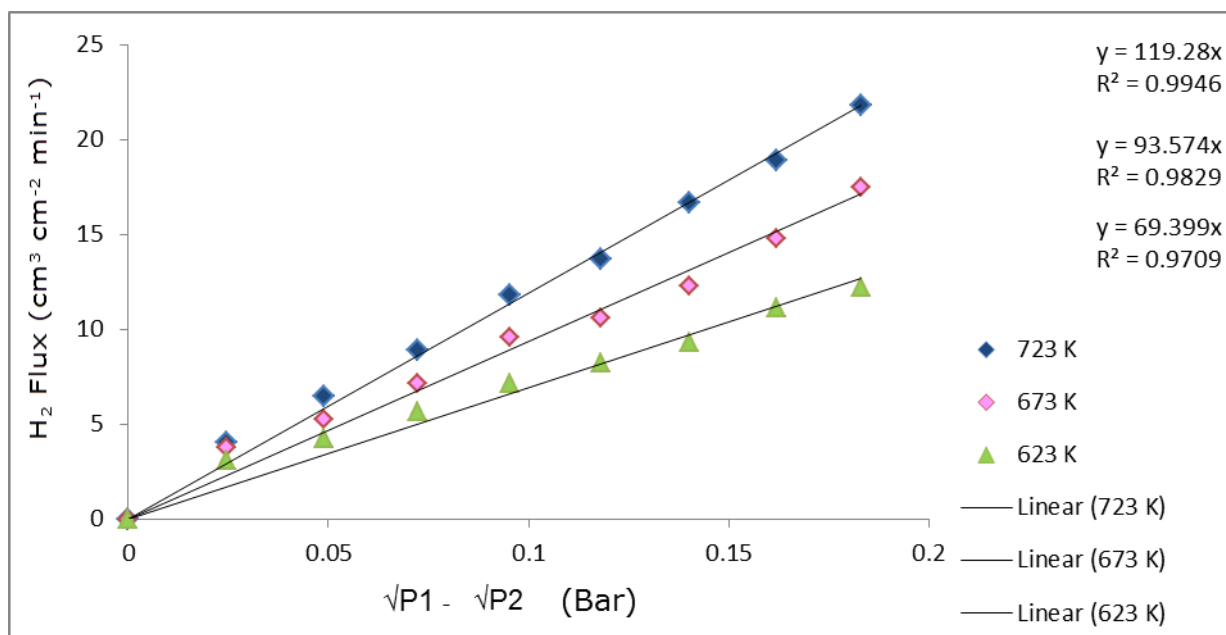


Figure 6.26: Hydrogen flux against partial pressure difference for the Pd3 membrane at low temperature to test for embrittlement

After the permeation test, the membrane was retrieved but there was no peeling off or cracks of the palladium layer hence no hydrogen embrittlement occurred. This is an indication that the Pd/Ag membrane effectively avoided the $\alpha - \beta$ miscibility gap at lower temperatures thus resisting the hydrogen embrittlement. Results for the permeation test at high temperature are displayed in Figure 6.28 and it shows an increase in hydrogen flux with temperature and transmembrane pressure difference giving activation energy of 15.76 kJ/mol.

The maximum hydrogen flux observed was $67.5 cm^3 cm^{-2} min^{-1}$ at 723 K which is higher than that of Pd1 (i.e. $41.0 cm^3 cm^{-2} min^{-1}$) and Pd2 ($54.5 cm^3 cm^{-2} min^{-1}$) under the same conditions. The maximum H_2/N_2 selectivity observed for the Pd3 membrane at low temperature was 16.52 at 723 K and 0.4 bar as shown in figure 6.27.

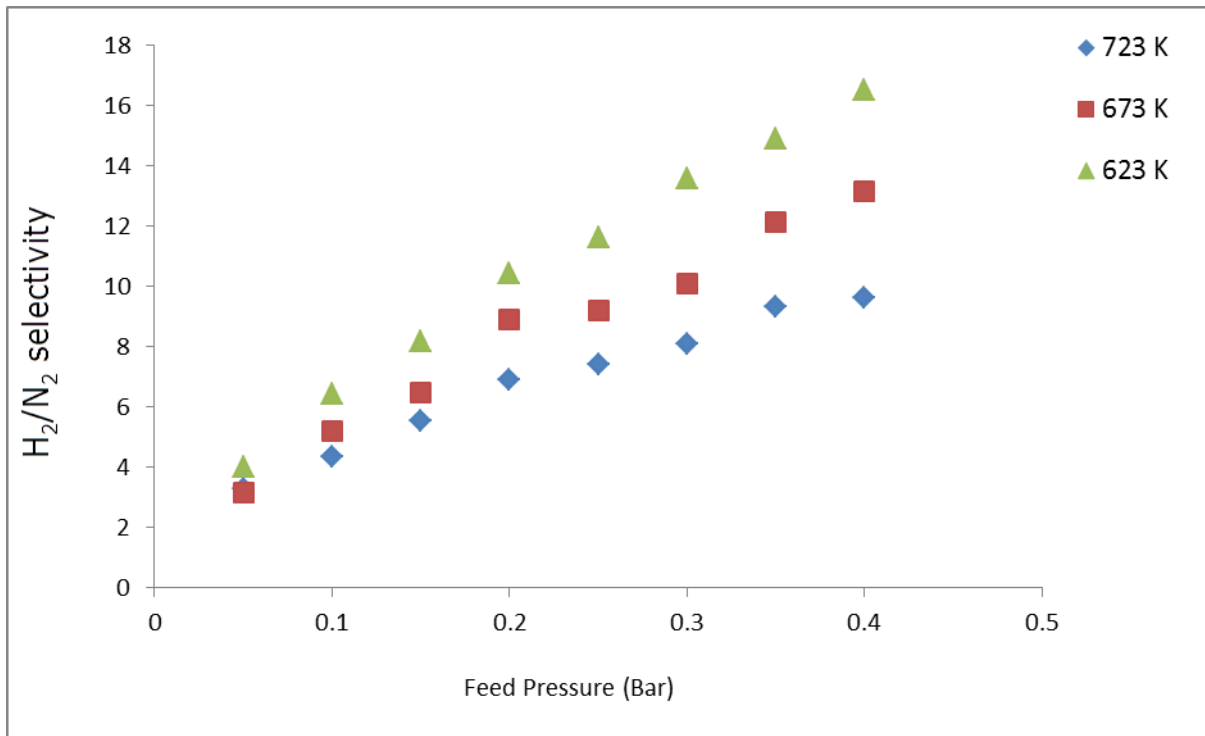


Figure 6.27: H₂/N₂ selectivity against feed pressure for the Pd3 membrane

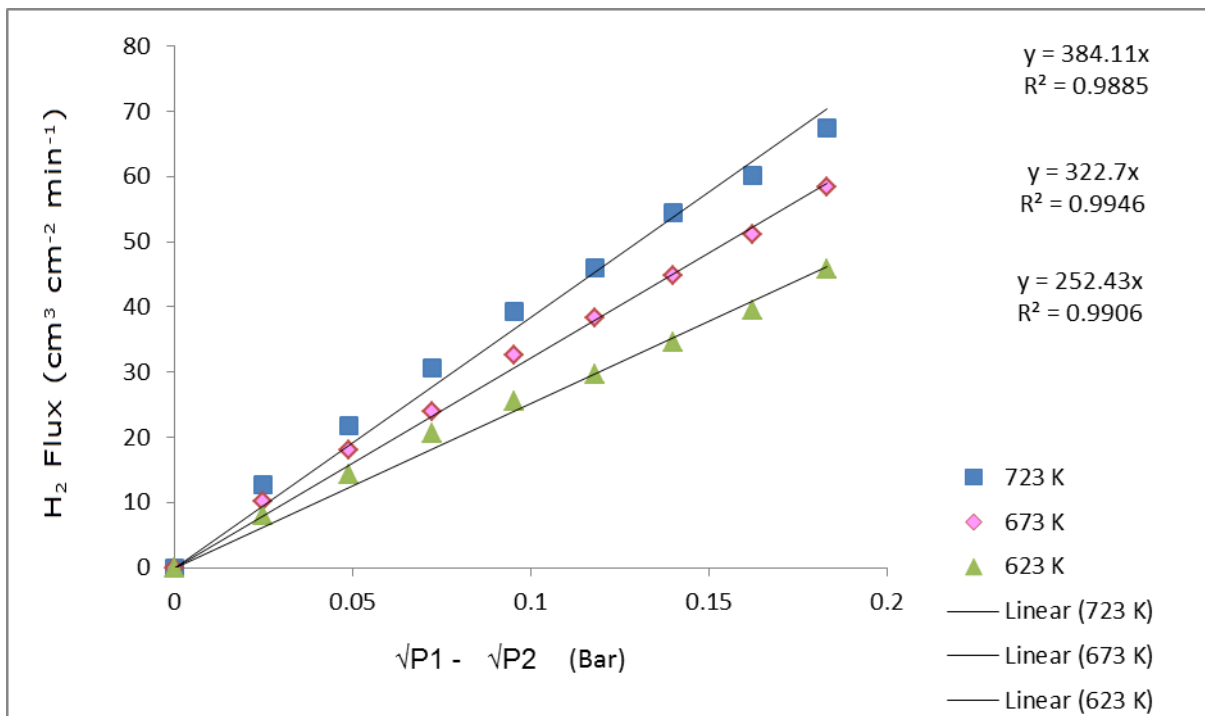


Figure 6.28: Hydrogen flux against partial pressure difference for the Pd3 membrane at high temperature.

6.3.3 Effect of Annealing Pd3 Membrane on Hydrogen Permeation

The membrane was annealed in hydrogen at 873, 773 and 673 for 10 hours to investigate the effect of annealing temperature on hydrogen permeation.

The annealing was carried out at 873, 773 and 673K. However, the temperature was allowed to equilibrate to 623K where at which hydrogen permeation measurement was carried out. The activation energy observed was 16.32 kJ/mol which was higher than that prior to annealing the membrane.

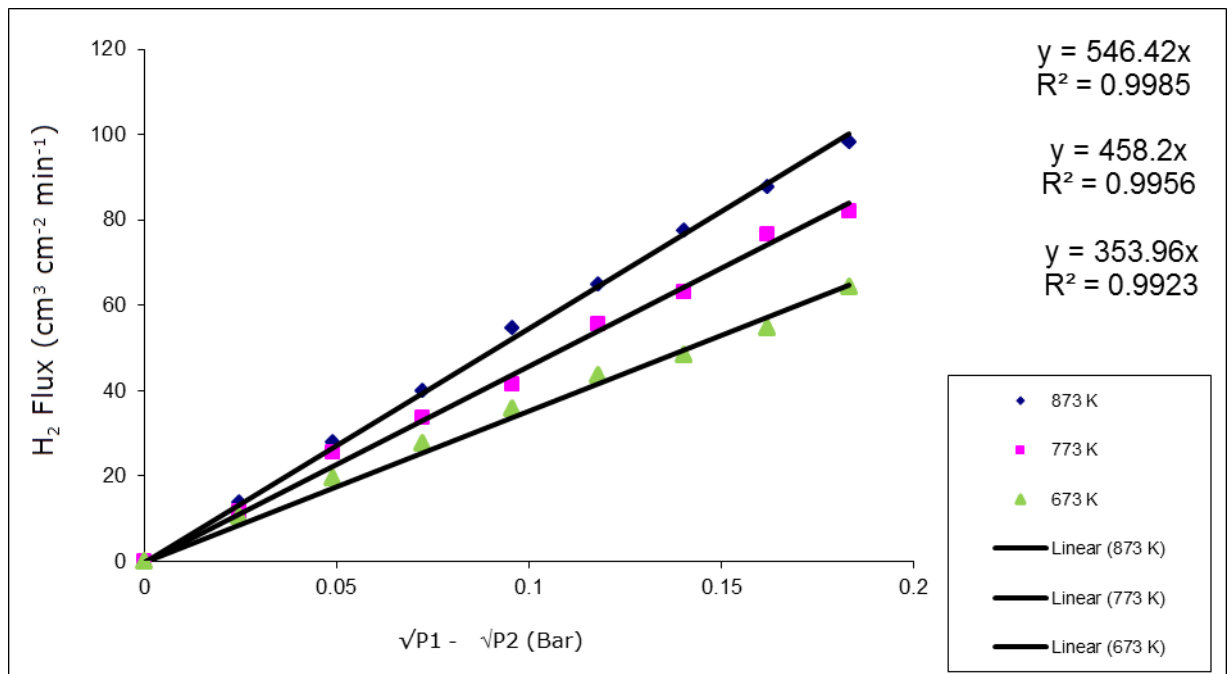


Figure 6.29: Hydrogen flux against partial pressure difference after annealing the Pd3 membrane

As shown in Figure 6.29, hydrogen permeation across the membrane after annealing obeys Sievert's law and a maximum hydrogen flux of $98.1 \text{ cm}^3 \text{ cm}^{-2} \text{ min}^{-1}$ was observed at 873 K which is higher than the hydrogen flux of the membrane prior to annealing i.e. $67.5 \text{ cm}^3 \text{ cm}^{-2} \text{ min}^{-1}$. The hydrogen flux for Pd3 membrane after annealing is higher than that for both Pd1 and Pd2 membranes i.e. $80.4 \text{ cm}^3 \text{ cm}^{-2} \text{ min}^{-1}$ and $94.5 \text{ cm}^3 \text{ cm}^{-2} \text{ min}^{-1}$ respectively. For the Pd2 membrane, there were no threats of Sn impurities since the sensitization

step was skipped. However, for Pd1 and Pd3 membranes, the threat of Sn impurities was real since the sensitization step was carried out with Tin solution.

6.3.4 Gas Separation and Hydrogen Purity

The objective of this test is to investigate the response of the Pd/Ag membrane to the inhibiting effect of these compounds to hydrogen permeation. The same hydrogen mixture with same composition for Pd1 and Pd2 membranes was used to investigate the gas separation properties of the Pd/Ag membrane named Pd3. As can be observed from Figure 6.30, the membrane was able to separate hydrogen from the gas mixture and also achieve a maximum hydrogen flux of $37.6 \text{ cm}^3 \text{ cm}^{-2} \text{ min}^{-1}$ which is about 2 fold higher than the flux for Pd1 membrane and higher than that of Pd2 membrane from the town gas mixture i.e. $17.8 \text{ cm}^3 \text{ cm}^{-2} \text{ min}^{-1}$ and $23.8 \text{ cm}^3 \text{ cm}^{-2} \text{ min}^{-1}$ respectively. This indicates that alloying with silver has enhanced hydrogen permeation and also achieve a Sievert driving force with bulk diffusion controlling hydrogen permeation ($n=0.5$) despite the thickness of the membrane ($2 \text{ }\mu\text{m}$) and the presence of CO and CO_2 in the mixture. The activation energy calculated was 19.42 kJ/mol .

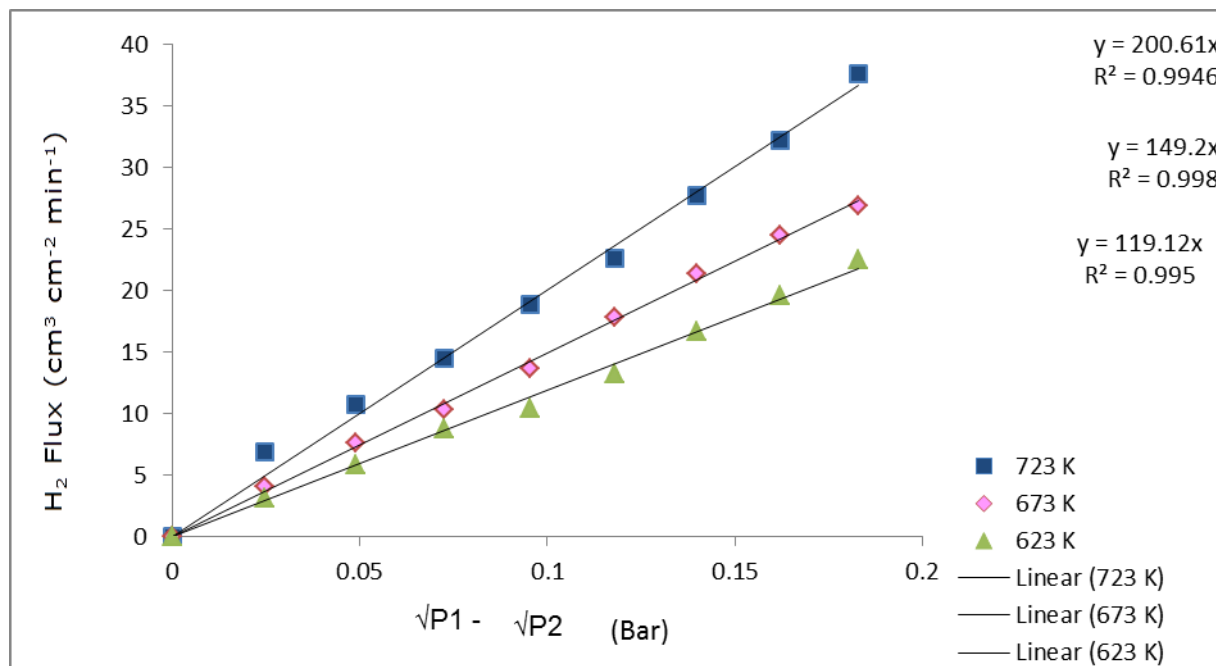


Figure 6.30: Hydrogen flux against partial pressure difference for mixed gas separation for the Pd3 membrane

The effect of annealing the Pd3 membrane for hydrogen separation from the gas mixture was also investigated at 873, 773 and 673 K. The results in Figure 6.31 show a maximum hydrogen flux of $40.9 \text{ cm}^3 \text{ cm}^{-2} \text{ min}^{-1}$ at 873 K and a transmembrane pressure difference of 0.4 bar. This is higher when compared to the hydrogen flux before the membrane was annealed and also higher compared to the annealed membranes Pd1 and Pd2 respectively. The activation energy was also higher at 20.85 kJmol^{-1} compared to that before the membrane was annealed at 19.42 kJmol^{-1} .

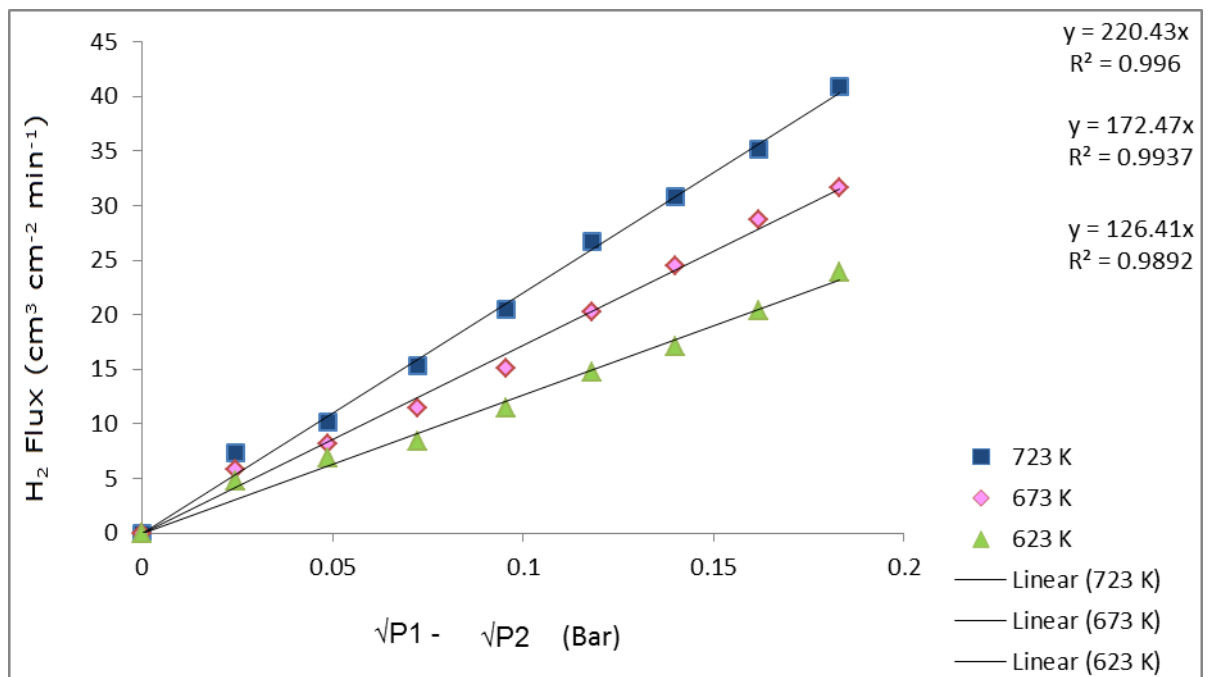


Figure 6.31: Hydrogen flux against partial pressure difference for hydrogen separation from gas mixture after annealing the Pd3 membrane.

The alloying with silver enhanced the separation of hydrogen from the gas mixture due to the ability of silver to suppress the inhibition effect of carbon monoxide. The component CO gas in the mixture inhibits hydrogen permeation through competitive adsorption by blocking the sites for permeation through reaction to reduce the hydrogen partial pressures. 23% Ag was used as shown in Table 3.5 on page 63 and the Ag is able to reduce the competitive adsorption effect of the CO thereby enhancing hydrogen permeation. The concentration of CO in the permeate stream permeate is shown in Table 6.4.

The silver enrichment increases the spacing in the metal lattice which counteracts the effect of CO and speeds up the permeation of hydrogen. Apart from enhancing hydrogen permeation and avoiding hydrogen embrittlement, alloying with silver also reduces the cost of production by reducing the amount of palladium to be used.

The results of investigation conducted for both single gas permeation and mixed gas separation implies that further addition of silver could enhance both hydrogen permeation and separation. However, high concentration of silver could lead to less sites for hydrogen permeation due to the 'competitive advantage' that silver enjoys over palladium.

Table 6.4: Flux of CO in the permeate stream before and after annealing Pd3 membrane

	Before annealing			After annealing		
	$(\text{cm}^3 \text{ cm}^{-2} \text{ min}^{-1})$			$(\text{cm}^3 \text{ cm}^{-2} \text{ min}^{-1})$		
Feed Pressure (Bar)	723 K	673 K	623 K	873 K	773 K	673 K
0.05	2.74E-04	7.95E-04	7.02E-04	8.63E-04	7.89E-04	7.23E-04
0.10	3.90E-04	8.76E-04	7.97E-04	8.95E-04	8.36E-04	7.81E-04
0.15	7.1E-04	9.36E-04	8.63E-04	9.27E-04	8.95E-04	8.39E-04
0.20	1.23E-03	9.85E-04	9.33E-04	9.59E-04	9.21E-04	8.94E-04
0.25	1.46E-03	1.02E-03	9.82E-04	9.88E-04	9.56E-04	9.29E-04
0.30	1.97E-03	1.26E-03	1.05E-03	9.93E-04	9.92E-04	9.63E-04
0.35	2.08E-03	1.89E-03	1.28E-03	1.03E-03	1.27E-03	1.05E-04
0.40	2.21E-03	2.45E-03	1.79E-03	1.26E-03	1.46E-03	1.27E-03

Table 6.5: Average hydrogen purity in the dry gas reformat for Pd3 membrane

Before annealing	

Temperature (K)	H ₂ Purity (%)
723	97.88
673	95.75
623	94.17
After annealing	
873	98.86
773	97.21
673	96.23

Table 6.4 shows the CO flux before and after annealing the membrane and it can be observed that annealing marginally reduced the amount of CO in the permeate stream. Table 6.5 shows the average hydrogen purity for the gas mixture separation before and after high temperature annealing in hydrogen. It can be observed that an optimum purity of 98.86% was observed after annealing the Pd3 membrane (Pd/Ag). The alloying with silver has led to an enhanced flux of hydrogen by suppressing the inhibiting effect of CO.

Table 6.6: Comparison of activation energy for composite membranes

Metallic layer	Support	Pore size (nm)	Thickness (μm)	n value	Activation Energy ($\text{kJ}\cdot\text{mol}^{-1}$)	Reference
Pd	Alumina	30	2	0.5 - 1	10– 28.30	This work
PdAg	Alumina	30	2	0.5 - 1	15– 20.85	This work
Pd	Alumina	n/a	1	0.85	8.8	24
PdAg	Alumina		1.6		35.20	2
PdAg	Alumina		1.7		4.4	25
PdAg	Alumina	0.1	2.5	0.5	17	26
Pd.	Alumina		3	0.5	10.3	2
PdAg	Alumina	30	6	1	8.43	23
Pd			7.5	0.61	11-12	27
PdAg	Alumina	150	8.6	0.5	8.22	28
Pd.			10.3	0.65	12.3	29

Pd		10-200	11.4	0.58	8.88	30
Pd.			15	0.65	10	31
PdAg.			20	0.76	10	32

As shown in Table 6.6, our observed values for activation energy are in agreement with the values obtained in literature. After the investigation for Pd3 membrane in this work, it is clear that a higher hydrogen flux was achieved and the cost of the membrane lowered compared to the Pd1 and Pd2 membranes. The cost target for palladium membranes as specified by the U.S department of energy's (DOE) for hydrogen separation for 2015 is that a membrane material should be less than \$100/ft² as shown in Table 6.7. Other organizations around the world working towards a sustainable energy system have also set their separate targets using the DOE's as a reliable benchmark. According to table 6.7, the 2011 target for membrane stability/durability is 1031 hours which is 43 days. However, this target was upgraded to 5 years for 2015.

In this regard, it is necessary to encourage research that could provide options for palladium with a view to meeting this technical cost target and also achieving highly stable membrane. It is this reason that necessitated our next set of investigation on silica membranes. Silica membranes offer unique options to palladium membranes in terms of cost and chemical stability in hydrogen production in membrane reactor applications and high temperature hydrogen separation [33]. It is for these reasons that investigations were conducted on silica membranes for hydrogen separation and purification.

Table 6.7: Technical targets for hydrogen separation using membranes (U.S DOE)

Performance Criteria	DOE target for 2015
H ₂ flux	300 ft ³ h ⁻³ ft ⁻²
Cost	<100 \$/ft ²
H ₂ purity	99.99%

Stability/Durability	5 years (2015) 1,031 hours (43 days: Target for 2011)
----------------------	--

6.3.5 Summary of observations for Pd3 membrane

The following observations were made during the investigation of hydrogen permeation in both single and mixed gas streams:

1. A maximum hydrogen flux of $98.1 \text{ cm}^3 \text{ cm}^{-2} \text{ min}^{-1}$ was observed after annealing the membrane at 873 K which is higher than the hydrogen flux for the palladium membranes prepared using both the conventional and modified electroless plating methods.
2. When the PdAg membrane was investigated at low temperature below 300°C , no hydrogen embrittlement was observed and the membrane didn't suffer from any cracks or peeling of the metallic layer. The alloying with silver was able to suppress the H_2 embrittlement.
2. The PdAg membrane achieved a higher hydrogen flux compared to the Pd membrane. Hydrogen permeation through the membrane obey Sievert's driving force for both single and mixed gas streams. This was in direct contrast to the observation for Pd-only membranes Pd1 and Pd2 where a deviation from Sievert's law was observed due to the effect of CO. This was due to the ability of the Ag to suppress the permeation inhibiting effect of CO.
3. The cost of the PdAg membrane was less compared to the Pd membranes Pd1 and Pd2 because less palladium precursor was used in the Pd3 membrane fabrication.
4. Hydrogen purity increased to 98.86% for the Pd3 membrane which is higher than 96.95% for the Pd2 membrane, also annealing in hydrogen enhanced hydrogen permeation through the membrane.

6.4 Silica Membranes SL1 & SL2

Two Silica membranes were fabricated using the porous big membrane tubular ceramic support of 6000 nm pore size. In the first instance, the Silica membrane was prepared using the conventional dip coating method where the Silica layer was deposited onto the ceramic support. A smooth and uniformly coated membrane named SL1 of thickness 24.63 μm was achieved. In the second instance, a modified dip coating method was used to deposit Silica layer of thickness 31.19 μm onto the porous ceramic alumina support.

The Silica membrane prepared using the modified dip coating method was named SL2. This section presents the results from the permeation investigations conducted on the two silica membranes prepared in this work: SL1 and SL2. Both single and mixed gas permeation tests were carried out for hydrogen and five other single gases namely H_2 , CO_2 , He, CH_4 , N_2 and Ar at temperature range from room temperature to 573 K and a transmembrane pressure difference from 0.05 to 0.4 bar. The selectivity of the membrane to hydrogen in relation to the five other single gases is also presented and discussed.

6.4.1 Single Gas Permeation Test for SL1 Membrane after first dip

Figure 6.32 shows the hydrogen permeance of the SL1 silica membrane after first dip showing an increase in permeance with decreasing temperature and pressure. The maximum permeance observed was $3.12 \times 10^{-7} \text{ mol m}^{-2} \text{ s}^{-1} \text{ Pa}^{-1}$ at 573 K. The dominant gas transport mechanism in porous membranes is Knudsen flow. In Knudsen diffusion, gas permeance is inversely proportional to the square root of temperature and molecular weight. Hence, a diffusing gas should have an independent relationship with temperature if the gas transport is governed by only Knudsen. This means that if the gas transport is Knudsen, then an increase or decrease in temperature should have no effect on gas permeation. However, it can be observed from figure 6.32 that the permeance increases with temperature which means that there is an effect of temperature on gas permeation through the membrane. The increase in hydrogen permeance with temperature indicates that hydrogen permeation through the silica membrane is mainly by activated surface

diffusion. Increasing the temperature of permeation contributes to the surface diffusion of the molecules and subsequently increased the movement of molecules within the pores.

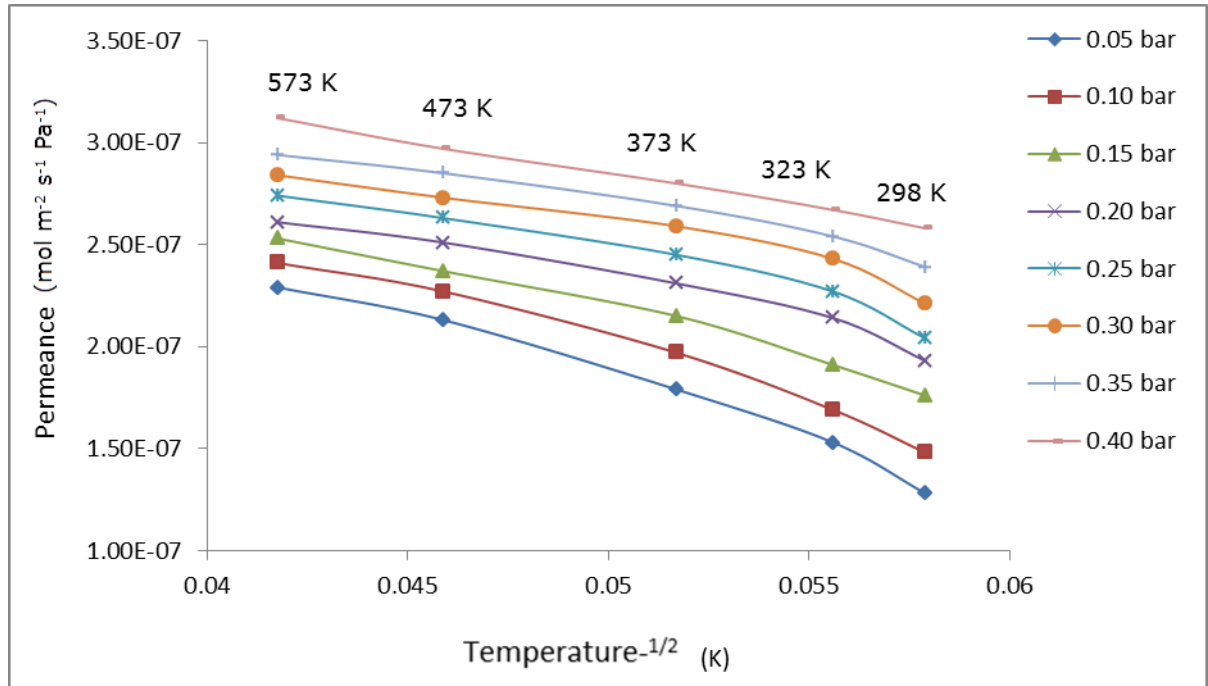


Figure 6.32: Hydrogen permeation against inverse square root of temperature for the SL1 membrane after first dip.

The permeance of hydrogen is at least one order of magnitude higher than the other gases. The results indicate the order of permeance as follows: $H_2 > He > CO_2 > CH_4 > N_2 > Ar$ which does not follow the order of molecular size as follows: $CH_4 (3.8 \text{ \AA}) > N_2 (3.64 \text{ \AA}) > Ar (3.4 \text{ \AA}) > CO_2 (3.3 \text{ \AA}) > H_2 (2.89 \text{ \AA}) > He (2.65 \text{ \AA})$. Comparing the two orders indicates that they do not agree which is an indication that the gas transport mechanism is other than Knudsen diffusion and governed by activated surface diffusion.

Table 6.8 shows the SL1 membrane selectivity to hydrogen with respect to the other 5 single gases at 573 K. The ideal selectivity of hydrogen with respect to all the single gases were above the respective theoretical Knudsen selectivity except H_2/Ar . However, there is also the contribution of viscous flow which is evident from the pressure dependency of hydrogen permeance. If the activated surface

diffusion and viscous flow occur in parallel, the sum total permeance of the adsorbable gases is given by equation 14 [33]:

$$Q_{\text{total}} = Q_{\text{surface diffusion}} + Q_{\text{viscous flow}} \dots\dots\dots \text{Eqn 14}$$

Normally, the pressure dependency on gas permeance is characteristic of viscous flow transport mechanism and depicts the possible presence of defects. When the hydrogen permeance is becoming more stable and independent of pressure, the Knudsen flow becomes more likely and will prevail when the pressure has no influence on hydrogen permeation. At the point when pressure has no effect on hydrogen permeation, there will be straight line relationship and this will give support to a strict Knudsen flow. The contribution of viscous flow could also result from the presence of cracks and defects in the membrane leading to a decrease in the rate of hydrogen permeation through the membrane. The deposited silica layer over the porous support will penetrate through the pores and repair some of the defects or pinholes on the porous support. In this regard, the higher the thickness of the silica layer, the more likelihood for eradication of pinholes and defects on the porous support but the higher the resistance to hydrogen permeation and the lower the permeance. However, the increase in permeance with upstream pressure is also a characteristic of the viscous flow mechanism but is normally associated with defects in the active silica layer.

Table 6.8: Ideal selectivity for hydrogen in relation to He, CO₂, CH₄, N₂ and Ar at 573 K for the SL1 membrane after first dip

Feed Pressure (Bar)	Ideal Selectivity H ₂ /CH ₄	Ideal Selectivity H ₂ /He	Ideal Selectivity H ₂ /Ar	Ideal Selectivity H ₂ /N ₂	Ideal Selectivity H ₂ /CO ₂	Knudsen Selectivity
0.05	4.35	1.62	5.39	2.63	3.30	H ₂ /He = 1.41
0.10	3.62	1.43	4.81	2.46	3.09	H ₂ /N ₂ = 3.73
0.15	3.36	1.38	4.45	2.36	2.97	H ₂ /CO ₂ = 4.67
0.20	3.25	1.32	4.24	2.16	2.88	H ₂ /CH ₄ = 2.82
0.25	3.18	1.28	4.13	2.01	2.79	H ₂ /Ar = 4.45
0.30	3.07	1.23	3.98	1.91	2.51	
0.35	3.02	1.20	3.77	1.79	2.33	
0.40	3.13	1.19	3.75	3.45	2.28	

As shown in Table 6.8, the maximum H₂/He selectivity observed was 1.62 at 573 K and 0.05 bar which was higher than the theoretical Knudsen selectivity of 1.41. The H₂/He selectivity decreases with pressure but increases with temperature in contrast to permeance which increases with pressure. The permeance of Helium follows the same trend as hydrogen but Helium shows slightly more stability at higher temperature as shown in figure 6.33. The maximum He permeance was $2.63 \times 10^{-7} \text{ mol m}^{-2} \text{ s}^{-1} \text{ Pa}^{-1}$ at 573 K which drops more sharply with pressure.

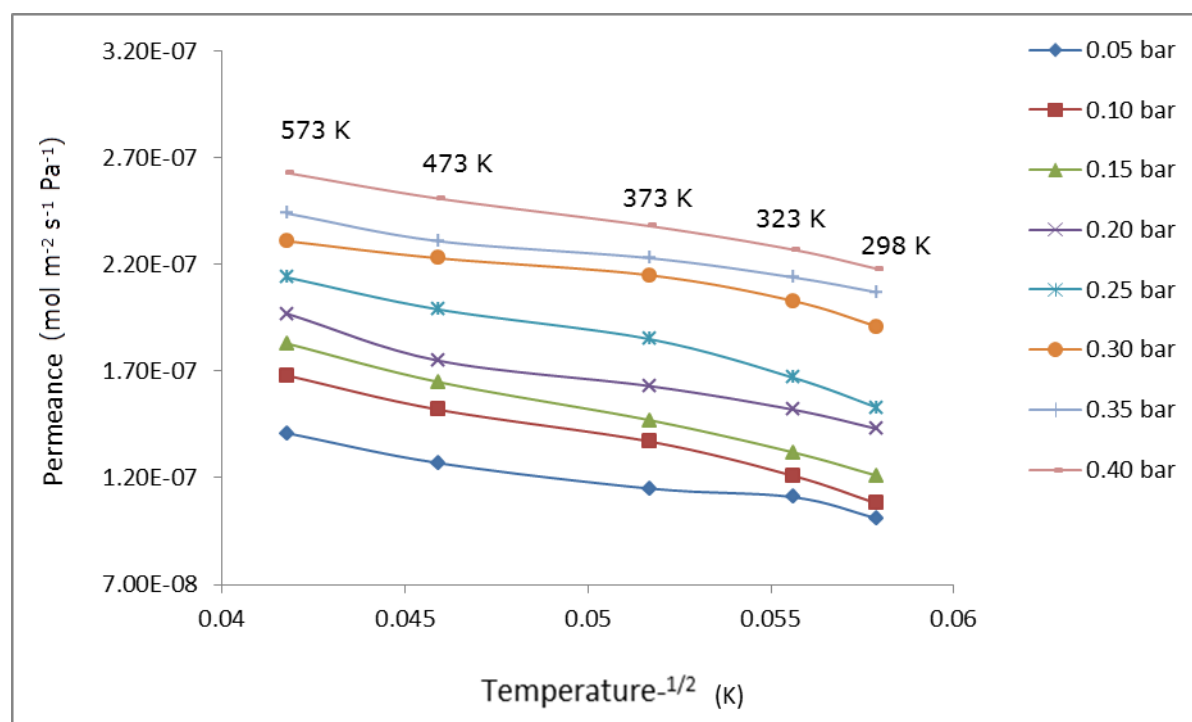


Figure 6.33: Helium permeance against inverse square root of temperature for the SL1 membrane after first dip.

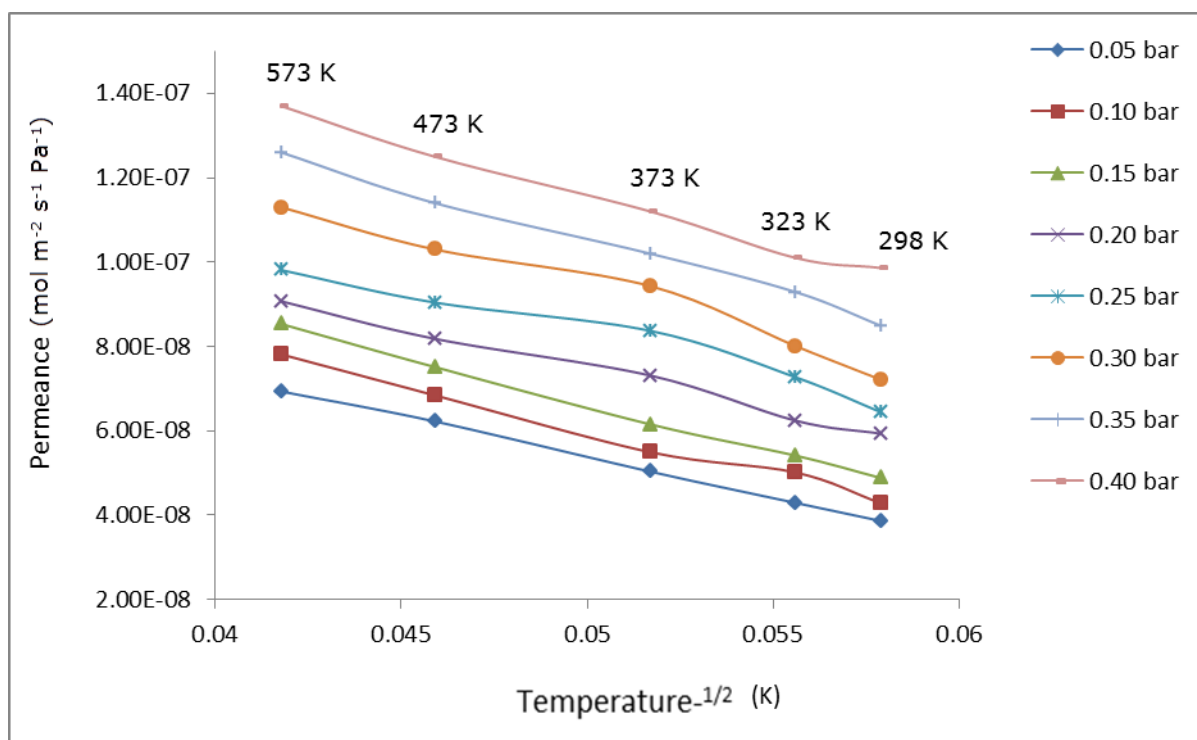


Figure 6.34: Nitrogen permeance against inverse square root of temperature for the SL1 membrane after first dip

The permeance of Nitrogen through membrane SL1 was also investigated under the same conditions as for hydrogen and Helium. As shown in Figure 6.34, the N_2 permeance increased with temperature and transmembrane pressure. The maximum permeance was $1.37 \times 10^{-7} \text{ mol s}^{-1} \text{ m}^{-2} \text{ Pa}^{-1}$ at 573 K and 0.4 bar which is lower than the hydrogen permeance under the same conditions.

The increase in permeance with increasing temperature indicates that N_2 transport is through activated surface diffusion. However, it can also be observed that the N_2 permeance is slightly more stable than both hydrogen and helium. The stability of N_2 permeance indicates that the effect of activated surface diffusion mechanism is reducing which implies that the likelihood of a Knudsen flow is more pronounced at lower temperature. Figure 6.35 shows the H_2/N_2 selectivity of the SL1 membrane. The maximum H_2/N_2 selectivity of the membrane was 2.63 at 573 K and a transmembrane pressure difference of 0.05 bar which is lower than the theoretical Knudsen selectivity of 3.73. However, the selectivity increases with temperature but decreases with increase in the transmembrane pressure difference.

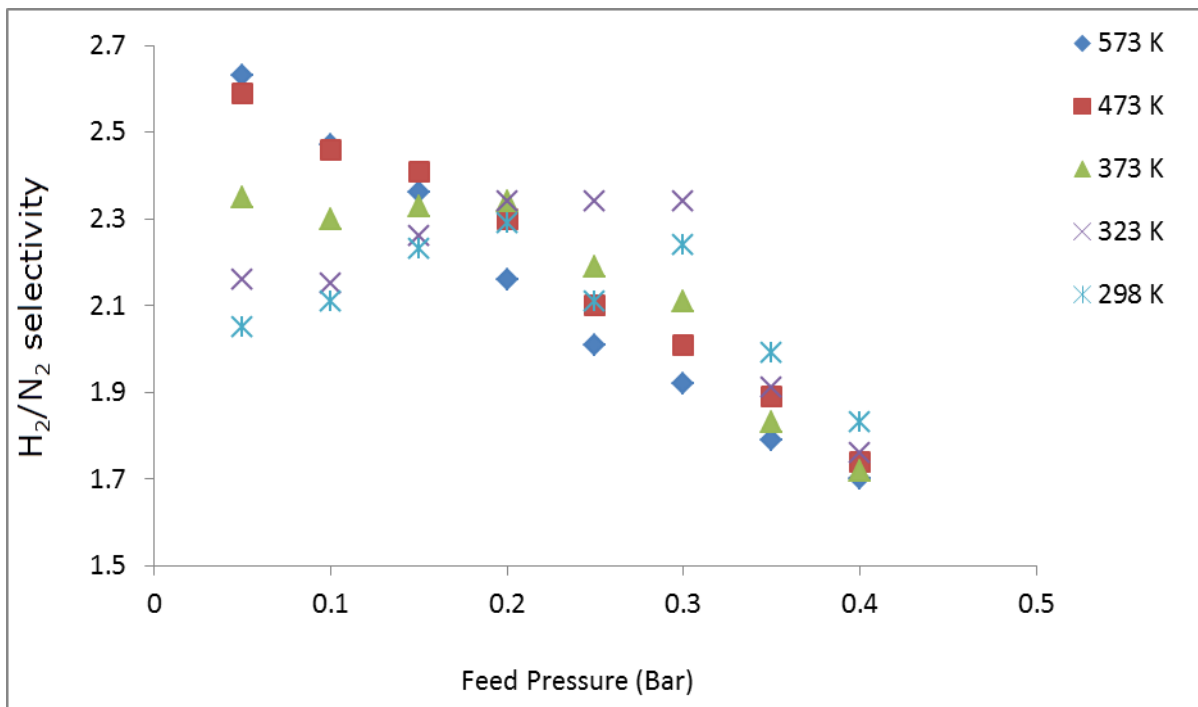


Figure 6.35: H₂/N₂ selectivity against inlet pressure after first dip for the SL1 membrane

The permeance of CO₂ through the SL1 membrane at different temperature for transmembrane pressure differential of 0.05 to 0.4 bar is shown in figure 6.36. It can be observed that the maximum permeance was $1.83 \times 10^{-7} \text{ mol m}^{-2} \text{ s}^{-1} \text{ Pa}^{-1}$ measured at 573 K and 0.05 bar. The CO₂ permeance exhibited the same behavior as H₂ and N₂ with activated surface diffusion mechanism governing the gas transport through the membrane with contribution of viscous flow.

Under the Knudsen transport mechanism, there exists an inverse dependence of gas permeance on gas molecular weight. CO₂ is a heavier gas compared to CH₄, and Ar but displayed higher permeance than these gases as shown in the order of permeance of the gases. show that CO₂ displayed a higher permeance compared to the other 3 heavier gases which is a further confirmation that the gas transport is activated surface diffusion with contribution of viscous flow.

The order of permeance of the heavier gases is CO₂ (3.3 A) > CH₄ (3.8 A) > N₂ (3.64 A) > Ar (3.4 A) but for Knudsen flow, it should be CH₄ (3.8 A) > N₂ (3.64 A) > Ar (3.4 A) > CO₂ (3.3). This indicates that the order of Knudsen flow was

not followed as CO₂ which has the highest permeance among the heavier gases should ordinarily have had the least under Knudsen flow. CO₂ permeates faster than N₂ which is in agreement with the order of molecular size or kinetic diameter of these gases i.e. CO₂ (3.3 Å) < N₂ (3.6 Å) since CO₂ with a lower size compared to N₂ is expected to find accommodation through the membrane pores more easily than N₂. However, this trend doesn't depict a Knudsen flow which is expected to be the other way round. The order of molecular size is normally expected to account for the ranking of gases in terms of their permeance in silica membranes under a molecular sieving transport mechanism.

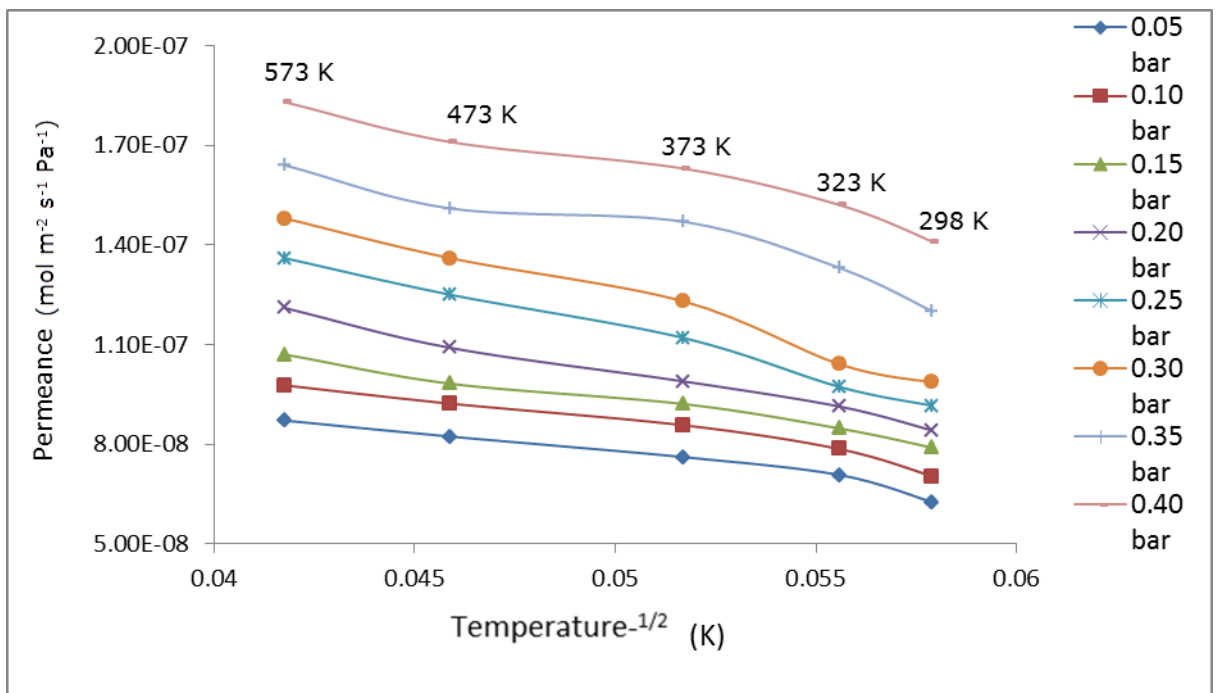


Figure 6.36: CO₂ permeance against inverse square root of temperature for the SL1 membrane after first dip

The H₂/CO₂ ideal selectivity was also determined based on the permeance ratio of the 2 gases under same temperature and transmembrane pressure. As shown in figure 6.37, the selectivity increases with temperature but decreases with transmembrane pressure differential and the highest selectivity was 3.61 observed at 298 K and 0.15 bar which is lower than the theoretical Knudsen selectivity of 4.67. Moreover, the selectivity can be improved by depositing another silica layer which will increase the density of the active layer and repair any possible defects or pinholes. However, the downside of depositing another

silica layer is reduction in the permeance of the membrane. This is in tandem with the norm in membrane processes where gas permeance is usually sacrificed to improve selectivity and vice versa.

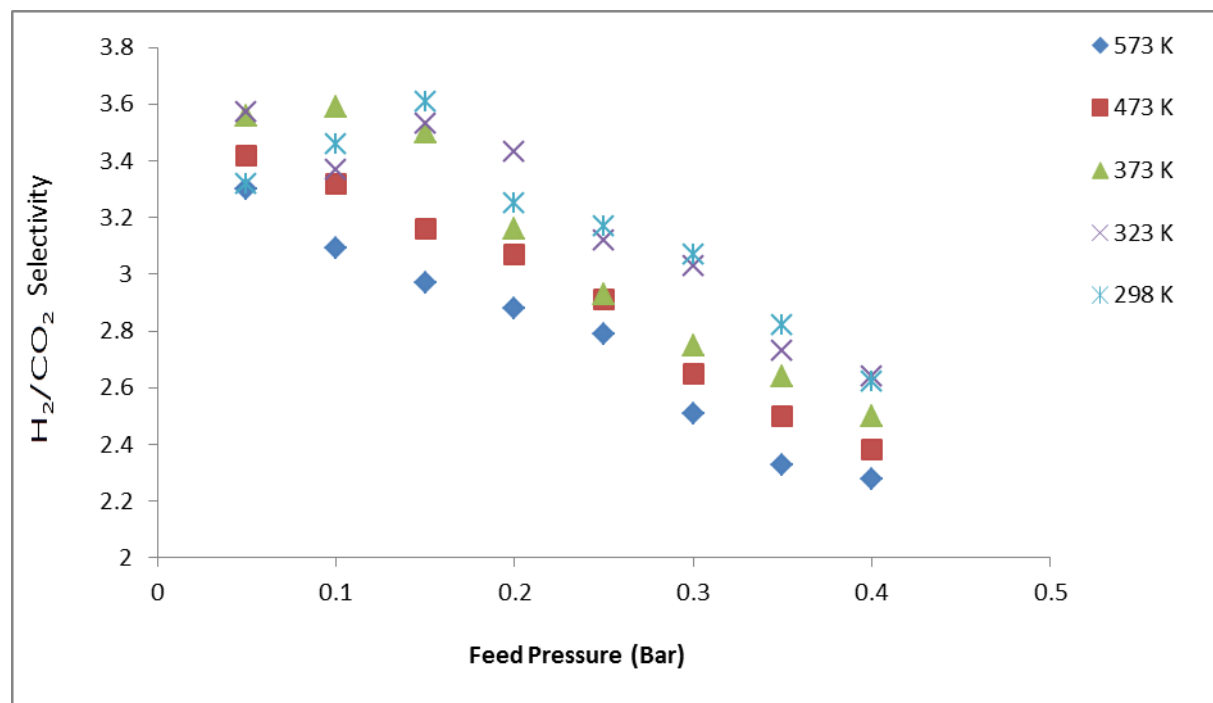


Figure 6.37: H₂/CO₂ selectivity against inlet pressure for the SL1 membrane after first dip

The permeance of CH₄ through the SL1 membrane was also investigated under the same conditions as for the other gases previously discussed in this section. The result shown in figure 6.38 indicate that the maximum permeance observed was $9.98 \times 10^{-8} \text{ mol m}^{-2} \text{ s}^{-1} \text{ Pa}^{-1}$ at 573 K and transmembrane pressure differential of 0.4 bar. The CH₄ permeance was higher than N₂ and Ar and as such does not follow the order of molecular size of the gases. CH₄ (3.8 Å) is a heavier gas compared to N₂ and Ar hence it is expected to encounter more resistance to permeation if the criteria for molecular differentiation is through size selectivity.

The lighter gases i.e. H₂ and He, permeated faster than CH₄, and the CH₄ permeance became more stable with increasing pressure and lower temperature which shows increasing tendency towards Knudsen diffusion. The decrease in CH₄

permeance was clearly more significant at lower temperature. This trend indicates that Knudsen flow is less likely at lower temperatures but more likely at higher temperature because the permeance remained stable.

For a Knudsen flow, the permeance should be independent of temperature. As observed from figure 6.39, the highest H_2/CH_4 selectivity observed is 4.47 at 473 K and 0.05 bar which is higher than the theoretical Knudsen selectivity i.e. 2.82. The relatively high selectivity is also another indication of the uniformity of the coated active silica layer. However, it can also be observed that CH_4 has a higher selectivity relative to hydrogen than He which is a lighter gas compared to CH_4 .

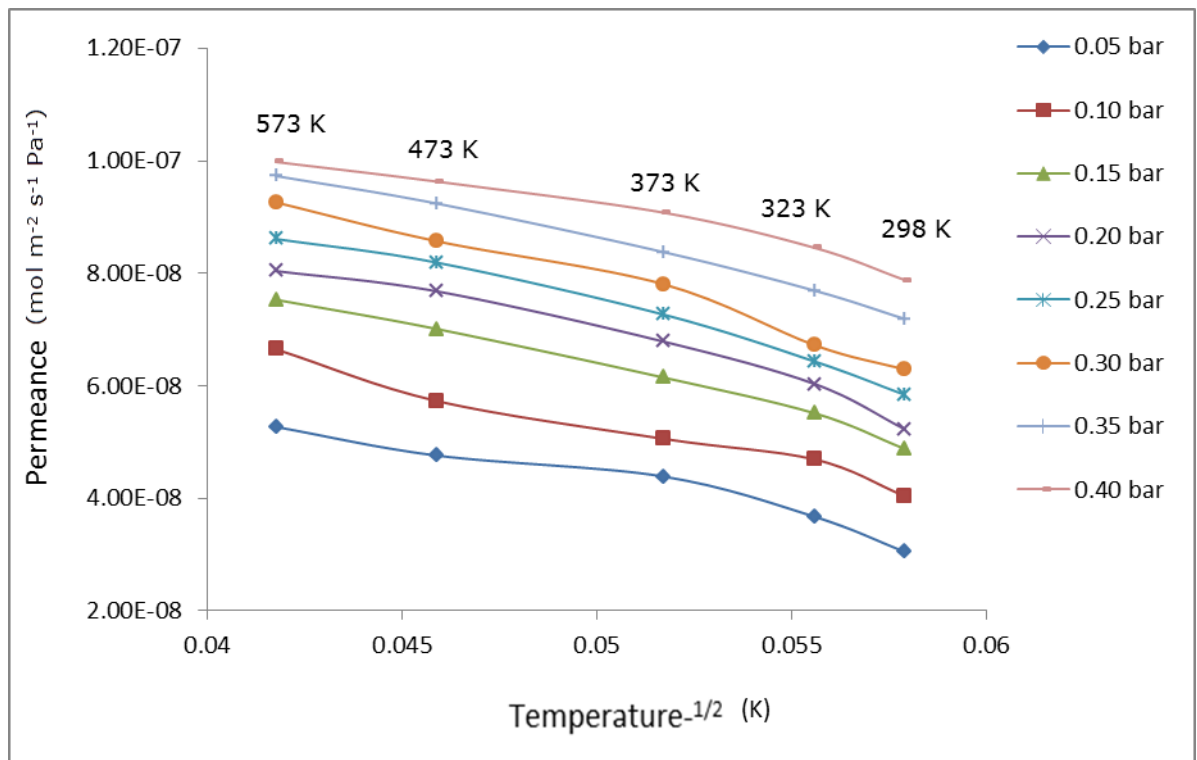


Figure 6.38: CH_4 permeance against inverse square root of temperature for the SL1 membrane after first dip.

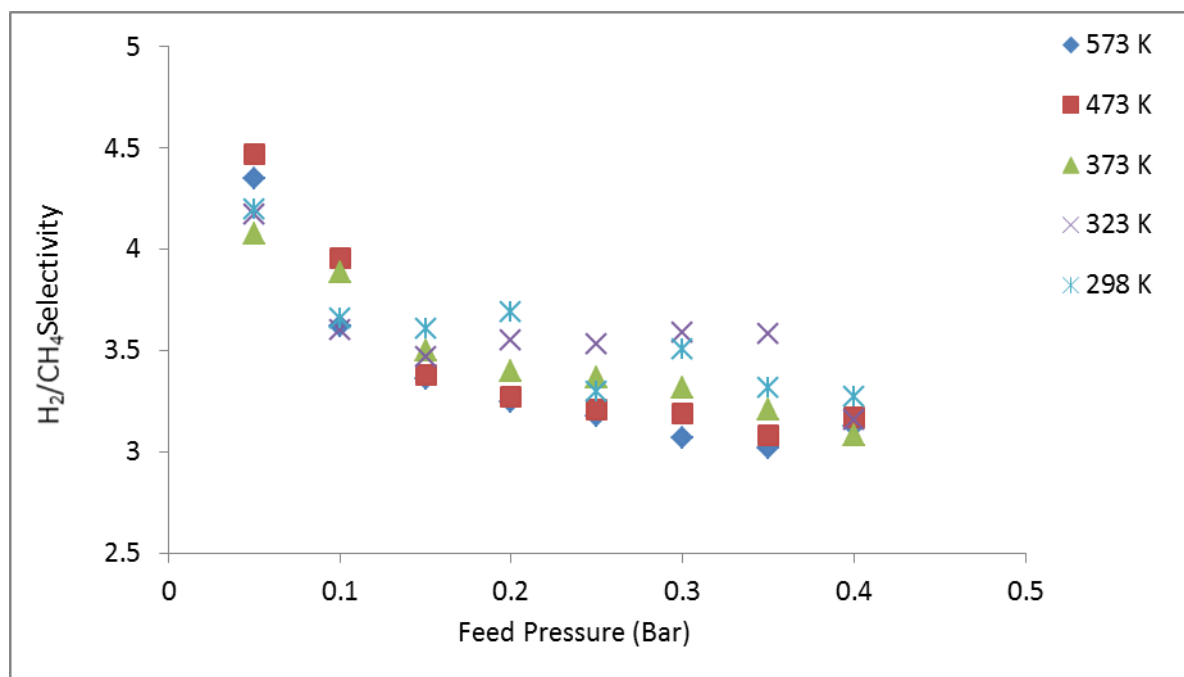


Figure 6.39: H₂/CH₄ selectivity for the SL1 membrane after first dip

The permeance of Ar through the SL1 membrane was also investigated under the same conditions as for the other gases. The results in figure 6.40 show an increase in permeance with increasing temperature which depicts an activated surface diffusion transport mechanism. However, Ar displayed the lowest permeance across the SL1 membrane compared to all the other gases albeit Ar is larger in size compared to H₂, He and CO₂ but lower in size compared to CH₄ and N₂. The maximum permeance observed was $8.32 \times 10^{-8} \text{ mol m}^{-2} \text{ s}^{-1} \text{ Pa}^{-1}$ at 573 K and transmembrane pressure differential of 0.4 bar. Also the permeance trend across the transmembrane pressure indicate that there is more stability for Ar permeance across the membrane compared to the other gases.

The permeation behavior of Ar across the SL1 membrane is governed by the activated surface diffusion mechanism with some contribution of viscous flow just like the other gases investigated. The highest H₂/Ar selectivity was 6.01 at 298 K and a transmembrane pressure difference of 0.05 bar which is higher than the theoretical Knudsen selectivity of 4.45. Ar with the lowest permeance displayed the highest selectivity relative to hydrogen.

However, if the permeance of hydrogen increases, then the H₂/Ar selectivity increases provided that the Ar permeance remains same as shown in figure 6.41.

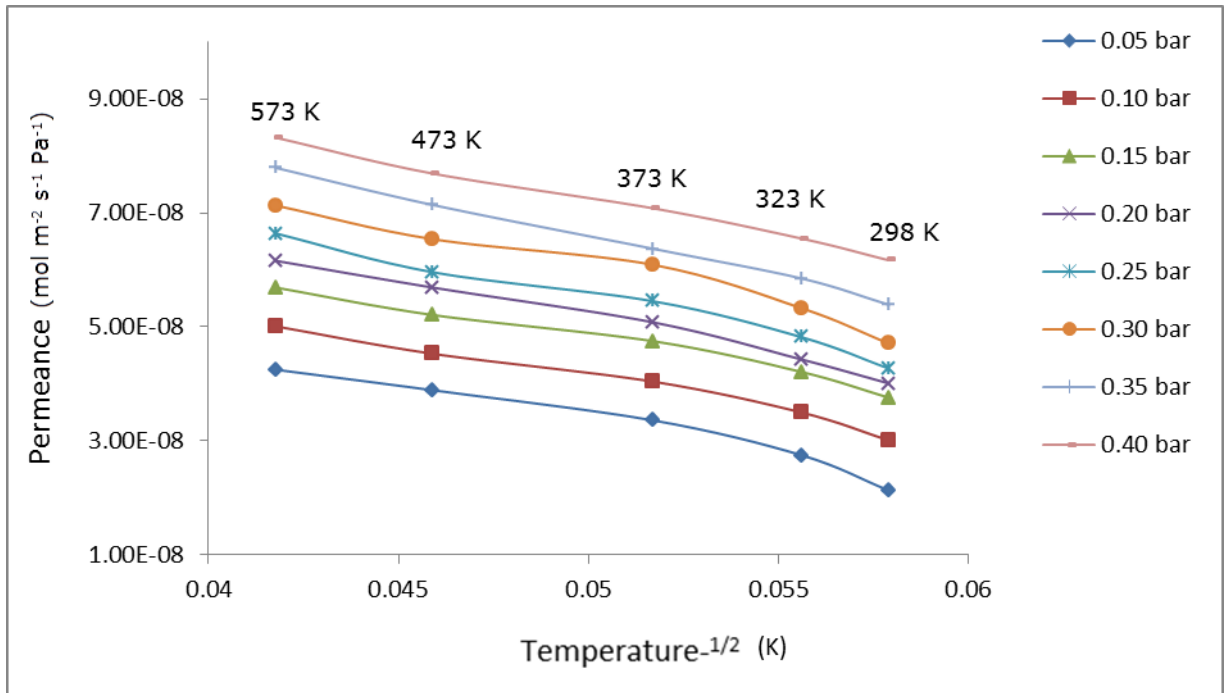


Figure 6.40: Ar permeance against the inverse square root of temperature for the SL1 membrane after first dip.

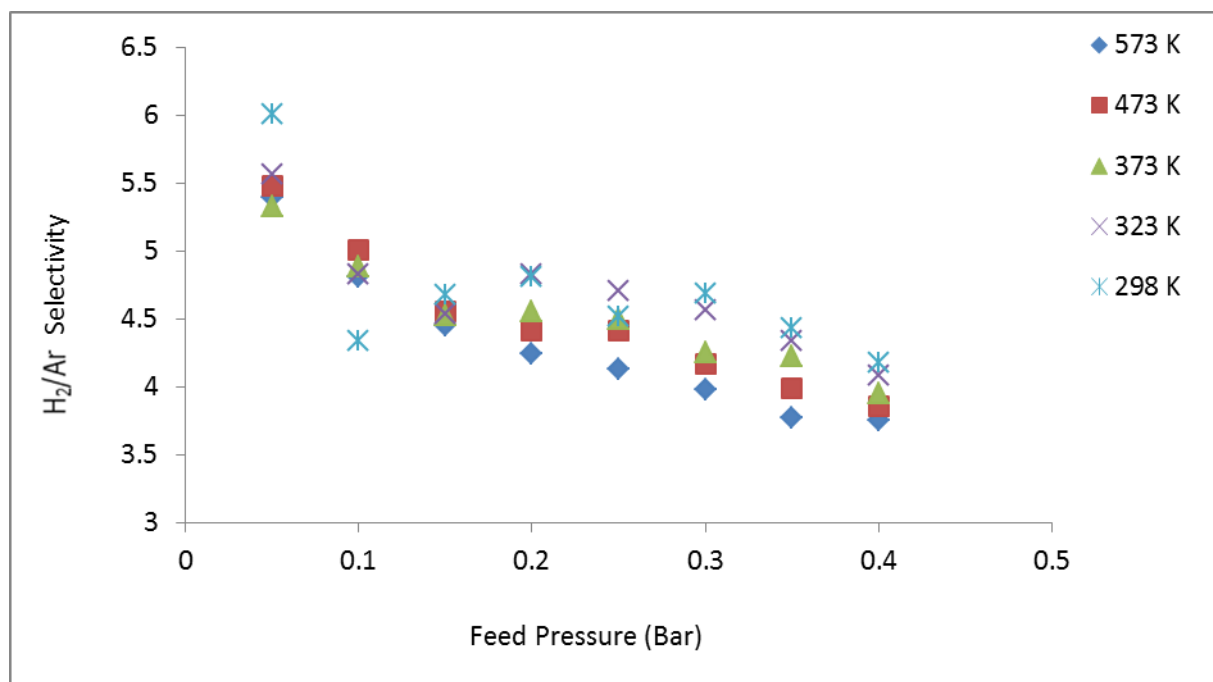


Figure 6.41: H₂/Ar selectivity for the SL1 membrane after first dip

6.4.2 Gas Permeation Through SL1 Membrane after second dip

Although the SL1 membrane showed high gas permeance especially for hydrogen, the membrane selectivity for hydrogen with respect to the other gases is low. For example, H₂ selectivity over CH₄, CO₂ and CO for silica membranes up to 1500 has been reported in literature [33]. It is necessary to devise a means of repairing any possible defects in the membrane support with a view to improving the support quality and by implication, the hydrogen permeation/selectivity of the membrane. This can be done by deposition of another silica layer. The second silica layer will plug any pinholes and repair any defects which impede membrane quality and loss of separation ability. Although it could repair any defects or pinholes in the membrane, the deposition of the second layer will also increase the gas permeation resistance of the membrane. After the second coating, an additional layer of thickness 18.06 μm was added which increased the total thickness of the active silica to 42.69 μm.

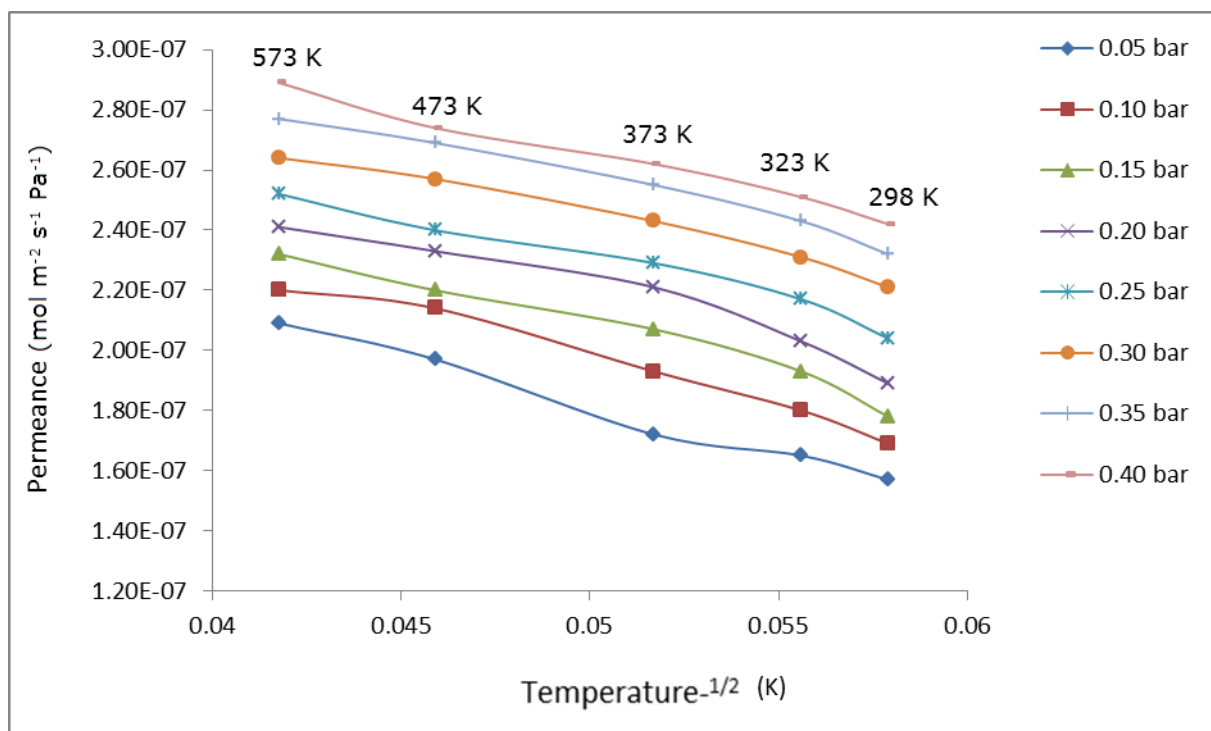


Figure 6.42: H₂ permeance against inverse square root of temperature for the SL1 membrane after second dip

Figure 6.42 shows hydrogen permeance after the second dip which is higher than the permeance of the 5 other single gases i.e He, CO₂, CH₄, N₂ and Ar. It was observed that the permeance of all the gases is lower than their respective permeance for the first coating. Hydrogen permeance was higher than Helium by about 1 order of magnitude which is attributed to the effect of higher temperature which opened up the pores for hydrogen permeation but this effect was less pronounced for the other 5 gases.

The highest permeance for hydrogen is $2.89 \times 10^{-7} \text{ mol m}^{-2} \text{ s}^{-1} \text{ Pa}^{-1}$ which is lower compared to $3.12 \times 10^{-7} \text{ mol m}^{-2} \text{ s}^{-1} \text{ Pa}^{-1}$ observed at 573 K and 0.4 bar for the first coating. The decrease in the permeance of hydrogen and the other gases is due to the increase in the silica layer thickness which increased the membrane resistance to permeation. The permeance after the second coating increased with increasing temperature which indicates that activated surface diffusion is the prevailing gas transport mechanism as was the case after the first coating.

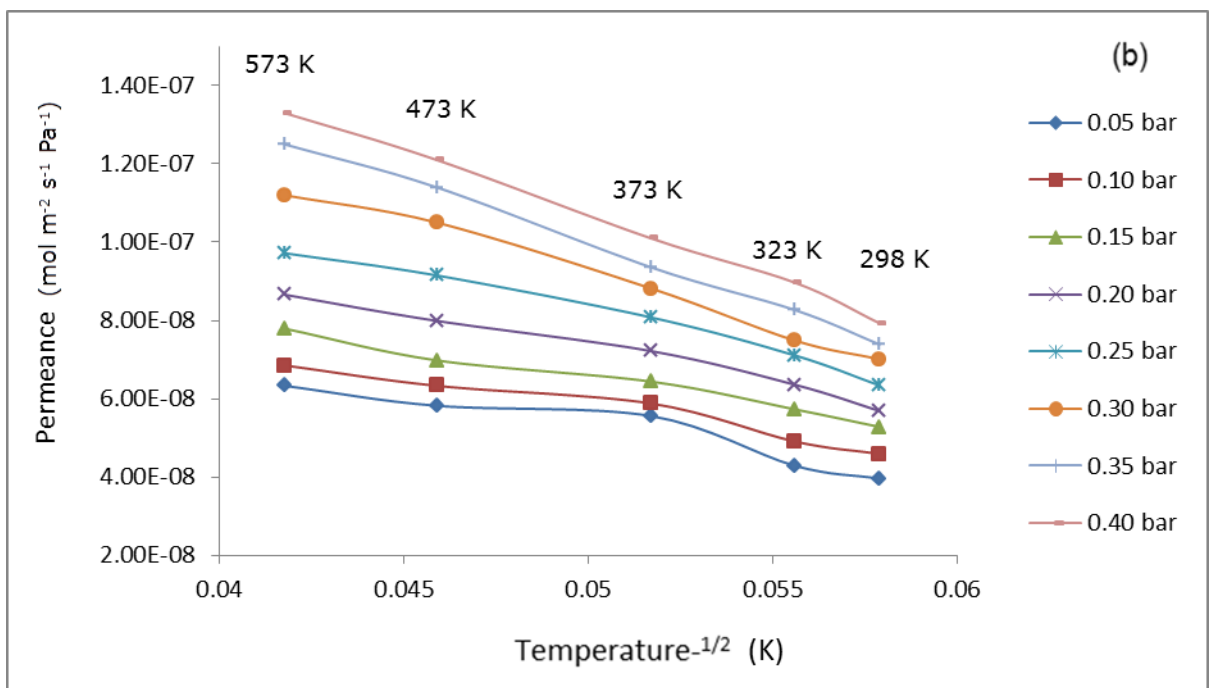
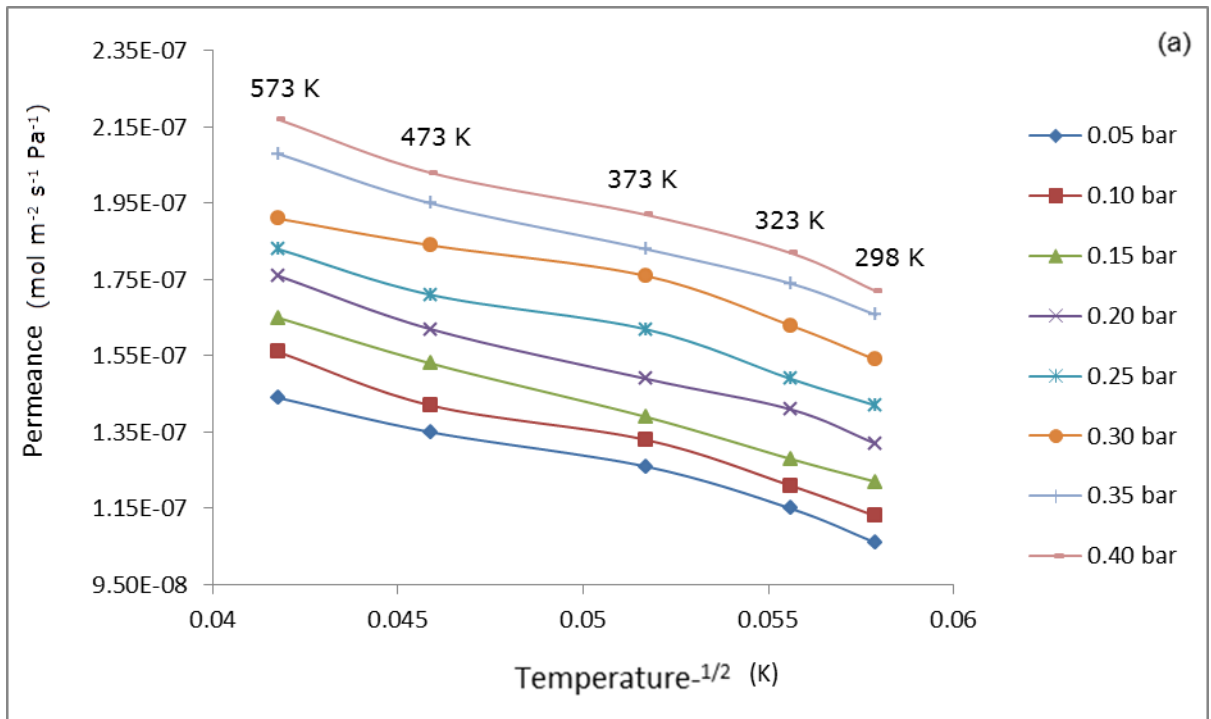


Figure 6.43: (a) He permeance and (b) CO₂ permeance against inverse square root of temperature for the SL1 membrane after the second dip

Figures 6.43 (a) and (b) show the plot of permeance of He and CO₂ respectively against the inverse of square root of temperature at different transmembrane pressure. The permeance of both gases $-2.17 \times 10^{-7} \text{ mol m}^{-2} \text{ s}^{-1} \text{ Pa}^{-1}$ and $1.33 \times$

$10^{-7} \text{ mol m}^{-2} \text{ s}^{-1} \text{ Pa}^{-1}$ - are comparably lower than their highest permeance at first coating i.e. $2.63 \times 10^{-7} \text{ mol m}^{-2} \text{ s}^{-1} \text{ Pa}^{-1}$ and $1.83 \times 10^{-7} \text{ mol m}^{-2} \text{ s}^{-1} \text{ Pa}^{-1}$ for He and CO_2 respectively.

It can also be observed that the permeance decreased with temperature which indicates an activated surface diffusion transport mechanism. One noticeable difference in the permeance of the 2 gases is that the permeance of He was more stable compared to that of CO_2 which indicated more propensity towards Knudsen diffusion for Helium compared to CO_2 . Temperature enhances surface diffusion because it promotes the mobility of the gas molecules within the pores of the membrane. The higher the temperature the higher the rate of diffusion of the gas through the pores of the membrane.

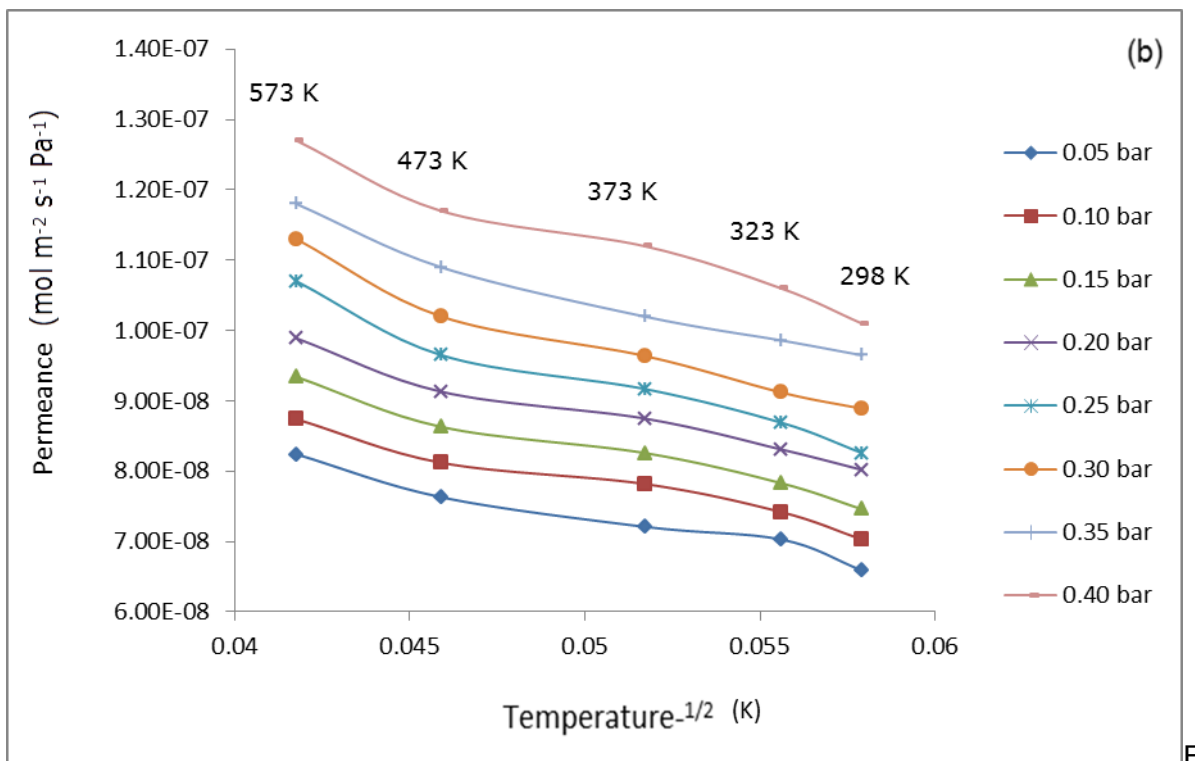
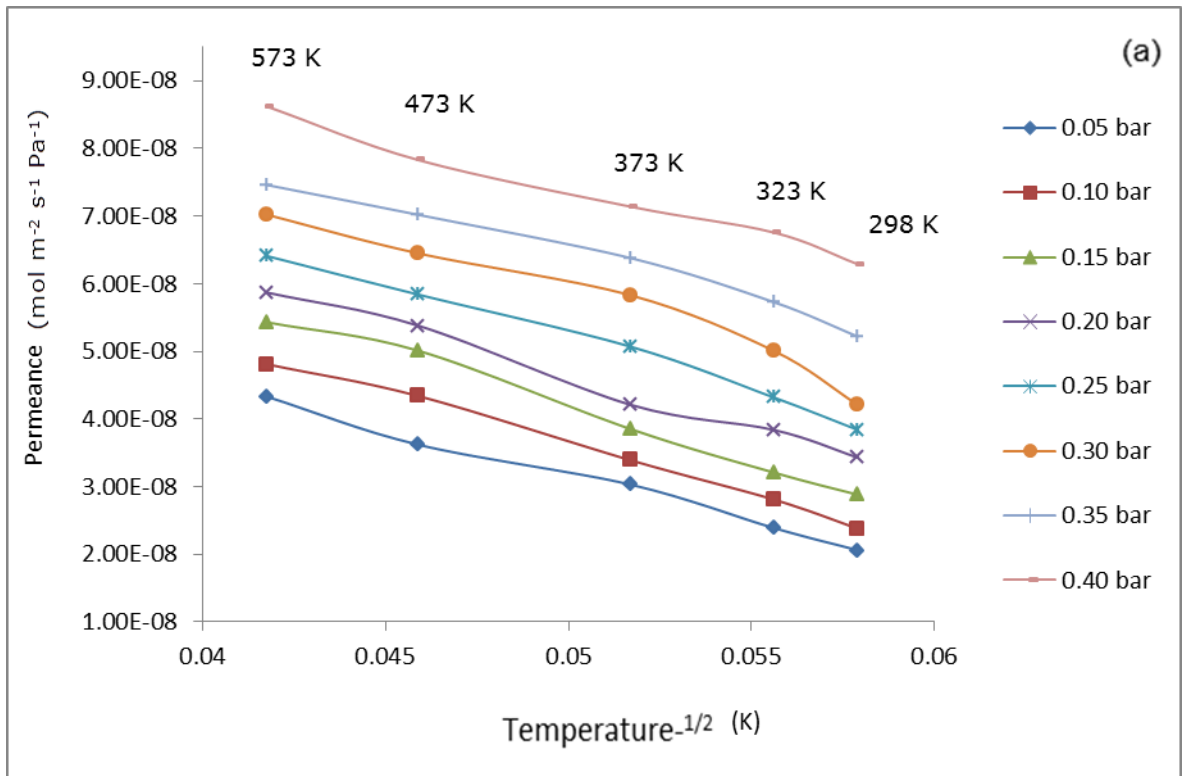


Figure 6.44: (a) CH₄ and (b) N₂ permeance against inverse square root of temperature for the SL1 membrane after the second dip

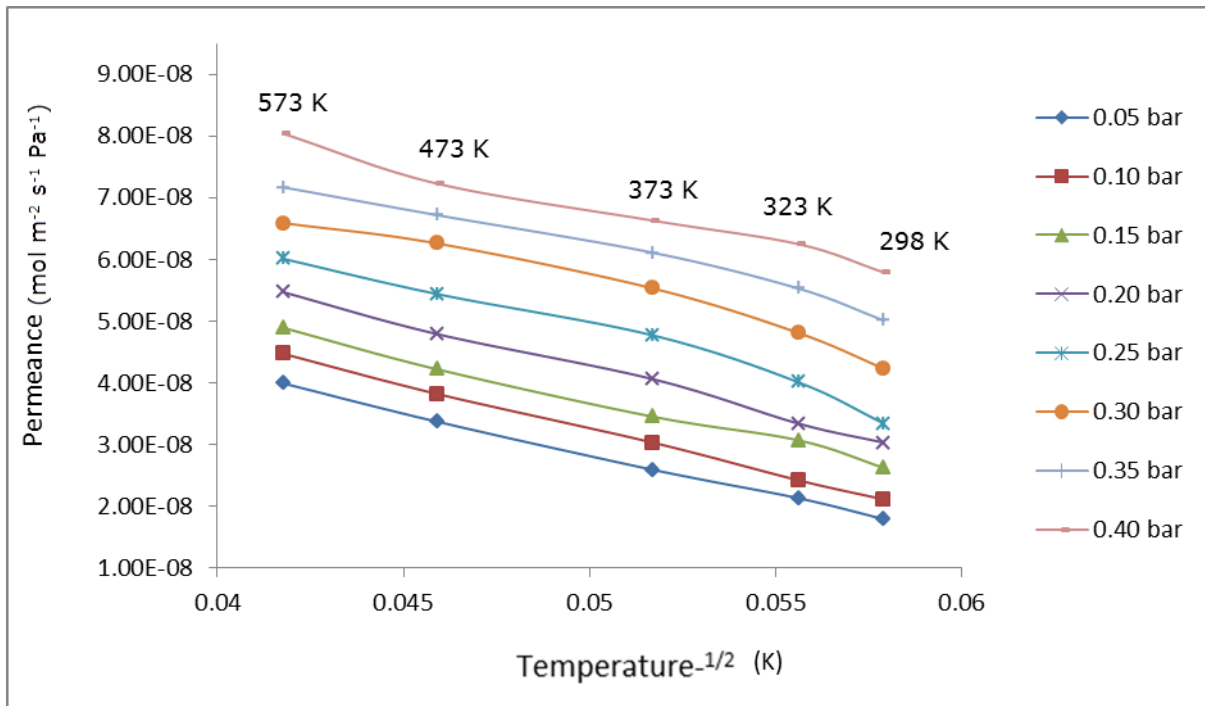


Figure 6.45: Ar permeance against square root of temperature for the SL1 membrane after the second dip

Figure 6.44 (a), (b) display the permeance of CH₄ and N₂ respectively and Figure 6.45 shows the permeance of Ar against the inverse square root of temperature at different pressure for the second coating. The same permeation behavior can be observed as in the first coating with a decrease in the permeance with increasing temperature. The permeance of both gases decreased with the additional layer to $8.62 \times 10^{-8} \text{ mol m}^{-2} \text{ s}^{-1} \text{ Pa}^{-1}$ and $1.27 \times 10^{-7} \text{ mol m}^{-2} \text{ s}^{-1} \text{ Pa}^{-1}$ for CH₄ and N₂ respectively.

The selectivity of the membrane after the second coating for hydrogen over the other five single gases was also investigated and compared with the H₂ selectivity for the second coating. The ideal selectivity results are displayed in Tables 6.9, 6.10, 6.11, 6.12 and 6.13. Fig. 6.45 shows the permeance of Ar for the second coating – $8.04 \times 10^{-8} \text{ mol m}^{-2} \text{ s}^{-1} \text{ Pa}^{-1}$

Table 6.9: H₂/He selectivity at different temperature and pressure for the SL1 membrane after second dip.

Feed Pressure (Bar)	573 K	473 K	373 K	323 K	298 K
0.05	1.38	1.35	1.36	1.38	1.41
0.10	1.33	1.38	1.39	1.40	1.40
0.15	1.38	1.40	1.38	1.42	1.44
0.20	1.37	1.44	1.41	1.46	1.44
0.25	1.41	1.44	1.48	1.44	1.43
0.30	1.41	1.44	1.53	1.56	1.46
0.35	1.45	1.51	1.45	1.44	1.50
0.40	1.45	1.43	1.37	1.43	1.48

Table 6.10: H₂/CH₄ selectivity at different temperature and pressure for the SL1 membrane after second dip

Feed Pressure (Bar)	573 K	473 K	373 K	323 K	298 K
0.05	2.21	2.17	2.24	2.22	2.22
0.10	2.29	2.36	2.36	2.36	2.32
0.15	2.26	2.36	2.41	2.56	2.34
0.20	2.27	2.35	2.41	2.34	2.26
0.25	2.34	2.41	2.38	2.32	2.22
0.30	2.36	2.36	2.69	2.57	2.22
0.35	2.37	2.40	2.27	2.23	2.16
0.40	2.38	2.34	2.11	2.13	2.14

Table 6.11: H₂/CO₂ selectivity at different temperature and pressure for the SL1 membrane after second dip

Feed Pressure (Bar)	573 K	473 K	373 K	323 K	298 K
0.05	2.39	2.16	2.00	1.38	1.68
0.10	2.47	2.30	2.09	1.88	1.69
0.15	2.49	2.36	2.09	1.88	1.67
0.20	2.53	2.33	2.12	1.85	1.63
0.25	2.52	2.36	2.10	1.81	1.60
0.30	2.51	2.34	2.42	2.05	1.59
0.35	2.54	2.37	2.02	1.81	1.59
0.40	2.50	2.26	1.90	1.73	1.58

Table 6.12: H₂/N₂ selectivity at different temperature and pressure after second dip

Feed Pressure (Bar)	573 K	473 K	373 K	323 K	298 K
0.05	2.28	2.38	2.34	2.37	2.40
0.10	2.35	2.47	2.50	2.46	2.40
0.15	2.34	2.52	2.52	2.53	2.49
0.20	2.36	2.49	2.50	2.50	2.47
0.25	2.44	2.55	2.53	2.44	2.36
0.30	2.48	2.55	2.61	2.67	2.39
0.35	2.52	2.64	2.47	2.43	2.40
0.40	2.54	2.58	2.39	2.35	2.38

Table 6.13: H₂/Ar selectivity at different temperature and pressure for the SL1 membrane after second dip

Feed Pressure (Bar)	723 K	673 K	623 K	573 K	523 K
0.05	2.734	2.78	2.75	2.71	2.73
0.10	2.74	2.86	2.83	2.74	2.75
0.15	2.74	2.84	2.84	2.74	2.76
0.20	2.75	2.78	2.78	2.74	2.69
0.25	2.78	2.82	2.78	2.64	2.60
0.30	2.78	2.77	3.15	3.01	2.57
0.35	2.73	2.80	2.67	2.62	2.54
0.40	2.67	2.6	2.44	2.47	2.50

The membrane selectivity for H₂ over all the gases decreased with pressure but increased with temperature for both the first and second coatings. For H₂/He after the second coating, the highest selectivity observed was 1.56 which is lower than 1.62 after the first coating as shown in Table 6.8. Both are higher than the theoretical Knudsen selectivity of 1.41. For H₂/CH₄, the highest selectivity observed was 2.69 after the second coating as shown in table 6.10 but this was lower than the highest selectivity i.e. 4.35 after the first coating. Both selectivities are higher than 2.82 which is the theoretical Knudsen selectivity. The same behavior was observed for H₂/CO₂ selectivity where the highest selectivity for the second coating i.e. 2.54 as shown in Table 6.11 is lower than that for the first coating i.e. 3.30. But in this case, the ideal selectivities for both the first and second coating were lower than the theoretical Knudsen selectivity of 4.67.

The H₂/N₂ selectivity however, was slightly higher for the second coating i.e. 2.67 as shown in Table 6.12 compared to the first coating- 2.63- but both are lower than the theoretical Knudsen selectivity of 3.73. The H₂/Ar selectivity decreased after the second dip from 5.39 for the first dip to 3.15 for the second dip.

The quality of the membrane can be improved so as to achieve a more selective membrane by polishing, however this method is adapted to flat surfaces hence tedious and repetitive. The use of thin intermediate layers is a more attractive option which can be used to generate a smooth surface to improve the chemical adhesion of the silica layer to the support.

6.4.3 Modification of the Alumina support with Boehmite sol for silica deposition

Modification of the tubular ceramic Alumina support with Boehmite sol prior to the silica deposition is one way of achieving a smooth and uniform surface for deposition of the silica layer and repairing any possible defects on the support. This is with a view to enhancing the hydrogen permeation behavior of the membrane. In this section, results are presented for the second stage of investigation on silica membranes where the alumina support was modified with Boehmite sol and investigated for hydrogen permeation and also the permeation of the 5 gases investigated for the SL1 membrane. The commercial alumina membrane of 6000 nm average pore size was dried in an oven for 2 hours at 65^o C after which it was calcined at 873 K for 10 hours at 2^o C/minute. The significance of the support modification with Boehmite is to produce smaller and more uniform pores, reduce surface roughness and ensure in a continuous structure. The small and uniform pores will result in a high hydrogen selective silica membrane.

After the calcination, the support was dipped in the Boehmite sol for 30 minutes after which it was dried overnight at room temperature. After drying, the support was calcined based on the same calcination cycle as before dipping. The weight gain method was used to calculate the thickness of the modified support. A smooth and uniformly coated silica membrane named SL2 with an estimated thickness of 31.19 μm was obtained. The intermediate Boehmite sol provided an intermediate region between the coarse macroporous silica support and the active silica layer. The modification of the α - alumina support with $\text{AlO}(\text{OH})$ sol prior to deposition of the silica layer results in a uniform surface for the deposition of a hydrogen selective silica layer. It was observed that the thickness

of the SL2 membrane has now increased compared to the thickness of membrane SL1 in which no support modification was carried out prior to deposition of the silica layer. This increase is due to the extra thickness of the Boehmite layer which will increase the resistance to permeation but will also fix defects or pinholes in the support and provide a smooth surface for the silica deposition.

6.4.4 Single Gas Permeation Tests for the SL2 membrane after first dip

The thickness of the SL2 membrane after modification with Boehmite sol and deposition of the silica layer was calculated as 31.19 μm . Single gas permeation tests were carried out for hydrogen and 5 other single gases as carried out for SL1 membrane at temperature and transmembrane pressure difference of 573, 473, 373, 323 and 298 K and 0.05 - 0.4 bar respectively.

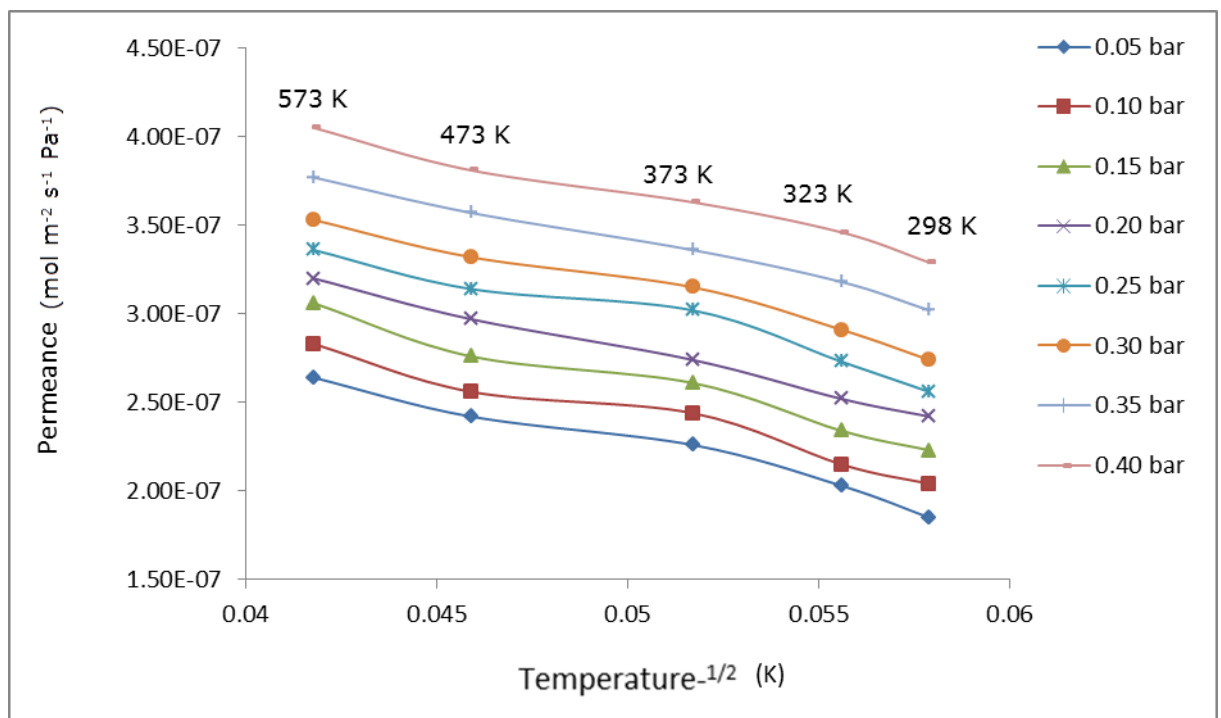


Figure 6.46: Hydrogen permeance against inverse square root of temperature for the SL2 membrane after first dip

It can be observed from Figure 6.46 that the maximum hydrogen permeance observed for the modified SL2 silica membrane of 30 nm average pore size is $4.05 \times 10^{-7} \text{ mol m}^{-2} \text{ s}^{-1} \text{ Pa}^{-1}$ at 573 K and transmembrane pressure differential of

0.4 bar. This is higher than the maximum hydrogen permeance for the unmodified silica membrane SL1 at first coating i.e $3.12 \times 10^{-7} \text{ mol m}^{-2} \text{ s}^{-1} \text{ Pa}^{-1}$ 10^{-6} at the same temperature and pressure differential. However, it can be observed that the increase in hydrogen permeance was more significant at lower temperature and more stable at higher temperature which indicates more propensity to Knudsen diffusion at higher temperature. It can be inferred that although the Boehmite layer increased the thickness of the membrane but served to fix the defects and pinholes associated with the membrane which enhance gas permeation through the membrane.

The increase in H₂ permeance also indicates that surface roughness has been minimized/eliminated and there is a more continuous structure and uniform pore size distribution. Apart from having a higher hydrogen permeance, the SL2 modified membrane also displayed a more stable hydrogen permeance than the SL1 unmodified membrane. This is as a result of the minimized surface roughness and continuous and uniform pore size distribution which enhance hydrogen permeation. The hydrogen permeance increases with increasing temperature and transmembrane pressure difference thus depicting a viscous flow and surface diffusion mechanism which was the case for the SL1 unmodified membrane.

The Boehmite is an intermediate layer which is meant to enhance gas permeation through the membrane by making the surface smoother and more uniform. However, as the boehmite layer is deposited, the thickness of the membrane increases and since gas permeation is inversely proportional to thickness, the permeance will decrease with an additional layer. However, the permeance increased when compared to the permeance before the modification of the support with Boehmite.

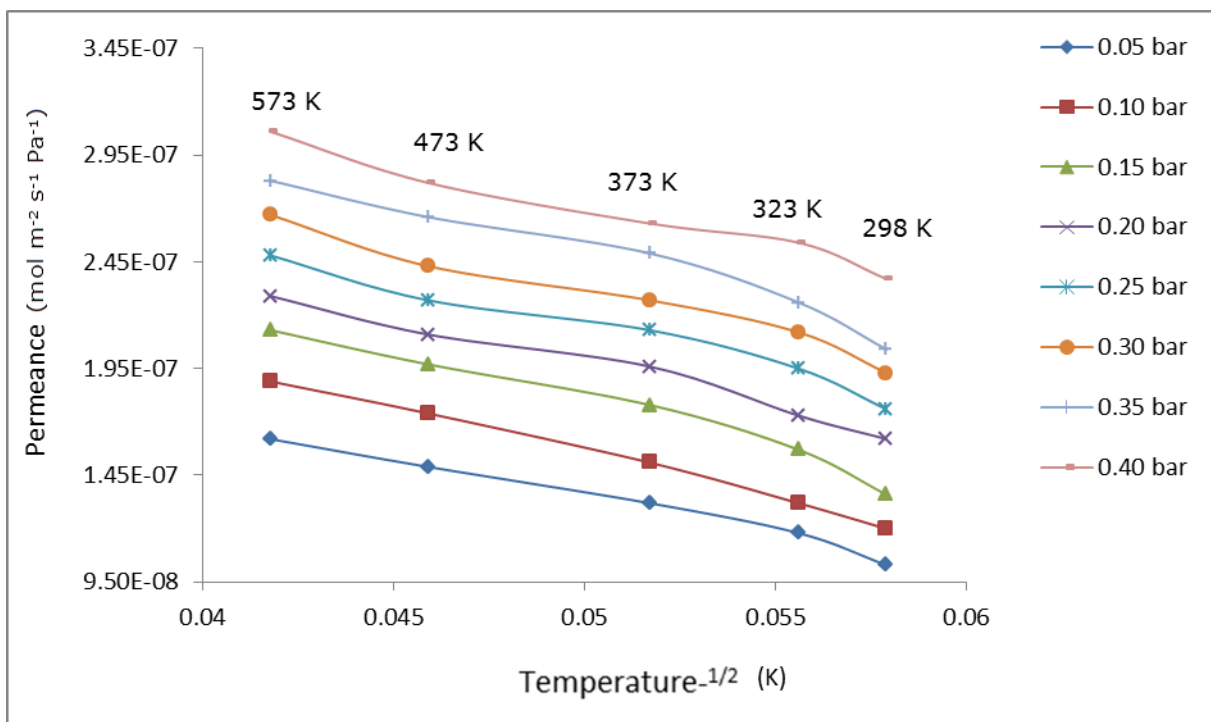


Figure 6.47: Helium permeance against inverse square root of temperature for the SL2 membrane after first dip

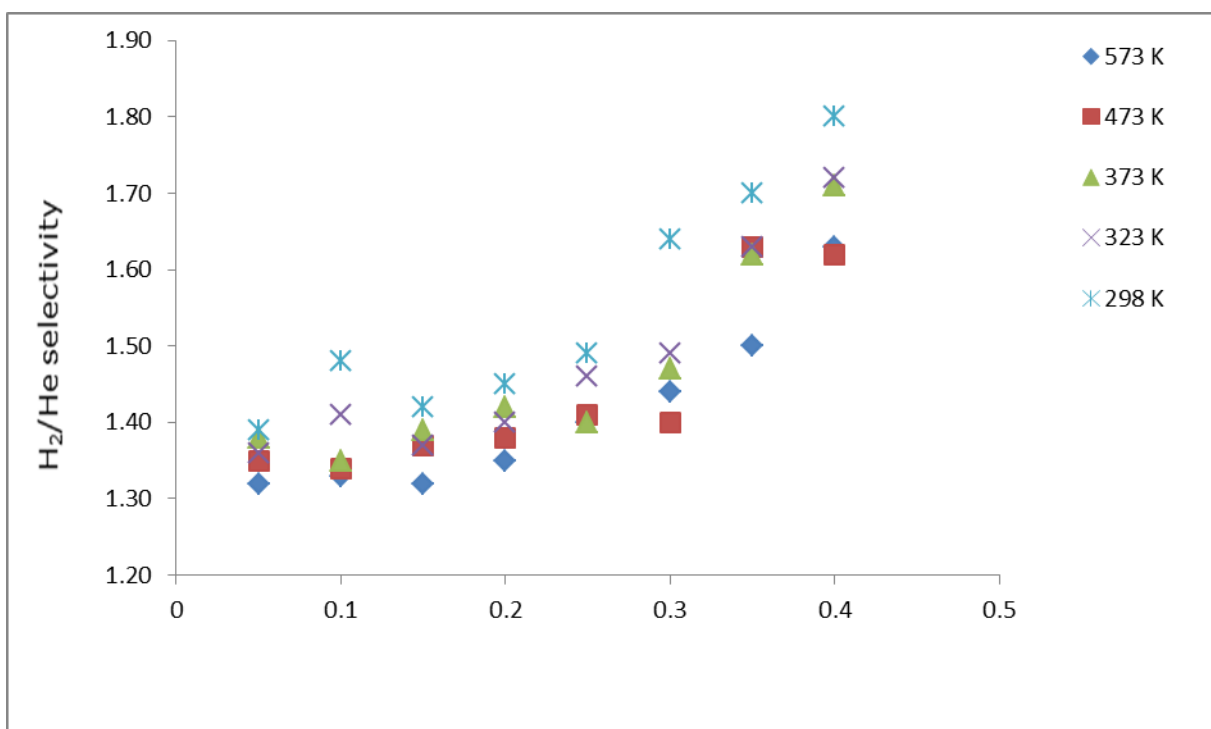


Figure 6.48: H₂/He selectivity for the SL2 membrane after first dip.

As can be observed from figure 6.47, the maximum helium permeance through the SL2 modified membrane at first coating increased to $3.06 \times 10^{-7} \text{ mol m}^{-2} \text{ s}^{-1} \text{ Pa}^{-1}$ from $2.63 \times 10^{-7} \text{ mol m}^{-2} \text{ s}^{-1} \text{ Pa}^{-1}$ for the unmodified SL1 membrane at 573 K and 0.05 bar. However, the He permeance was more stable compared to the H₂ permeance although it showed a little wobble at low temperature i.e. 323 and 298 K. In fact, the Helium permeance was largely unaffected by the increase in the transmembrane pressure. This is a departure from the transport mechanism for He permeation in SL1 which was clearly dominated by surface diffusion transport mechanism with some contribution of viscous flow.

As shown in figure 6.48, the maximum H₂/He selectivity for both the SL1 and SL2 membranes was almost same but different temperature and pressure conditions: 1.62 for the SL1 at 0.05 bar and 573 K and 1.80 for the SL2 membrane at 298 K and 0.40 bar. However, both values are higher than the theoretical Knudsen selectivity of 1.41 which indicates that the permeance of H₂ and He increased proportionately when the membrane was modified.

The H₂/He selectivity for both membranes was clustered at low temperatures but generally decreased at higher temperature for the SL1 membrane.

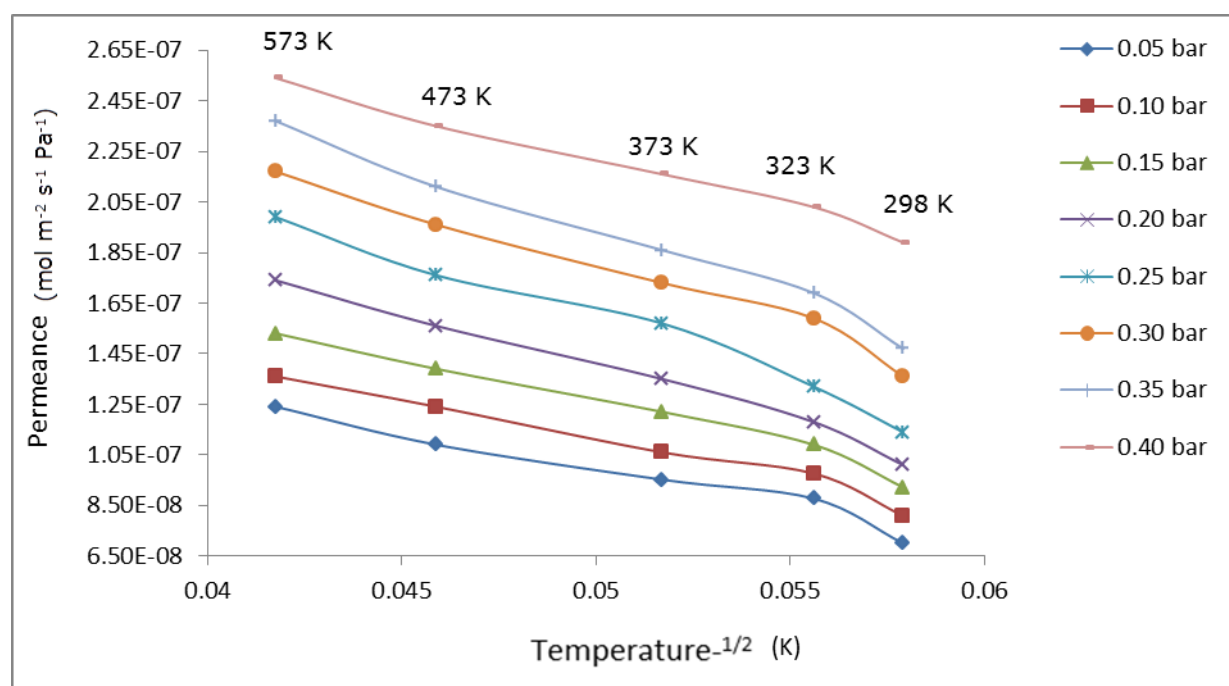


Figure 6.49: CO₂ permeance against inverse square root of temperature for the SL2 membrane after first dip.

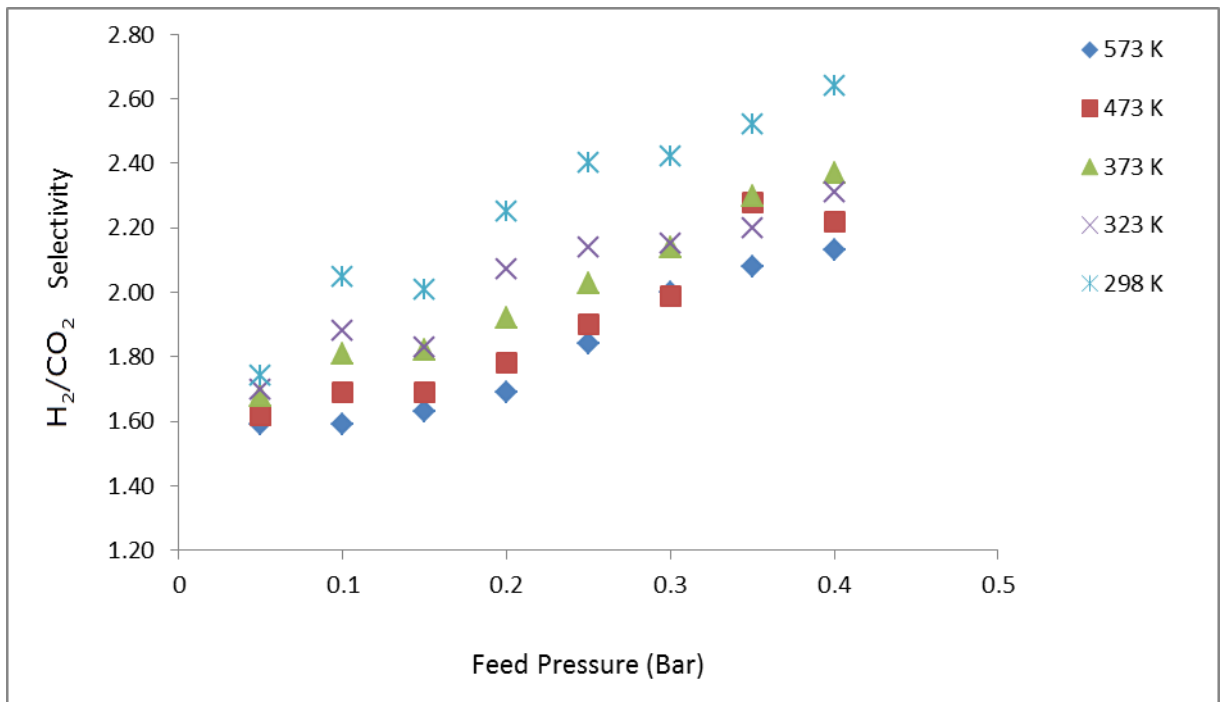


Figure 6.50: H₂/CO₂ selectivity for the SL2 membrane after first dip

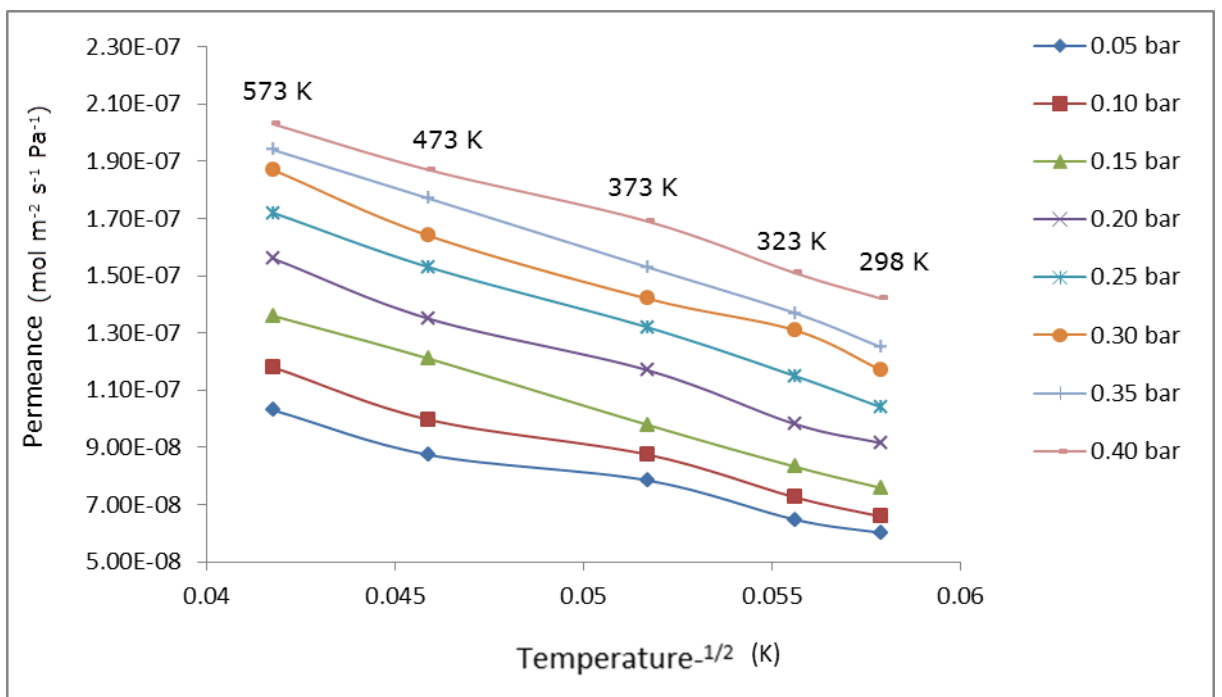


Figure 6.51: CH₄ permeance against inverse square root of temperature for the SL2 membrane after first dip.

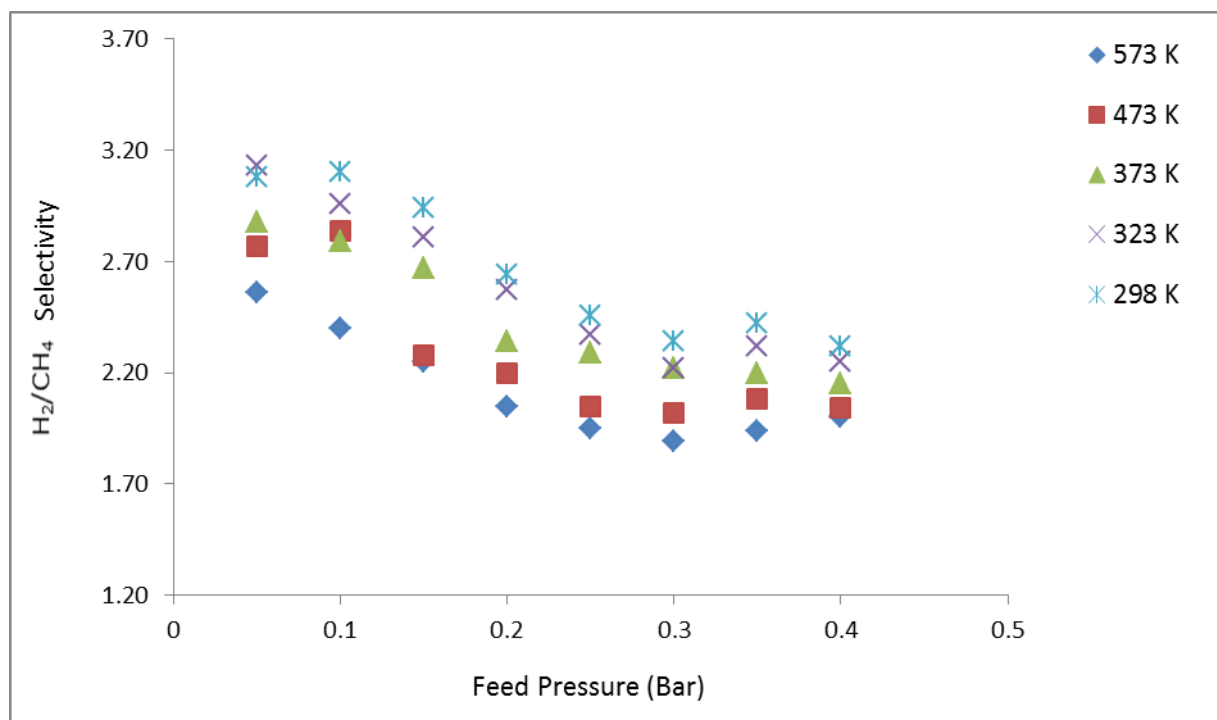


Figure 6.52: H₂/CH₄ selectivity at different temperature for the SL2 membrane after the first dip

The CO₂ and CH₄ permeance and H₂/CO₂ and H₂/CH₄ selectivity of the SL2 membrane after the first dip is shown in Figures 6.49 – 6.52. It can be observed that there is an increase in the permeance of both gases with increase in temperature and transmembrane pressure difference which suggests that surface diffusion controls gas permeation through the membrane with contribution of viscous flow. For the SL2 modified membrane, the highest CO₂ permeance is $2.54 \times 10^{-7} \text{ mol m}^{-2} \text{ s}^{-1} \text{ Pa}^{-1}$ which is higher than the CO₂ permeance of $1.83 \times 10^{-7} \text{ mol m}^{-2} \text{ s}^{-1} \text{ Pa}^{-1}$ for the SL1 membrane while the highest permeance for CH₄ is $2.03 \times 10^{-7} \text{ mol m}^{-2} \text{ s}^{-1} \text{ Pa}^{-1}$ which is higher than the CH₄ permeance for the SL1 membrane after the first coating i.e. $9.98 \times 10^{-8} \text{ mol m}^{-2} \text{ s}^{-1} \text{ Pa}^{-1}$.

One observed difference in the gas permeation behavior of SL1 as against that of SL2 is that the permeance of CH₄ decreased more slowly for SL2 as against a deeper drop for SL1. The highest H₂/CO₂ selectivity was 2.64 at 298 K and a transmembrane pressure of 0.4 bar which is lower than the theoretical Knudsen selectivity of 4.67.

The increase in permeance for the SL2 membrane and the corresponding decrease in selectivity is conventionally correct and stems from the fact that there was an increase in the permeance for both hydrogen and CO₂ after modification with AlOOH sol. For the H₂/CH₄ selectivity, the highest selectivity observed was 3.13 at 323 K for a transmembrane pressure difference of 0.05 bar which is higher than the theoretical Knudsen selectivity of 2.82. The highest H₂/CH₄ selectivity for SL2 membrane is however lower than same for the SL1 membrane which is 4.35 at same temperature and transmembrane pressure.

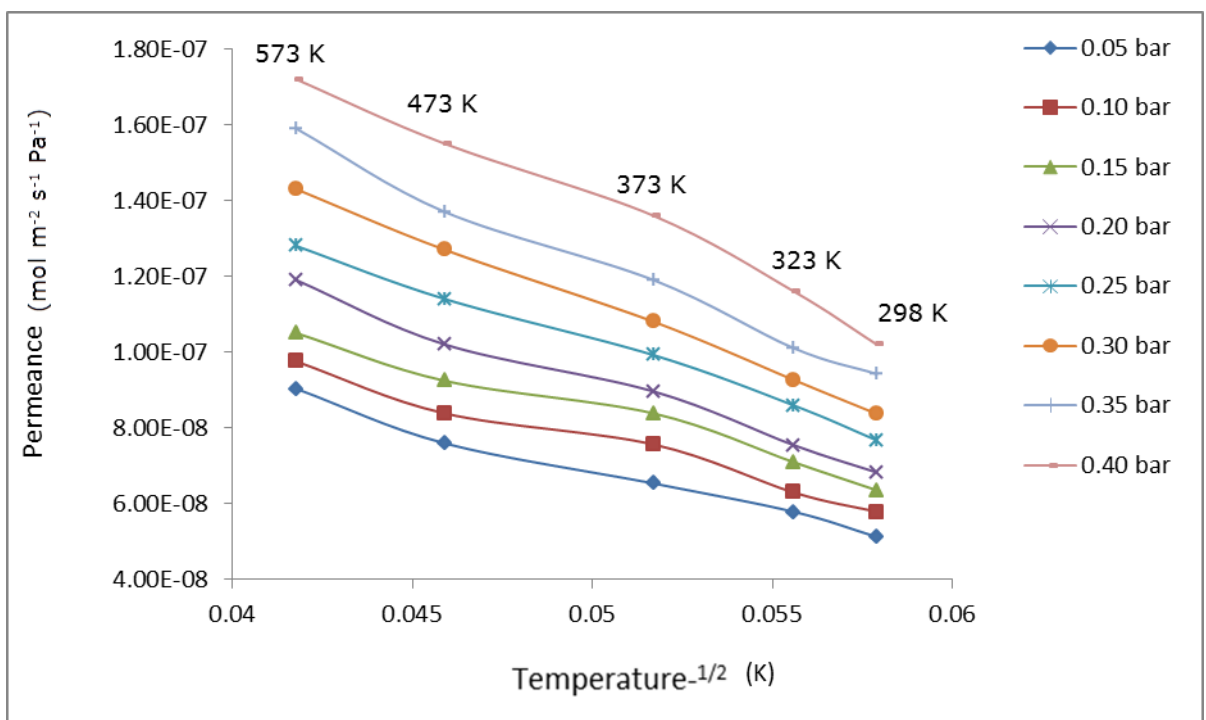


Figure 6.53: N₂ permeance against inverse square root of temperature for the SL2 membrane after the first dip.

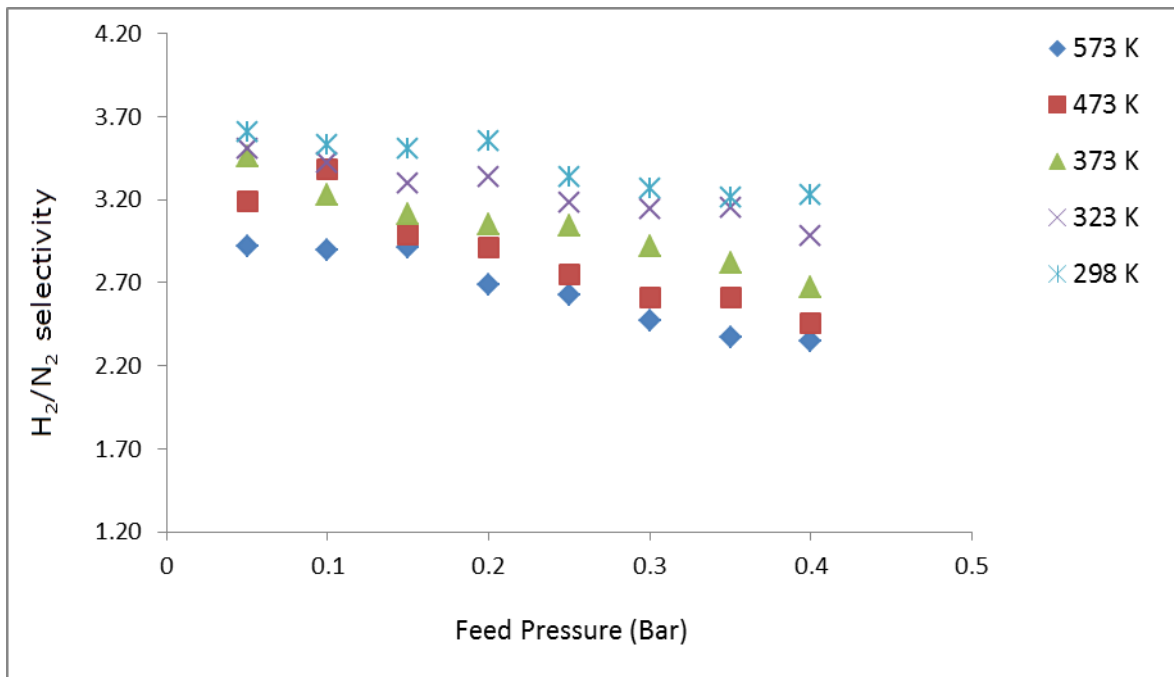


Figure 6.54: H_2/N_2 selectivity at different temperature for the SL2 membrane after first dip

The permeance of N_2 and H_2/N_2 selectivity is also shown in Figures 6.53 and 6.54 respectively. However, the H_2/N_2 selectivity increased from 2.63 for the SL1 membrane to 3.61 for the SL2 membrane at 298K K and 0.05 bar. The ideal selectivity for both membranes is lower than the theoretical Knudsen value of 3.73. For the SL2 membrane, the difference in permeance at different pressure was less significant compared to the SL1 membrane but the stability of both membranes in terms of the applicable gas transport mechanism is identical. The drop in gas permeance with decreasing temperature also confirms surface diffusion as the dominant gas transport mechanism with contribution of viscous flow.

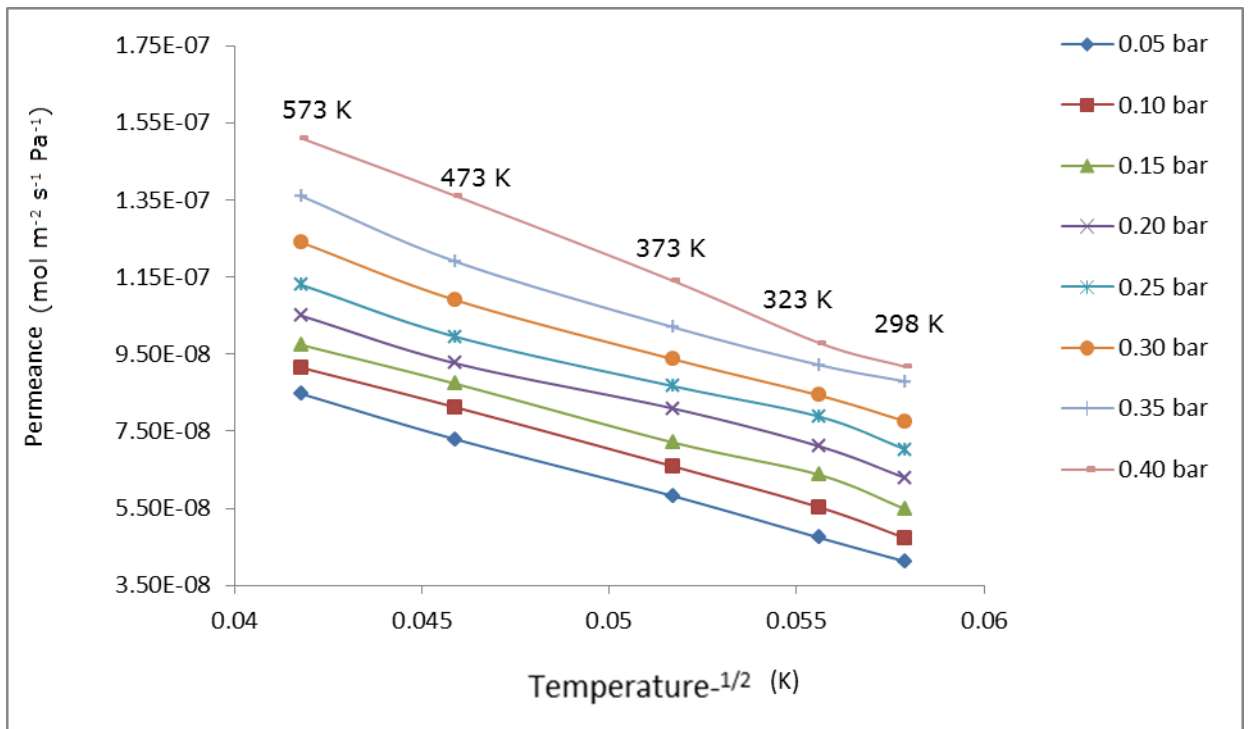


Figure 6.55: Ar permeance against the inverse square root of temperature for the SL2 membrane after first dip

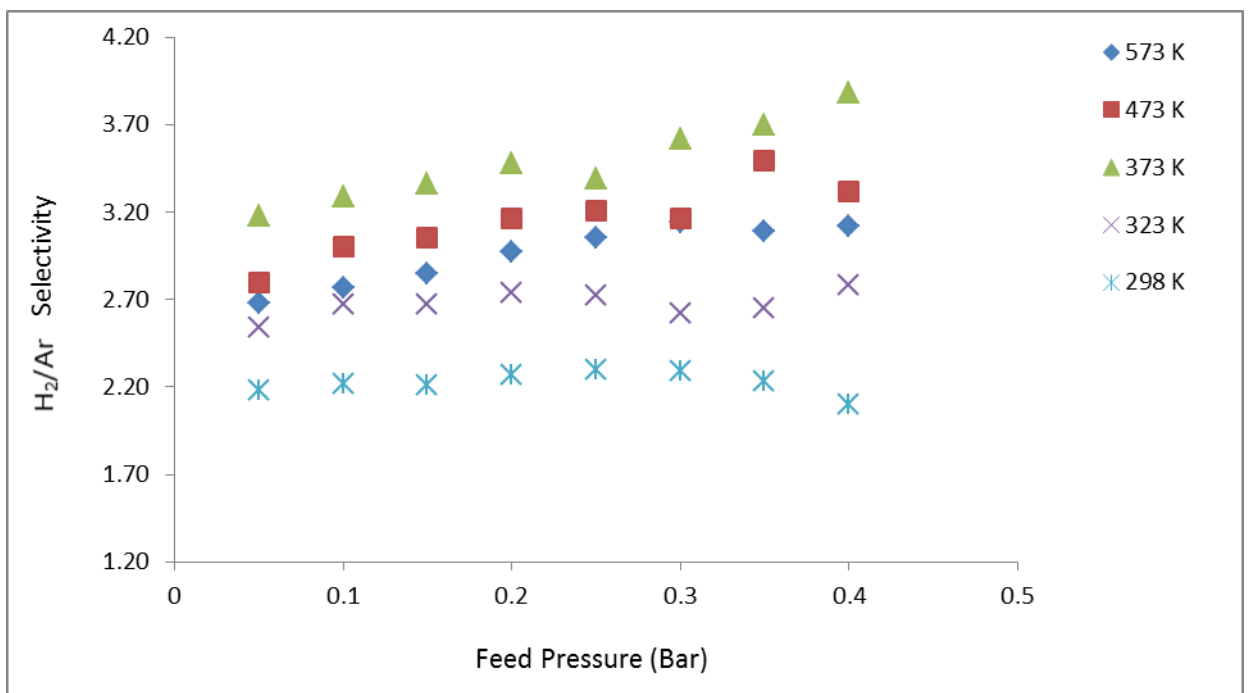


Figure 6.56: H₂/Ar selectivity at different temperature for the SL2 membrane after first dip

From the Ar permeance shown in Figure 6.55, it can be observed that the permeance increased from $8.32 \times 10^{-8} \text{ mol m}^{-2} \text{ s}^{-1} \text{ Pa}^{-1}$ for SL1 membrane to $1.51 \times 10^{-7} \text{ mol m}^{-2} \text{ s}^{-1} \text{ Pa}^{-1}$ for the SL2 membrane. From figure 6.56, it can be observed that the highest H_2/Ar selectivity observed was 3.88 at 373 K and 0.4 bar which is above the theoretical Knudsen selectivity of 4.45.

6.4.5 Single Gas Permeation Tests for the Modified Silica Membrane after Second Dip

A second silica layer was deposited on the SL1 membrane after the first dip using the same procedure as for the first coating. The thickness of the second silica layer was calculated as $19.70 \mu\text{m}$ which brought the total thickness of the SL2 membrane to $50.89 \mu\text{m}$. The significance of the second layer deposition is to repair any defects or pinholes in the silica layer for improved gas permeation and selectivity. A uniformly coated membrane with a continuous silica layer was obtained. However, the thickness of the membrane increased to $50.89 \mu\text{m}$ owing to the additional silica layer.

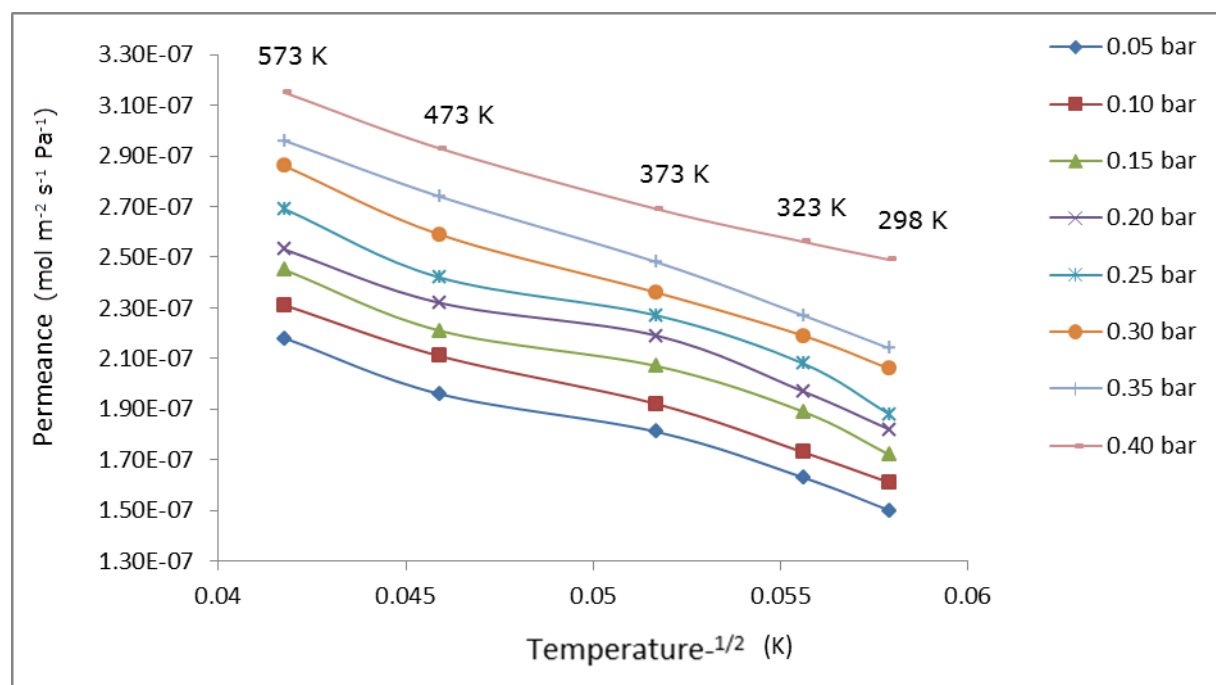


Figure 6.57: Hydrogen permeance against inverse square root of temperature for the SL2 membrane after second dip

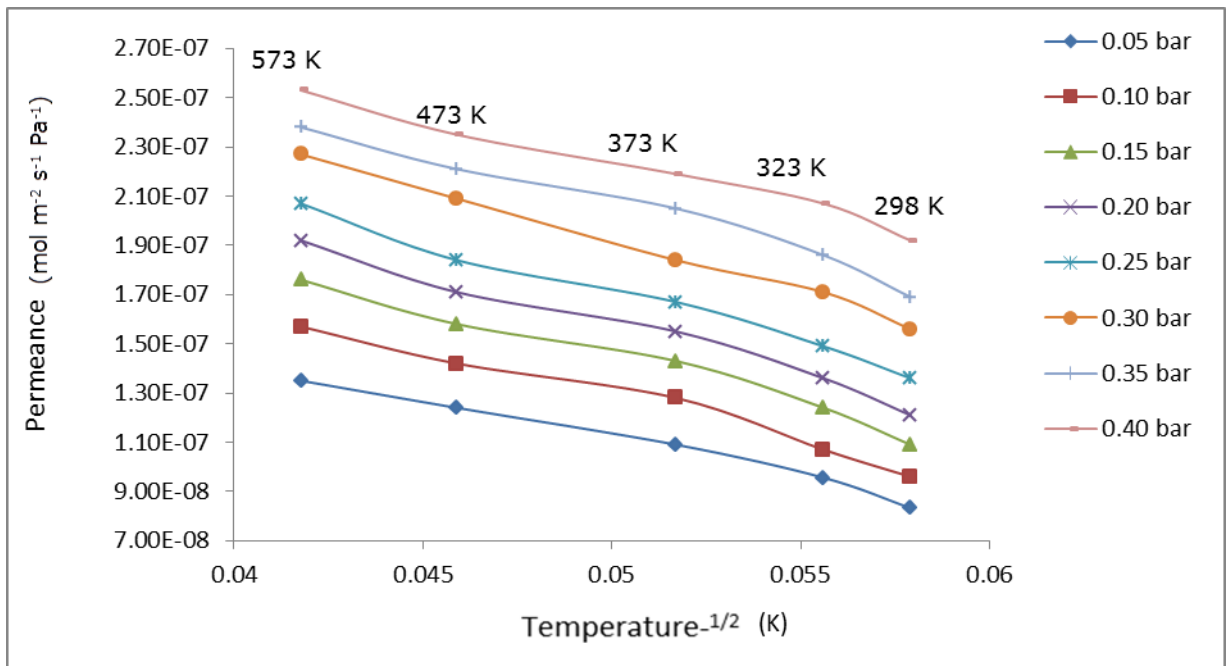


Figure 6.58: Helium permeance against the inverse square root of temperature for the SL2 membrane after second dip

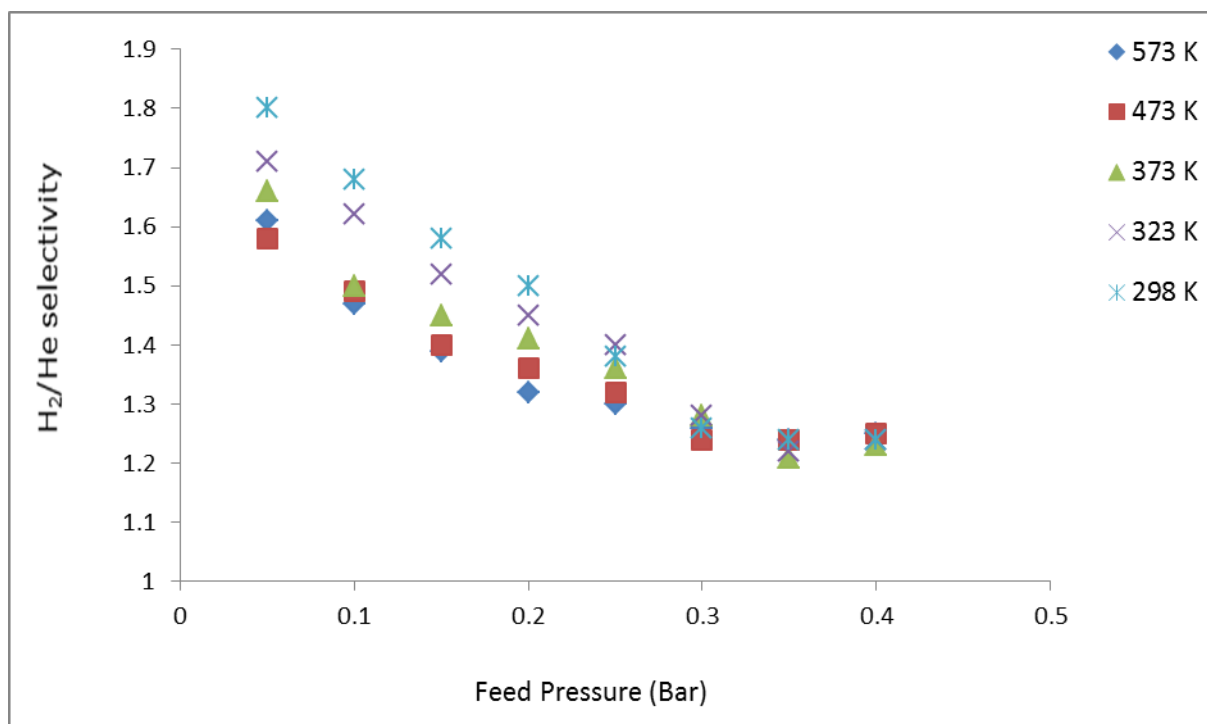


Figure 6.59: H₂/He selectivity at different temperatures for the SL2 membrane after second dip.

It can be observed from figure 6.57 that hydrogen permeance decreased with temperature and differential pressure with a maximum of $3.15 \times 10^{-7} \text{ mol m}^{-2} \text{ s}^{-1} \text{ Pa}^{-1}$ at 573 K and 0.4 bar. This indicates more resistance to permeation compared to $4.05 \times 10^{-7} \text{ mol m}^{-2} \text{ s}^{-1} \text{ Pa}^{-1}$ for the SL2 membrane after the first coating which confirms that there could be some defects or pinholes in the alumina support. This is because the hydrogen permeance has now increased for the same type of support under the same conditions except that in this case the support was modified.

The H₂ permeance is less stable compared to the He permeance in figure 6.58 which means that there is more likelihood for Knudsen diffusion in He than in H₂. The modification with AlO (OH) sol has improved the surface structure and morphology of the membrane which enhanced hydrogen permeation through the membrane. As shown in figure 6.59, the highest H₂/He ideal selectivity was 1.80 at 298 K and 0.05 bar which is higher than the theoretical Knudsen selectivity of

1.41. The ideal selectivity increased with temperature but became more stable with increasing transmembrane pressure.

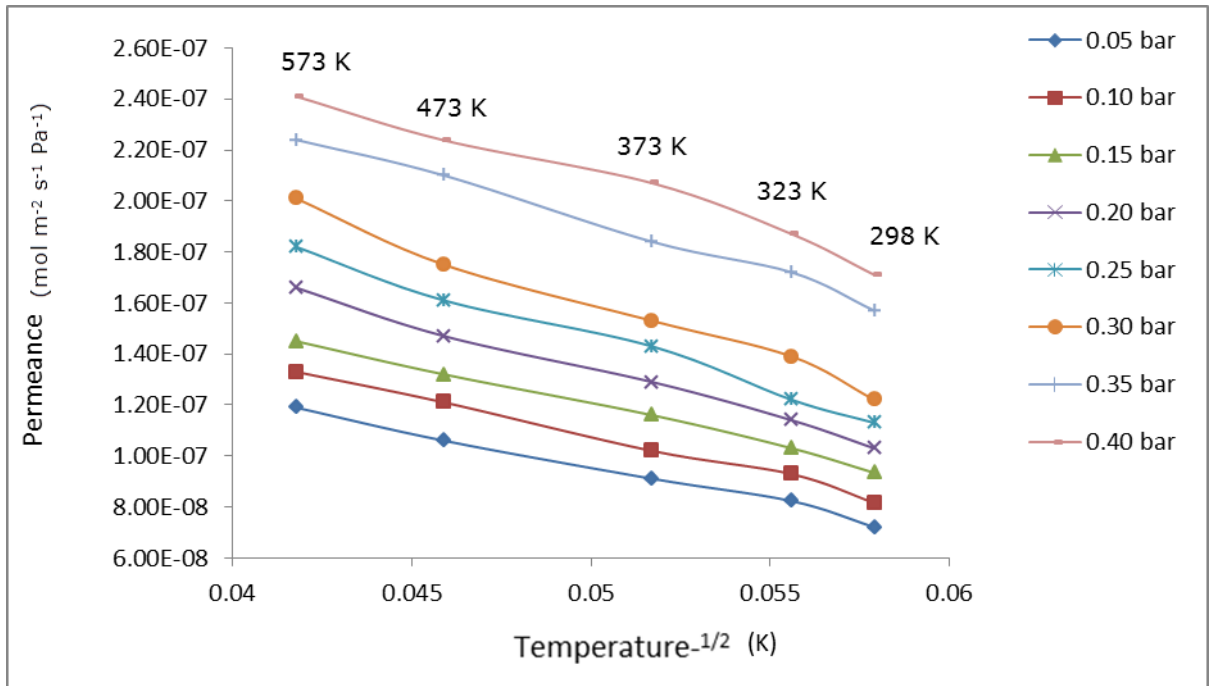


Figure 6.60: CO₂ permeance against inverse square root of temperature for the SL2 membrane after second dip.

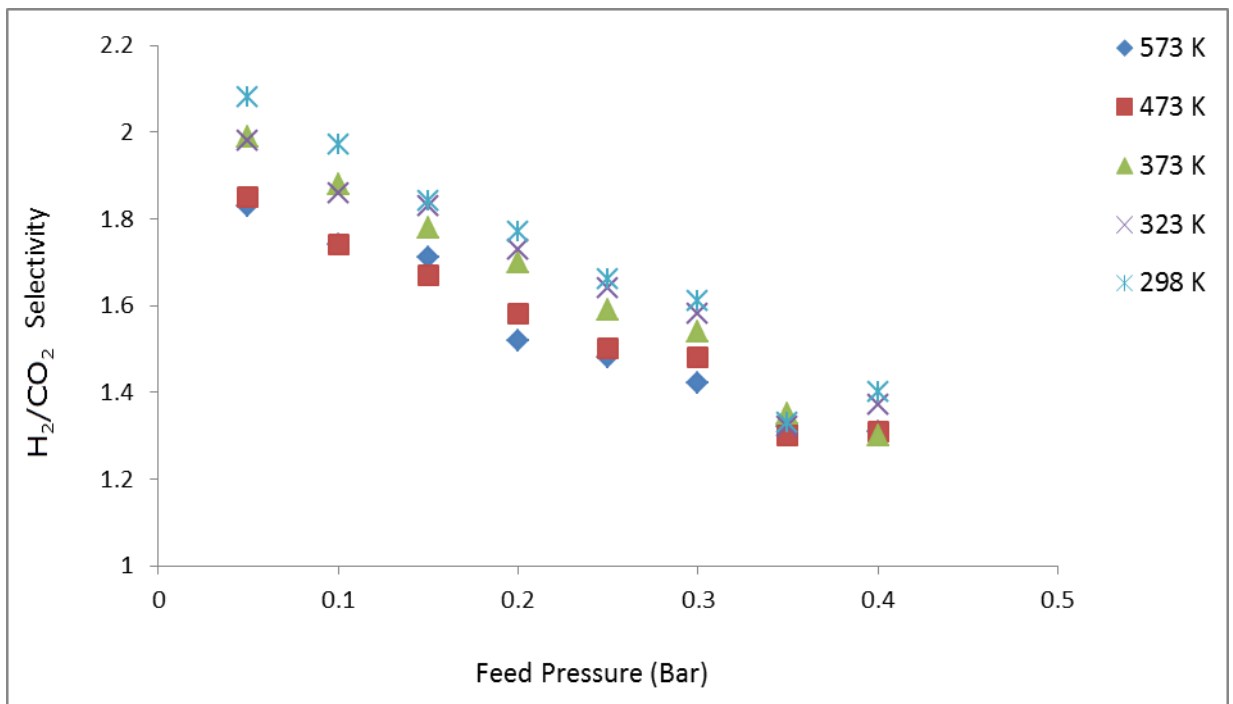


Figure 6.61: H₂/CO₂ selectivity at different temperature for the SL2 membrane after second dip

Figures 6.60 and 6.61 show the CO₂ permeance and H₂/CO₂ selectivity for the SL2 membrane after second dip. It can be observed that there is a decrease in the CO₂ after the second coating from $2.54 \times 10^{-7} \text{ mol m}^{-2} \text{ s}^{-1} \text{ Pa}^{-1}$ to $2.41 \times 10^{-7} \text{ mol m}^{-2} \text{ s}^{-1} \text{ Pa}^{-1}$ which could be attributed to the increased resistance to permeation after the second coating. The highest H₂/CO₂ selectivity after the second coating was 2.08 at 298 K and 0.05 bar which was below the theoretical Knudsen selectivity of 4.67.

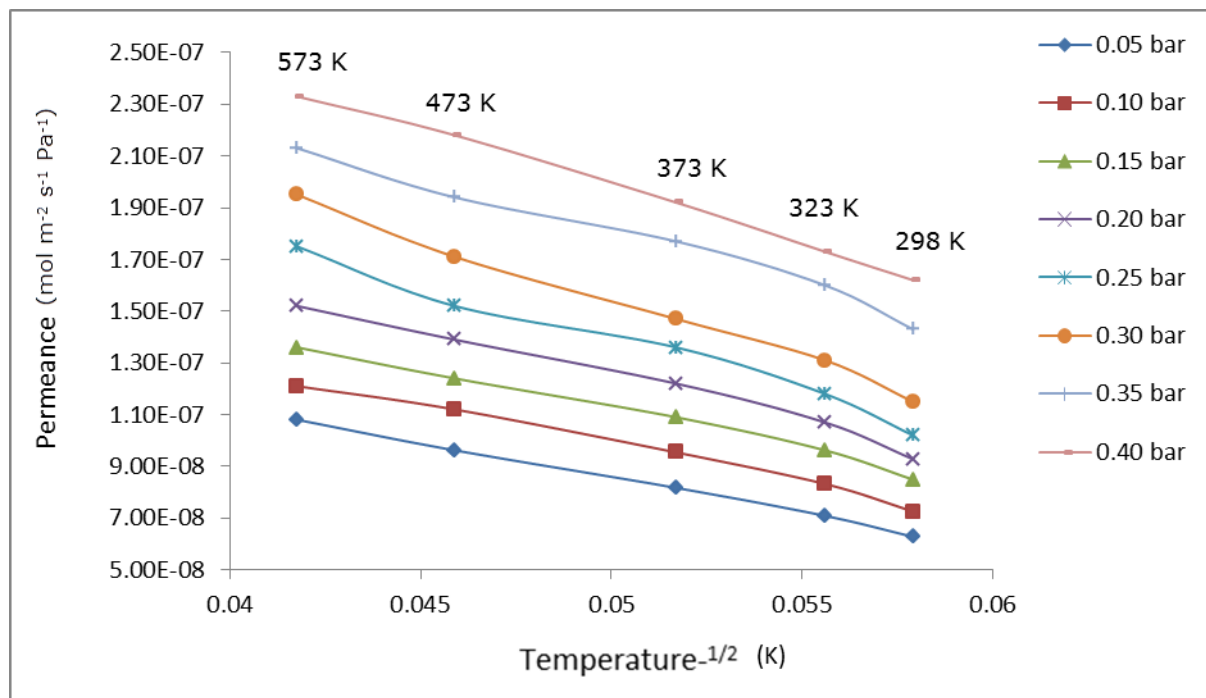


Figure 6.62: CH₄ permeance against inverse square root of temperature for the SL2 membrane after second dip

The CH₄ permeance is shown in Figure 6.62 and it decreased with temperature and transmembrane pressure after the second dip but appears to be more stable with increasing transmembrane pressure which depicts increased deviation from activated surface diffusion and closeness to Knudsen diffusion. The maximum

CH₄ permeance after the second coating was $2.33 \times 10^{-7} \text{ mol m}^{-2} \text{ s}^{-1} \text{ Pa}^{-1}$ at 573 K and 0.4 bar.

The H₂/CH₄ selectivity is shown in figure 6.63 and it increases with temperature with the highest selectivity of 2.39 at 289 K and 0.05 bar which is lower than the theoretical Knudsen selectivity of 2.82. However, after the first coating the highest H₂/CH₄ selectivity observed was 3.13 at 323 K and 0.05 bar which is higher than the theoretical Knudsen selectivity. This indicates that the H₂/CH₄ selectivity of the membrane decrease after the second coating.

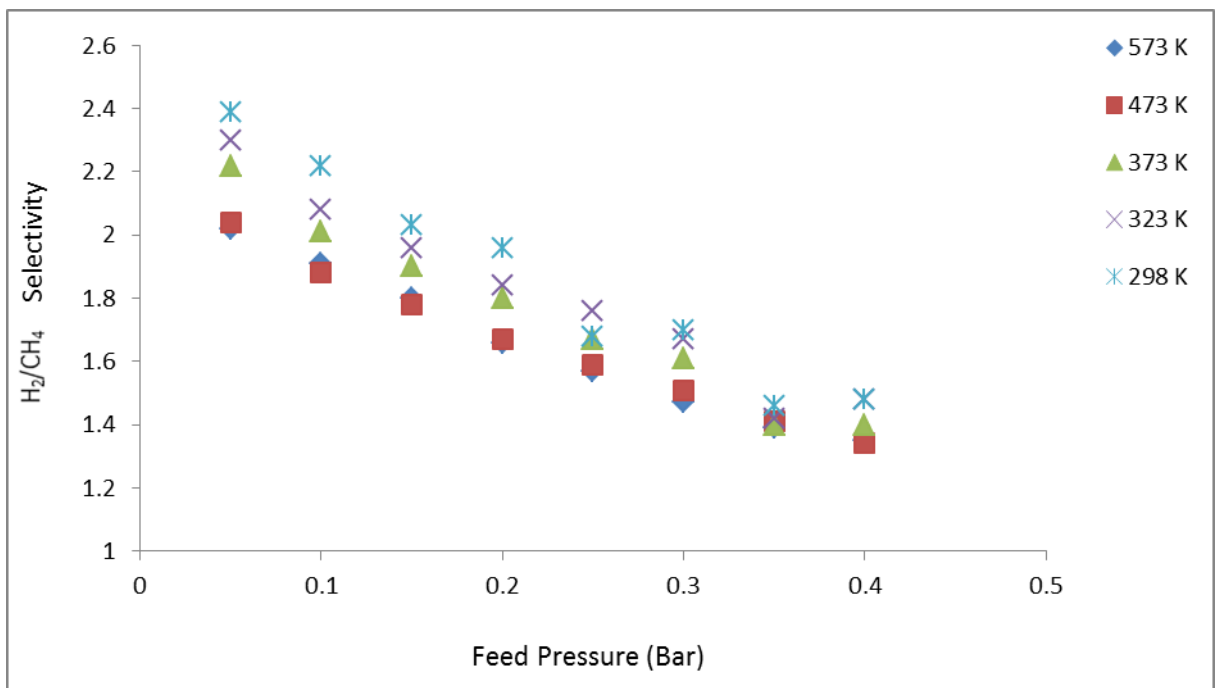


Figure 6.63: H₂/CH₄ selectivity at different temperature for the SL2 membrane after second dip

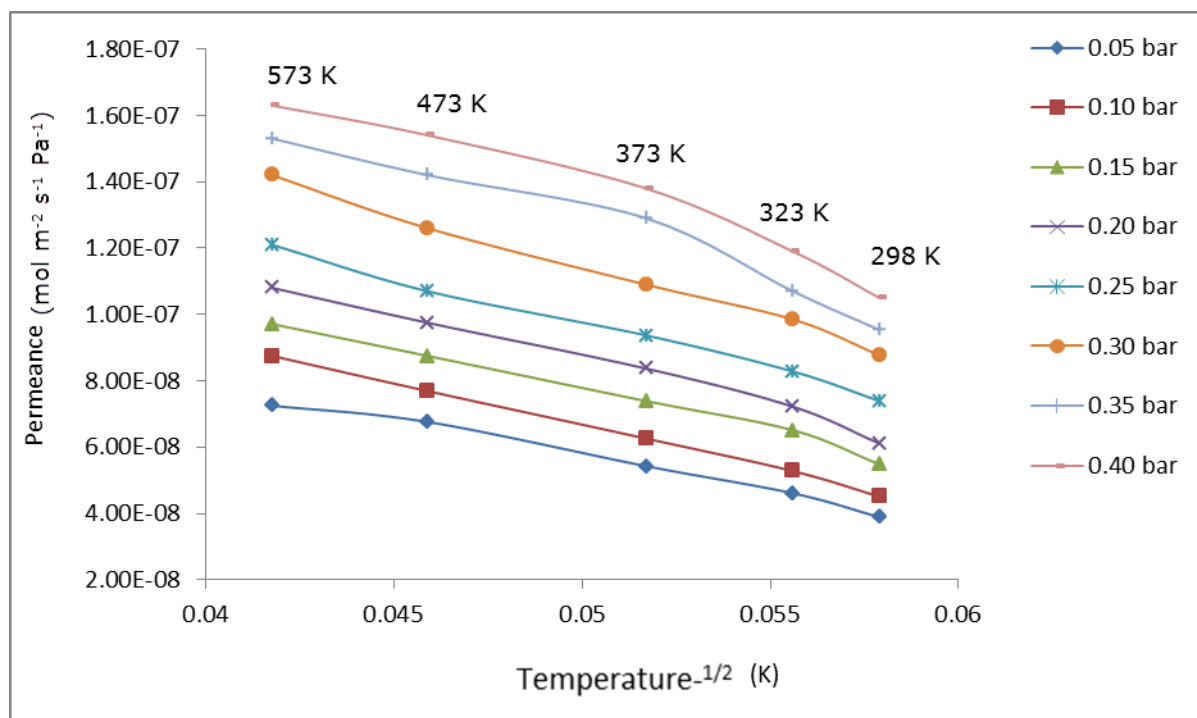


Figure 6.64: N₂ permeance against inverse square root of temperature for the SL2 membrane after second dip

The maximum N₂ permeance for the SL2 membrane shown in figure 6.64 decreased after the second coating to $1.63 \times 10^{-7} \text{ mol m}^{-2} \text{ s}^{-1} \text{ Pa}^{-1}$ from $1.72 \times 10^{-6} \text{ mol m}^{-2} \text{ s}^{-1} \text{ Pa}^{-1}$ for the first coating but the decrease was relatively stable with increasing transmembrane pressure. The same trend was observed after the first coating which relates to a closer tendency towards Knudsen diffusion. The H₂/N₂ selectivity is shown in figure 6.65 and it can be observed that the maximum selectivity was 3.18 at 573 K which increased with temperature and pressure.

The highest H₂/N₂ selectivity was 3.86 at 298 K and 0.05 bar which is higher than the theoretical Knudsen selectivity of 3.73. However, the highest H₂/N₂ selectivity after the first coating was 3.61 at 298 K and 0.05 bar which is lower than the theoretical Knudsen selectivity of 3.73. This indicates a decrease in selectivity of the SL2 membrane after deposition of the second layer.

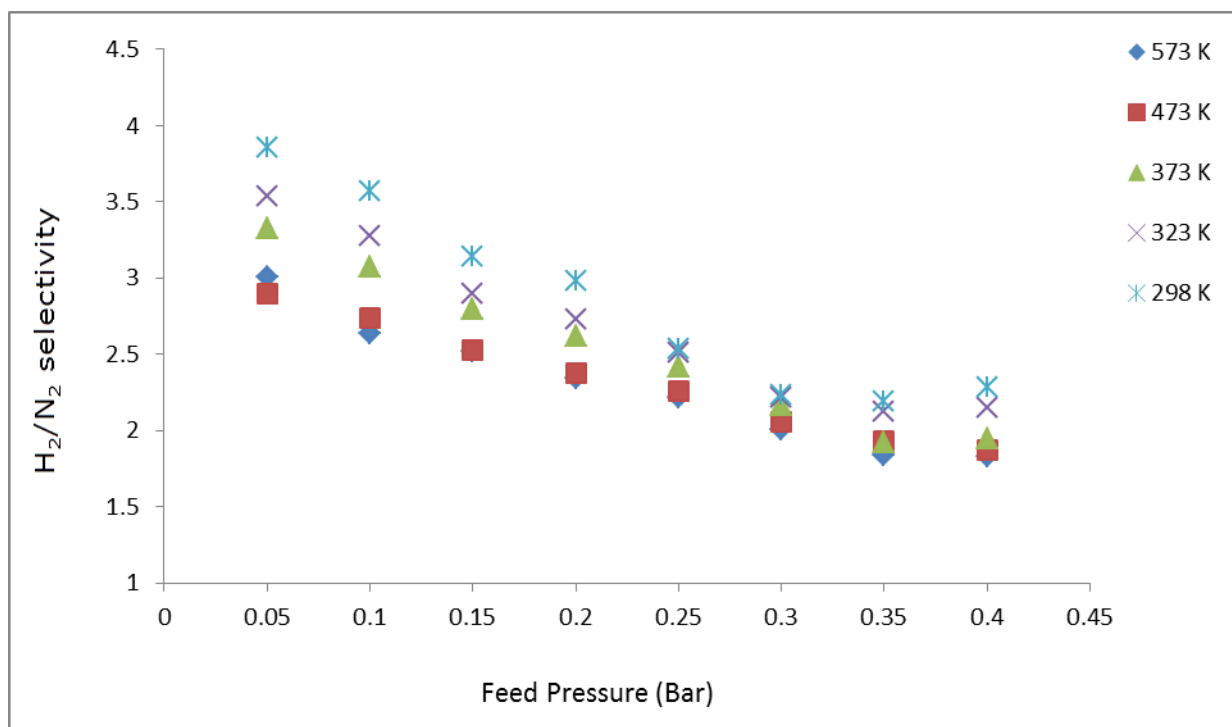


Figure 6.65: H₂/N₂ selectivity for the SL2 membrane after second dip

The Ar permeance through the SL2 membrane also decreased after deposition of the second silica layer as shown in Figure 6.66 due to the increased resistance to permeation. The Ar permeance for SL2 membrane after the first coating was $1.51 \times 10^{-7} \text{ mol m}^{-2} \text{ s}^{-1} \text{ Pa}^{-1}$ which dropped to $1.38 \times 10^{-7} \text{ mol m}^{-2} \text{ s}^{-1} \text{ Pa}^{-1}$. After the first coating, the highest H₂/Ar selectivity was 3.88 at 373 K and 0.4 bar which was lower than the theoretical Knudsen selectivity of 4.45 as shown in figure 6.67. However, after the second coating, the selectivity dropped to 3.16 at 298 K and 0.05 bar which is lower than the theoretical Knudsen selectivity.

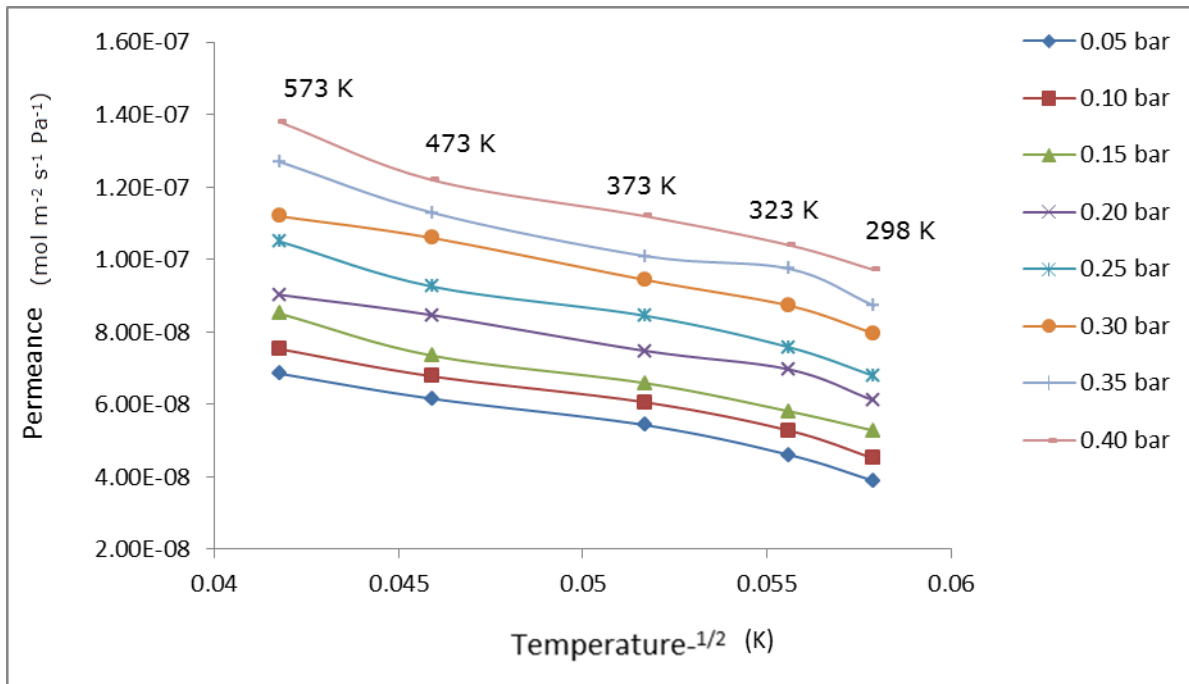


Figure 6.66: Ar permeance against the inverse square root of temperature for the SL2 membrane after second dip

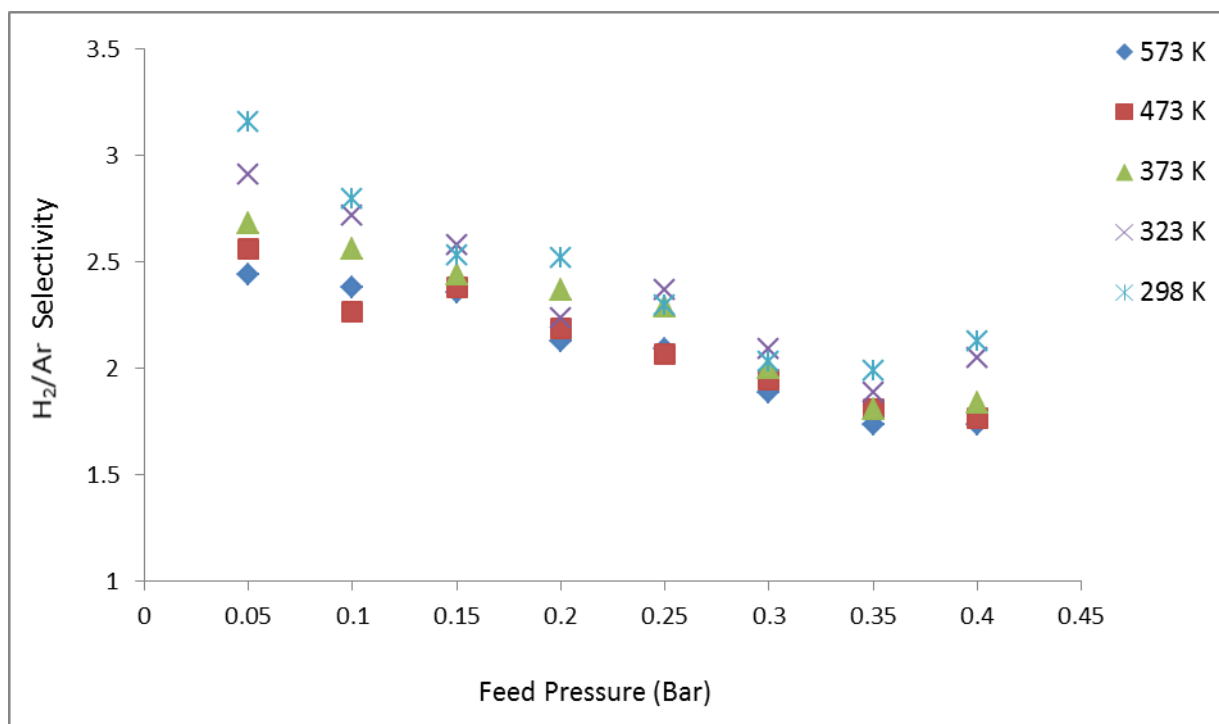


Figure 6.67: H_2/Ar selectivity at different temperature for the SL2 membrane after second dip

Table 6.14: Comparison of hydrogen permeance SL1 and SL2 at 573 K and 0.4 bar after the first and second dips

Temp. (K)	SL1 (1 st coating) (mol m ⁻² s ⁻¹ Pa ⁻¹)	SL1 (2 nd coating) (mol m ⁻² s ⁻¹ Pa ⁻¹)	SL2 (1 st coating) (mol m ⁻² s ⁻¹ Pa ⁻¹)	SL2 (2 nd coating) (mol m ⁻² s ⁻¹ Pa ⁻¹)
573	3.12×10^{-7}	2.89×10^{-7}	4.05×10^{-7}	3.15×10^{-7}
473	2.97×10^{-7}	2.74×10^{-7}	3.81×10^{-7}	2.93×10^{-7}
373	2.80×10^{-7}	2.62×10^{-7}	3.63×10^{-7}	2.69×10^{-7}
323	2.67×10^{-7}	2.51×10^{-7}	3.46×10^{-7}	2.56×10^{-7}
298	2.58×10^{-7}	2.42×10^{-7}	3.29×10^{-7}	2.49×10^{-7}

Permeance for all the gases decreased when an additional layer was deposited on the SL2 membrane which indicates that the increase in thickness resulted in an increase in the membrane resistance to permeation. The inference is that the low hydrogen selectivity is due to the adsorption ability of the other 5 gases i.e CO₂, N₂, CH₄, He and Ar through the silica membrane. A comparison of H₂ permeance for the SL2 membrane at second coating is shown in Table 6.14 and it can be observed that there was a decrease in H₂ permeance with increasing thickness after the first coating.

6.4.6 Gas Permeance against Kinetic Diameter

The permeance of hydrogen and the other gases investigated for the 6000 nm silica membrane modified with AlOOH sol is in the order H₂ > He > CO₂ > CH₄ > N₂ > Ar. However, the order of the gas permeance was not in tandem with the order of the kinetic diameter which is CH₄ > N₂ > Ar > CO₂ > H₂ > He. It would have been 'expected' that the gas permeance will follow the order of kinetic diameter since the permeance is related to the size, molecular dimensions and also the pore structures.

Hydrogen has lower kinetic diameter compared to CO₂, CH₄, Ar and N₂ but has the highest permeance through the silica membrane at the temperature investigated i.e 298, 323, 373, 473 and 573 K. Also Helium which has the lowest kinetic diameter has a higher permeance compared to all the gases except Hydrogen. The trend can be explained in terms of the diffusion and sorption of the gas molecules through the membrane. Hydrogen has a greater diffusivity through the silica membrane compared to the other gases.

6.4.7 Gas Permeance against Molecular Weight

The order of molecular weight of the gases investigated is CO₂ > Ar > N₂ > CH₄ > He > H₂. The order of gas permeance didn't follow the order of molecular weight of the gases. In fact, it is nearly an inverse relationship except for CO₂ which has the largest molecular weight but is the third in the permeance ranking. Hydrogen with the lowest molecular weight has the highest permeance. The

gases with higher molecular weight display lower permeance due to the higher resistance to permeation. Hence Ar, N₂, CH₄ with higher molecular weight show low permeance due to the resistance they encounter and have a lower permeance compared to H₂ and He. This phenomenon could also explain the increase in gas permeance with increase in temperature because increase in temperature should expectedly enhance gas permeation through the pores of the membrane. H₂ and He with lower molecular weights show a higher permeance compared to the gases with higher molecular weight due to the surface diffusion phenomenon and the low resistance to permeation.

6.4.8 Observations for SL1 and SL2 membranes

From the investigations for gas permeation through the SL1 and SL2 membranes prepared through the dip coating method, the following observations are drawn:

1. Hydrogen displayed higher permeance compared to the 5 other gases.
2. Gas permeance increased with temperature and transmembrane pressure difference but decreased with the number of coatings as a result of increased thickness and by implication enhanced resistance to permeation.
3. The membrane selectivity for hydrogen in respect of the other 5 gases generally increased with temperature but decreased with pressure.
4. Silica membranes are cheaper to produce compared to palladium membranes

The silica membranes investigated in this work for hydrogen permeation produced low selectivity and moreover the hydrogen permeance through the silica membranes could be enhanced. It is therefore necessary to look further into other alternatives membranes with a view to achieving higher hydrogen permeance and selectivity at low cost. Alumina ceramic membranes are options in hydrogen permeation and can withstand high temperature and pressure.

Our next set of investigations involved testing hydrogen permeation through ceramic alumina membranes.

6.5 Ceramic Alumina Membranes

This section presents results and discussions for both the commercial ceramic Alumina membrane AM0 of 6000 nm average pore size and the modified membrane AM1. The AM0 membrane is a commercial ceramic alumina membrane not graded with any layer while the AM1 membrane of thickness 10.65 μm at first dip was prepared by depositing a layer of Boehmite over the porous ceramic alumina support using the dip coating method.

6.5.1 Single Gas Permeation Test for the Commercial Ceramic Alumina Support AM0

The permeance of hydrogen and the other 5 gases (He, CO₂, CH₄, N₂, Ar) for the unmodified ceramic α - alumina support AM0 and the modified γ -alumina membrane AM1 were investigated at pressure differential 0.05, 0.10, 0.15, 0.20, 0.25, 0.30, 0,35 and 0.4 bar and temperature 573, 473, 373, 323 and 298 K. Figure 6.68 shows the hydrogen permeance at different temperature and feed pressure for the commercial alumina membrane AM0.

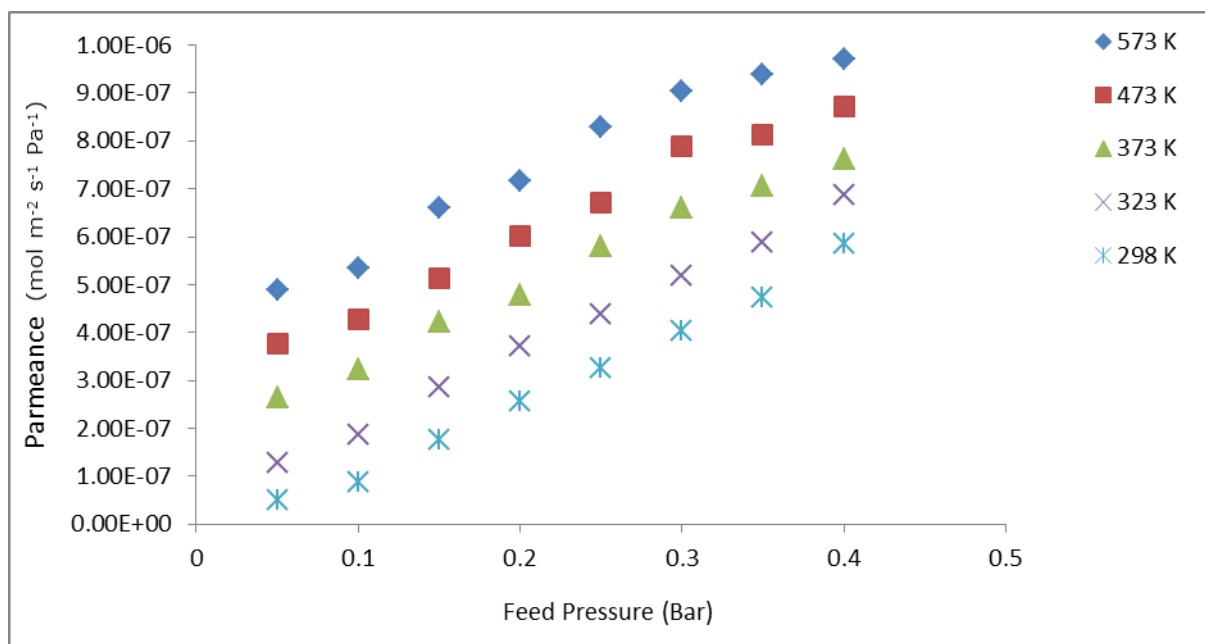


Figure 6.68: Hydrogen permeance against feed pressure for the ceramic alumina support AM0

The increase in H₂ permeance with increase in temperature and differential pressure indicates a direct relationship between temperature and pressure with hydrogen permeance. The same trend was observed for the other gases i.e. He, CO₂, CH₄, N₂ and Ar as shown in figure 6.69 where it can be observed that the gas permeance increased with increasing temperature and pressure. However, the temperature effect was more significant for hydrogen compared with the other 5 gases. The highest permeance for hydrogen was $9.72 \times 10^{-7} \text{ mol m}^{-2} \text{ s}^{-1} \text{ Pa}^{-1}$ observed at 573 K and a feed pressure of 0.4 bar. Hydrogen has the highest permeance compared to the other gases which indicates higher mobility of hydrogen molecules through the membrane pores as a result of the temperature effect leading to increasing permeance.

The increase in gas permeance with temperature indicates that activated surface diffusion is the gas transport mechanism with some contribution of viscous flow. Surface adsorption is generally inversely proportional to temperature as reported by Li, X et al (2012) [34] and Wu et al (1993) [35] [36]. In their work and in line with this phenomenon, this group reported a decrease in hydrogen permeance with temperature. However, in this investigation, the reverse was the case because gas permeance increases with temperature hence the high temperature

enhances the surface diffusion of Hydrogen in the alumina membrane. The increase in H₂ permeance with increasing feed pressure also indicates a viscous flow gas transport mechanism [37]. The increase in gas permeance with increasing temperature also indicates that the rate of viscous flow is increasing hence the resistance to permeation is reduced as the temperature is increased [34].

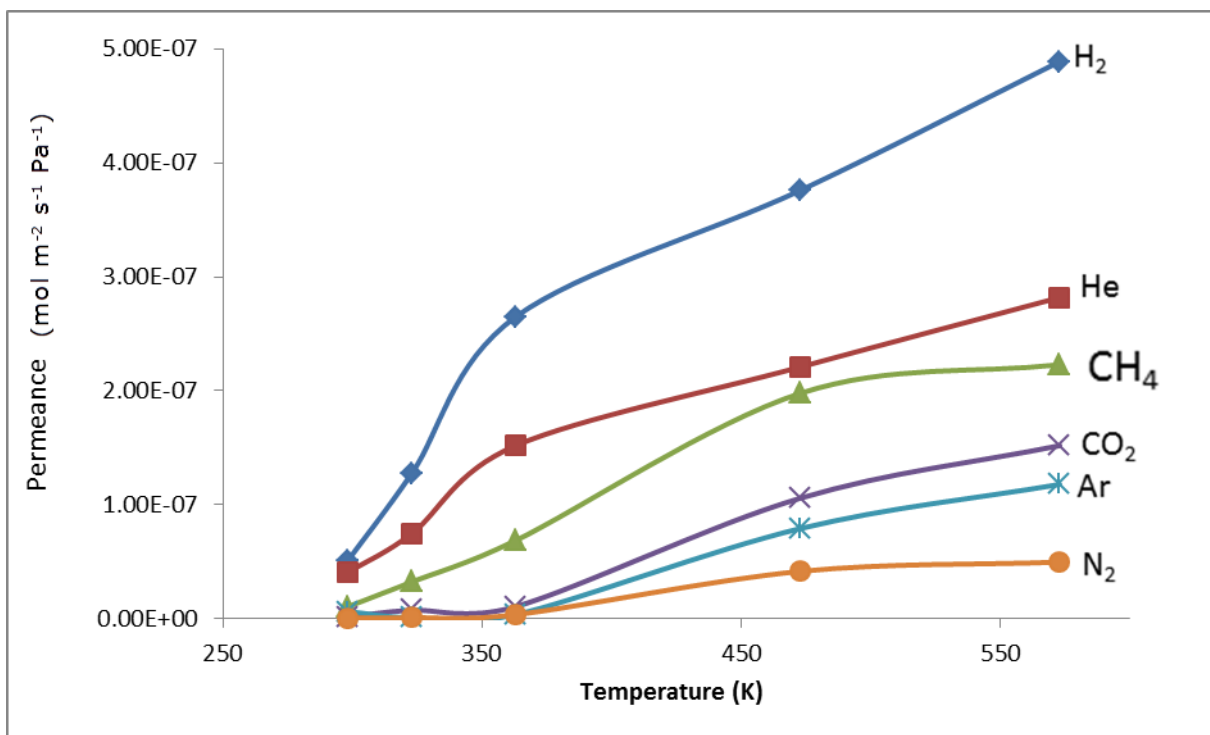


Figure 6.69: Gas permeance against temperature at 0.05 bar for the Alumina support.

It can be observed that at 0.05 bar, hydrogen permeance was almost same with Helium permeance but as the temperature increased, hydrogen permeance gradually increased more drastically while He permeance decreased very slowly. The same trend was observed for the other gases, CO₂, CH₄, N₂ and Ar which also increased slowly. The rapid increase in the permeance of hydrogen indicates that hydrogen permeance is dependent on temperature and differential pressure which indicates a viscous flow mechanism.

The observed maximum permeance for hydrogen is $4.89 \times 10^{-7} \text{ mol m}^{-2} \text{ s}^{-1} \text{ Pa}^{-1}$ which is at least one order of magnitude higher than the permeances of the other gases at same temperature and pressure. An increase in permeance with temperature indicates a gas transport mechanism other than Knudsen because in Knudsen diffusion, gas permeance will be independent of pressure and will decrease with temperature. This suggests that the gas transport mechanism in this investigation is activated surface diffusion with contribution of viscous flow.

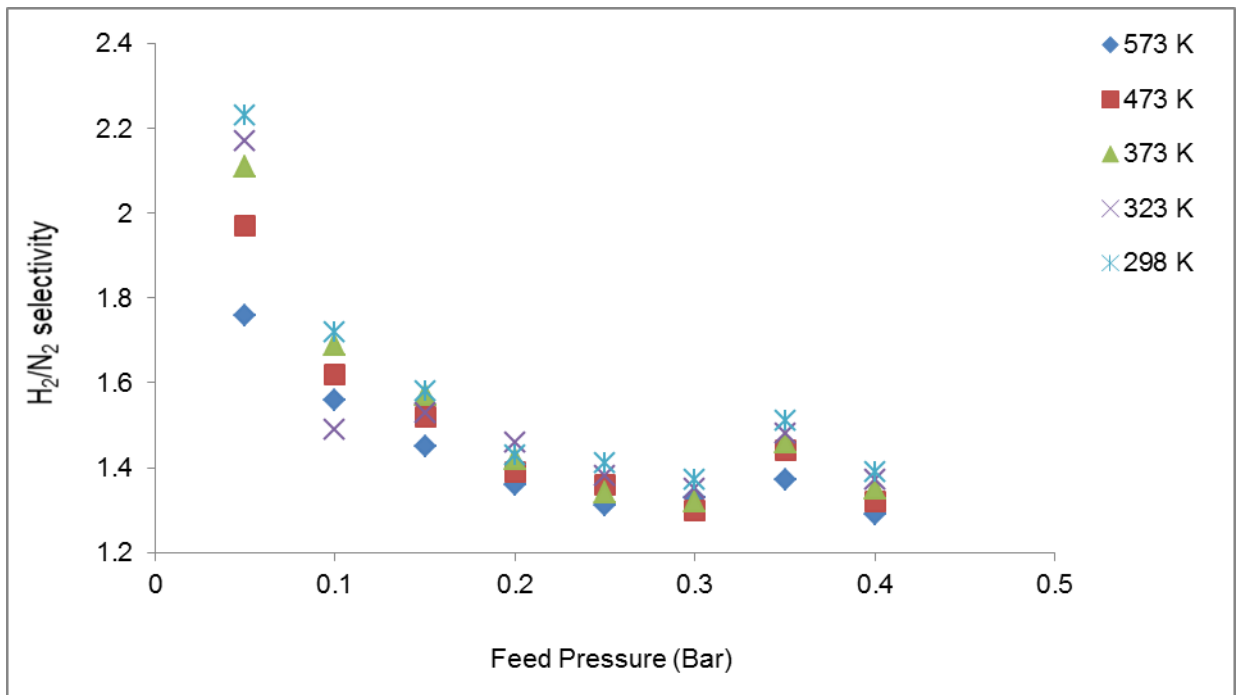


Figure 6.70: H_2/N_2 selectivity against feed pressure for the alumina support AMO

It can be observed from figure 6.70 that the H_2/N_2 selectivity is in the range 1.29 – 2.23 and the highest selectivity -2.23- at 0.05 bar and 298 K is lower than the theoretical Knudsen selectivity of 3.73 and indicates that the gas transport mechanism is activated surface diffusion with contribution of viscous flow. This is because for Knudsen diffusion, the selectivity would have been higher than theoretical Knudsen selectivity. Although there was no particular trend for gas selectivity for all the gases investigated, the selectivity generally increases with temperature but decreases with pressure which also suggests a viscous flow transport mechanism.

Tables 6.15, 6.16 and 6.17 show the H₂/N₂, H₂/CO₂ and H₂/Ar selectivity. From the results, none of the selectivities was above the theoretical Knudsen selectivity values. The low selectivity can be attributed to the decrease in the contribution of surface adsorption in gas permeation through the membrane and a contribution of viscous flow regime. The low selectivity could also be attributed to defects or pin holes in the membrane which also indicates viscous flow gas transport mechanism. The H₂/He selectivity is in the range 1.08 – 1.22.

It should be noted that the membrane displayed selectivity for all the gases relative to hydrogen although it was low and below the theoretical Knudsen value. In terms of gas permeance/molecular weight relationship, results indicate that H₂ and He with lower molecular weight permeated faster than the other gases i.e. CO₂, N₂, CH₄ and Ar. The permeance of the gases investigated doesn't follow the order of the molecular weight of the gases which is as follows: CO₂ (44.01) > Ar (39.948) > N₂ (28.0134) > CO (28.011) > CH₄ (16.044) > He (4.02) > H₂ (2.016).

Table 6.15: H₂/N₂ and H₂/He selectivity for the Alumina support AM0

Feed Pressure (Bar)	H ₂ /N ₂ Selectivity					H ₂ /He Selectivity				
	573 K	473 K	373 K	323 K	298 K	573 K	473 K	373 K	323 K	298 K
0.05	1.78	1.97	2.11	2.17	2.23	1.22	1.18	1.13	1.17	1.15
0.10	1.56	1.62	1.69	1.49	1.72	1.13	1.21	1.14	1.15	1.11
0.15	1.45	1.52	1.51	1.53	1.58	1.16	1.13	1.18	1.17	1.12
0.20	1.36	1.39	1.42	1.46	1.43	1.17	1.19	1.15	1.16	1.14
0.25	1.31	1.36	1.34	1.38	1.41	1.10	1.14	1.18	1.13	1.18
0.30	1.33	1.3	1.32	1.35	1.37	1.15	1.11	1.14	1.11	1.09
0.35	1.37	1.44	1.46	1.48	1.51	1.14	1.16	1.19	1.18	1.13
0.40	1.29	1.32	1.35	1.37	1.39	1.16	1.12	1.16	1.13	1.08

Table 6.16: H₂/CO₂ and H₂/CH₄ selectivity for the Alumina support AM0

Feed Pressure (Bar)	H ₂ /CO ₂ Selectivity					H ₂ /CH ₄ Selectivity				
	573 K	473 K	373 K	323 K	298 K	573 K	473 K	373 K	323 K	298 K
0.05	1.24	1.31	1.35	1.28	1.19	1.53	1.71	1.82	1.93	1.67
0.10	1.27	1.20	1.23	1.22	1.18	1.39	1.54	1.49	1.63	1.58
0.15	1.21	1.26	1.23	1.28	1.18	1.29	1.31	1.46	1.52	1.63
0.20	1.29	1.28	1.34	1.33	1.24	1.23	1.31	1.25	1.28	1.29
0.25	1.11	1.13	1.15	1.14	1.16	1.17	1.19	1.23	1.28	1.31
0.30	1.10	1.12	1.17	1.09	1.12	1.14	1.15	1.19	1.18	1.17
0.35	1.15	1.12	1.18	1.14	1.15	1.12	1.17	1.16	1.19	1.16
0.40	1.12	1.14	1.15	1.14	1.16	1.14	1.19	1.14	1.18	1.16

Table 6.17: H₂/Ar selectivity for the Alumina support AM0

Feed Pressure (Bar)	H ₂ /Ar Selectivity				
	573 K	473 K	373 K	323 K	298 K
0.05	2.21	2.32	2.45	2.29	2.54
0.10	1.86	2.23	2.28	2.25	2.71
0.15	1.76	2.09	2.16	2.19	2.58
0.20	1.66	2.11	2.06	1.93	2.82
0.25	1.61	1.97	2.01	1.76	2.23
0.30	1.42	1.77	1.82	1.73	1.89
0.35	1.48	1.78	1.63	1.59	1.57
0.40	1.25	1.64	1.53	1.59	1.62

6.5.2. Gas Permeance against Kinetic Diameter for the AM0 Membrane

There was a correlation between the order of permeance of the gases and their kinetic diameter as shown in figure 6.71. The order of permeance didn't exactly follow the order of kinetic diameter of the gases for the alumina membrane. **Order of kinetic Diameter:** CH₄ (3.8)>N₂ (3.64)>Ar (3.4)>CO₂ (3.3)>H₂ (2.89)>He (2.65) The order of permeance of the gases is as follows: H₂>He>CO₂>CH₄>Ar>N₂

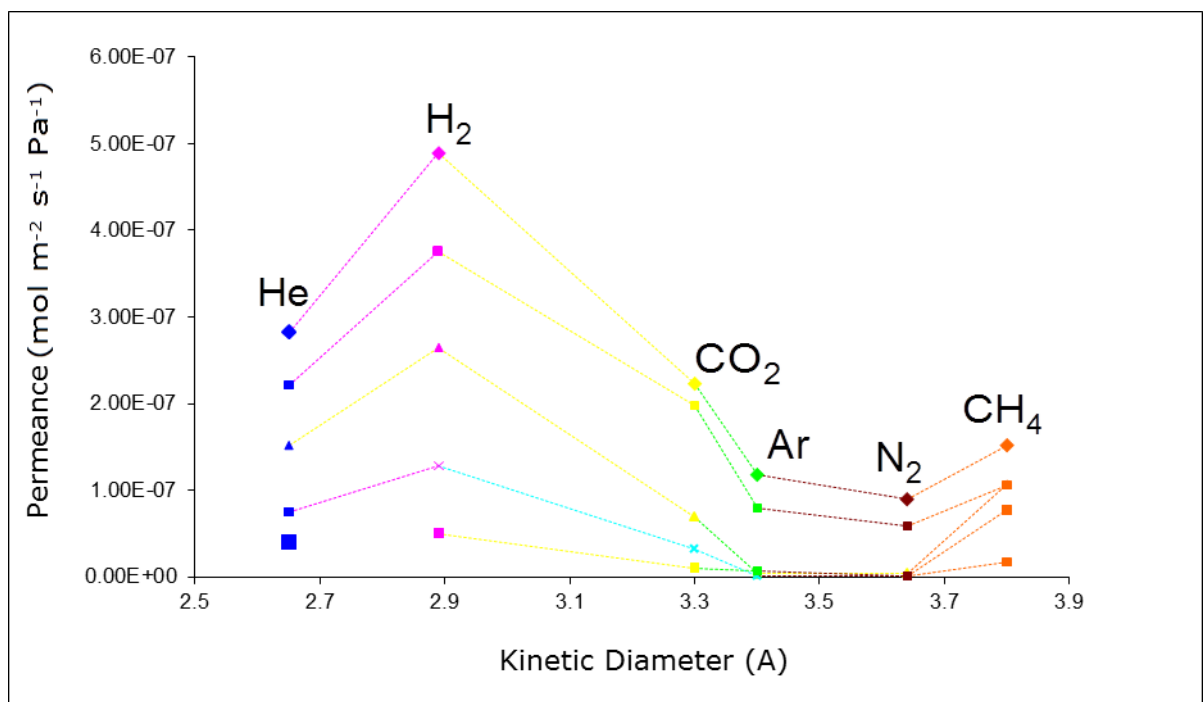


Figure 6.71: gas permeance against kinetic diameter at 573 K and 0.05 bar for the alumina support AM0

The Order of permeance is as follows: H₂>He>CO₂>CH₄>Ar>N₂

Hydrogen permeated faster than all the other 5 gases despite having a lower kinetic diameter (2.89 Å) than all the gases except He (2.65 Å). The observed permeance of H₂, He and CO₂ with lower K.D was much higher than that of N₂, Ar and CH₄ with higher K.D. H₂ with a smaller K.D can fill the pores of the membrane more readily than the CH₄, N₂ and Ar with higher K.D at low temperature where these smaller molecules have better mobility within the membrane pores [36].

The higher permeance of H₂ is due to the effect of surface diffusion through the alumina membrane. This trend also suggests viscous flow mechanism in the H₂ transport through the membrane. There is a higher hindrance to permeation for the heavier gases- CO₂, Ar, N₂ and CO while the lighter gases permeated faster through the membrane.

6.5.3 Gas Permeation Tests for the Modified Alumina Membrane AM1

To plug any pin holes or defects and enhance hydrogen permeation, the Al₂O₃ tubular support was modified with Boehmite sol through successive deposition of layers using the dip coating method. The thickness of the membrane was calculated using the weight gain method as 10.65 μm. Figure 6.72 shows the hydrogen permeance of the modified γ-alumina membrane AM1 after the first coating. The thickness of the membrane after first coating determined using the weight gain method is 10.65 μm. The results indicate that a maximum H₂ permeance observed is $9.85 \times 10^{-7} \text{ mol m}^{-2} \text{ s}^{-1} \text{ Pa}^{-1}$ was observed at 573 K and 0.4 bar which represents an increase of $1.3 \times 10^{-8} \text{ mol m}^{-2} \text{ s}^{-1} \text{ Pa}^{-1}$ compared to the hydrogen permeance before the modification of the support with Boehmite sol.

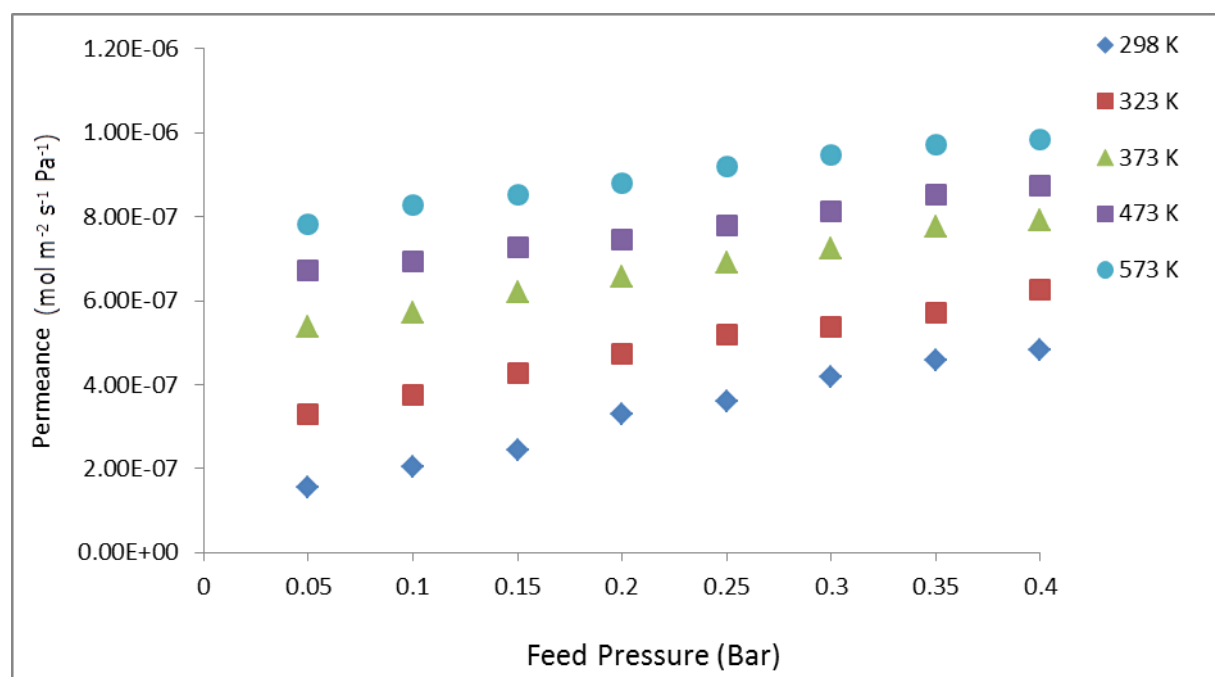


Figure 6.72: Hydrogen permeance against feed pressure for the modified AM1 membrane after first dip

The modification enhanced surface diffusion of hydrogen molecules through the membrane pores leading to increased hydrogen permeance with increasing temperature and pressure. Molecular diffusion has been known to enhance the permeance of gases in nanoporous inorganic membranes hence these gas molecules with higher diffusivity permeate faster than those with lower diffusivity [34]. Hydrogen is more diffusive than CO₂ hence hydrogen molecules enjoy more mobility and can retain in the permeate stream longer than CO₂ and by implication exhibit a higher permeance compared to CO₂ [34]. Just as in the gas permeance for the AM1 membrane, Hydrogen permeance increased with increase in pressure which suggested that viscous flow existed in the gas transport for all the gases investigated. The H₂ permeance increased with temperature but decreased with the number of coatings as more layers of the Boehmite sol were deposited as a result of the increased resistance to permeation.

In the modified membrane, the pore size is expected to decrease due to the additional layer of the AlO (OH) sol as the sol occupies parts of the membrane pores. The increase in gas permeance is attributable to the enhanced solubility of hydrogen through the porous support as a result of the temperature and pressure effect. Impliedly, the resistance to H₂ permeation decreases as the permeation temperature is increased which indicates that increasing the temperature enhances surface diffusion and enhanced gas permeation. The same trend was observed for the other gases based on the same order of permeance as follows: H₂>He>CO₂>CH₄>N₂>Ar. It can be observed from figure 6.72 that hydrogen permeance at 298 K was higher compared to that of the unmodified AM0 membrane. Also the increase in gas permeance was more drastic between 298 – 373 K but it became more stable between 373 – 573 K. This indicates that the effect of temperature is more significant at lower temperature.

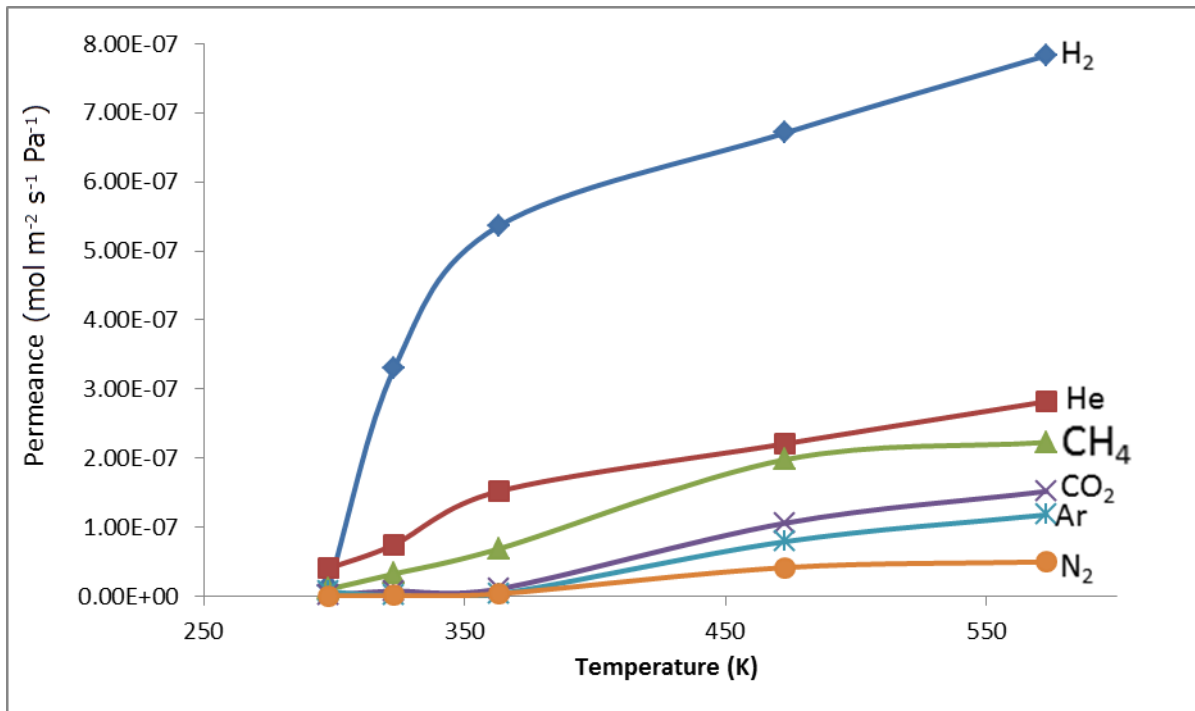


Figure 6.73: Gas permeance against temperature at 0.05 bar for the AM1 membrane after first dip

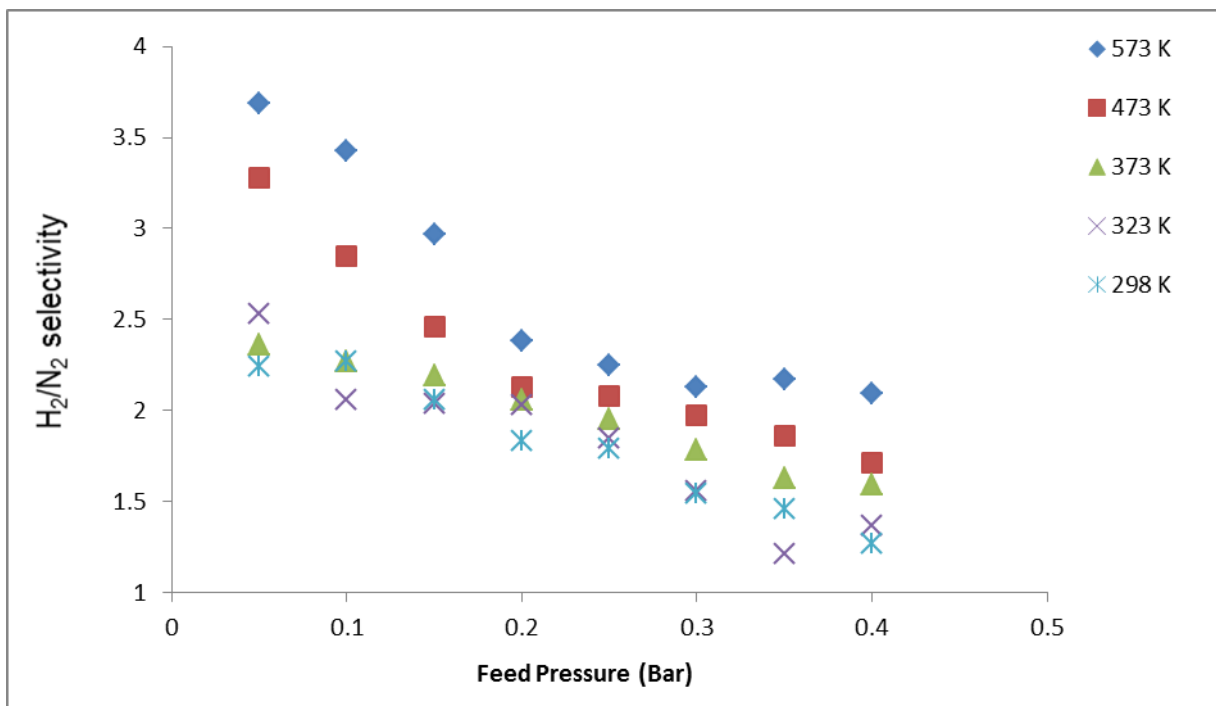


Figure 6.74: H₂/N₂ selectivity against feed pressure for the AM1 membrane

The membrane selectivity for hydrogen in respect of He, N₂ and CO₂ is shown in figure 6.74 and Tables 6.18, 6.19 and 6.20. It can be observed from figure 6.74 and Table 6.18 that the maximum H₂/N₂, H₂/CO₂ and H₂/He permselectivity are 3.69, 1.96 and 1.52 was measured for the γ -alumina at 573 K and 0.05 bar. The H₂/He selectivity 1.52 is higher than the theoretical Knudsen selectivity of 1.41 while the H₂/N₂ selectivity 3.69 is slightly lower than the theoretical Knudsen selectivity of 3.73. Also, as shown in Table 6.19, the maximum H₂/CO₂ selectivity is 2.09 and lower than the theoretical Knudsen value of 4.67. In the same vein, the H₂/CO₂ permselectivity of 1.35 was observed at 373 K and 0.05 bar for the modified Al₂O₃ substrate at 298 K which is below the theoretical Knudsen selectivity.

It can be observed from Table 6.18 that the H₂/N₂ selectivity is in the range 1.21 – 3.69 which indicates that the highest selectivity is above the theoretical Knudsen value of 3.73. This is a departure from the highest H₂/N₂ selectivity for the unmodified AM0 membrane -2.23- which was below the Knudsen value. The higher selectivity above the Knudsen value indicates that the gas transport mechanism is Knudsen diffusion with contribution of viscous flow.

The same trend was observed for H₂/He where the selectivity range is 1.07 – 1.52 which is above the theoretical Knudsen value. However, as shown in Table 6.19, the H₂/CO₂ selectivity was observed to be below the Knudsen selectivity and is in the range 1.19 – 1.96. Also, the same scenario was observed for H₂/CH₄ which was in the range 1.15 – 2.01. The H₂/Ar selectivity also decreased from the highest value of 2.82 for the AM0 membrane at 298 K and 0.20 bar to 2.76 for the AM1 membrane at 298 K and 0.05 bar as shown in Table 6.20.

Table 6.18: H₂/N₂ and H₂/He selectivity for the AM1 membrane after first dip

Feed Pressure (Bar)	H ₂ /N ₂ Selectivity					H ₂ /He Selectivity				
	573	473	373	323	298	573	473	373	323	298
0.05	3.69	3.28	2.36	2.53	2.24	1.52	1.47	1.29	1.25	1.23
0.10	3.43	2.85	2.27	2.06	2.27	1.47	1.25	1.26	1.28	1.17
0.15	2.97	2.46	2.19	2.04	2.06	1.42	1.22	1.21	1.21	1.13
0.20	2.38	2.13	2.06	2.03	1.83	1.38	1.21	1.20	1.24	1.07
0.25	2.25	2.08	1.95	1.85	1.79	1.26	1.28	1.17	1.15	1.16
0.30	2.13	1.97	1.78	1.56	1.54	1.29	1.19	1.09	1.19	1.18
0.35	2.17	1.86	1.63	1.21	1.46	1.31	1.22	1.11	1.16	1.16
0.40	2.09	1.71	1.59	1.37	1.27	1.24	1.27	1.16	1.15	1.21

Table 6.19: H₂/CO₂ and H₂/CH₄ selectivity for the Alumina membrane AM1 after first dip

Feed Pressure (Bar)	H ₂ /CO ₂ Selectivity					H ₂ /CH ₄ Selectivity				
	573	473	373	323	298	573	473	373	323	298
0.05	1.96	1.66	1.75	1.63	1.58	1.93	1.96	1.87	2.01	1.75
0.10	1.73	1.50	1.53	1.52	1.42	2.03	1.74	1.25	1.79	1.83
0.15	1.81	1.44	1.44	1.47	1.39	2.09	1.62	1.34	1.74	2.09
0.20	1.76	1.39	1.52	1.24	1.21	1.67	1.48	1.21	1.26	1.29
0.25	1.59	1.36	1.26	1.20	1.19	1.72	1.35	1.25	1.23	1.21
0.30	1.62	1.28	1.21	1.25	1.23	1.55	1.40	1.26	1.21	1.17
0.35	1.25	1.32	1.22	1.26	1.26	1.41	1.47	1.21	1.17	1.22
0.40	1.27	1.27	1.27	1.22	1.18	1.38	1.37	1.20	1.12	1.15

Table 6.20: H₂/Ar selectivity for the Alumina membrane AM1 after first dip

Feed Pressure (Bar)	H ₂ /Ar Selectivity				
	573 K	473 K	373 K	323 K	298 K
0.05	2.21	2.34	2.49	2.52	2.76
0.10	2.27	2.16	1.88	2.24	2.71
0.15	2.18	1.21	1.92	2.13	2.34
0.20	1.93	1.93	2.37	2.07	1.92
0.25	1.62	1.67	1.51	3.01	2.02
0.30	1.72	1.61	1.42	1.53	1.94
0.35	1.58	1.45	1.35	1.55	1.45
0.40	1.63	1.24	1.29	1.42	1.26

6.5.4 Gas permeance and Selectivity after Second Dip for the AM1 Membrane

After the permeation test for the first coating, a second layer of the AlO (OH) sol was deposited using the dip coating method. The thickness of the AM1 membrane increased to 19.37 μm as a result of an additional layer of 8.72 μm which presents increased resistance to hydrogen permeation. The membrane was also dried and calcined using the same procedure as for the first coating.

Gas permeation tests were carried out at 573, 473, 373, 323 and 298 K to investigate the hydrogen permeance and selectivity of the membrane. The maximum hydrogen permeance was $5.89 \times 10^{-7} \text{ mol m}^{-2} \text{ s}^{-1} \text{ Pa}^{-1}$ observed at 573 K and 0.05 bar as shown in figure 6.75 which is lower than the maximum hydrogen permeance after the first coating. The thickness of the membrane increased almost 2 fold after the second dip thus significantly increasing the membrane's resistance to gas permeation. It can be observed that gas permeance increased with temperature and pressure which was the same trend observed after the first coating although the gas permeance was lower compared to the second coating.

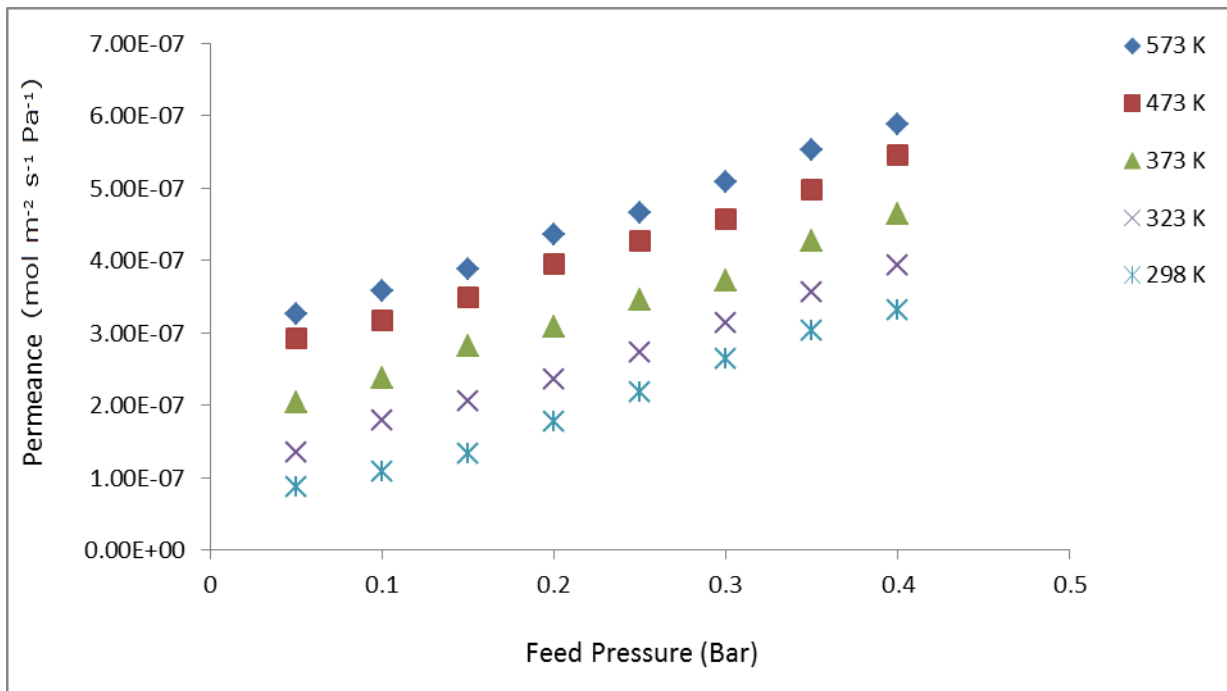


Figure 6.75: Hydrogen permeance against feed pressure for the alumina membrane AM1 after second dip.

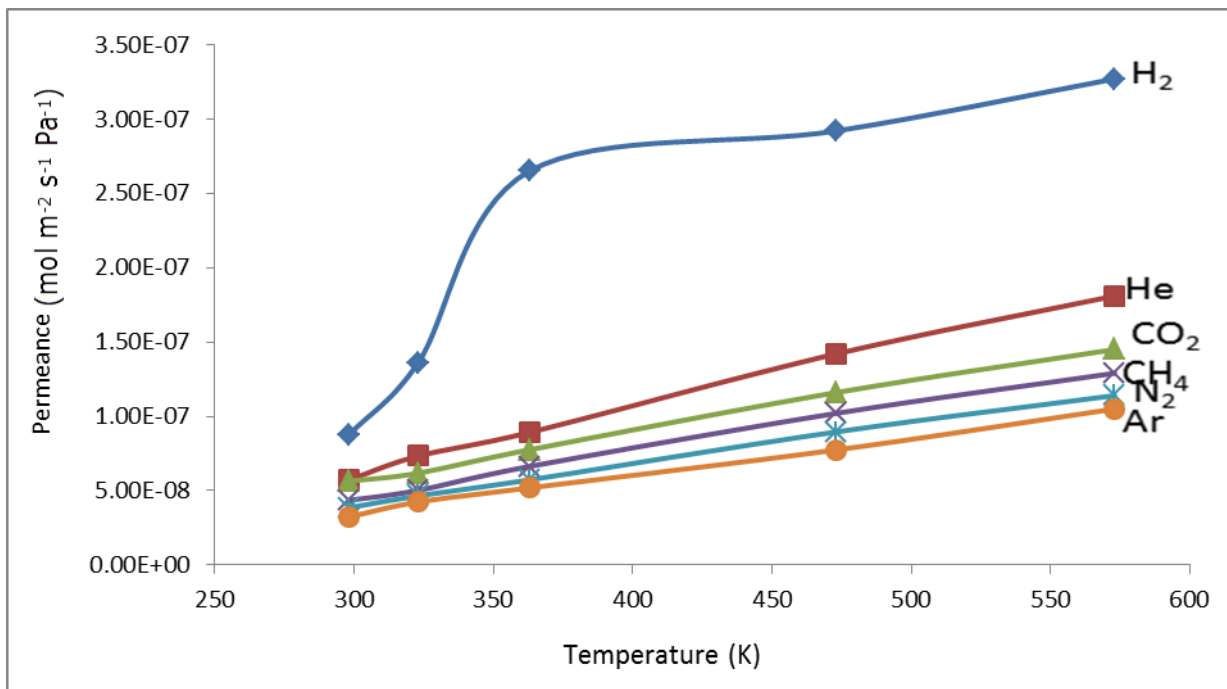


Figure 6.76: Gas permeance against temperature at 0.05 bar for the AM1 membrane after the second dip.

From figure 6.76, it can be observed that there was a more drastic increase in hydrogen permeation compared to the 5 other gases. The permeance of the other 5 gases was less affected by the increase in temperature compared to the results after the first dip. This could be attributed to the increased thickness of the membrane. The effect of temperature is determined by the thickness of the membrane and as more layers are deposited, the effect of temperature becomes less pronounced. It can be observed from Table 6.21 that the H₂/N₂ selectivity range 1.22 – 3.51 with the highest selectivity of 3.51 observed at 298 K and 0.05 bar which was below the theoretical Knudsen value of 3.73.

This indicates that the highest H₂/N₂ selectivity has decreased after the second dip from 3.69 to 3.51 however, the H₂/N₂ highest selectivity observed after the first dip was 3.69 at 573 K and 0.05 bar while after the second dip, it was 3.51 at 0.05 bar and 298 K. For the H₂/He selectivity, as observed in Table 6.21, the range observed was 1.15 – 2.18 which is above the theoretical Knudsen selectivity of 1.41 and also higher than the maximum selectivity after the first dip -1.53.

The H₂/He selectivity increased from 1.53 to 2.18 after the second dip. In Table 6.22, it can be observed that the H₂/CO₂ selectivity observed was in the range 1.28 – 2.53 which is lower than the theoretical Knudsen selectivity although it increased from 1.96 after the first dip to 2.53 after the second dip. A similar observation was made for the maximum H₂/CH₄ selectivity as shown in Table 6.23 which increased after the second dip from 2.09 to 2.96 which is higher than the theoretical Knudsen selectivity of 2.82 and suggests that the gas transport mechanism is Knudsen diffusion with contribution of viscous flow. The observed H₂/Ar selectivity is in the range 1.12 – 3.09 as shown in Table 6.23 which is lower than the theoretical Knudsen selectivity of 4.45.

Table 6.21: H₂/He selectivity for the Alumina membrane AM1 after second dip

Feed Pressure (Bar)	H ₂ /N ₂ Selectivity					H ₂ /He Selectivity				
	573 K	473 K	373 K	323 K	298 K	573 K	473 K	373 K	323 K	298 K
0.05	1.59	2.09	1.96	2.09	3.51	1.42	1.45	1.21	1.31	2.18
0.10	1.62	1.74	1.75	2.12	2.53	1.29	1.48	1.29	1.27	1.91
01.5	1.53	1.48	1.48	1.75	1.62	1.28	1.23	1.20	1.25	1.70
0.20	1.47	1.56	1.45	1.61	1.51	1.20	1.27	1.24	1.26	1.56
0.25	1.31	1.25	1.42	1.53	1.73	1.16	1.21	1.21	1.21	1.20
0.30	1.23	1.29	1.41	1.67	1.74	1.22	1.18	1.17	1.15	1.26
0.35	1.25	1.22	1.48	1.52	1.75	1.26	1.19	1.19	1.17	1.18
0.40	1.26	1.26	1.25	1.56	1.62	1.32	1.17	1.23	1.18	1.22

Table 6.22: H₂/CO₂ and H₂/CH₄ selectivity for the Alumina membrane AM1 after second dip

Feed Pressure (Bar)	H ₂ /CO ₂ Selectivity					H ₂ /CH ₄ Selectivity				
	573 K	473 K	373 K	323 K	298 K	573 K	473 K	373 K	323 K	298 K
0.05	1.62	1.94	2.03	2.05	2.53	1.90	2.02	2.21	2.51	2.96
0.10	1.59	1.92	1.72	1.89	2.01	1.82	1.73	2.95	1.93	1.98
01.5	1.43	1.63	1.57	1.52	1.79	1.63	1.52	1.73	1.76	1.87
0.20	1.67	1.56	1.42	1.63	1.52	1.93	1.63	1.57	1.52	1.62
0.25	1.28	1.49	1.61	1.67	1.39	1.52	1.65	1.28	1.40	1.49
0.30	1.32	1.51	1.55	1.74	1.57	1.27	1.52	1.44	1.38	1.27
0.35	1.58	1.57	1.40	1.45	1.62	1.21	1.43	1.39	1.45	1.23
0.40	1.38	1.53	1.31	1.56	1.69	1.56	1.41	1.28	1.46	1.22

Table 6.23: H₂/Ar selectivity for the Alumina membrane AM1 after second dip

Feed Pressure (Bar)	H ₂ /Ar Selectivity				
	573 K	473 K	373 K	323 K	298 K
0.05	1.60	1.93	1.93	2.20	3.09
0.10	1.57	1.79	1.86	1.79	2.21
0.15	1.42	1.58	1.75	1.68	2.13
0.20	1.36	1.49	1.22	1.49	1.64
0.25	1.24	1.26	1.25	1.23	1.85
0.30	1.51	1.15	1.27	1.22	1.56
0.35	1.12	1.18	1.16	1.18	1.21
0.40	1.23	1.27	1.23	1.21	1.27

6.5.5 Gas Permeance and Selectivity after Third Dip

After the third dip, the thickness of the modified membrane AM2 increased to 27.11 μm as a result of an additional layer of 7.74 μm thickness which enhanced the membrane resistance to hydrogen permeation. The enhanced resistance to hydrogen permeation after the third dip resulted in a decrease in the hydrogen permeance from $5.89 \times 10^{-7} \text{ mol m}^{-2} \text{ s}^{-1} \text{ Pa}^{-1}$ after the second coating to $4.20 \times 10^{-7} \text{ mol m}^{-2} \text{ s}^{-1} \text{ Pa}^{-1}$ as shown in figure 6.77.

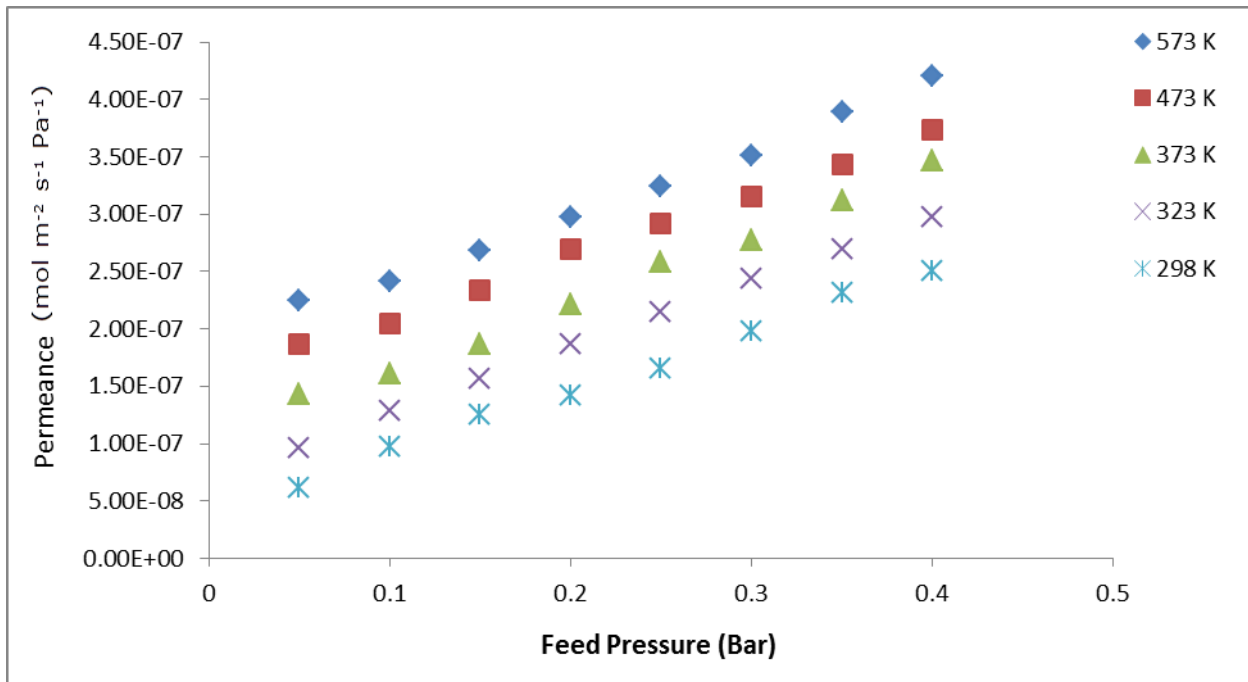


Figure 6.77: Hydrogen permeance against feed pressure for the AM1 membrane after third dip

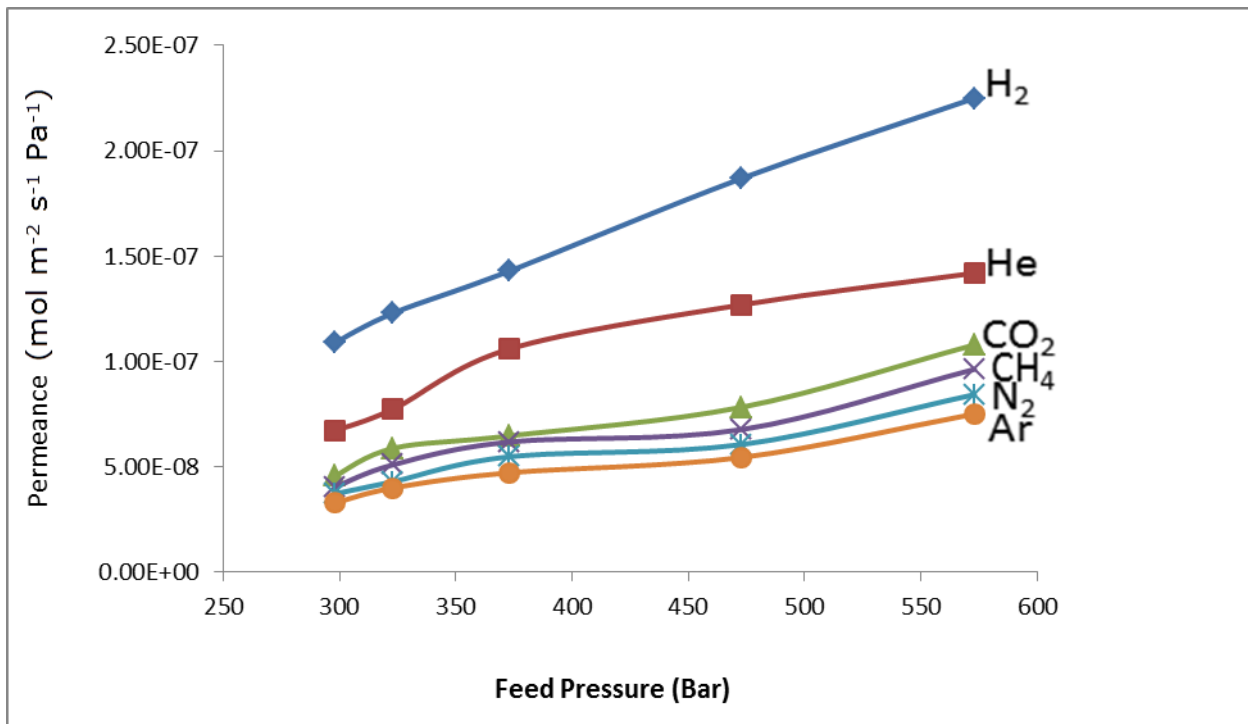


Figure 6.78: Gas permeance against temperature at 0.05 bar for the AM1 membrane after third dip.

Gas permeance increased with temperature and pressure as shown in figure 6.78 which represents gas permeance at 0.05 bar and temperature 298 – 573 K. However, it can be observed that the temperature effect was more significant for hydrogen and helium permeation compared to the results after the second dip. The other gases also displayed increasing permeance with temperature especially Helium. Compared to the results after the second dip, it can be observed that the increased thickness has less effect on temperature for the third dip.

It can be observed from Table 6.24 that the H₂/N₂ selectivity is in the range 1.95 – 4.57 which represents an increase compared to the selectivity after the second dip. The membrane displayed hydrogen selectivity relative to all the gases except CO₂. As shown in Table 6.26, for H₂/Ar selectivity, it is only after the third dip that a value above Knudsen was achieved as against the previous 2 dips where the value was below Knudsen in both dips.

Table 6.24: H₂/N₂ and H₂/CO₂ selectivity for the alumina membrane AM1 after third dip

Feed Pressure (Bar)	H ₂ /N ₂ Selectivity					H ₂ /He Selectivity				
	573 K	473 K	373 K	323 K	298 K	573 K	473 K	373 K	323 K	298 K
0.05	4.57	4.21	3.79	3.23	3.19	1.42	1.54	1.51	1.63	1.71
0.10	3.88	3.95	4.24	3.51	3.42	1.26	1.27	1.46	1.48	1.63
01.5	3.19	3.63	3.88	3.57	3.55	1.22	1.21	1.38	1.41	1.41
0.20	2.59	2.69	3.21	2.75	3.23	1.26	1.20	1.43	1.39	1.17
0.25	2.63	2.41	2.73	2.72	3.45	1.31	1.25	1.21	1.25	1.24
0.30	2.08	2.55	2.44	2.97	2.91	1.19	1.17	1.09	1.19	1.19
0.35	1.95	2.29	2.19	2.45	3.01	1.53	1.26	1.11	1.12	1.22
0.40	2.03	2.87	2.21	2.26	2.73	1.17	1.22	1.16	1.23	1.18

Table 6.25: H₂/CO₂ and H₂/CH₄ selectivity for the Alumina membrane AM1 after third dip

Feed Pressure (Bar)	H ₂ /CO ₂ Selectivity					H ₂ /CH ₄ Selectivity				
	573 K	473 K	373 K	323 K	298 K	573 K	473 K	373 K	323 K	298 K
0.05	2.21	2.48	2.42	2.71	2.63	1.95	3.02	2.71	2.54	2.58
0.10	1.93	2.21	2.33	2.58	2.85	2.24	2.56	2.63	2.26	2.47
0.15	1.24	1.85	2.17	2.25	2.21	1.84	1.95	2.12	2.04	2.14
0.20	1.53	1.71	1.82	1.69	1.73	1.66	1.82	1.97	1.96	2.56
0.25	1.45	1.68	1.73	1.54	1.86	1.51	1.73	2.05	1.73	2.18
0.30	1.36	1.73	1.50	1.49	1.66	1.56	1.75	1.84	1.61	1.90
0.35	1.42	1.52	1.53	1.38	1.57	1.43	1.63	1.73	1.68	1.73
0.40	1.25	1.36	1.36	1.41	1.55	1.39	1.59	1.67	1.62	1.66

Table 6.26: H₂/Ar selectivity for the Alumina membrane AM1 after third dip

Feed Pressure (Bar)	H ₂ /Ar Selectivity				
	573 K	473 K	373 K	323 K	298 K
0.05	5.21	5.52	5.52	4.85	4.43
0.10	4.95	5.07	5.24	4.20	4.50
0.15	4.56	4.93	4.44	3.85	3.86
0.20	4.06	4.23	4.25	3.65	3.21
0.25	3.50	3.60	3.74	3.14	3.74
0.30	3.32	4.02	3.77	3.25	3.55
0.35	3.07	3.75	3.62	3.52	3.62
0.40	2.86	3.42	3.26	3.27	3.73

6.5.6 Gas permeance after fourth Dip

After depositing the fourth AlO (OH) layer, the thickness of the AM2 membrane increased to 34.85 μm due to an increased 7.74 μm thickness of the fourth layer. However, after the 4th coating, only hydrogen and CO₂ permeated through the membrane. While hydrogen permeated through the membrane at all the temperatures investigated, CO₂ permeance was observed at all temperature investigated except room temperature (573, 473, 373 and 323 K and transmembrane pressure difference of 0.05 – 0.4 bar). As shown in figure 6.79, the maximum hydrogen permeance observed is $8.50 \times 10^{-8} \text{ mol m}^{-2} \text{ s}^{-1} \text{ Pa}^{-1}$ at 573 K and 0.4 bar which indicates a significant decrease in the hydrogen permeance of $3.35 \times 10^{-7} \text{ mol m}^{-2} \text{ s}^{-1} \text{ Pa}^{-1}$ compared to the results after the third dip.

The maximum CO₂ permeance observed was $6.73 \times 10^{-8} \text{ mol m}^{-2} \text{ s}^{-1} \text{ Pa}^{-1}$ observed at 573 K and 0.4 bar which is lower than that after the third coating. The inability of the other gases i.e. He, N₂, CH₄ and Ar to permeate through the membrane is attributable to the enhanced thickness of the membrane. There was not enough driving force for the gases to overcome the membrane resistance to permeation as a result of the increased thickness of the membrane. From the H₂/CO₂ selectivity of the membrane shown in Table 6.27, it can be observed that the maximum selectivity was 1.28 at 473 K and 0.05 bar which is lower than the theoretical Knudsen selectivity of 4.67. The observed trend through the permeation investigation is that the H₂/CO₂ selectivity has been consistently below Knudsen at successive dips.

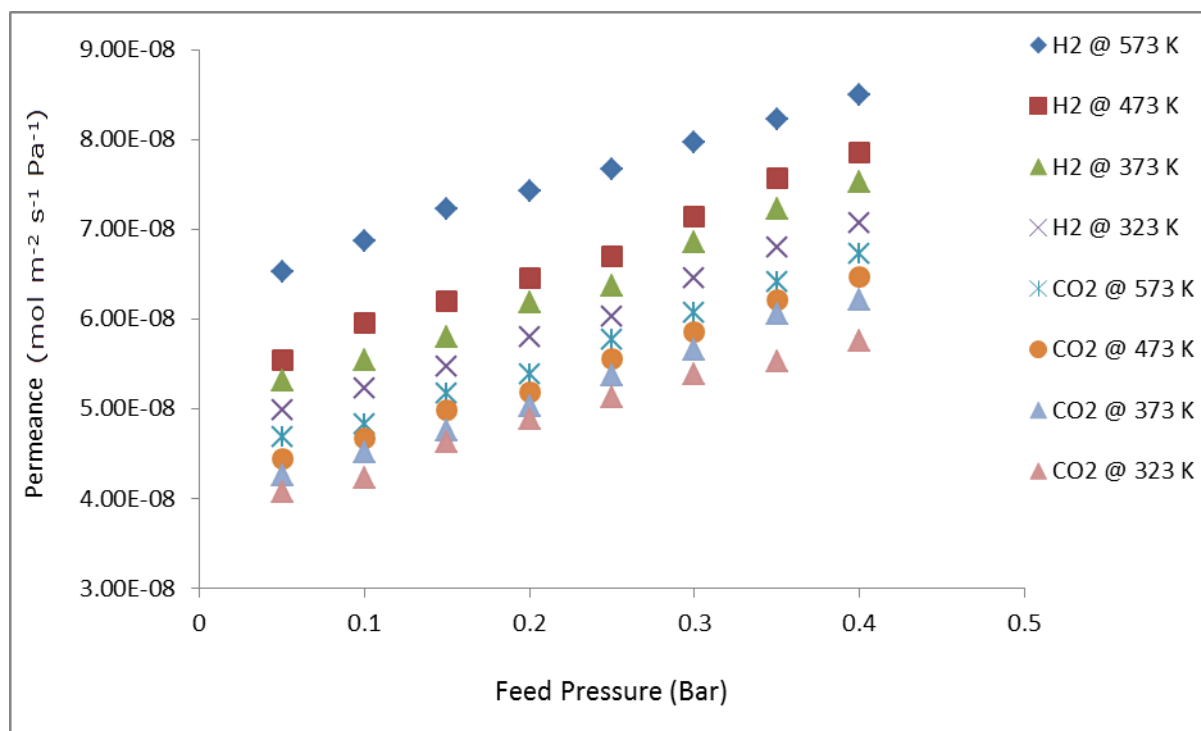


Figure 6.79: H₂ and CO₂ permeance against feed pressure for the AM1 membrane after fourth dip.

Table 6.27: H₂/CO₂ selectivity for the Alumina membrane AM1 after fourth dip

Feed Pressure (Bar)	H ₂ /CO ₂ Selectivity			
	573 K	473 K	373 K	323 K
0.05	1.16	1.22	1.20	1.22
0.10	1.12	1.26	1.15	1.19
0.15	1.18	1.06	1.06	1.20
0.20	1.05	1.08	1.02	1.02
0.25	1.07	1.12	1.01	1.06
0.30	1.15	1.19	1.04	1.02
0.35	1.09	1.21	1.17	1.09
0.40	1.10	1.16	1.05	1.01

6.5.7 Hydrogen Permeance after fifth Dip

After the 5th dip, the thickness of the AM1 membrane increased to 41.63 μm after the deposition of the 5th layer of 6.78 μm thickness. However, only hydrogen permeated through the membrane and no other gas permeance was observed. Hydrogen is more diffusive compared to the other gases investigated hence there was enough driving force for it to permeate through the membrane despite the increased thickness resulting from the 5 successive layers deposited over the porous support. The maximum hydrogen permeance decreased to $6.93 \times 10^{-8} \text{ mol m}^{-2} \text{ s}^{-1} \text{ Pa}^{-1}$ as shown in figure 6.80 due to the increased resistance to permeation as a result of the additional layer. The significance of this investigation is that at certain thickness, the AlO (OH) modified alumina membrane can permeate only hydrogen. This is important especially for scaling up purposes and also in the search for more options for hydrogen permeation using composite membranes.

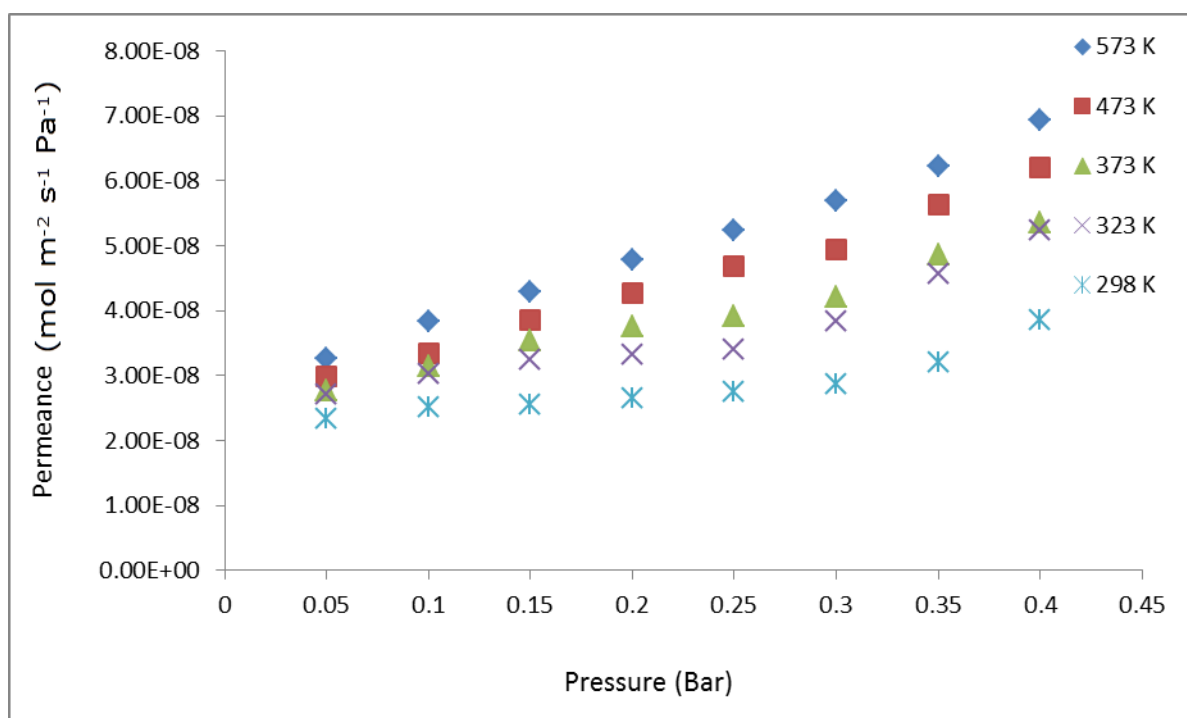


Figure 6.80: Hydrogen permeance against feed pressure for the AM1 membrane after fifth dip

6.5.8 Observations for the AM0 and AM1 Membranes

The following observations were made from the investigations for modification of alumina support using Boehmite sol:

1. Alumina membranes show good adaptability for hydrogen permeation when modified with Boehmite.
2. Alumina membranes when modified with Boehmite sol at a certain thickness permeates only hydrogen but not the other 5 gases: He, CO₂, N₂, CH₄ and Ar.
3. The findings for the modified membrane AM2 are significant especially for scaling up purposes.
4. Alumina supports modified with Boehmite sol present options in hydrogen purification in terms of cost.

6.5.9 References

1. Zhang, K. & Lin, Y.S. (2009). Effect of metal-support interface on hydrogen permeation through palladium membranes. *American institute of chemical engineers*. 55, 3:630-639.
2. Cheng, Y. S., Pena, M.A., Fierro, J.L., Hui, D.C.W. & Yeung, K.L. (2002). Performance of alumina, zeolite, palladium, Pd-Ag alloy membranes for hydrogen separation from town gas mixture. *Journal of membrane science*, 204: 329-340.
3. Guazzone, F., Engwall, E. E. & Ma, H, Y. (2006). Effects of surface activity, defects and mass transfer on hydrogen permeance and n -value in composite palladium-porous stainless steel membranes. *Catalysis Today*, 118: 24-31.
4. Souleimanova, R.S., Mukasyan, A. & Varma, A. (2004). Palladium membranes formed by electroless plating with osmosis: Hydrogen permeation studies. *American institute of chemical engineers*, 48, 2:262-268
5. LI, X., Liu, T.M., Huang, D., Fan, Y.Q. & Xu, N.P. (2009). Preparation and Characterisation of Ultrathin palladium membranes . *Industrial Engineering Chemical Research*. 48: 2061-2065.
6. Kikuchi, E. & Uemiya, S. (1991). Preparation of supported thin palladium-silver alloy membranes and their characteristics for hydrogen separation. *Gas separation & Purification*. 5, 4:261-266.
7. Ilias, S., Su, N., Udo, U.I. & King, F.G. (1997). Application of electroless deposited thin-film palladium composite membrane in hydrogen separation. *Separation science and technology*. 32, 1-4: 487-504.
8. Li, A., Liang, W. & Hughes, R. (1999). Fabrication of defect-free Pd/ α -Al₂O₃ composite membranes for hydrogen separation. *Thin film solids*. 350:106-112.

9. Regonini, D., Jaroenworarluck, A., Stevens, R. & Bowen, C.R. (2010). Effect of heat treatment on the properties and structure of TiO₂ nanotubes: phase composition and chemical composition. *Surface and Interface Analysis*, 43, 3:139-144.
10. Samavat, F., Ahmad, P.T., Mahmoodi, F., Samavat, M.F. & Tavakoli, M.H.(2012). The effect of annealing on the size and morphology of palladium nanoparticles. *American journal of condensed matter physics*, 2, 3:73-75.
11. Roa, F. & Way, J.D. (2005). The effect of air exposure on palladium-copper composite membranes. *Applied surface science* 240 (2005) 85-104.
12. Gielens, F.C., Tong, H.D., Vorstman, M.A.G. & Keurentjes, J.T.F. (2007). Measurement and modeling of hydrogen transport through high flux palladium membranes. *Journal of membrane science*, 289:15-25.
13. Ward, L.T. & Dao, T. (1999). Model of hydrogen permeation behaviour in palladium membranes. *Journal of membrane science*. 153: 211-231.
14. Hou, K. & Hughes, R. (2002). The effect of external mass transfer, competitive adsorption and coking on hydrogen permeation through thin Pd/Ag membranes. *Journal of membrane science*, 206: 119-130.
15. Amano, M., Nishimuro, C. & Komaki, M. (1990). Effects of high concentration CO and CO₂ on Hydrogen permeation through the palladium membrane. *Materials Transactions, JIM*. 31: 5: 404-408.
16. Hara, S., Sakaki, K. & Itoh, N. (1999). Decline in Hydrogen permeation due to concentration polarization and CO hindrance in a palladium membrane reactor. *Ind. Eng. Chem. Res.* 38:4913-4918.
17. Amandusson, H., Ekedahl, L.-G. & Dannelun, H. (2000). The effect of CO and O₂ on hydrogen permeation through palladium membrane. *Applied surface science* 153: 259-267.
18. Li, A., Grace, J.R. & Lim, J.C. (2007). Preparation of thin Pd-based composite membranes on planar metallic substrate. Part 11: Preparation of membranes by electroless plating and characterisation. *Journal of membrane science* 306:159-165.

19. Souleimanova, R.S., Mukasyan, A. & Varma, A. (2004). Palladium membranes formed by electroless plating with osmosis: Hydrogen permeation studies. *American institute of chemical engineers*, 48, 2:262-268.
20. Yun, S. & Oyama, T.S. (2011). Correlations in palladium membranes for hydrogen separation: A review. *Journal of membrane science*, 375 (1-2): 28-45.
21. Hatlevik, O., Gade, K.S., Keeling, K.M., Thoen, M.P., Davidson, A.P. & Way, J.D. (2010). Palladium and palladium alloy membranes for hydrogen separation and production: History, fabrication strategies, and current performance. *Separation and Purification Technology*, 73: 59-64.
22. Zhang, X., Xiong, G. & Yang, W. (2008). A modified electroless plating technique for thin dense palladium composite membranes with enhanced stability. *Journal of membrane science*. 314: 226-237.
23. Chee, C. & Gobina, E. (2010). Ultra-thin palladium technologies enable future commercial deployment of PEM fuel cell systems. *Membrane technology*, Vol. 2010, Issue 3, 6-13.
24. Haag, S., Burgard, M., Amer, J. & Ernst, B. (2008). Thin palladium layer deposited on ceramic materials: application in hydrogen transport and catalytic membrane process. *International journal of surface science & engineering*, 2:3-4.
25. Zeng, G., Shi, L., Liu, Y., Zhang, Y. & Sun, Y. (2014). A simple approach to uniform PdAg alloy membranes: Comparative study of conventional and silver concentration-controlled co-plating. *International journal of hydrogen energy*, 1-10.
26. Pizzi, D., Worth, R., Baschetti, G.M., Sarti, G.C. & Noda, K. (2008). Hydrogen permeability of a 2.5 μm palladium – silver membranes deposited on ceramic support. *Journal of membrane science*, 446 – 453.

27. Weyten, H., Luyten, J., Keizer, K., Willems, L. & Leysen, R. (2000). Membrane performance: the key issues for dehydrogenation reactions in a catalytic membrane reactor. *Catalysis Today*, Vol. 56:3.
28. Guo, Y., Lu, G., Wang, Y. and Wang, R. (2003). Preparation and characterization of Pd-Ag/ceramic composite membrane and application to enhancement of catalytic dehydrogenation of isobutane, *Separation & purification technology*. 32: 271.
29. Li, A., Liang, W. & Hughes, R. (2000). Fabrication of dense palladium composite membranes for hydrogen separation. *Catalysis Today*, Vol. 56:45.
30. Collins, J.P. and Way, J.D. (1993). Preparation and characterization of a composite palladium-ceramic membrane, *Industrial engineering chemical research*. 32: 3006.
31. Hoellein, V., Thornton, M., Quicker, P. and Dittmeyer, R. (2001). Preparation and characterization of palladium composite membranes for hydrogen removal in hydrocarbon dehydrogenation membrane reactors. *Catalysis Today*, Vol. 67:33.
32. Uemiya, S., Matsuda, T. and Kikuchi, E. (1991). Hydrogen permeable palladium-silver alloy membrane supported on porous ceramics. *Membrane Science*. Vol. 56:315.
33. Gu, Y. & Oyama, S.T. (2007). Ultrathin, hydrogen-selective silica membranes deposited on alumina-graded structures prepared from size-controlled boehmite sols. *Journal of Membrane science*, 306:216-227.
34. Li, X. & Liang, B. (2012). Permeance of pure vapors in porous γ -Al₂O₃/ α -Al₂O₃ ceramic membrane, *Journal of the Taiwan Institute of Chemical Engineering*, (43): 339-346.

35. Wu, JCS., Yang, WS. & Lin, LW. (1993). Gas permeation properties of porous alumina membranes. *Petrochemical Technology*, 22:735–8.
36. Suda, H. & Haraya, K. (1997). Gas permeation through micropores of carbon molecular sieve membranes derived from Kapton polyimide. *Journal of physical chemistry*, 101: 3988-3994.
37. Othman, M.B., Mukhtar, H. & Ahmad, A.L. (2004). Gas permeation characteristics across nanoporous inorganic membranes. *IIUM Engineering Journal*, Vol. 5. No. 2: 17-32.

CHAPTER 7

7.0 Conclusions and Recommendations for Future Work

7.1 Validation of Results

The Uniformity of coating has a significant effect on the hydrogen permeation behavior of the membrane. A more uniformly coated and shiny finish was obtained for the Pd/Ag (Pd3) membrane from the codeposition electroless plating method. The Pd3 membrane displayed the highest hydrogen flux compared to the Pd2 and Pd1 membranes prepared using the modified and conventional electroless plating methods respectively. Apart from the uniformity of coating, other factors could also account for the higher hydrogen flux observed for the Pd3 membrane such as presence of leaks from graphite seals and loose bolts and nuts from the membrane reactor during the permeation tests.

In the course of this work, it was observed that it is very important to fix the graphite seals at both ends of the membrane and replace them periodically. There is also the need to properly install the membrane reactor onto the permeation test rig and tighten the bolts and nuts properly as loose bolts and nuts could result in gas leaks. Also, when the membrane reactor is removed from the test rig, it should be cleaned properly from the inside such that no particles are left which could distort the placement of the membrane in the reactor. The modification of the support with Boehmite Sol before deposition has resulted in enhanced hydrogen permeation for both the Palladium, Silica and Ceramic Alumina membranes. The Pd1 membrane was prepared without any surface modification with Boehmite but the 2-step sensitization and activation process was conducted before deposition of the palladium layer. When the ceramic support was modified with Boehmite before deposition for the Pd2 membrane, the hydrogen flux increased. However, the third membrane Pd3 prepared using the codeposition electroless plating method, a higher hydrogen flux compared to both Pd1 and Pd2 membranes was observed.

For the Silica membranes, the SL2 membrane modified with Boehmite displayed a higher hydrogen permeance compared to the SL1 membrane which was not modified with Boehmite. The modified ceramic Alumina membrane AM1 also displayed a higher hydrogen permeance compared to the AM0 membrane.

The Boehmite Sol plugs any defects or pinholes on the porous support thereby enhancing hydrogen permeation through the membrane.

7.2 Conclusions

Hydrogen separation and purification using inorganic composite membranes has been widely accepted as a viable option. However, it is still early days to posit that the challenges in palladium, silica and alumina membranes in hydrogen processes have been fully investigated and addressed. The major challenge in palladium membranes is how to achieve, thin defect free palladium layer with uniform densification of the active palladium layer, durability and high hydrogen recovery. The threat of impurities as inhibitors to hydrogen permeation and separation has also posed major challenge to the application of palladium membranes in hydrogen separation. Another challenge in palladium membranes has been cost and the ability to withstand harsh operating conditions.

The summary of the conclusions in this work is as follows:

1. The Pd/Ag membrane (Pd3) prepared in this work displayed a higher hydrogen flux compared to the Pd membranes prepared using the conventional electroless plating method (Pd1) and the modified electroless plating method (Pd2).
2. A maximum hydrogen flux of $98.1 \text{ cm}^3 \text{ cm}^{-2} \text{ min}^{-1}$ was observed for the Pd/Ag membrane prepared using the codeposition electroless plating method after annealing the membrane in hydrogen at 873 K. This was higher than the maximum hydrogen for both palladium membranes prepared using the conventional electroless plating method ($80.4 \text{ cm}^3 \text{ cm}^{-2} \text{ min}^{-1}$) and the modified electroless plating method ($94.5 \text{ cm}^3 \text{ cm}^{-2} \text{ min}^{-1}$) under same conditions.
3. Annealing the membrane in hydrogen at higher temperature enhanced the hydrogen flux through the membrane. The Pd/Ag membrane displayed the highest flux at 873 K.

4. The Pd/Ag membrane prepared in this work achieved a hydrogen purity of 98.86% and increase in temperature results increasing hydrogen purity. Hydrogen purity through the palladium membranes was enhanced in 2 ways: By annealing at high temperature and alloying with silver.

5. The effect of carbonaceous contaminant carbon monoxide in hydrogen permeation through palladium membranes and the pressure exponent n was also investigated. CO cause deviations from Sievert's law but annealing the palladium membrane at high temperature decreases the inhibition of CO to hydrogen permeation through palladium membranes.

6. A modified method for electroless plating was developed which skips the sensitization step during support modification. A maximum hydrogen flux of 9 was achieved using the method compared to the conventional method which involves the 2 step sensitization and activation. The modified method also reduced the effect of contamination in the active Pd layer in hydrogen permeation through palladium membranes. Through this method, it was observed that Tin impurities during sensitization also contribute to inhibiting hydrogen permeation through palladium membranes and by extension, deviations from Sievert's driving force.

7. The effect of carbonaceous contaminant carbon monoxide in hydrogen permeation through palladium membranes and the pressure exponent n was also investigated. CO cause deviations from Sievert's law but annealing the palladium membrane at high temperature decreases the inhibition of CO to hydrogen permeation through palladium membranes.

8. CO inhibits hydrogen permeation in palladium membranes. However, this effect decreases with increase in temperature and can be suppressed by alloying with silver. Alloying with silver drastically dampens the effect of CO in hydrogen permeation and achieved a sievert's driving force with n value of 0.5.

The Pd/Ag membrane produced in this work also achieved a higher hydrogen flux compared to the Pd-only membrane.

9. Silica membranes were investigated as alternatives and it was observed that these membranes display low hydrogen permeation compared to palladium membranes. However, silica membranes present veritable options to palladium membranes in terms of cost.

10. Silica membranes permeated other gases, He, CO₂, N₂, CH₄ and Ar which is in contrast to a dense defect free palladium membrane that permeates only hydrogen.

11. A method of achieving cost effective alumina membranes for hydrogen permeation was also developed through modification of the commercial alumina support with Boehmite sol. It was concluded that at certain Boehmite layer thickness of the alumina support, only hydrogen can permeate through the membrane. This is significant in scaling up of inorganic membranes for hydrogen processes

12. In the surface modification method for alumina membranes, it was observed that the mean free path for intermolecular travel during collisions, decrease with the number of Boehmite layers. This was attributed to the decrease in pore size of the membrane with increase in layer thickness. The boehmite layers deposited onto the membrane surface lead to a change in the pore structure of the membrane with the pore size decreasing as a result of the additional layers. The decreased pore size results in enhanced resistance to hydrogen permeation and also serves to repair any possible defects/pinholes in the pore structure of the membrane.

7.2 Recommendations for Future Work

This work recorded some achievements based on the results from the several experimental investigations that were conducted. However, research is an ongoing process and certain areas will form the basis for future work. These are:

1. To investigate the effect of CO on hydrogen permeation at high temperature above 873 K so as to provide a better understanding of how temperature suppress deviation from Sievert's driving force in hydrogen permeation so as to provide a better understanding of how temperature suppress deviation from Sievert's driving force in hydrogen permeation through palladium membranes.
2. To investigate the effect of CO on deviations from Sievert's law based on the grain sizes of the membrane. It is an area where not much work has been carried and will provide a better understanding as to how CO inhibits hydrogen permeation in palladium membrane.
3. To investigate the use of sweep gas in hydrogen separation using palladium and palladium alloy membranes at high temperature in terms of the effect of these sweep gases in cushioning the effect of contaminants such as CO on hydrogen permeation
4. To investigate the effect of varying the concentration of Pd and Ag during codeposition to ascertain how it affects hydrogen permeation at different temperature and pressure.
5. To investigate how the rate of electroless plating could affect the uniformity of coating of the palladium layer by varying the electroless plating time and membrane thickness. This is one way of addressing the problems of surface roughness and pin holes that could occur during electroless plating which affects densification and uniformity of coating.

6. To investigate the durability and long term stability of Palladium membranes to establish the active life of each membrane which will be beneficial in terms of time and resources especially for scaling up purposes.

7. To investigate the hydrogen separation and the effect of high temperature annealing in Silica membranes for a better understanding on how the membrane's hydrogen permeation behavior and selectivity can be enhanced.

8. To investigate Hydrogen transport in alumina membranes from the relationship between mean free path and the pore size of the membrane at high temperature This will provide a better understanding of the applicable transport mechanism for hydrogen permeation. This is from the basis of the surface modification method for alumina membranes developed in this work.

Appendices

Appendix A: GC Method for Gas Analysis

```

*****
GC Workstation Multi Instrument - Method Listing - Wed Aug 10 16:11:18 201
Method: Alkali Test Method
*****
*****
*****
3800 GC
*****
Module Address: 44

Valve Table
-----
Valve 1: Gas Sampling Valve
  Initial: Fill
  0.01 min: Fill
  5.50 min: Fill

Valve 2: Gas Sampling Valve
  Initial: Fill
  0.01 min: Inject
  5.50 min: Fill

Front Injector Type 1041
-----
Oven Power: On
Temperature: 150 C

Middle Injector Type 1041
-----
Oven Power: On
Temperature: 150 C

Front Injector EFC Type 4
-----
Pressure   Rate   Hold   Total
 (psi) (psi/min) (min) (min)
-----
    12.5    0.00    3.50    3.50

Time   Total Flow
 (min) (ml/min)
-----
Initial      40

Middle Injector EFC Type 4
-----
Pressure   Rate   Hold   Total
 (psi) (psi/min) (min) (min)
-----
    32.0    0.00    3.00    3.00

Time   Total Flow
 (min) (ml/min)
-----
Initial      40

Column Oven
-----
Coolant: On
Enable Coolant at: 50 C
Coolant Timeout: 10.00 min
Stabilization Time: 0.30 min

Temp   Rate   Hold   Total
 (C) (C/min) (min) (min)
-----
    30    0.0    5.50    5.50

Front TCD Detector
-----
Oven Power: On
Temperature: 125 C
Electronics: On
Filament Temp: 150 C
Time Constant: Slow
Temp Limit: 390 C
Carrier Gas: He

Time   Range   Autozero   Polarity
 (min)

```

```

-----
Initial      0.05    yes    positive
3.00        0.05    yes    positive
-----
Middle FID Detector
-----
Oven Power: Off
Temperature: 50 C
Electronics: Off
Time Constant: Slow

Time      Range  Autozero
(min)
-----
Initial    9      yes
-----
Output Port A
-----
Time      Signal  Attenuation
(min)     Source
-----
Initial   Middle    1
-----
Output Port B
-----
Time      Signal  Attenuation
(min)     Source
-----
Initial   Front    1
-----
Output Port C
-----
Time      Signal  Attenuation
(min)     Source
-----
Initial   Front    1
-----
Data Acquisition
-----
Detector Bunch Rate : 4 points (10.0 Hz)
Monitor Length : 64 bunched points (6.4 sec)
Front FID/TSD Scale: 10 Volts
Middle FID/TSD Scale: 10 Volts
Rear FID/TSD Scale: 10 Volts

Integration Parameters  Address 44  Channel Front
-----
Subtract Blank Baseline : No
Initial S/N Ratio       : 5
Initial Peak Width      : 4 sec
Initial Tangent Height % : 10%
Monitor Noise           : Before every run
Measurement Type        : Peak Area
Initial Peak Reject Value : 1000 counts
Report Unidentified Peaks : Yes
Report Missing Peaks    : No
Normalize Results       : No

Calibration Setup      Address 44  Channel Front
-----
Calculation Type       : External Standard
Number of Calibration Levels: 1
Curve Origin           : Force
Curve Fit              : Linear
Weighted Regression    : (None)
Replicate Treatment    : Keep Replicates Separate
Replicate Tolerance    : Always add new replicates
  Out-of-Tolerance Action : No Action
Calibration Range Tolerance : 50.0%
  Out-of-Tolerance Action : No Action

Verification Setup     Address 44  Channel Front
-----
Deviation Tolerance    : 100.0%
  Out-of-Tolerance Action : No Action

Peak Table  Address 44  Channel Front

```

```

-----
Reference Peaks Time Windows:Width: 0.10 min. Retention Time 2.0%
Other Peaks Time Windows :Width: 0.05 min. Retention Time 11.0%

Peak Name      : H2
Attributes     : Ref:N Std:N RRT:N Lock:N Group:0 Time: 0.571 min
Uses Standard  :
Level 1 Amount: 50
Coefficients   : +0.0000e+000x^3 +0.0000e+000x^2 +0.0000e+000x +0.0000e+000

Peak Name      : N2
Attributes     : Ref:N Std:N RRT:N Lock:N Group:0 Time: 1.250 min
Uses Standard  :
Level 1 Amount: 4
Coefficients   : +0.0000e+000x^3 +0.0000e+000x^2 +0.0000e+000x +0.0000e+000

Peak Name      : CH4
Attributes     : Ref:N Std:N RRT:N Lock:N Group:0 Time: 2.060 min
Uses Standard  :
Level 1 Amount: 8
Coefficients   : +0.0000e+000x^3 +0.0000e+000x^2 +0.0000e+000x +0.0000e+000

Peak Name      : CO
Attributes     : Ref:N Std:N RRT:N Lock:N Group:0 Time: 2.453 min
Uses Standard  :
Level 1 Amount: 28
Coefficients   : +0.0000e+000x^3 +0.0000e+000x^2 +0.0000e+000x +0.0000e+000

Peak Name      : CO2
Attributes     : Ref:N Std:N RRT:N Lock:N Group:0 Time: 4.581 min
Uses Standard  :
Level 1 Amount: 10
Coefficients   : +0.0000e+000x^3 +0.0000e+000x^2 +0.0000e+000x +0.0000e+000

```

Time Events Table Address 44 Channel Front

```

-----
Width Event : 0.1688 0.5 sec
Width Event : 4.3433 4.0 sec
Width Event : 5.0700 8.0 sec

```

Report Format: Module 3800 Address 44 Channel Front

```

-----
Title :
Print Chromatogram : Yes
Chromatogram Options:
Start Retention Time : 0.00 minutes
End Retention Time : 1440.00 minutes
Length in Pages : 1
Initial Chart Speed : 0.0 cm/min
Minutes per Tick : 1.0
Autoscale : On
Time Events : On
Chromatogram Events : On
Retention Times : On
Peak Names : On
Baseline : On

```

```

Print Results : Yes
Results Options:

```

```

Units :
Number of Decimal Digits : 4
Show Peak Group Totals : Yes
Run Log : Off
Error Log : Off
Calibration Report : Off
Revision Log : On
Notes : Off
Method Notes : Off
Convert Results to ASCII?: Off

```

```

Calibration Block Reports
Print Report : No
Convert Report to ASCII?: Off

```

```

Print Copies : 1

```

Figure A.1: A Scanned copy of Alkali Test Method used in the Varian HP 3800 Gas Chromatograph for Gas Analysis

Appendix B: Typical GC Chromatogram Result for Single Gas Hydrogen Permeation Test

```

Print Date: Fri Oct 07 17:25:30 2011          Page 1 of 1
Title :
Run File : C:\star\data\0.05 bar H2 300 C.run
Method File : C:\star\Alkali Test Method 1.mth
Sample ID : Manual Sample

Injection Date: 10/7/2011 5:19 PM      Calculation Date: 10/7/2011 5:24 PM
Operator : ike                          Detector Type: 3800 (10 Volts)
Workstation: RG02701                    Bus Address : 44
Instrument : varian star #1              Sample Rate : 10.00 Hz
Channel : Front = TCD                   Run Time : 5.497 min

** GC Workstation Multi Instrument Version 6.41 ** 01141-2588-C69-24B5 **

Run Mode : Analysis
Peak Measurement: Peak Area
Calculation Type: Percent

Peak No.   Peak Name   Result      Ret.   Time   Area   Sep.   Width   Status
           ( )         (min)  Offset (counts) Code (sec) Group Codes
-----
1 H2       99.9153    0.555  -0.016  9480426  BB  7.6   0
2         0.0847    0.855   0.000   8035     TS  0.0   0
-----
Group 0    100.0000          -0.016  9488461
-----
Totals:    100.0000          -0.016  9488461

Total Unidentified Counts :      8035 counts
Detected Peaks: 2      Rejected Peaks: 0      Identified Peaks: 1
Multiplier: 1      Divisor: 1      Unidentified Peak Factor: 0
Baseline Offset: -78 microVolts      LSB: 1 microVolts
Noise (used): 125 microVolts - monitored before this run
Manual injection

Data Handling: All Coefficients for All Peaks are Zero
Data Handling: Default to A%
*****

```

Figure B1: A Scanned copy of the result for hydrogen single gas permeation test using the Varian HP 3800 Gas Chromatograph

Title :
Run File : C:\star\data\0.05 bar H2 300 C.run
Method File : C:\star\Alkali Test Method 1.mth
Sample ID : Manual Sample
Injection Date: 10/7/2011 5:19 PM Calculation Date: 10/7/2011 5:24 PM
Operator : ike Detector Type: 3800 (10 Volts)
Workstation: RG02701 Bus Address : 44
Instrument : varian star #1 Sample Rate : 10.00 Hz
Channel : Front = TCD Run Time : 5.497 min
** GC Workstation Multi Instrument Version 6.41 ** 01141-2588-C69-24B5 **
Chart Speed = 3.54 cm/min Attenuation = 497 Zero Offset = 2%
Start Time = 0.000 min End Time = 5.497 min Min / Tick = 1.00

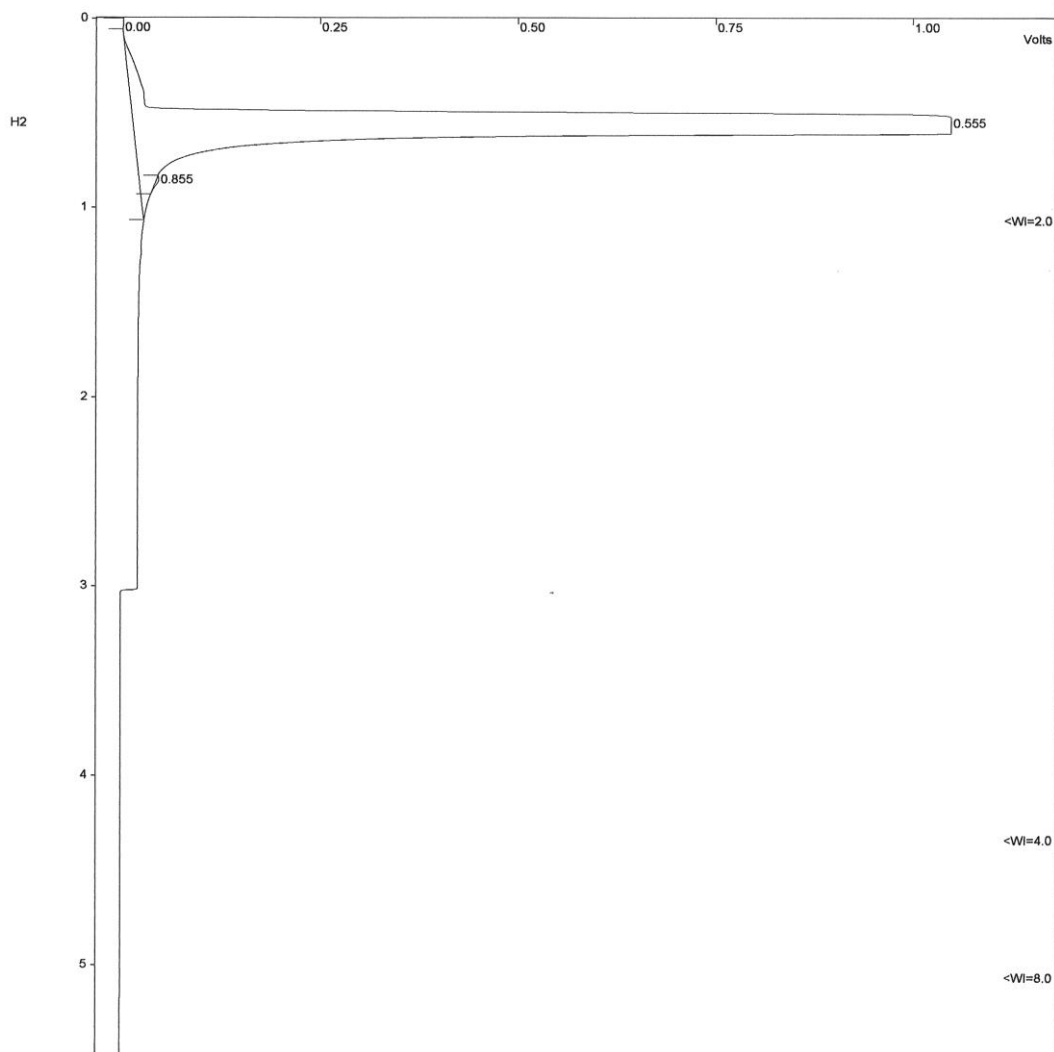


Figure B2: A Scanned copy of the Gas Chromatogram showing clear hydrogen peak based on the result shown in figure B1.

Appendix C: Typical GC Chromatogram Result for Mixed Gas Hydrogen Permeation Test

```

Print Date: Wed Nov 30 16:20:46 2011          Page 1 of 1
Title :
Run File : c:\star\data\3800.44.run
Method File : C:\star\COPY of Alkali Test Method 1.mth
Sample ID : Manual Sample

Injection Date: 11/30/2011 4:15 PM      Calculation Date: 11/30/2011 4:20 PM

Operator :                               Detector Type: 3800 (10 Volts)
Workstation: RG02701                     Bus Address : 44
Instrument : Varian GC3800                 Sample Rate : 10.00 Hz
Channel : Front = TCD                      Run Time : 5.497 min

** GC Workstation Multi Instrument Version 6.41 ** 01141-2588-C69-24B5 **

Run Mode : Analysis
Peak Measurement: Peak Area
Calculation Type: Percent

Peak No.   Peak Name   Result      Ret. Time   Time Offset   Area   Sep. 1/2   Width   Status
           ( )         (min)      (min)      (counts)     Code (sec) Group Codes
-----
1 H2       99.0260      0.495     -0.076     8137159     BB  7.0      0
2         0.0564      0.758     0.000     4638        TS  0.0      0
3 N2       0.0510      1.151     -0.099     4191        BB  2.5      0
4 CO       0.1239      2.419     -0.034     10180       BV  0.0      0
5         0.0646      2.622     0.000     5304        VV  0.0      0
6         0.0139      2.742     0.000     1141        VB  0.0      0
7         0.6643      3.011     0.000     54585       BB  4.9      0
-----
Group 0    100.0001      -0.209     8217198
-----
Totals:    100.0001      -0.209     8217198

Total Unidentified Counts :      65668 counts
Detected Peaks: 17      Rejected Peaks: 10      Identified Peaks: 3
Multiplier: 1      Divisor: 1      Unidentified Peak Factor: 0
Baseline Offset: -80 microVolts      LSB: 1 microVolts
Noise (used): 18 microVolts - monitored before this run
Manual injection
Data Handling: All Coefficients for All Peaks are Zero
Data Handling: Default to A%
*****

```

Figure C1: A Scanned copy of result for hydrogen mixed gas separation test using the Varian HP 3800 Gas Chromatograph showing the gas retention times.

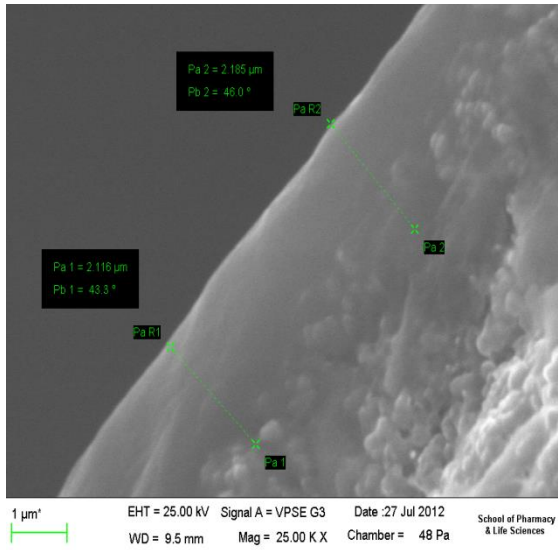
Appendix D: Membrane Characterization: SEM and EDXA for Pd1

Membrane

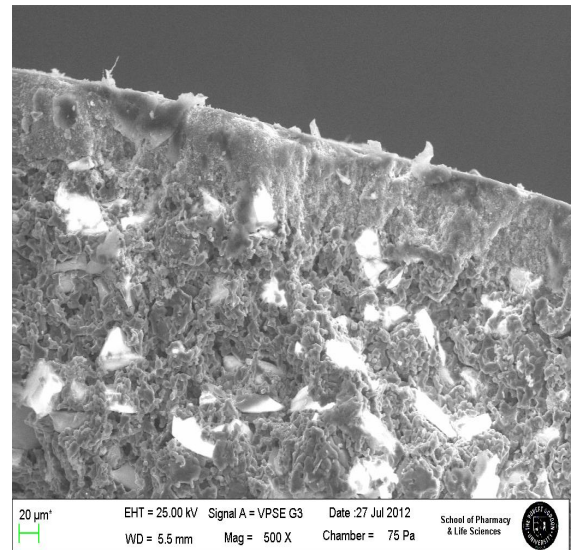
The Pd1 membrane was characterized using the Leo Model S430 Scanning Electron Microscopy (SEM) which is linked online with Energy Dispersive X-ray Analysis (EDXA) to obtain the morphological and structural features of the membrane. Small pieces of the membrane were broken after the permeation tests and used to obtain the elemental composition of the membrane from the energy dispersive x-ray analysis (EXDA).

The SEM micrographs in Figure D1 (A-C) show the Pd layer at inner, outer and cross sections as a thin layer with a thickness of 2 μm . The image also demonstrates a reasonably clear interface between the Pd layer and the macroporous alumina support which suggests a good adhesion of the layer with the support. It can also be observed that the grain sizes are initially small and uniform around the edges but became open inwards while the outer section has bigger grain sizes. Small sol particles results in immediate formation of a gel layer and avoidance of pore clogging.

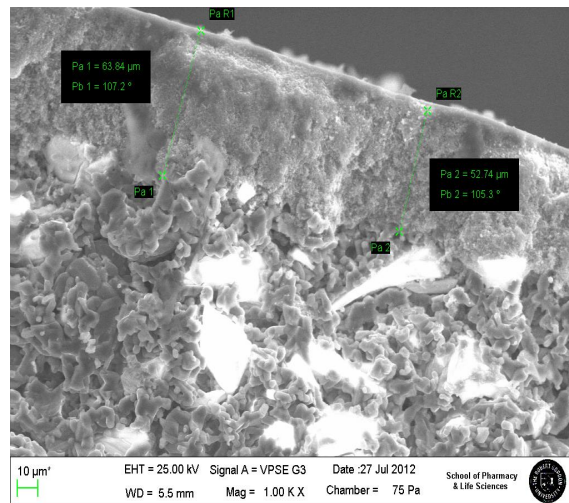
Figure D2 shows the EDXA results indicating the elemental peaks while figure D3 shows the elemental composition of the palladium membrane which indicates the presence of Pd and other elements. The elements from the alumina support are Al and Ti while Pd is from the metallic layer. Sn is from the solution used in the sensitization step during the 2 step support modification. However, it can also be observed from figure D3 that there are other elements such as Na, C and O which could be from the water used in the preparation of the solution and other possible handling imperfections. Pd has the highest weight % of 56.75 while Sn also is reasonably present in the sample at 3.54 %. The Sn could contaminate the active layer and impede hydrogen permeation.



(A). Cross section



(B). Outer section



(C). Inner section

Figure D1: SEM Micrographs for Pd1 membrane showing (C) Inner (B) Outer and (A) Cross Section

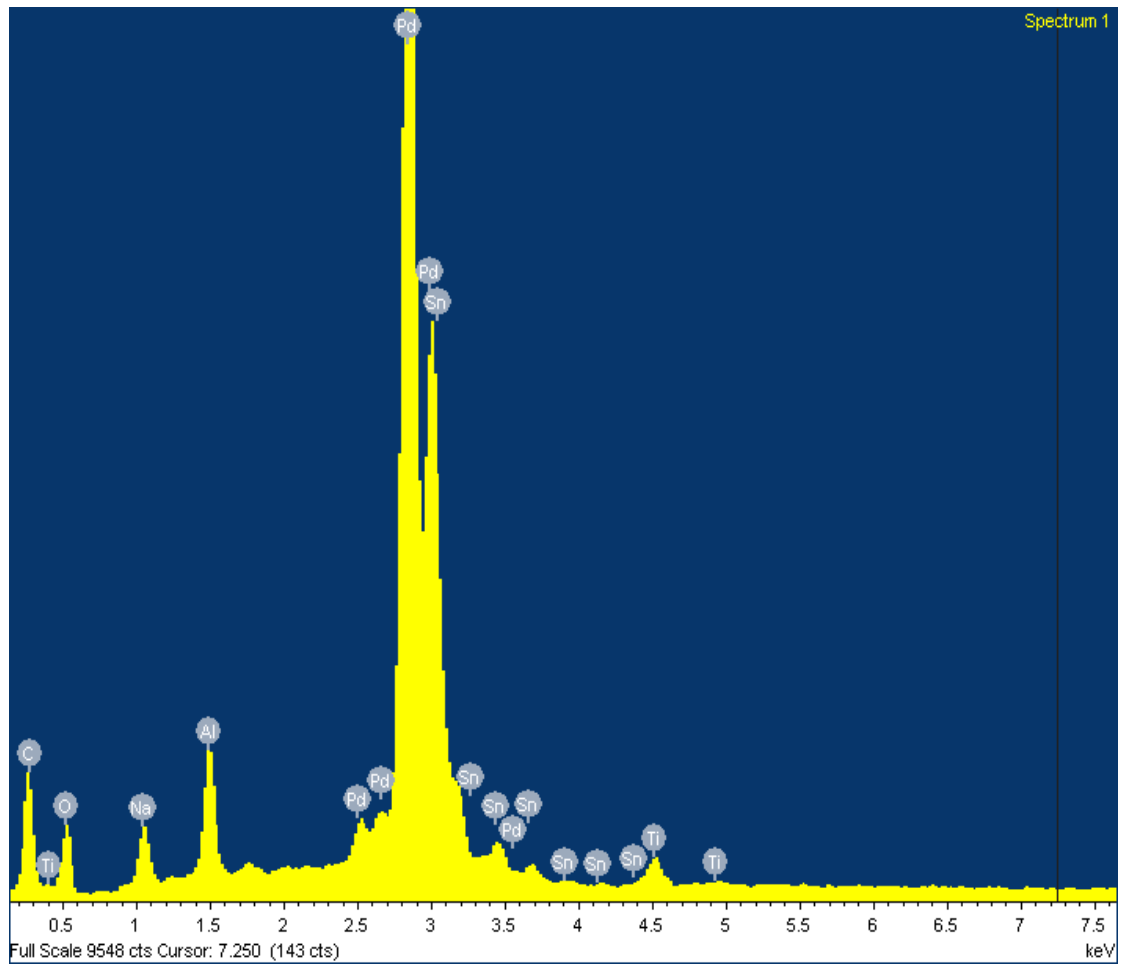


Figure D2: EDXA spectrum showing elemental peaks for the Pd1 membrane

Spectrum processing :

Peaks possibly omitted : 1.760, 18.650 keV

Processing option : All elements analyzed (Normalised)

Number of iterations = 3

Standard :

C CaCO₃ 1-Jun-1999 12:00 AM

O SiO₂ 1-Jun-1999 12:00 AM

Na Albite 1-Jun-1999 12:00 AM

Al Al₂O₃ 1-Jun-1999 12:00 AM

Ti Ti 1-Jun-1999 12:00 AM

Pd Pd 1-Jun-1999 12:00 AM

Sn Sn 1-Jun-1999 12:00 AM

Element	Weight%	Atomic%
C K	14.79	38.57
O K	18.65	36.50
Na K	2.56	3.49
Al K	2.72	3.16
Ti K	0.98	0.64
Pd L	56.75	16.70
Sn L	3.54	0.93
Totals	100.00	

Figure D3: Elemental composition for the Pd1 membrane

Appendix E: Calculation of Hydrogen Flux

The flux for hydrogen through the Palladium membrane was calculated at each temperature and transmembrane pressure. Only the small support (OD= 7.34 mm, ID= 10.07 mm) was used to deposit thin palladium films and the hydrogen flux calculations apply to only the palladium membranes.

The following presents a sample calculation for Hydrogen flux through the palladium membranes from the measured values and stated conditions:

Transmembrane Pressure difference: 0.4 bar

Temperature : 350⁰ C (623 K)

Membrane O.D = 10.07

Pd Layer thickness = 2.116 μm

Hydrogen flow rate = 1.117 L/min

Sample Calculation:

Flux = Flow rate/ Area

To calculate the area (Small membrane):

To determine r_2 (radius for O.D) and r_1 (radius for I.D)

O.D = 10.07 mm

= 0.01007 m

To determine the O.D, there is need to include the Pd layer (Pd layer 2 μm):

$$\mathbf{O.D} = (0.01007 + 2 \times 10^{-6}) \text{ m}$$

$$= 0.01007$$

$$r_2 = \frac{0.010702}{2} = 0.005351 \text{ m}$$

$$\lambda = \frac{c}{d}, \text{ Therefore } c = d \times \lambda$$

$$\text{Area} = \lambda r^2$$

$$A = \text{Circumference} (0.005351^2 \times 3.142)$$

$$A = (10.07 \times 3.142)^2 (0.00002863 \times 3.142)$$

$$= 1130.26 \times 0.00002863$$

$$= 0.10164 \text{ m}^2$$

$$= 1016.4 \text{ cm}^2$$

$$\text{Hydrogen flow rate} = 1.117 \text{ L/min}$$

$$= 1117 \text{ cm}^3 \text{ min}^{-1}$$

$$\text{Hydrogen flux} = \frac{1117}{1016.4}$$

$$= 1.10 \text{ cm}^3 \text{ cm}^{-2} \text{ min}^{-1}$$

Appendix F: Sample Calculation of Gas Permeance and Selectivity

The permeance of the single gases was calculated for the Silica and Alumina membranes. The big support was used to fabricate the Silica and Alumina.

Sample calculation of Gas permeance:

Transmembrane Pressure difference: 0.4 bar

Temperature : 300⁰ C (573 K)

Membrane O.D = 25.91 mm

Membrane I.D = 20.07 mm

He flow rate = 0.184 L/min

Molar volume of a gas at S.T.P = 22.4 L

$$\lambda = \frac{c}{d}, \text{ Therefore } c = d \times \lambda$$

$$\text{Area} = \lambda r^2$$

To calculate the area of the Palladium membrane with O.D of 10.07 mm

O.D = 25.91 mm

Radius r = O.D/2

= 25.91/2 = 12.96 mm

= 0.01296

A =Circumference (0.01296² × 3.142)

A = (12.96×3.142)² (0.0001678 × 3.142)

= 40.72 × 0.00052722

= 0.02146 m²

= 214.87 cm²

$$\text{Permeance} = \frac{(0.184/60/22.4)}{214.87 \times 40000}$$

$$= 1.59 \times 10^{-11} \text{ mol m}^{-2} \text{ s}^{-1} \text{ pa}^{-1}$$

Sample calculation for Selectivity:

Stated conditions from permeation experiment:

Differential Pressure = 0.25 bar

Temperature = 573 K

H₂ permeance = $3.23 \times 10^{-6} \text{ mol m}^{-2} \text{ s}^{-1} \text{ Pa}^{-1}$

CO₂ permence = $1.41 \times 10^{-6} \text{ mol m}^{-2} \text{ s}^{-1} \text{ Pa}^{-1}$

$$\text{Selectivity } \alpha_{H_2/CO_2} = \frac{3.23 \times 10^{-6}}{1.41 \times 10^{-6}}$$

$$= 2.29$$

Appendix G: Calculation of Thickness for Silica Membrane

The weight gain method was used to calculate the thickness of the silica and alumina layers in both membranes. The method involves weighing the support before and after deposition of the silica layer. For both membranes, the big size membrane with the following specification was used: I.D = 20.07 mm, O.D= 26.0 mm, Effective length = 0.32 m

Silica membrane SL1 after first dip: (Conventional method):

First Dip in Silica Solution:

$$\text{Weight of membrane} = 279.80 \text{ g}$$

$$\text{Weight after dipping} = 293.5 \text{ g}$$

$$\text{Weight after drying and calcination} = 281.30 \text{ g}$$

$$\begin{aligned}\text{Weight gain} &= \text{Weight after drying} - \text{Weight of Membrane} \\ &= 281.30 - 279.80 \\ &= 1.50 \text{ g}\end{aligned}$$

$$\text{Surface Area} = \lambda D L$$

Where D is the Outer Diameter of the membrane, L is the effective length of the membrane.

$$D = 2.6 \text{ cm}$$

$$L = 0.32 \text{ m}$$

$$\begin{aligned}\text{Surface Area} &= 3.142 \times 2.6 \times 32 \\ &= 261.41 \text{ cm}^2\end{aligned}$$

$$\text{Density of Silicone} = 2.33 \text{ g/cm}^3$$

$$\begin{aligned}\text{Volume} &= \text{weight gain/density} \\ &= 1.50 \text{ g}/2.33 \text{ gcm}^3 \\ &= 0.64377 \text{ cm}^3\end{aligned}$$

$$\begin{aligned}
\text{Thickness} &= \text{Volume} / \text{Surface Area} \\
&= 0.64377 \text{ cm}^3 / 261.41 \text{ cm}^2 \\
&= 0.0024627 \text{ cm} \\
&= 24.627 \text{ } \mu\text{m}
\end{aligned}$$

Second Dip in Silica Solution:

Weight of membrane after permeation test = 280.7 g

Weight after dipping = 295.1 g

Weight after drying and calcination = 281.8 g

$$\begin{aligned}
\text{Weight gain} &= \text{Weight after drying} - \text{Weight of Membrane} \\
&= 281.8 - 280.7 \\
&= 1.1 \text{ g}
\end{aligned}$$

Thickness based on same procedure used for the first dip = 18.06 μm

So to obtain the total thickness, the thickness for the second dip should be added to the thickness for the first dip:

$$24.627 + 18.06 = 42.687 \text{ } \mu\text{m}$$

Therefore, after the first and second dips the thickness of the SL1 membrane is 42.687 μm .

First Dip Silica membrane SL2 (Modified method)

It should be noted that for the modified method, the support was dipped in Boehmite solution prior to the deposition of the Silica layer.

Weight of support = 276.7 g

Weight after dipping in Boehmite solution = 279.3 g

Weight after drying = 277.9 g

Weight after dipping in Silica Solution = 287.5 g

Weight after drying and calcination = 278.4

Weight gain = 278.6 - 276.7

= 1.9 g

Thickness of the membrane based on the procedure in calculating the thickness after first dip = 31.19 μm

Second dip Silica membranes SL2 (Modified method):

Weight of support after permeation test = 278.1 g

Weight after dipping in Boehmite solution = 278.9 g

Weight after drying = 278.3 g

Weight after dipping in Silica solution = 298.4 g

Weight after drying and calcination = 279.2

Weight gain = 279.3 - 278.1

= 1.2 g

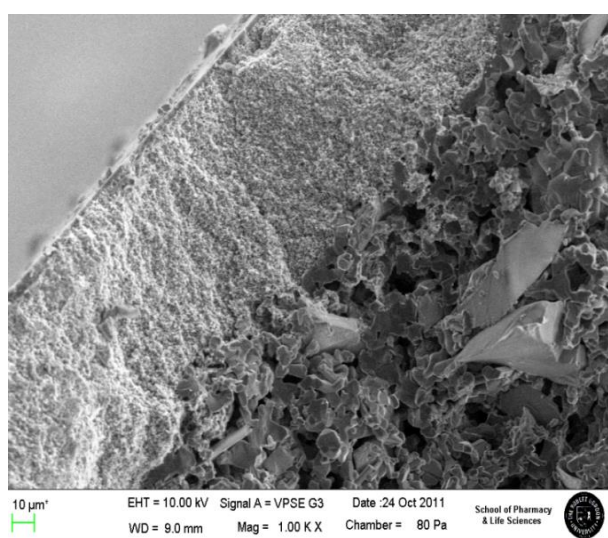
Thickness = 19.70 μm

Therefore, the thickness of the SL2 membrane after the first and second dips =
27.91 μm + 19.70 μm
= 50.89 μm

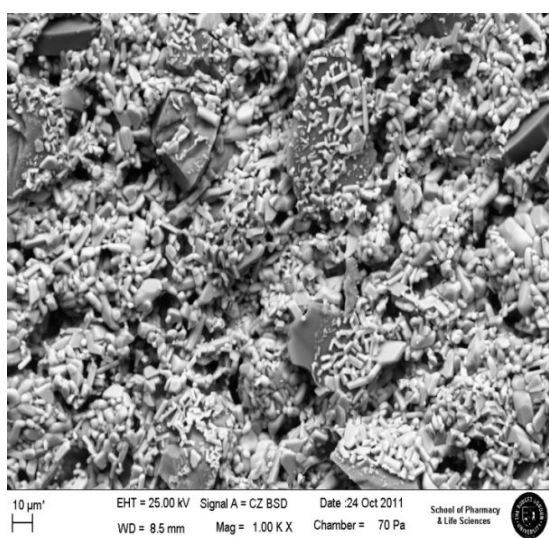
Therefore, after the first and second dips, the thickness of the silica membrane prepared using the modified dip coating method is 50.89 μm

Appendix H: Membrane Characterisation for Ceramic Alumina Membrane

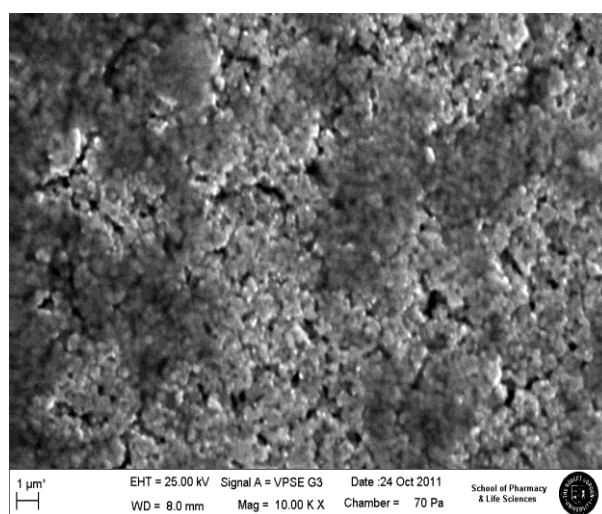
The SEM micrographs and EDXA elemental composition of the α -alumina membrane AM1 are shown in Figure 5.2 and Table 5.1 respectively. The morphology of the cross section is shown in Figure 5.2 (a). The outer section in Figure 5.2 (b) shows a more homogeneous pore structure with a smaller grain size compared to both the inner and cross sections. Smaller grain sizes usually lead to better gas selectivity of the membrane due to the relatively smaller boundaries associated with small grains.



(a) Cross section



(b) Inner Section



(c) Outer section

Figure H1: SEM Micrographs of Ceramic Alumina Membrane AM0

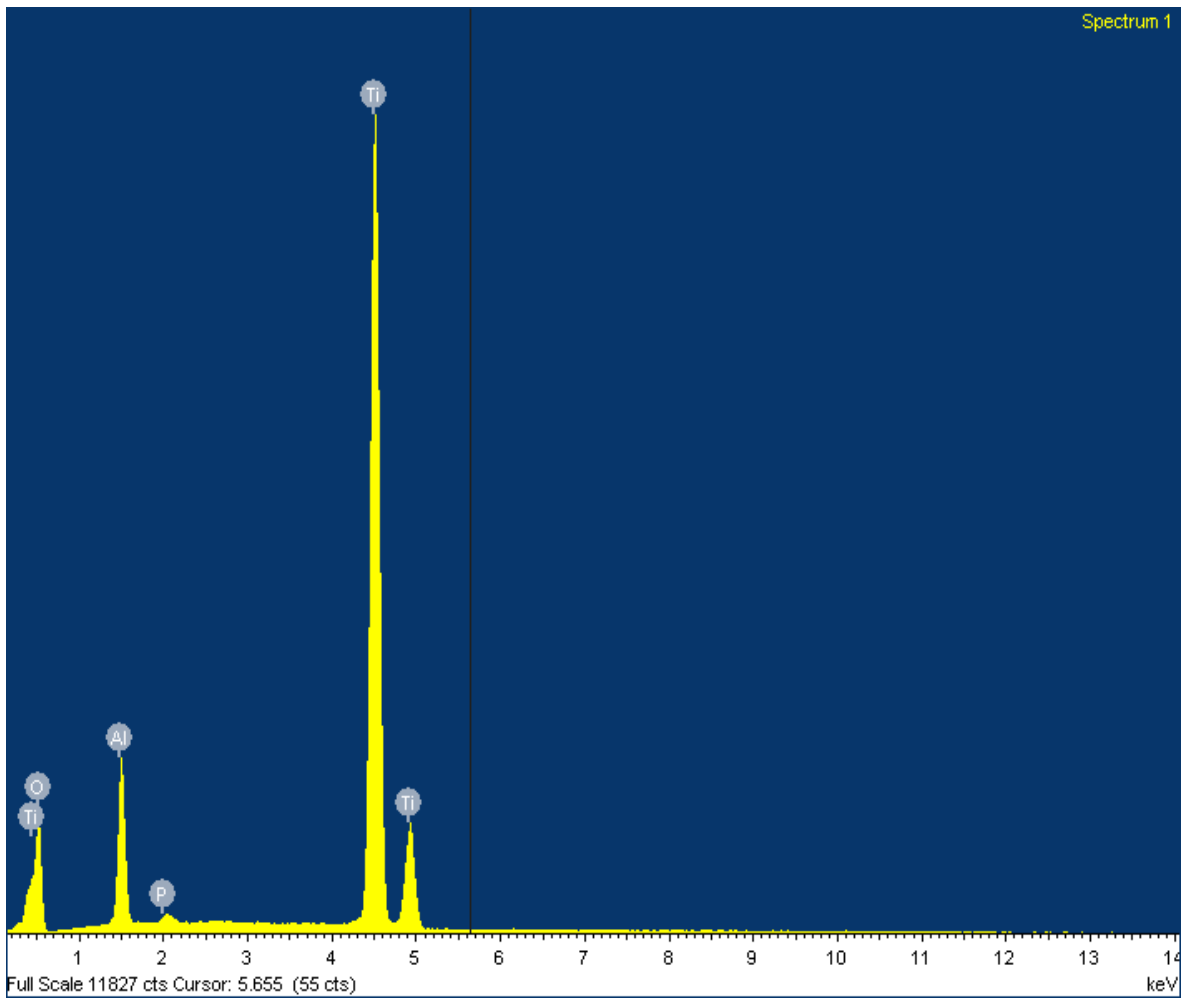


Figure H2: EDXA Results for Ceramic Alumina Membrane AM0

Spectrum processing :

No peaks omitted

Processing option : All elements analyzed (Normalised)

Number of iterations = 4

Standard :

O SiO2 1-Jun-1999 12:00 AM

Al Al2O3 1-Jun-1999 12:00 AM

P GaP 1-Jun-1999 12:00 AM

Ti Ti 1-Jun-1999 12:00 AM

Element	Weight%	Atomic%
O K	49.67	72.96
Al K	6.06	5.28
P K	0.13	0.10
Ti K	44.14	21.66
Totals	100.00	

Figure H3: Elemental Composition of Ceramic Alumina Membrane AM0

Appendix I: Calculation of Thickness for Modified Ceramic Alumina Membrane AM1

First Dip AM1 membrane:

Weight of the Support before dipping = 277.6 g

Weight of membrane after dipping = 281.3 g

Weight of membrane after drying and calcination = 278.7 g

Weight gain = Weight after drying – Weight of Membrane
= 278.7 – 277.6 g
= 1.1 g

Surface Area = $\lambda D L$

Where D is the Outer Diameter of the membrane, L is the effective length of the membrane.

D= 2.6 cm

L = 0.32 m

Surface Area = $3.142 \times 2.6 \times 32$
= 261.41 cm²

Density of Alumina 3.95 g/cm³

Volume = weight/density
= 1.1 g/3.95 gcm³
= 0.278481 cm³

Thickness = Volume/ Surface Area
= 0.278481 cm³/261.41 cm²
= 0.0010653 cm
= 10.65 μ m

Second dip AM1 membrane:

Weight of the AM1 membrane after permeation test = 278.5 g

Weight of membrane after dipping = 283.6 g

Weight of membrane after drying and calcination = 279.4 g

$$\begin{aligned}\text{Weight gain} &= \text{Weight after drying} - \text{Weight of Membrane} \\ &= 279.4 - 278.5 \\ &= 0.9 \text{ g}\end{aligned}$$

Thickness after second dip = 8.72 μm

$$\begin{aligned}\text{Total thickness} &= 10.65 + 8.72 \\ &= 19.37 \mu\text{m}\end{aligned}$$

Third Dip AM1 membrane:

Weight of the AM1 membrane after permeation test = 279.3 g

Weight of membrane after permeation test = 279.3 g

Weight of membrane after drying and calcination = 280.1 g

$$\begin{aligned}\text{Weight gain} &= \text{Weight after drying} - \text{Weight of Membrane} \\ &= 279.9 - 279.3 \\ &= 0.8 \text{ g}\end{aligned}$$

Thickness = 7.74 μm

Total thickness after first, second and third dips:

$$\begin{aligned}&= 19.37 + 7.74 \\ &= 27.11 \mu\text{m}\end{aligned}$$

Fourth Dip AM1 membrane:

Weight of the AM1 membrane after permeation test = 279.8 g

Weight of membrane after dipping = 289.8 g

Weight of membrane after drying and calcination = 280.6 g

Weight gain = Weight after drying – Weight of Membrane

$$= 280.6 - 279.8$$

$$= 0.8 \text{ g}$$

Thickness = 7.74 μm

Total thickness = 27.11 + 7.74

$$= 34.85 \text{ } \mu\text{m}$$

Fifth Dip AM1 membrane:

Weight of the AM1 membrane after permeation test = 280.5 g

Weight of membrane after dipping = 295.7 g

Weight of membrane after drying and calcination = 281.3 g

Weight gain = Weight after drying – Weight of Membrane

$$= 281.2 - 280.5$$

$$= 0.7 \text{ g}$$

Thickness = 6.78 μm

Total thickness = 34.85 + 6.78 = 41.63 μm

